

DISSERTATION

**GRID SIZE SELECTION FOR 2-D HYDROLOGIC MODELING
OF LARGE WATERSHEDS**

Submitted by

Darcy Kay Molnár

Department of Civil Engineering

In partial fulfillment of the requirements

for the Degree of Doctor of Philosophy

Colorado State University

Spring 1997

UMI Number: 9735027

UMI Microform 9735027
Copyright 1997, by UMI Company. All rights reserved.

**This microform edition is protected against unauthorized
copying under Title 17, United States Code.**

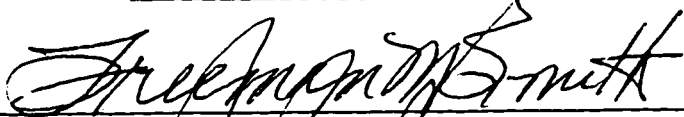
UMI
300 North Zeeb Road
Ann Arbor, MI 48103

COLORADO STATE UNIVERSITY

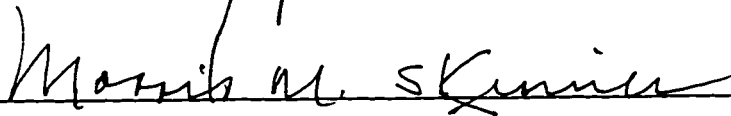
April 3, 1997

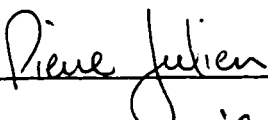
WE HEREBY RECOMMEND THAT THE DISSERTATION PREPARED UNDER OUR SUPERVISION BY DARCY K. MOLNÁR ENTITLED GRID SIZE SELECTION FOR 2-D HYDROLOGIC MODELING OF LARGE WATERSHEDS BE ACCEPTED AS FULFILLING IN PART REQUIREMENTS FOR THE DEGREE OF DOCTOR OF PHILOSOPHY.

Committee on Graduate Work

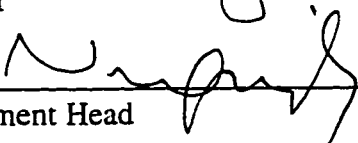








Advisor



Department Head

ABSTRACT OF DISSERTATION
GRID SIZE SELECTION FOR 2-D HYDROLOGIC MODELING
OF LARGE WATERSHEDS

An important aspect of applying hydrologic models to large watersheds is the determination of an appropriate scale at which the spatial variability governing rainfall-runoff processes is preserved. A method to select suitable grid sizes for hydrologic modeling of large areas is developed by meeting the following objectives: 1) application of the CASC2D distributed-parameter model in order to examine the effects of increasing grid size; 2) determination of drainage patterns and runoff behavior, assuming impervious conditions; and 3) evaluation of pervious runoff, resulting in the definition of peak discharge as a function of equilibrium conditions.

The CASC2D model is applied to two watersheds, draining 21 km² and 560 km² respectively, using grid sizes ranging from 30x30 m to 1x1 km. The effects of grid resolution of estimated watershed characteristics, network characteristics, and runoff hydrographs are evaluated. At increasing grid size, the total number of cells decreases, the percentage of overland cells decreases, and drainage density decreases. As a result of these changes, hydrographs simulated using coarse resolutions typically have higher peak runoff rates and earlier times to peak. Consequently, in calibrating and verifying the model at coarser resolutions, the parameters representing overland and channel roughness coefficients are to be increased.

Assuming impervious runoff conditions, and using GIS-GRASS capabilities for data analysis and manipulation, it is possible to generate maps depicting the drainage areas (A_d) corresponding to individual grid cells in the basin. At increasing grid size, the distribution of A_d corresponding to overland cells is significantly changed. In contrast, the distribution of A_d corresponding to channel cells is not affected by grid resolution. The raster maps of drainage areas are used to develop maps of the time to equilibrium (T_e) and equilibrium discharge (Q_e) for individual cells. These give a graphical representation of the basin's response to a particular rainfall event. Since the distribution of A_d for channel cells does not change as a result of increasing grid size, complete and partial equilibrium conditions in the channel are also not affected by grid size.

Based on the definition of dimensionless parameters Q^* (Q_p/Q_e) and T^* (T_f/T_e), partial and complete equilibrium conditions are evaluated, assuming a variety of rainfall properties. The Green-Ampt infiltration scheme is used, and pervious runoff is defined as a function of average hydraulic conductivity (\bar{K}_z) and average rainfall intensity (\bar{i}), which are found to accurately represent runoff when $A_d > 1 \text{ km}^2$. Appropriate grid resolutions for simulations are defined using Q^* and T^* , which incorporate watershed and rainfall characteristics. By definition, the grid size selected for simulations on large watersheds is small enough to preserve essential characteristics governing rainfall-runoff processes, but large enough to be used effectively and efficiently.

Darcy K. Molnár
Civil Engineering Department
Colorado State University
Fort Collins, CO 80523
Spring 1997

ACKNOWLEDGMENTS

I especially would like to extend my appreciation to my advisor, Pierre Julien, whose constant guidance and encouragement made this study possible. I would also like to thank Jorge Ramírez, Morris Skinner, and Freeman Smith for serving on my committee and for providing useful insights and recommendations. My husband Peter, my parents, and my family have provided unending support. I am deeply grateful to them. And finally, I would like to thank the many friends, colleagues, and instructors who have helped me accomplish this work.

Financial support was granted through the Center for Geosciences.

TABLE OF CONTENTS

LIST OF TABLES	viii
LIST OF FIGURES.....	ix
LIST OF SYMBOLS	xii
CHAPTER 1: INTRODUCTION	
1.1 Introduction.....	1
1.2 Study objectives.....	4
1.3 Approach.....	5
CHAPTER 2: LITERATURE REVIEW	
2.1 Modeling watershed hydrology.....	8
2.2 Scaling issues.....	11
2.3 GIS and hydrological models.....	16
2.4 The concept of a watershed time to equilibrium.....	18
2.5 Future needs/trends in hydrological modeling.....	23
CHAPTER 3: MODEL DESCRIPTION	
3.1 The model	25
3.2 Governing equations	26
3.2.1 Precipitation	26
3.2.2 Infiltration	27
3.2.3 Overland flow routing.....	28
3.2.4 Channel flow routing	32
3.3 CASC2D scaling issues	33
CHAPTER 4: SMALL-SCALE SIMULATIONS	
4.1 Goodwin Creek input data	36
4.1.1 Defining grid resolutions	39
4.1.2 Rainfall runoff events	41
4.2 Model calibration and validation	42
4.2.1 Calibrating to outlet conditions.....	46
4.2.2 Calibrating to sub-basin conditions	54
4.2.3 Validation results	58
4.3 Summary	62

CHAPTER 5: LARGE-SCALE SIMULATIONS	
5.1 Hickahala-Senatobia input data	64
5.2 CASC2D simulations.....	69
5.2.1 Fine grid resolution	69
5.2.2 Coarse grid resolutions	73
5.3 Summary	81
 CHAPTER 6: SIMULATING IMPERVIOUS WATERSHED CONDITIONS	
6.1 Introduction.....	85
6.2 Goodwin Creek	89
6.2.1 Evaluating complete equilibrium conditions	89
6.2.2 Peak discharge as a function of T^*	96
6.3 Hickahala-Senatobia	98
6.3.1 Evaluating complete equilibrium conditions	98
6.3.2 Peak discharge as a function of T^*	103
6.4 Effects of grid size on cell drainage area.....	106
6.5 Analysis of impervious runoff conditions on two watersheds.....	113
6.6 Summary	115
 CHAPTER 7: SIMULATING PERVIOUS WATERSHED CONDITIONS	
7.1 Introduction.....	117
7.2 Goodwin Creek	119
7.3 Hickahala-Senatobia	121
7.4 Quantifying infiltration effects.....	124
7.4.1 Simulating complete equilibrium conditions	124
7.4.2 Goodwin Creek rainfall events	131
7.5 Analysis of pervious runoff conditions on two watersheds	137
7.6 Summary	142
 CHAPTER 8: APPLICATION	
8.1 Methodology	145
8.2 Example	147
 CHAPTER 9: SUMMARY AND CONCLUSIONS.....	
	151
 REFERENCES	 157
 APPENDICES	
Appendix A: CASC2D source code	163
Appendix B: Input data.....	178
Appendix C: Calibration data	186
Appendix D: GRASS programs used in analysis.....	193
Appendix E: Results from pervious simulations at coarse resolutions.....	195
Appendix F: Calculating an equivalent channel roughness	200

LIST OF TABLES

<u>Table</u>	<u>Content</u>	<u>Page</u>
3.1	Processes simulated using CASC2D	35
4.1	Goodwin Creek watershed characteristics at increasing grid size	40
4.2	Rainfall-runoff conditions for rainfall events	43
4.3	Variations in parameters calibrated for outlet conditions	47
4.4	Model parameters determined as a result of calibration run 1	49
4.5	Model parameters determined as a result of calibration run 2	51
4.6	Variations in parameters in sub-basin calibration of event 1	54
4.7	Variations in parameters in sub-basin calibration of event 2	56
5.1	Hickahala-Senatobia watershed characteristics at increasing grid size	68
5.2	Drainage areas associated with sub-basins at increasing grid sizes	78
7.1	Parameters used in simulations at 416 ft resolution	133
7.2	Infiltration effects at Goodwin Creek outlet	134
B.1	Green and Ampt parameters based on soil texture	179
B.2	Description of CASC2D input parameters	179
B.3	Goodwin Creek rainfall events	183
C.1	Parameter values used for trial simulations at a 416 ft grid size	186
C.2	Parameter values used for trial simulations at a 832 ft grid size	187
C.3	Parameter values used for trial simulations at a 1248 ft grid size	187
C.4	Parameter calibration for sub-basins (event 1)	189
C.5	Parameter calibration for sub-basins (event 2)	191

LIST OF FIGURES

<u>Figure</u>	<u>Content</u>	<u>Page</u>
2.1	Complete and partial equilibrium hydrographs	19
3.1	A two dimensional model grid mesh	26
3.2	Raster-based description of overland flow routing scheme	28
3.3	Representation of a channel cell	32
4.1	Goodwin Creek basin	37
4.2a	Goodwin Creek elevation map at a 416 ft grid size	38
4.2b	Goodwin Creek soil map at a 416 ft grid size	38
4.2c	Goodwin Creek landuse map at a 416 ft grid size	38
4.3	Slope in upland areas as a function of grid resolution	41
4.4	Goodwin Creek at increasing grid sizes	42
4.5	Rainfall rates recorded at rain gage 1, located at the outlet	44
4.6	Sample calibration results	47
4.7	Simulated outlet hydrograph for event 1	49
4.8	Simulated sub-basin hydrographs for event 1	50
4.9	Simulated outlet discharge for event 2	52
4.10	Simulated sub-basin hydrographs for event 2	53
4.11	Calibrating to sub-basin conditions, event 1	55
4.12	Calibrating to sub-basin conditions, event 2	57
4.13a	Goodwin Creek simulated outlet discharge, event 3	59
4.13b	Goodwin Creek simulated discharge at gage 3, event 3	60
4.14a	Goodwin Creek simulated outlet discharge, event 4	60
4.14b	Goodwin Creek simulated discharge at gage 3, event 4	61
5.1	Hickahala-Senatobia basin	64
5.2	Hickahala-Senatobia digital elevation map (100 ft grid size)	65
5.3	Hickahala-Senatobia sub-basins and network at a 1000 ft grid size	67
5.4	Hickahala-Senotobia upland slopes at increasing grid size	68
5.5	Hickahala-Senatobia simulation results at a 100 ft grid size	72
5.6	Hickahala-Senatobia at increasing grid sizes	75
5.7a	Simulated hydrographs at 1000 ft resolution with impervious conditions	76
5.7b	Simulated hydrographs at 2000 ft resolution with impervious conditions	77
5.7c	Simulated hydrographs at 3000 ft resolution with impervious conditions	77
5.8a	Simulated hydrographs at 1000 ft resolution with pervious conditions	79
5.8b	Simulated hydrographs at 2000 ft resolution with pervious conditions	79
5.8c	Simulated hydrographs at 3000 ft resolution with pervious conditions	79
5.9	Simulated discharge at increasing grid size	80

5.10	Required calculation time for the simulation of a 12 hr event	83
6.1	Goodwin Creek equilibrium discharge hydrographs	90
6.2	Spatial variability of equilibrium discharge on the Goodwin Creek basin	92
6.3	Spatial variability of drainage area on the Goodwin Creek basin	92
6.4	Spatial variability of time to equilibrium on the Goodwin Creek basin	93
6.6a	Distribution of basin-wide Q_e at increasing grid size, Goodwin Creek	94
6.6b	Distribution of basin-wide A_d at increasing grid size, Goodwin Creek	94
6.6c	Distribution of basin-wide T_e at increasing grid size, Goodwin Creek	95
6.7a	Peak discharge assuming impervious conditions (416 ft grid size)	96
6.7b	Peak discharge assuming impervious conditions (832 ft grid size)	97
6.7c	Peak discharge assuming impervious conditions (1248 ft grid size)	97
6.8	Spatial variability of drainage area on the Hickahala-Senatobia basin	100
6.9	Spatial variability of equilibrium discharge on the Hickahala-Senatobia basin	101
6.10	Spatial variability of the time to equilibrium on the Hickahala-Senatobia basin	101
6.11a	Distribution of basin-wide A_d at increasing grid size, Hickahala-Senatobia	102
6.11b	Distribution of basin-wide Q_e at increasing grid size, Hickahala-Senatobia	102
6.11c	Distribution of basin-wide T_e at increasing grid size, Hickahala-Senatobia	103
6.12a	Peak discharge assuming impervious conditions (1000 ft grid size)	104
6.12b	Peak discharge assuming impervious conditions (2000 ft grid size)	105
6.12c	Peak discharge assuming impervious conditions (3000 ft grid size)	105
6.13	Range of peak overland discharge and peak channel discharge	106
6.14	Distribution of A_d on Goodwin Creek as determined by GRASS	108
6.15a	Distribution of A_d corresponding to Goodwin Creek channel cells	108
6.15b	Distribution of A_d corresponding to Goodwin Creek overland cells	109
6.16a	Distribution of A_d as a function of grid resolution	110
6.16b	Distribution of A_d/A_g as a function of grid resolution	110
6.17	Defining the minimum channel drainage area as a function of total area	112
6.18	Runoff length as a function of total drainage area	113
6.19	Partial and complete equilibrium conditions on an impervious watershed	114
7.1a	Peak runoff rates on Goodwin Creek for $\bar{K}_s / i = 1.0$	120
7.1b	Peak runoff rates for on Goodwin Creek $\bar{K}_s / i = 0.5$	120
7.1c	Peak runoff rates on Goodwin Creek for $\bar{K}_s / i = 0.2$	121
7.2a	Peak runoff rates on Hickahala-Senatobia for $\bar{K}_s / i = 1.0$	123
7.2b	Peak runoff rates on Hickahala-Senatobia for $\bar{K}_s / i = 0.5$	123
7.2c	Peak runoff rates on Hickahala-Senatobia for $\bar{K}_s / i = 0.2$	124
7.3a	Equilibrium hydrographs $\bar{K}_s / i = 1.0$	126
7.3b	Equilibrium hydrographs $\bar{K}_s / i = 0.5$	126
7.3c	Equilibrium hydrographs $\bar{K}_s / i = 0.2$	127
7.4a	Distribution of basin-wide i_{eq}/i (416 ft grid size)	128
7.4b	Distribution of basin-wide i_{eq}/i (832 ft grid size)	129
7.4c	Distribution of basin-wide i_{eq}/i (1248 ft grid size)	129
7.5a	Effects of drainage area on i_{eq}/i for overland cells	130
7.5b	Effects of drainage area on i_{eq}/i for channel cells	130

7.6	Effect of rainfall variability on peak discharge for rainfall events on Goodwin Creek	132
7.7	Infiltration conditions for events 1 and 3	136
7.8	Effects of infiltration on complete equilibrium conditions	138
7.9	Partial and complete equilibrium conditions at $\bar{K}_s / \bar{i} = 1.0$	139
7.10	Partial and complete equilibrium conditions at $\bar{K}_s / \bar{i} = 0.5$	140
7.11	Partial and complete equilibrium conditions at $\bar{K}_s / \bar{i} = 0.2$	140
7.12	Channel runoff conditions for pervious simulations	144
B.1	Goodwin Creek observed stage and discharge at the outlet	183
B.2	Coefficient of variation of average rainfall rates for Goodwin Creek events	184
B.3	Coefficient of variation of maximum rainfall rates for Goodwin Creek events	185
C.1	Simulated hydrographs from calibration runs at a 416 ft resolution	187
C.2	Simulated hydrographs from calibration runs at a 832 ft resolution	188
C.2	Simulated hydrographs from calibration runs at a 1248 ft resolution	188
C.4	Peak discharge and time to peak for trial calibration runs	188
C.5	Peak discharge for sub-basin calibration runs (event 1)	189
C.6	Effects of increasing grid size on sub-basin hydrographs (event 1)	190
C.7	Peak discharge for sub-basin calibration runs (event 2)	191
C.8	Effects of increasing grid size on sub-basin hydrographs (event 2)	192
E.1a	Peak runoff rates on Goodwin Creek for $\bar{K}_s / \bar{i} = 1.0$ (832 ft grid size)	196
E.1b	Peak runoff rates on Goodwin Creek for $\bar{K}_s / \bar{i} = 0.5$ (832 ft grid size)	196
E.1c	Peak runoff rates on Goodwin Creek for $\bar{K}_s / \bar{i} = 0.2$ (832 ft grid size)	196
E.2a	Peak runoff rates on Goodwin Creek for $\bar{K}_s / \bar{i} = 1.0$ (1248 ft grid size)	197
E.2b	Peak runoff rates on Goodwin Creek for $\bar{K}_s / \bar{i} = 0.5$ (1248 ft grid size)	197
E.2c	Peak runoff rates on Goodwin Creek for $\bar{K}_s / \bar{i} = 0.2$ (1248 ft grid size)	197
E.3a	Peak runoff rates on Goodwin Creek for $\bar{K}_s / \bar{i} = 1.0$ (2000 ft grid size)	198
E.3b	Peak runoff rates on Goodwin Creek for $\bar{K}_s / \bar{i} = 0.5$ (2000 ft grid size)	198
E.3c	Peak runoff rates on Goodwin Creek for $\bar{K}_s / \bar{i} = 0.2$ (2000 ft grid size)	198
E.4a	Peak runoff rates on Goodwin Creek for $\bar{K}_s / \bar{i} = 1.0$ (3000 ft grid size)	199
E.4b	Peak runoff rates on Goodwin Creek for $\bar{K}_s / \bar{i} = 0.5$ (3000 ft grid size)	199
E.4c	Peak runoff rates on Goodwin Creek for $\bar{K}_s / \bar{i} = 0.2$ (3000 ft grid size)	199

LIST OF SYMBOLS

<u>Symbol</u>	<u>Description</u>
A	channel flow cross-section
A_{ch}	cross-sectional area of the channel
A_d	drainage area
A_{d_min}	drainage area reflecting the minimum threshold for channel cells
A_g	drainage area corresponding to a single grid cell
Δ	ratio representing variations in calibration parameters
C	Courant number
C_v	coefficient of variation
dt	time step
dx	cell width
e	excess rainfall
E	elevation
f	infiltration rate
F	total infiltrated depth
g	gravitational acceleration
h	surface depth of flow
h_{ch}	depth of flow in the channel
H_f	capillary pressure head at the wetting front
i	rainfall intensity
\bar{i}	average rainfall intensity
i_{eq}	equivalent rainfall intensity
K_s	hydraulic conductivity at normal saturation
\bar{K}_s	average hydraulic conductivity at normal saturation
L	runoff length
L_{d_min}	runoff length associated with A_{d_min}
L_e	equilibrium length under impervious conditions
L_g	grid length
L_{g_max}	largest grid size corresponding to equilibrium conditions
L_{g_min}	smallest grid size corresponding to equilibrium conditions
L_s	length scale
M_d	soil moisture deficit
n	Manning coefficient
n_{ch}	channel Manning coefficient
n_{eq}	equivalent channel Manning coefficient
n_{ol}	overland Manning roughness

R	hydraulic radius of channel
S	runoff slope
S_d	detention storage
S_{fx}	friction slopes in x direction
S_{fy}	friction slopes in y direction
S_{ox}	bed slopes in x direction
S_{oy}	bed slopes in y direction
Δt	computational time step
t_s	time associated with infiltration conditions
t_p	ponding time
T_e	time to equilibrium under impervious conditions
T_{e_bas}	time to equilibrium for the entire basin
T_{e_ce}	time to equilibrium under pervious conditions
T_c	time of concentration
T_{obs}	observed time to peak
T_p	time to peak
T_r	rainfall duration
T[*]	dimensionless time, equal to T_r/T_e
T[*]_{ce}	dimensionless time corresponding to complete equilibrium conditions
T[*]_{out}	dimensionless time corresponding to runoff conditions at the outlet
u	average velocity in the x direction
v	average velocity in the y direction
value_{trial}	parameter value used in calibration runs
value_{trial 1}	parameter value used in trial 1 of calibration runs
q_l	lateral inflow rate per unit length, into or out of the channel
q_x	unit flow rate in x-direction
q_y	unit flow rate in y-direction
Q	total discharge in the channel
Q_e	equilibrium discharge under impervious conditions
Q_{e_eq}	equilibrium discharge under pervious conditions
Q_{obs}	observed discharge
Q_p	peak discharge
Q[*]	dimensionless discharge, equal to Q_p/Q_e
Q[*]_{ce}	dimensionless discharge corresponding to complete equilibrium
Q[*]_{ch}	dimensionless discharge corresponding to channel cells
Q[*]_{max}	maximum dimensionless discharge corresponding to overland cells
Q[*]_{min}	minimum dimensionless discharge corresponding to overland cells
Q[*]_{out}	dimensionless discharge corresponding to runoff at the outlet
W	grid size
W_{ch}	channel width

Chapter I

INTRODUCTION

1.1 INTRODUCTION

Hydrological models have been developed with two purposes: to improve our understanding of physical systems, and as predictive tools. The goal in hydrological modeling is to capture the essence of the physical controls of soil, vegetation, and topography on runoff production. The variance of the rainfall-runoff response of a watershed should be governed by factors such as the variance of soil properties, the variance of overland roughness coefficients, routing conditions in the channel network, as well as by the spatial variability of rainfall in time and space.

A variety of models have been developed and tested on small-scale watersheds, based on empirically derived equations. Distributed parameter models have taken these results and extended their applicability to larger scales. The use of distributed models for runoff determination on large watersheds is complicated by the need to establish a spatial scale which will accurately represent the variability in physical basin characteristics. This spatial scale has been defined as a function of basin characteristics such as topography, drainage density, degree of soil saturation, geomorphology, and rainfall characteristics. The challenge in hydrological modeling of large watersheds is to determine a scale at

which spatial variability can be neglected, with average characteristics of a given area providing sufficient information for accurate modeling of basin runoff generation.

The CASC2D model is a two-dimensional distributed parameter model which can be used in the analysis of spatial variability on a cell by cell basis. Average characteristics are defined per square grid cell. The model incorporates three types of data requirements: 1) excess precipitation, as the mass input to the system; 2) basin and network physical characteristics; and 3) physical laws governing surface runoff. The process of evaluating runoff as a function of the three types of data involves looking at the hydrological component (rainfall input), the hydraulic component (overland and channel flow), and the geomorphic component (basin geomorphology, overland plane characteristics, stream network characteristics). The choice of a grid size for CASC2D rainfall-runoff simulations could affect all three components of the model. For example: in evaluating excess precipitation, rainfall rates are interpolated from point measurements to average rates per grid element (hydrological component); the spatial variability of basin characteristics such as soil and landuse types are assumed constant within each grid cell (hydraulic component); and the applicability of point based equations representing physical laws may not be justified on large grid cells (geomorphic component).

The CASC2D model has been successfully applied to basins less than 50 km² (Saghafian 1992, Ogden 1992, Doe and Saghafian 1992). The applicability of the model on large watersheds has yet to be tested. The current availability of watershed input data in the form of GIS (geographic information systems) raster maps has increased the feasibility of simulating runoff generation on large basins. With current advances in GIS technology, watershed input data is becoming readily available at grid sizes as fine as 30

meters. For modeling purposes, the complexity of the basin and network at such a fine scale require intense data manipulation and long computation times. A coarser resolution would require less input data and less computation time, although spatial variability in watershed characteristics may be lost as a result of the larger grid size. In order to effectively and accurately represent runoff processes on large watersheds, an appropriate scale must be defined at which essential characteristics governing hydrologic, hydraulic, and geomorphic processes are preserved, but for which data requirements are reduced and computation time is limited.

The watershed time to equilibrium (T_e) represents a basin's response to rainfall. T_e is defined as a function of rainfall intensity and the hydraulic parameters affecting overland and channel flow. Under complete equilibrium conditions, the equilibrium discharge (Q_e) is linearly related to rainfall intensity (i). Conceptually, if the entire watershed reaches equilibrium, the evaluation of peak runoff should not be affected by grid resolution. Regardless of upland spatial variability, peak discharge will be a constant value, equal to product of the drainage area (A_d) and the rainfall intensity (i). When equilibrium conditions are not reached, spatial variability becomes important. The grid size selected for modeling purposes may have a significant impact on the accuracy of runoff estimations. In this case, peak discharge will be a non-linear function of rainfall intensity (i).

Infiltration effects will increase the time to equilibrium (T_e) and decrease the equilibrium discharge (Q_e), as compared to impervious conditions. An analysis of runoff conditions using the concept of a watershed time to equilibrium provides a dimensionless approach to the evaluation of rainfall-runoff processes on large basins. Appropriate grid

sizes for hydrological modeling can be selected as a function of the dimensionless parameter Q^* , which is equal to peak discharge (Q_p) divided by equilibrium discharge (Q_e), and the dimensionless parameter T^* , which is equal to rainfall duration (T_r) divided by the time to equilibrium (T_e). These dimensionless parameters are related to specific watershed characteristics and rainfall properties. The definition of grid resolutions which accurately and effectively represent rainfall-runoff processes on large watersheds, based on watershed characteristics and rainfall properties, will extend the applicability of 2-D hydrological modeling.

1.2 STUDY OBJECTIVES

The main objective of this research is to recommend appropriate grid sizes for hydrological simulations on large watersheds. In order to do so, the following objectives are defined:

1. Simulation of rainfall-runoff events using grid sizes ranging from 30x30 m to 1x1 km, so as to evaluate the effects of grid resolution on estimates of watershed and network characteristics, as well as the effects on hydrologic and hydraulic processes;
2. Attempt to model a 560 km² watershed using a 30x30 m grid size;
3. Simulation of impervious and pervious runoff, with the determination of complete and partial equilibrium conditions on individual grid cells in a basin;
4. Quantification of infiltration effects and pervious runoff response through the evaluation of the relationships governing peak runoff rates for both uniform and spatially-varied rainfall events;
5. Development of a method to select appropriate grid sizes for large-scale simulations, using dimensionless parameters Q^* and T^* , where $Q^* = Q_p/Q_e$ and $T^* = T_r/T_e$.

1.3 APPROACH

The intent of the study is to evaluate conditions for the large-scale application of 2-D hydrologic models such as CASC2D. The availability of raster-based input data makes it possible to evaluate runoff conditions on individual cells throughout the basin. This capability can be used in describing the spatial variability of the rainfall-runoff response of both overland and channel cells, so as to evaluate grid scales which are appropriate for simulations on large watersheds.

The following requirements are set forth as the scope of the study:

- Data collection at the grid finest resolution possible, for a small-scale watershed and a large-scale watershed located in the same geographic region;
- Aggregation of input data to coarser grid resolutions;
- Application of the CASC2D distributed model to a 21 km² basin (8 mi²);
- Application of the CASC2D distributed model to a 560 km² basin (219 mi²);
- Evaluation of peak discharge (Q_p) for all grid cells within each basin, for a variety of impervious and pervious conditions;
- Evaluation of complete equilibrium conditions for individual cells, with the determination of time to equilibrium (T_e) and equilibrium discharge (Q_e);
- Evaluation of partial equilibrium conditions for individual cells, where peak discharge is a non-linear function of rainfall intensity, using dimensionless parameters Q^* and T^* ;
- Evaluation of the basin-wide response to varying rainfall intensities resulting in partial and complete equilibrium conditions, using dimensionless parameters Q^* and T^* ;

- Determination of appropriate grid resolutions for large-scale simulations based on the requirement that complete equilibrium be reached on individual grid cells.

The objectives of the study are met in the following manner. In Chapter 1 the scope of the research is introduced, study objectives are defined, and the research approach is outlined. Chapter 2 summarizes related literature, covering the topics of hydrological models, scaling issues, and the concept of watershed complete and partial equilibrium conditions. In Chapter 3 the CASC2D model is presented, with an emphasis on numerical formulations and data requirements, as well as a discussion of possible effects of increased grid size on CASC2D simulations. Chapters 4 and 5 present a model-oriented approach to understanding the effects of grid resolution on rainfall-runoff simulations. In Chapter 4 the model is calibration and validated on a 21 km² watershed, using grid sizes up to 400x400 m. Scaling issues encountered in the simulations are discussed. In Chapter 5, the results from model calibration on a small scale are extended to a 560 km² watershed. The rainfall-runoff response is simulated using grid sizes ranging from 30x30 m to 1x1 km. The effects of grid resolution on large-scale simulations are summarized, with comments on the relative effects of channel routing versus overland routing. Chapters 6 and 7 present a conceptual approach to understanding the effects of grid resolution on hydrological simulations. Dimensionless parameters Q^* (where $Q^* = Q_p/Q_e$) and T^* (where $T^* = T_r/T_e$) are defined and used in the analysis of rainfall-runoff generation, for both partial and complete equilibrium conditions. In Chapter 6, simulations are performed on the two watersheds assuming impervious runoff conditions. Basin-wide response to rainfall is evaluated as a function of drainage areas corresponding to cells throughout the basin. Chapter 7 presents rainfall-

runoff simulations performed assuming pervious conditions. The effects of infiltration are quantitatively defined with regard to Q^* and T^* . Conclusions are drawn as to the effects of infiltration and runoff generation in upland areas for uniform and non-uniform rainfall events. In Chapter 8, the results from Chapters 4, 5, 6, and 7 are used to define a method by which appropriate grid sizes can be selected for large-scale simulations. The method is then tested on the 560 km² watershed. In Chapter 9 research results are summarized and final conclusions are made.

Chapter II

LITERATURE REVIEW

2.1 MODELING WATERSHED HYDROLOGY

Hydrological models are defined as models which attempt to simulate natural processes governing the generation of runoff on basins. From the moment a raindrop lands on the earth's surface, various mechanisms play an important role in determining where the raindrop will be located in 1, 2, or 3 hr. Scientists have been successful in simulating point processes such as interception, infiltration, and evapo-transpiration using equations derived from fundamental physics. The challenge in more recent years has been to integrate these equations to the hillslope or catchment scale, in order to simulate basin-wide hydrological response. Spatial integration to catchment scale is not straightforward, due to typical nonlinear catchment response (Goodrich and Woolhiser, 1991). A variety of hydrological models deal with the components of rainfall-runoff generation in different ways, giving more or less attention to specific components.

Models have successfully been used to simulated large-scale events, but the question remains: Are these models true to the physics of the system, or are they simply 'fitting' parameters on a case-by-case basis? Grayson et al. (1992a) warn that it is possible to obtain 'good fits' when representing the wrong processes. What is the role of calibration when simulating events on large watersheds? Watersheds vary greatly in

terms of physical characteristics such as soil types, landuse types, upland runoff lengths and slopes, channel morphology. Coupled with the variations in watershed characteristics are variations in rainfall characteristics such as rainfall intensity, duration, and spatial variability. Initial soil moisture and base flow in a channel are additional factors which influence the rainfall-runoff response of a basin.

Several models have been developed which spatially integrate watershed characteristics over a given area. Heterogeneity within the area is neglected, resulting in simplified runoff conditions. The major concern with lumped models is the difficulty in obtaining a single representative value of a spatially variable parameter that would lead to an accurate prediction of the mean basin response (Moore and Gallant, 1991). Simulation results could be drastically affected by the single value chosen to represent a particular parameter. In addition, the problem with using measured parameter values for physically based models is that the scales at which measurements are performed are typically too small to enable integration of spatial variability (Dunne, 1982; James and Burges, 1982; Beven, 1983; Wood, 1983).

Moore et al. (1993) state that the Thiessen, isohyetal, and reciprocal-distance-squared methods used to estimate areal precipitation are not capable of accurately representing the spatial distribution of temporally varying, fine time-resolution rainfall intensities on a catchment. These methods are also not effective in handling moving storm cells. When the only precipitation information available is a daily point rainfall estimate, it becomes extremely difficult to represent the temporal variability of rainfall intensities, especially in highly convective regions.

As model developers try to improve upon work already done and come up with better approaches to simulating rainfall events at large scales, they must consider lessons learned from previous work. Klemes (1986) warns that a good mathematical model must work well for the right reasons and must reflect, even if only in a simplified form, the essential features of the physical prototype. Hillel (1986) suggests that a model should not be too complex, and that it should have a limited number of parameters - parameters with a physically-based significance. Hillel goes on to state that a model need not depict a phenomenon much more accurately than our ability to measure it, nor should a model pretend to do too much, as there is no such thing as THE model.

Grayson et al. (1992b) point out that catchment response is typically 'well behaved'. Most hydrographs are smooth and predictable. There appears to be dichotomy between the variability of the natural system (e.g. variability in measured values of hydraulic conductivity) and the relatively well behaved output of the system. A complex model should not be required in order to reproduce the well behaved response of catchments. Grayson et al. conclude by stating that in order to advance the art and science of hydrological modeling, a good conceptual understanding of the processes, the variability, and the behavior of natural systems is needed.

Beven (1989) summarizes the challenges facing model developers by noting that future developments in physically-based modeling will need to take into consideration the theory of the lumping of subgrid scale processes, the need for closer correspondence between equations and field processes, and the need for rigorous assessment of uncertainty in model predictions.

2.2 SCALING ISSUES

There are two approaches to studying scaling issues in hydrology: a model-oriented approach and an approach using dimensional analysis and similarity concepts (Blösch and Sivapalan, 1995). A model-oriented approach focuses on the scaling of state variables, model parameters, inputs, and conceptualizations. An approach using dimensional analysis and similarity concepts deals with complex hydrological processes in a much more simple fashion. In the past decades, hydrologists have used both approaches in attempting to understand the nature of watershed runoff generation and its relation to watershed characteristics. These studies have led to a wide range of conclusions, primarily pertaining to small scale basins. Some of these studies, dating back to the 1970's, are summarized herein.

Black (1970, 1972) and Black and Cronn (1975), in their studies of small scale watersheds using a rainfall simulator, determined that if conditions are saturated, morphometric features of the basin have little or no effect on the runoff hydrograph, but if conditions are not saturated these features do affect the hydrograph. They also concluded that drainage density is not a sensitive indicator of runoff behavior, that the slope and basin relief will have over-riding effects.

Klein (1976) argues that in small catchments the form of the hydrograph will be dominated by the overland flow response, while subsurface flows will be too highly delayed to contribute to peak flows. Klein states that a break occurs around 300 km²: smaller basins have peakier responses, while larger basins have more attenuated hydrographs. In large catchments, especially in humid areas, routing times through the channel network may be long enough that the hydrograph form could become dominated

by subsurface flow contributions. Kirkby (1976) also supports the theory that in very large catchments, channel flow routing times are long enough that the shape of the hydrograph is dominated by the topology of the network itself.

Rodriguez-Iturbe and Valdes (1979), along with Gupta et al. (1980), related basin response to basin geomorphology using a statistical approach. The bifurcation ratio (R_B), the length ratio (R_L), the area ratio (R_A), and the slope ratio (R_S) were used to relate the characteristics of streams of different orders within the watershed. In their presentation of the GIUH (geomorphic instantaneous unit hydrograph), Rodriguez-Iturbe and Valdes (1979) defined peak discharge and time to peak as a function of the R_B , R_L , R_A , and R_S ratios, assuming a constant velocity in the channels and the independence of flow pathways. Their conclusions point to the effects of geomorphology in determining rainfall-runoff conditions.

With regard to the effects of soil and vegetative properties on rainfall-runoff processes, Milly and Eagleson (1987) examined the effects of spatial variability of soil and vegetation on spatially and temporally averaged hydrologic fluxes. From their studies they concluded that an equivalent homogeneous soil can reproduce average behavior only when there is little initial variability. Loague (1988) examined the impact of spatially variable rainfall and soil information on runoff predictions by aggregating detailed hydraulic conductivity and rainfall data to coarser resolutions. According to Loague's analyses, accurate representation of the spatial variability of hydraulic conductivity appears to be more critical than accurate representation of spatially varied rainfall rates. In addition, he found that obtaining accurate estimates of runoff variables

such as time to peak (T_p), peak discharge (Q_p), and runoff volume required different spatial scales.

According to Beven et al. (1988), water flow pathways depend on hillslope morphology, especially where surface or near surface flows are the major mechanism by which water reaches a stream channel. Beven states that the channel network can be described using Strahler's area ratio and Horton's bifurcation, slope, and length ratios. He concludes that runoff can thus be described using ratios of bifurcation, length, slope, and area.

Moore et al. (1993) suggest that if a single process in the landscape dominates the rainfall-runoff response, then a simple lumped model may be able to simulate the behavior if a quasi-distributed representation of the effect of that process can be incorporated into the model. They propose an index approach, based on simplified representations of the underlying physics of two processes. These processes are the distribution of soil water content in a landscape and the susceptibility of landscapes to erosion by water.

In the application of hydrologic models, Bruneau et al. (1995) suggest that the space and time resolution used for model calculations is a compromise between the accuracy required, available accurate data, and computational demands of using smaller space and time steps. They state that physically-based models are most sensitive to water content at saturation, flow resistance in the channel network and soils, and initial conditions of simulations. In their study of hydrological space-time sensitivity using TOPMODEL on a 12 km² watershed, they determined that the ideal simulation conditions were at a 30-50 m spatial resolution and a 1-2 hr time resolution.

Beven (1995) states that the assumption that a model which is applicable at small scales can be applied to larger scales using 'effective' parameter values is an inadequate approach to the scaling problem. He goes on to suggest a disaggregated approach to hydrologic modeling, where sub-dividing into smaller areas would better reflect hydrological heterogeneity.

Farajalla and Vieux (1995) evaluated correct resolutions for distributed modeling of surface runoff, based on the effects of spatially variable infiltration. They determined that the correct resolution should capture the essential variability of infiltration parameters, and that the resolution is related to the fractal dimension of the parameter surface. Based on their analysis of infiltration, and earlier analyses of hydraulic roughness (Farajalla and Vieux, 1994), they state that the entropy curve is useful in describing, a priori, the spatial variability and for identification of critical cell resolution. The rate of change of entropy is defined as the Hurst coefficient (H), which is a measure of spatial variability. Their results indicate that the critical resolution is approximately 1209 m. At a fine resolution, no new information is captured and model results are reproducible. At a coarser resolution variability is lost and model output is inconsistent. They concluded that an appropriate grid resolution for surface runoff modeling will be dependent on size of catchment and the spatial variability of the parameters affecting the hydrological process.

A concept which has gained a great deal of attention in the past decade is the concept of a representative elementary area (REA). DeCoursey (1996) provides an extensive review of the theory behind the REA, and gives examples of studies in which the concept was evaluated using specific hydrological models. Wood et al. (1988) were

the first to define areas of similar hydrologic response as REA's, based on the theory that runoff generation is a multi-scale phenomenon with different length scales characterizing soil, topography, and rainfall variability. By definition, the REA must be a length scale larger than the length scale characteristic of rapidly varying components of the hydrological response, yet smaller than the length scale of slowly varying components. The basis of the REA is that when variability is integrated over a large enough area, the effects of small-scale variability are attenuated (Sivapalan et al., 1987; Wood et al., 1988, 1990). Wood et al. (1990) applied TOPMODEL to a 11.7 km² catchment and found the area representative of hydrological processes to be approximately 1 km². This was the same area determined in earlier studies by Wood et al. (1988). Wood and Lakshmi (1993) extended the analysis using TOPMODEL to evaluate catchment evapo-transpiration during inter storm periods. Goodrich et al. (1993) evaluated the REA using KINEROSR, which is a research version of the KINEROS model. They identified two different REA sizes for the two catchment areas used in the study. Their results indicate that the REA will be a function of the DEM resolution used in its development and the catchment size. Blöschl et al (1995) evaluated the REA using the THALES model, which simulates hydrologic response and includes flow routing. According to their results, flow routing does not seem to have an effect on the REA. DeCoursey (1996) summarizes the studies of the REA concept, to date, by stating that the REA depends on catchment properties and climatic characteristics. At a small scale the REA will vary as a function of topographic features and the correlation length of soil characteristics. At a large scale, the REA will vary as a function of vegetation, geologic and geomorphic structures, and rainfall correlation length scales.

2.3 GIS AND HYDROLOGICAL MODELS

According to Maidment (1993), coupling geographic information systems (GIS) with hydrologic modeling will provide methods of doing things more quickly and efficiently, and will open up new fields of study that have previously been inaccessible. The use of GIS increases the potential for describing spatial variability, and will thus extend the applicability of hydrologic modeling in addressing regional or continental scale processes.

In an effort to take advantage of the large amount of data currently available in GIS format, modelers are increasingly adapting computer-based distributed parameter hydrological models to the GIS environment. Advances in computer technology have made it possible to efficiently handle large amounts of data. Computation times have been greatly decreased. These improvements point to seemingly endless capabilities for hydrological modeling, especially the modeling of mesoscale systems. A number of studies have been performed in order to evaluate the potential for linking hydrological models to a GIS.

Gao et al. (1993) linked a GIS with a distributed rainfall-runoff model. They used GIS to provide a dynamic description of the hydrologic response (soil moisture redistribution, runoff generation, stream flow variation) occurring in the watershed. They concluded that if properly used, GIS are powerful tools which will enhance the efficiency and effectiveness of numerical models and will also simplify the analysis of spatially distributed phenomena such as model-scale issues in surface hydrology.

Chairat and Delleur (1993) interfaced the physically based hydrologic model, TOPMODEL, with a GIS. GIS data management and manipulation capabilities were

used to derive topographic parameters. They evaluated the trade-off between the accuracy of digital elevation models (DEMs) and the accuracy of results from the hydrologic model.

Warwick and Hanes (1994) used ARC/INFO GIS to generate input parameters for the HEC-1 hydrologic model. Tedious and labor intensive tasks were effectively performed by ARC/INFO, but the outflow hydrographs resulting from the spatially aggregated parameters were not any more accurate than those obtained using traditional methods of runoff simulation. They concluded that the lack of input data cannot be overcome by technological advances.

Garbrecht and Martz (1994) used GIS data to evaluate the grid size dependency of parameters extracted from a digital elevation model (DEM). The drainage properties extracted from the DEM included the critical source area, the number of channel links, the total channel length, the mean channel link slope, and the watershed drainage density. Based on their studies, they stated that the number of channel links, the total channel length, and the drainage density decrease with increasing grid size. They defined a network reference area as the mean area draining directly into channel links, and concluded that a DEM should have a grid area less than 5 percent of the network reference area in order to be able to reproduce important drainage features within an accuracy of approximately 10 percent.

Clearly the transition to a GIS environment presents some challenges. With the advent of this technology, new problems arise. Scientific advancement must be motivated by the desire to understand nature and accurately represent physical processes, not by the desire to create sophisticated graphical images which may not represent reality.

Key points to consider in the transition to a GIS environment relate primarily to scaling issues. In particular, the spatial variability of input parameters such as soil properties should be taken into account and consideration must be given to the overall effects of scale and accuracy on GIS databases. A challenge in adapting models to the GIS environment is to successfully merge data from different sources, different resolutions, different accuracies, and different data structures. The first step in doing so is to determine at what scales geographic data provide enough information for runoff simulations.

2.4 THE CONCEPT OF A WATERSHED TIME TO EQUILIBRIUM

The watershed time to equilibrium (T_e) is a measure of the wave travel time of the most hydraulically remote point in the basin to the outlet of the basin. T_e is representative of the interaction of a storm with the watershed, and is an indication of the basin response time. It is evaluated as a function of storm characteristics, as well as watershed physical and geometrical properties. Woolhiser (1975, 1977) has described in great detail the concept of partial and complete equilibrium hydrograph conditions, using the watershed time to equilibrium as a reference parameter.

The watershed time to equilibrium can be estimated, based on the de St. Venant equations and the Manning resistance equation, as (Woolhiser, 1977):

$$T_e = \left(\frac{nL}{i^{2/3} S^{1/2}} \right)^{3/5} \quad (2.1)$$

where T_e = time to equilibrium

i = rainfall intensity

n = Manning roughness coefficient

S = runoff slope

L = runoff length

The nature of the surface runoff hydrograph, under uniform rainfall conditions, will depend on the rainfall duration (T_r). If $T_r/T_e > 1$, complete equilibrium occurs. Under equilibrium conditions, surface runoff increases linearly with rainfall intensity, warranting the use of linear methods such as the unit hydrograph (UH) and the instantaneous unit hydrograph (IUH). If $T_r/T_e < 1$, the runoff hydrograph is in partial equilibrium. Under partial equilibrium conditions, the relationship between rainfall and peak runoff is non-linear and must be evaluated using non-linear methods. Fig. 2.1 gives examples of complete and partial equilibrium hydrographs.

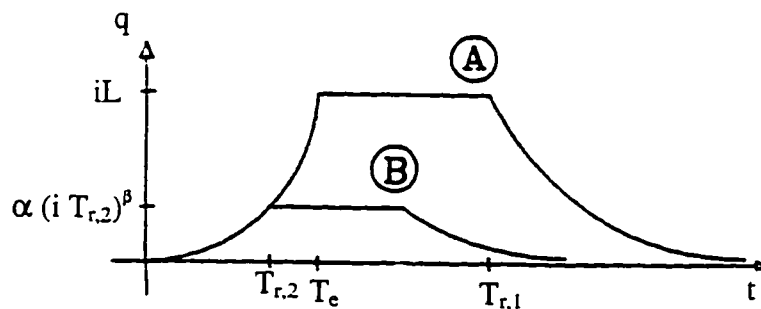


Fig. 2.1: Complete and partial equilibrium hydrographs

In Fig. 2.1, hydrograph A corresponds to complete equilibrium conditions, since the rainfall duration ($T_{r,1}$) is greater than the time to equilibrium (T_e). The peak equilibrium discharge (q) is equal to rainfall intensity (i) multiplied by runoff length (L). Hydrograph B corresponds to partial equilibrium conditions, where the rainfall duration ($T_{r,2}$) is less than T_e . In this case peak discharge (q) is evaluated as a function of rainfall intensity (i), rainfall duration ($T_{r,2}$), and constants alpha (α) and beta (β).

The relationship between T_e , watershed characteristics, and rainfall properties has been analytically derived for well defined simple geometries. Kinematic T_e was derived by Lighthill and Whitham (1955) using the method of characteristics for a rectangular plane sloping in a single direction. Henderson and Wooding (1964) performed similar studies. Agiralioglu (1984, 1988), also using the method of characteristics, derived integral forms of T_e for converging and diverging planes.

Wooding (1965a, 1965b, 1966) derived an analytical solution for a hydraulic model of kinematic flow over a plane V-shaped catchment. Wooding went on to evaluate the relative effects of overland and channel routing on time to equilibrium. He applied uniform rainfall for a finite duration, where the line stream outflow was laterally supplied by overland flow. With channel and overland flow treated separately, he defined λ as the ratio of the stream response time to the catchment response time. Wooding concluded that if λ is large, there is a delay in the arrival time of the flood peak, and a reduction in the peak amplitude. This condition would apply to a large basin. If λ is small, then the stream flow tends to the catchment outflow, as is the case on small basins. Woolhiser and Goodrich (1988) later specified that if λ is greater than 0.5, channel effects dominate runoff, and if λ is less than 0.5, overland flow plane characteristics will dominate.

More recent studies have looked at applying the concept of time to equilibrium to specific watersheds. Sivapalan and Wood (1986) derived quasi-analytical expressions for time to peak and infiltration under conditions of spatially variable soils with a uniform rainfall and constant soil properties with spatially variable rainfall. They concluded that

rainfall is expected to play an important role in rainfall-runoff modeling since the correlation length of rainfall is usually larger than that of soil hydraulic conductivity.

A study by Julien and Moglen (1990) evaluated the effect of spatial variability in slope (S), surface roughness (n), surface length (L), and rainfall intensity (i) on 1-D runoff characteristics. They defined a length scale which delineates similarity conditions for spatially-varied surface runoff. If the runoff length is less than the length scale, the rainfall-runoff relationship is nearly independent of spatial variability in hydrologic parameters. If the runoff length is greater than the length scale, the rainfall-runoff relationship is sensitive to spatial variability. They also found that the time to equilibrium of spatially varied systems is approximately equal to the time to equilibrium of spatially averaged values of hydrologic parameters. The distribution of peak discharges changes drastically as the value of T_r/T_e approaches unity. Variability in peak discharge was found to be most sensitive to rainfall intensity. Julien and Moglen's findings lead them to conclude that it should be possible to analyze extreme events (high intensity, long duration) with larger grids, as long as the grids have a runoff length which is greater than the length scale.

In order to determine the effects of T_r/T_e on runoff events, Ogden (1992) evaluated hydrologic model sensitivity to spatial variability in statistically equivalent rainfall fields. In his analysis of two basins, he concluded that runoff timing and magnitude are directly influenced by rain duration (T_r). Some of his observations include:

- Peak discharge always occurred at times greater than $0.5T_e$,

- The variability in hydrograph timing is larger than the variability in peak discharge for short rainfall events ($T_r/T_e < 0.3$),
- The variability in peak discharge increases and the variability in peak timing decreases when $0.3 < T_r/T_e < 0.6$, and
- When $T_r/T_e > 0.8$, there is very little variability in both peak discharge and time to peak.

Time to equilibrium (T_e) at the outlet is determined by the wave travel time through a flow path originating at the most hydraulically remote point in the watershed. T_e is not to be confused with the time to concentration (T_c), which is the time for the most remote point in the basin to contribute to the outlet runoff. According to studies performed by Saghafian and Julien (1995), the most hydraulically remote point in a watershed is stationary for spatially uniform rainstorms, but may vary for spatially distributed storms. In their analysis of Macks Creek (32.2 km²) using non-uniform rainfall conditions, the furthest distance geometrically was different from the furthest hydraulic point, resulting in a time to equilibrium less than the time to equilibrium corresponding to a uniform storm. Saghafian and Julien also found that infiltration significantly delays runoff when δ/K is large (representing highly pervious conditions), where $\delta = (1-S)\theta_e H_f$, and where S is initial saturation, θ_e is effective porosity, H_f is capillary pressure head, and K is saturated hydraulic conductivity. For pervious conditions, they assumed that the time to equilibrium was a function of t_s (a time associated with infiltration) and the time to equilibrium corresponding to excess rainfall ($i-K$). For highly pervious conditions, t_s was found to approach the ponding time (t_p). For near impervious conditions, t_s was found to be approximately equal to $17\delta/K$. Saghafian and Julien also determined that for small values of λ (as defined by Wooding,

1965a), the grid size used in calculations should be much less than the overland runoff length. Small values of λ correspond to runoff conditions on small basins.

From analytical derivations using simple geometries, to studies on actual watershed basins, conclusions regarding the concept of a time to equilibrium emphasize the effects of spatial variability of watershed characteristics and rainfall properties. Yet the literature lacks formulations which are applicable to large watersheds. The time to equilibrium of natural watersheds is not easily evaluated, due to the complexities of the spatial distribution of topography, surface resistance, soil types, infiltration parameters, rainfall distribution, and a time-varying infiltration process. The results from small scale studies can be used to extend our understanding of a watershed time to equilibrium to mesoscale events on large basins.

2.5 FUTURE NEEDS/TRENDS IN HYDROLOGICAL MODELING

A wide range of conclusions have been made regarding the differences in response between small and large basins, yet there is no underlying theory to explain why these differences take place. The success of hydrologic modeling depends on the accurate prediction of the amount of rainfall which becomes “effective” rainfall, and on the accurate definition of runoff processes from overland regions to the channel outlet. These processes will depend on scale. In the development of watershed models, certain assumptions have been made in order to extrapolate known physical processes to larger scales. Such assumptions include the lumping of homogeneous units, and the application of algorithms and parameters used to define subprocesses at the scale of the homogeneous units. In order to decrease the complexity of models, these assumptions must be accepted as necessary.

A more realistic approach to understanding the differences between small and large basin responses involves the use of dimensionless parameters and similarity concepts. Technical advances in computers and the increasing availability of watershed data now make it possible to simulate a wide range of conditions, both in terms of watershed physical characteristics and rainfall characteristics, and it is now possible to examine the effects of spatial variability in a much more detailed manner. The concept of a watershed time to equilibrium provides a dimensionless approach to evaluating the nature of rainfall-runoff conditions at all scales. This concept can be used in determining scales which will be appropriate for simulations on large watersheds.

Chapter III

MODEL DESCRIPTION

3.1 THE MODEL

CASC2D is a physically based distributed watershed model which simulates the hydrologic response of a watershed, subject to spatially-temporally varied rainfall. The major components of CASC2D are interception, infiltration, and runoff routing. Once interception and infiltration are accounted for, excess rainfall becomes surface runoff. Runoff is then routed as overland flow, based on a 2-D explicit finite difference (FD) technique, or as channel flow, based on an explicit FD technique.

As described by Julien and Saghafian (1991), the model has been formulated using to the de St. Venant equations of continuity and momentum to describe the mechanics of both overland flow and channel flow. Overland flow is generally a two-dimensional process which is controlled by spatial variations in slope, surface roughness, excess rainfall, and other parameters. The diffusive wave approximation is used as a simplified form of the de St. Venant momentum equation. The diffusive wave is selected because it has been found to be applicable in regions of small slope and or high roughness, and for its ability to represent stored water. The continuity and momentum equations are applied by superimposing a grid mesh on the watershed. A numerical solution is evaluated for individual grid cells of width (W). Rainfall intensity, soil

characteristics, and watershed characteristics are assumed constant within each grid element, but can vary from one element to another. Fig. 3.1 illustrates a typical grid mesh used in CASC2D, where W is the grid size. k represents the x-coordinate, and j represents the y-coordinate.

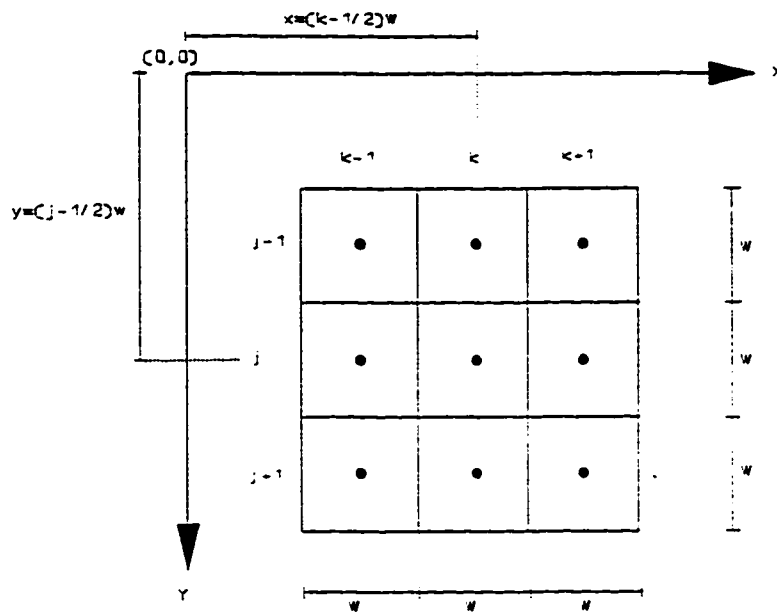


Fig. 3.1: A two dimensional model grid mesh (from Saghaian, 1992)

CASC2D has been incorporated into the GRASS (geographic analysis support system) environment, which supports the grid element structure of the model. The raster-based structure in GRASS accommodates variations in watershed characteristics such as slope, surface roughness, width of the runoff plane, soil characteristics, as well as space and time distribution of rainfall.

3.2 GOVERNING EQUATIONS

3.2.1 Precipitation

Precipitation is determined using either rain gage data or radar data. At each computational time step, a rainfall intensity rate must be estimated for every grid element within the watershed. If gage data is used, an interpolation scheme based on the inverse

distance squared approximates spatial variability of rainfall throughout the watershed based on recorded gage values. If radar data is used, rainfall intensities are specified on a cell by cell basis, based on the resolution of the radar data. Again an interpolation scheme is used if the radar data is not available basin-wide. At each time step, all cells in the basin are assigned a rainfall rate.

3.2.2 Infiltration

Infiltration is evaluated using the Green-Ampt infiltration scheme, requiring input values of soil hydraulic conductivity, capillary pressure, and moisture deficit. A table of Green-Ampt parameters for various soil types is shown in Appendix B (Table B.1). Each grid cell, based on the dominant soil type, is assigned corresponding soil parameters. Once the rainfall intensity has been determined for each grid element, the infiltration rate is calculated as:

$$f^{t+\Delta t} = K_s \left(1 + \frac{H_f M_d}{F^t + \frac{\Delta t}{2} f^{t+\Delta t}} \right) \quad (3.1)$$

where Δt = computational time step

t = time

f = infiltration rate

K_s = hydraulic conductivity at normal saturation (m/s)

H_f = capillary pressure head at the wetting front (m)

M_d = soil moisture deficit

F = total infiltrated depth

For a given time step, either all water infiltrates or a surface depth remains. This surface depth is then routed overland.

3.2.3 Overland flow routing

The spatial variability of watershed characteristics governing overland flow is defined within a raster-based system. Characteristics are assumed homogeneous within a single cell. Flow is routed overland based on the elevation associated with the center of the cell (Fig. 3.2).

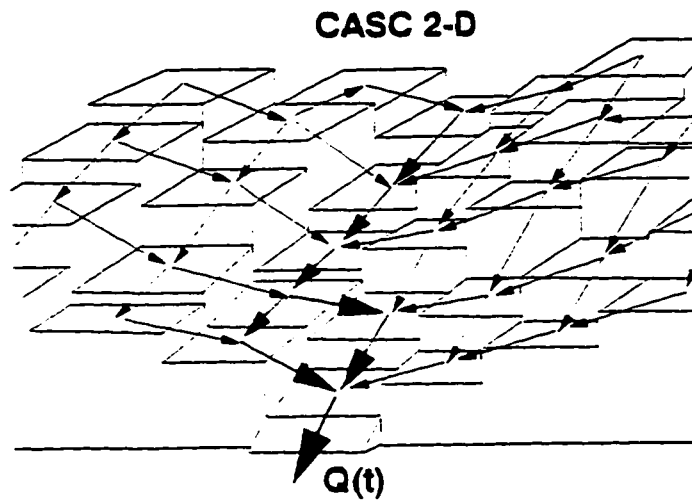


Fig. 3.2: Raster-based description of overland flow routing scheme (from Julien et al., 1995)

The de Saint-Venant equations of continuity and momentum are used in describing mechanics of overland flow. The two-dimensional continuity equation in partial differential form is:

$$\frac{\partial h}{\partial t} + \frac{\partial q_x}{\partial x} + \frac{\partial q_y}{\partial y} = e \quad (3.2)$$

where h = surface depth of flow

q_x = unit flow rate in x-direction

q_y = unit flow rate in y-direction

e = excess rainfall ($i - f$), where i = rainfall intensity and f = infiltration rate

The momentum equation is derived by equating the net forces per unit mass to the acceleration of flow. The differential form of the momentum equation, described for both the x and y directions, is:

$$\frac{\partial u}{\partial t} + u \frac{\partial u}{\partial x} + v \frac{\partial u}{\partial y} = g (S_{ox} - S_{fx} - \frac{\partial h}{\partial x}) \quad (3.3a)$$

$$\frac{\partial v}{\partial t} + u \frac{\partial v}{\partial x} + v \frac{\partial v}{\partial y} = g (S_{oy} - S_{fy} - \frac{\partial h}{\partial y}) \quad (3.3b)$$

where u, v = average velocities in the x and y directions, respectively

S_{ox}, S_{oy} = bed slopes in x and y directions, respectively

S_{fx}, S_{fy} = friction slopes in x and y directions, respectively

g = gravitational acceleration

The left-hand side of Eq. (3.3a) and (3.3b) represent local and convective acceleration terms, while the right-hand side of the momentum equations describe net forces along the x and y directions.

The kinematic wave approximation to the momentum equations has been the basis of many rainfall-runoff models. This approximation assumes that all terms in Eq. (3.3a) and (3.3b), except for the bed and friction slopes, are negligible. Yet the kinematic wave cannot predict backwater effects (Beven, 1985). The diffusive approximation is able to simulate backwater effects, and is considered applicable for overland flow over rough surfaces and for channel flow (Julien and Saghafian, 1991). The momentum equations based on the diffusive wave approximation reduce to:

$$S_{fx} = S_{ox} - \frac{\partial h}{\partial x} \quad (3.4a)$$

$$S_{fy} = S_{oy} - \frac{\partial h}{\partial y} \quad (3.4b)$$

where S_{ox} , S_{oy} = bed slopes in x and y directions, respectively

S_{fx} , S_{fy} = friction slopes in x and y directions, respectively

h = flow depth

In order to evaluate discharge, a general stage-discharge relationship is defined, with α and β representing constants which define the flow regime:

$$q = \alpha h^\beta \quad (3.5)$$

Assuming turbulent flow over a rough boundary, the Manning empirical resistance equation is used and the stage-discharge relationship reduces to:

$$q = \frac{S_f^{1/2}}{n} h^{5/3} \quad (3.6)$$

The differential forms of the continuity and momentum equations are applied to all cells, assuming a finite difference representation of the watershed. Flow is routed overland, from grid cell to grid cell, according to the mass conservation principle. For an incompressible fluid the net amount of mass (volume) entering an element over a short period of time is proportional to the change in mass (volume) within the element. A first order approximation of the continuity equation for element (j,k), at given time t, assuming two-dimensional flow, is applied in evaluating the flow depth such that:

$$h^{t+\Delta t}(j,k) = h^t(j,k) + \bar{e}\Delta t - \left[\frac{q_x^t(k \rightarrow k+1) - q_x^t(k-1 \rightarrow k)}{W} \right] \Delta t - \left[\frac{q_y^t(j \rightarrow j+1) - q_y^t(j-1 \rightarrow j)}{W} \right] \Delta t \quad (3.7)$$

where $h^{t+\Delta t}(j,k)$ = flow depth at element (j,k) at time $t + \Delta t$

$h^t(j,k)$ = flow depth at element (j,k) at time t

Δt = time step duration

\bar{e} = average excess rainfall rate over one time step

$q_x^t(k \rightarrow k+1)$ = unit flow rate in x-direction at time t, between (j,k) and (j,k+1)

$q_x^t(k-1 \rightarrow k)$ = unit flow rate in x-direction at time t, between (j,k-1) and (j,k)

$q_y^t(j \rightarrow j+1)$ = unit flow rate in y-direction at time t, between (j,k) and (j+1,k)

$q_y^t(j-1 \rightarrow j)$ = unit flow rate in y-direction at time t, between (j-1,k) and (j,k)

W = square element size = grid size

At a given time step, the unit flow rate at any grid cell depends on the flow direction, which is determined by the sign of the friction slope. Based on the diffusive wave approximation to the momentum equation, the friction slope in the x and y directions are calculated as:

$$S_{fx}^t(k-1 \rightarrow k) = S_{ox}(k-1 \rightarrow k) - \frac{h^t(j,k) - h^t(j,k-1)}{W} \quad (3.8a)$$

$$S_{fy}^t(j-1 \rightarrow j) = S_{oy}(j-1 \rightarrow j) - \frac{h^t(j,k) - h^t(j-1,k)}{W} \quad (3.8b)$$

Knowing elevation values (E) at every grid cell, the bed slopes are evaluated as:

$$S_{ox}(k-1 \rightarrow k) = \frac{E(j,k) - E(j,k-1)}{W} \quad (3.9a)$$

$$S_{oy}(j-1 \rightarrow j) = \frac{E(j,k) - E(j-1,k)}{W} \quad (3.9b)$$

Once the friction slope (S_f) has been calculated and the flow direction determined, unit discharge is evaluated assuming turbulent flow, which is approximated as:

$$q_x^t(k-1 \rightarrow k) = \frac{1}{n(j,k-1)} \left[h^t(j,k-1) \right]^{5/3} \left[S_{fx}^t(k-1 \rightarrow k) \right]^{1/2} \quad \text{if } S_{fx}^t(k-1 \rightarrow k) \geq 0 \quad (3.10a)$$

$$q_{x^t(k-1 \rightarrow k)} = -\frac{1}{n(j,k)} \left[h^t(j,k) \right]^{5/3} \left[-S_{fx^t(k-1 \rightarrow k)} \right]^{1/2} \text{ if } S_{fx^t(k-1 \rightarrow k)} < 0 \quad (3.10b)$$

The flow rate in the y-direction is calculated in a similar fashion. The above equations are also used to evaluate flow from element (j,k) to element (j+1,k) in the x-direction and to element (j,k+1) in the y-direction. The calculations are performed on all grid cells within the watershed.

3.2.4 Channel flow routing

The channel network is defined as a series of channel links, each of which is divided into a number of channel nodes. One channel node corresponds to a single grid cell. Channel characteristics, including channel width, depth, Manning roughness n, and bed elevation are defined for each channel node (Fig. 3.3).

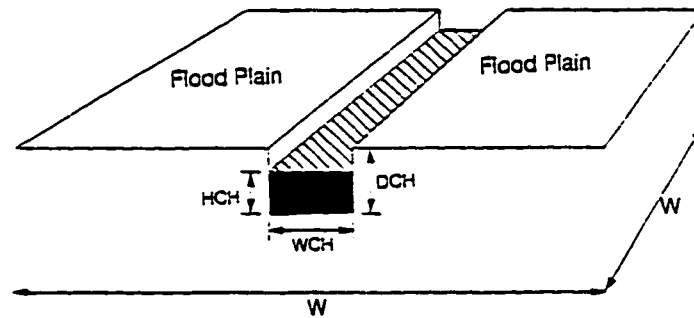


Fig. 3.3: Representation of a channel cell
(from Julien et al., 1995)

When overland runoff reaches a channel cell, a one-dimensional diffusive channel flow equation is used to route the flow. The continuity equation for channel flow, corresponding to a finite channel width, is:

$$\frac{\partial A}{\partial t} + \frac{\partial Q}{\partial x} = q_i \quad (3.11)$$

where A = channel flow cross-section

Q = total discharge in the channel

q_1 = lateral inflow rate per unit length, into or out of the channel

Assuming turbulent flow conditions in the channel, the Manning resistance equation is applicable and channel discharge rates are calculated as:

$$Q = \frac{1}{n} A R^{2/3} S_f^{1/2} \quad (3.12)$$

where n = channel Manning roughness

A = area of channel cross-section

R = hydraulic radius

S_f = friction slope

The equations used in determining friction slope (S_f) on overland cells, based on the diffusive wave approximation to the momentum equation, are used for channel cells as well, with bed slope (S_o) being calculated as a function of bed elevations in the channel network. Channel routing proceeds from the first order links in the upper-most parts of the basin towards the outlet watershed.

3.3 CASC2D SCALING ISSUES

The CASC2D model has been effectively used in simulating runoff events on small watersheds, including Macks Creek (32 km²), and Goodwin Creek (21 km²). Studies have been performed by Ogden (1992), Saghafian (1992), and Johnson (1993), with grid sizes ranging from 150 m to 400 m. Today computers are capable of handling large amounts of data effectively and efficiently, and watershed input data is becoming increasingly available at grid resolutions as fine as 30x30 m. As a result of current data

availability and computer advances, the applicability of the CASC2D model can be extended, increasing the potential for the simulation of rainfall-runoff on large watersheds.

The objective of this research is to examine the possibility of extending the applicability of the model to larger basins, with coarser grid resolutions. All components of the model formulation must be considered in order to evaluate the effects of grid size on CASC2D simulations. Conclusions made with regard to grid size effects and large-scale applicability will depend on assumptions of the model, the physical laws representing hydrological processes, and the numerical schemes incorporated into the model.

Key assumptions of the CASC2D model are as follows:

1. Hortonian surface runoff mechanism;
2. The loss of infiltrated water, which does not re-appear as subsurface runoff;
3. Homogeneity is assumed within a cell, whereby cell characteristics are represented by a single value;
4. Uniform depth and discharge are assumed on individual grid cells.

The model simulates rainfall-runoff in two distinct phases: hydrological processes and hydraulic processes. The parameters governing these processes are summarized in Table 3.1.

In the interest of extending the applicability of CASC2D to larger watersheds, the effects of grid resolution will be evaluated, and appropriate grid sizes for large-scale simulations will be defined. Simulations using coarser grid resolutions require less input data, and computation times are greatly decreased. Yet the spatial heterogeneity which

governs rainfall-runoff processes may be lost if large grid sizes are used. An ideal grid size for simulations on large watersheds will be small enough to accurately represent physical processes governing rainfall-runoff conditions, but large enough to warrant the applicability of the model on watersheds up to 1000 km². With this criterion in mind, the CASC2D model was applied to two basins in Mississippi which drained areas of approximately 21 km² and 560 km². The effects of grid resolution were evaluated using grid sizes ranging from 30x30 m to 1x1 km, with computational time steps ranging from 5 seconds to 30 seconds.

Table 3.1: Processes simulated using CASC2D

	Process	Parameters and unknowns
Hydrological	Rainfall Interception/Depression storage Infiltration	spatial and temporal distribution detention storage (S_d) hydraulic conductivity (K_s) capillary pressure (H_f) moisture deficit (M_d)
Hydraulic	Overland routing Channel routing	slope (S), overland roughness (n_{ol}) slope (S), channel roughness (n_{chan}), channel width, channel depth

Chapter IV

SMALL-SCALE SIMULATIONS

4.1 GOODWIN CREEK INPUT DATA

Goodwin Creek is a 21 km² watershed located in north-western Mississippi. The creek is a tributary of Long Creek, which flows into Yacona River, one of the main rivers in the Yazoo River Basin. The watershed climate is humid. Elevations range from 71 meters to 128 meters above sea level. In overland regions, 50% of the basin has a slope less than 0.02 and 15% of the regions have slopes greater than 0.03. Landuse types are described as cultivated areas (13%) or idle land such as pasture or forest (87%). The dominant soil types are silt loam and fine sandy loam. Channel slopes range from 0.0017 to 0.017, with an average channel slope of 0.004.

Goodwin Creek is an experimental basin monitored by the National Sedimentation Laboratory of the Agricultural Research Service (ARS), located in Oxford, MS. Due to the abundance of data available, engineers at Waterways Experiment Station (WES) in Vicksburg, MS, have used CASC2D to simulate rainfall-runoff events on Goodwin Creek. Over ten years of rainfall and runoff data are available for the watershed. Precipitation measurements have been recorded at 17 raingages located throughout the basin. Discharge, including sediment measurements, has been recorded at

14 flow gaging stations located throughout the drainage network. These raingage and stream gage locations are shown in Fig. 4.1.

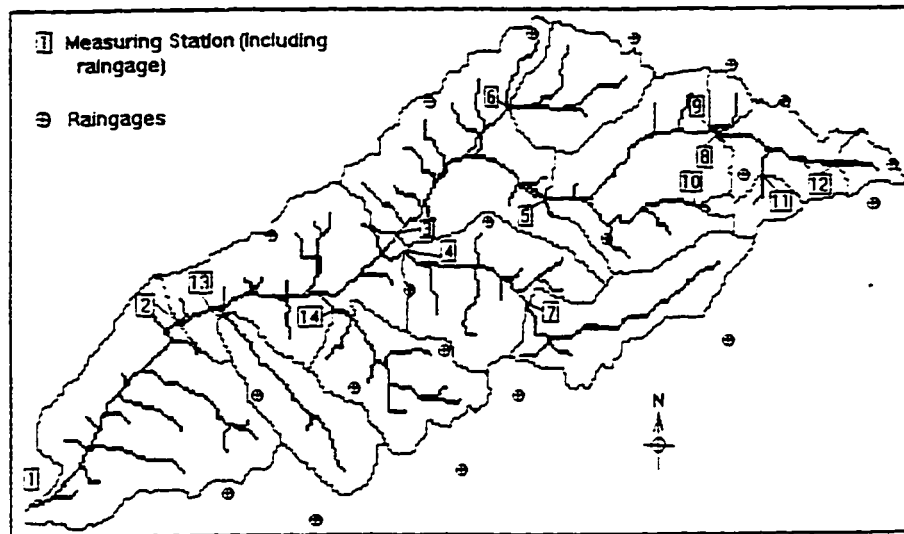


Fig. 4.1: Goodwin Creek basin
(from Blackmarr, 1995)

Input data for runoff simulations on Goodwin Creek were primarily obtained from WES, where CASC2D had been used in a study of rainfall-runoff models (Johnson 1993, Johnson et al. 1993). In Johnson's study, simulations were performed using a 416 ft (127 m) grid size. Since all the input data were available at a 416 ft grid size, this resolution was selected as a starting point for the analysis of grid size effects on CASC2D simulations. Input data in the form of raster maps included a digital elevation map, a soil type map, and a landuse map (see Fig. 4.2a, 4.2b, 4.2c). The soil map was used to determine infiltration parameters corresponding to each soil type. The landuse map was used to determine resistance to flow in overland areas. Channel data for Goodwin Creek included width, depth, and roughness coefficients for individual stream segments (see Appendix B for values).



Fig. 4.2a: Goodwin Creek elevation map at a 416 ft grid size

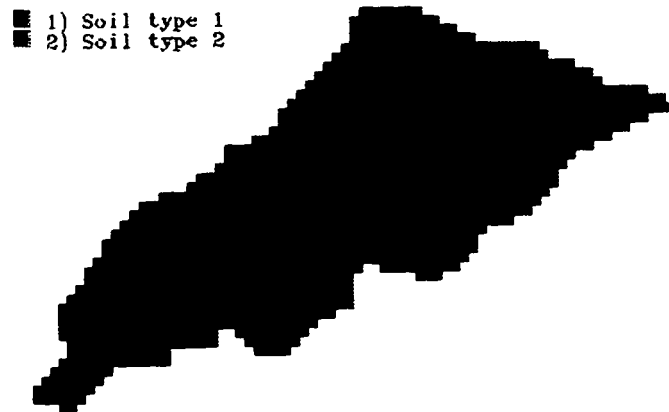


Fig. 4.2b: Goodwin Creek soil map at a 416 ft grid size

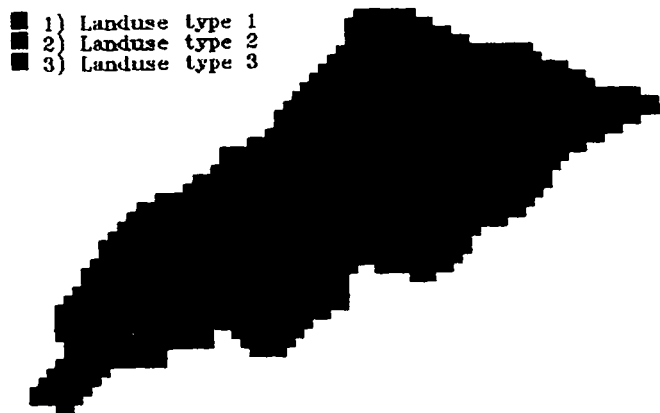


Fig. 4.2a: Goodwin Creek landuse map at a 416 ft grid size

4.1.1 DEFINING GRID RESOLUTIONS

The objective of this research being to look at the effects of increasing grid size on CASC2D simulations, two additional grid resolutions were selected for the analysis. Since the original data was at a 416 ft grid size, grid sizes of 832 ft (254 m) and 1248 ft (380 m) were chosen. Original input data were aggregated in order to develop elevation, soil, and manning roughness raster maps at the larger grid sizes. A simple approach to aggregation was applied, using GRASS (geographical resources analysis support system) capabilities for data manipulation. When a coarser resolution is defined in GRASS, the cell value at the original resolution which is nearest to the center of the larger cell is designated as the value corresponding to the cell at the coarser resolution (see Appendix D for details, *g.region* program).

In addition to the aggregation of raster map data, the channel network was defined at the larger resolutions, based on its original location. Channel slopes were known for individual links throughout the network. All channel properties, include channel slope, were preserved at the coarser resolutions.

Data aggregation to larger grid sizes affected the representation of certain watershed characteristics. The GRASS platform was used to evaluate the effects of increasing grid size on the representation of basin area, the number of channel cells, the number of overland cells, and drainage density. These characteristics are summarized in Table 4.1, for the three resolutions used in the analysis. The total number of grid cells is reduced from 1290 cells at a 416 ft grid size to 140 cells at a 1248 ft grid size. This represents a decrease in the required amount of computation time for CASC2D simulations. The drainage density, evaluated as the ratio of the total channel length to the

drainage area, drops from 1.3 km^{-1} at a 416 ft grid size to 1.15 km^{-1} at a 1248 ft grid size. This change in the representation of the channel network will have an impact on the relative contributions of overland flow and channel routing in rainfall-runoff simulations. The ratio of the number of channel cells to the total number of cells also increases as grid size increases. The implication of this change, in terms of the CASC2D formulation, is that at a 416 ft grid size overland flow is converted to channel flow on 16.4 percent of the total area. At a 1248 ft grid size, overland flow is converted to channel flow on 43.6 percent of the area. Once water reaches the channel, it is routed directly towards the outlet. Consequently, the increased ratio of channel cells to total cells leads to a more significant effect of channel routing at increasing grid size.

Table 4.1: Goodwin Creek watershed characteristics at increasing grid size

	416 ft (127 m)	832 ft (254 m)	1248 ft (380 m)
Drainage area [km^2]	20.74	20.71	20.26
Total number of grid cells	1290	322	140
Number of channel cells	212	101	61
Ratio of channel cells to total cells [%]	16.4	31.4	43.6
Ratio of overland cells to total cells [%]	83.6	68.6	56.4
Total length of channel [km]	26.88	25.36	23.20
Drainage density [km^{-1}]	1.30	1.24	1.15

The analysis of topographic maps corresponding to increasing grid sizes shows that upland slopes decrease as grid size is increased (Fig. 4.3). As a result of data aggregation at larger grid sizes, elevation information is lost. These changes will also have an impact on upland runoff rates, which are evaluated as a function of friction slope (S_f), and where friction slope is related to bed slope (S_o) through the momentum equation (see Eq. 3.8a, 3.8b, 3.10a, and 3.10b).

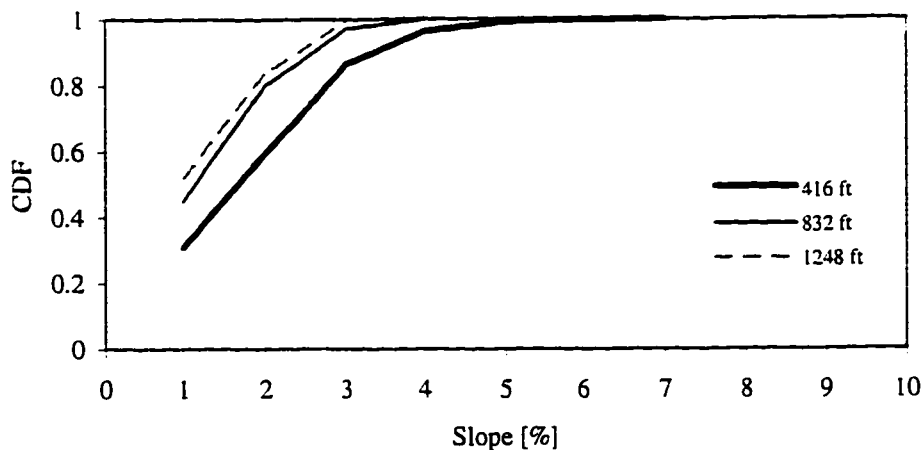


Fig. 4.3: Slope in upland areas as a function of grid resolution

As reflected by the decrease in drainage density corresponding to coarser resolutions, the total length of the channel network is shortened. The channel network at increasing grid size is shown in Fig. 4.4. For modeling purposes, the network has been divided into 19 links. Each link is assigned a specific width, depth, and roughness coefficient. Stream gages are located on sub-basins throughout the channel network. Gage locations for sub-basin discharge measurements are shown in Fig. 4.4 at the 416 ft grid size. Discharge conditions in the channel network are a function of bed slope. In order to reduce the effects of grid size on rainfall-runoff simulations, bed elevations have been defined such that channel slopes are constant at all three grid resolutions.

4.1.2 RAINFALL-RUNOFF EVENTS

Over 10 years of rainfall and runoff data are available for Goodwin Creek. Rainfall data includes precipitation measurements at 17 rain gages, at one minute intervals during high intensity rainstorms. Runoff data is available for 14 stream gages located throughout the network. Based on previous simulation studies done on Goodwin Creek (Johnson, 1993), four rainfall-runoff events were selected for the calibration and validation of the CASC2D model (for more information, see Appendix B, Table B.3).

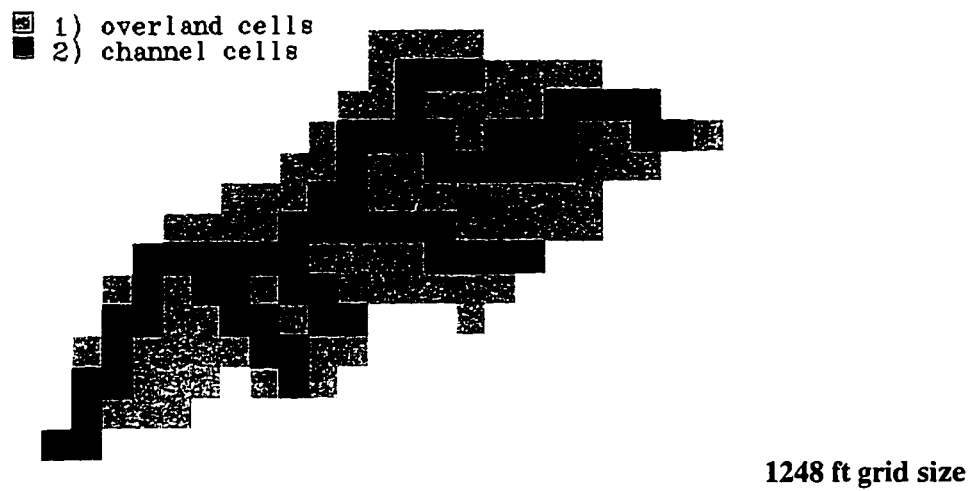
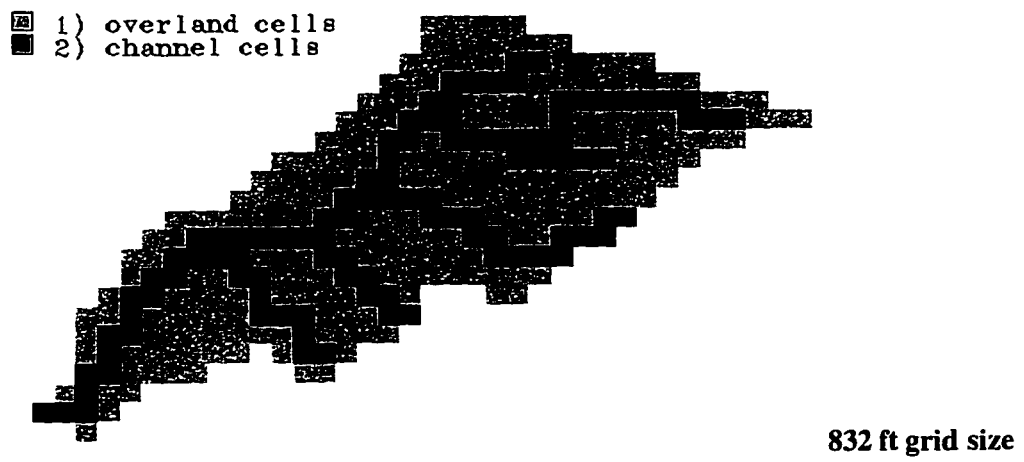
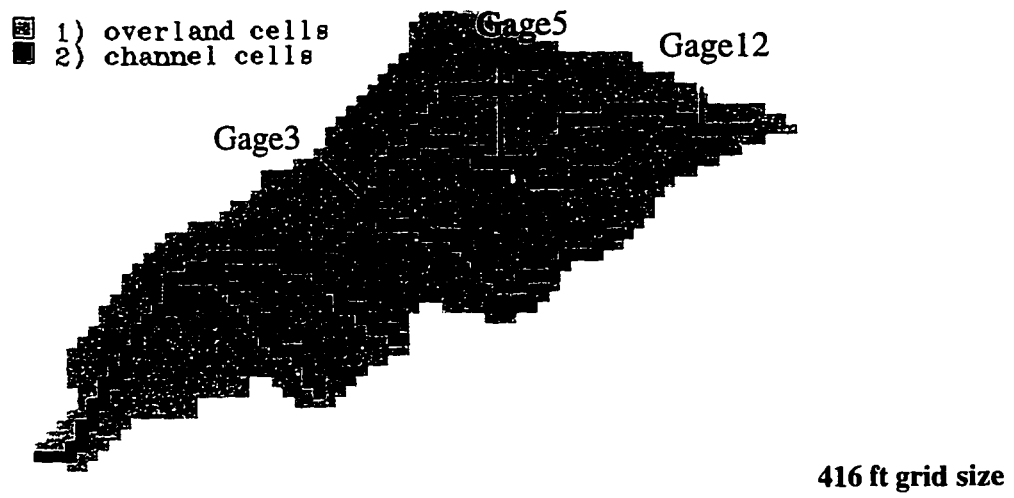


Fig. 4.4: Goodwin Creek at increasing grid sizes

Conditions for the four events are summarized in Table 4.2. Events 1, 2, and 3 lasted approximately 3.5 hr, 6 hr, and 7 hr respectively. Event 4 lasted over 24 hr. The largest volume of rainfall fell during event 4, and the smallest volume of rainfall fell during event 2. The average rainfall rate was calculated as the total rainfall volume divided by the duration of the storm, and corresponded very closely to the mean value of the instantaneous rainfall rates measured throughout the basin. A final distinction between the events was that event 1 was preceded by very little rainfall, while the other three events were preceded by significant amounts of rainfall.

Table 4.2: Rainfall-runoff conditions for rainfall events

	Rainfall duration	Rainfall preceding event	Average rainfall rate	Rainfall volume
Event 1	211 min	very little	0.811 in/hr (5.72E-6 m/s)	1,503,472 m ³
Event 2	361 min	significant amount	0.224 in/hr (1.58E-6 m/s)	711,970 m ³
Event 3	407 min	significant amount	0.340 in/hr (2.40E-6 m/s)	1,213,651 m ³
Event 4	1,869 min	significant amount	0.186 in/hr (1.31E-6 m/s)	2,865,181 m ³

Observed rain gage data from 17 rain gages was used in defining the temporal and spatial variability rainfall rates corresponding to each event (see location of gages in Fig. 4.1). The temporal variability of rainfall corresponding to measured precipitation at rain gage 1, which is located at the outlet, is shown in Fig. 4.5. At each time step, rainfall rates on individual grid cells throughout the basin were determined by interpolation, using the inverse distance squared method. The spatial variability of average and maximum rainfall rates throughout the basin is presented in Appendix B, Fig. B.2 and Fig. B.3.

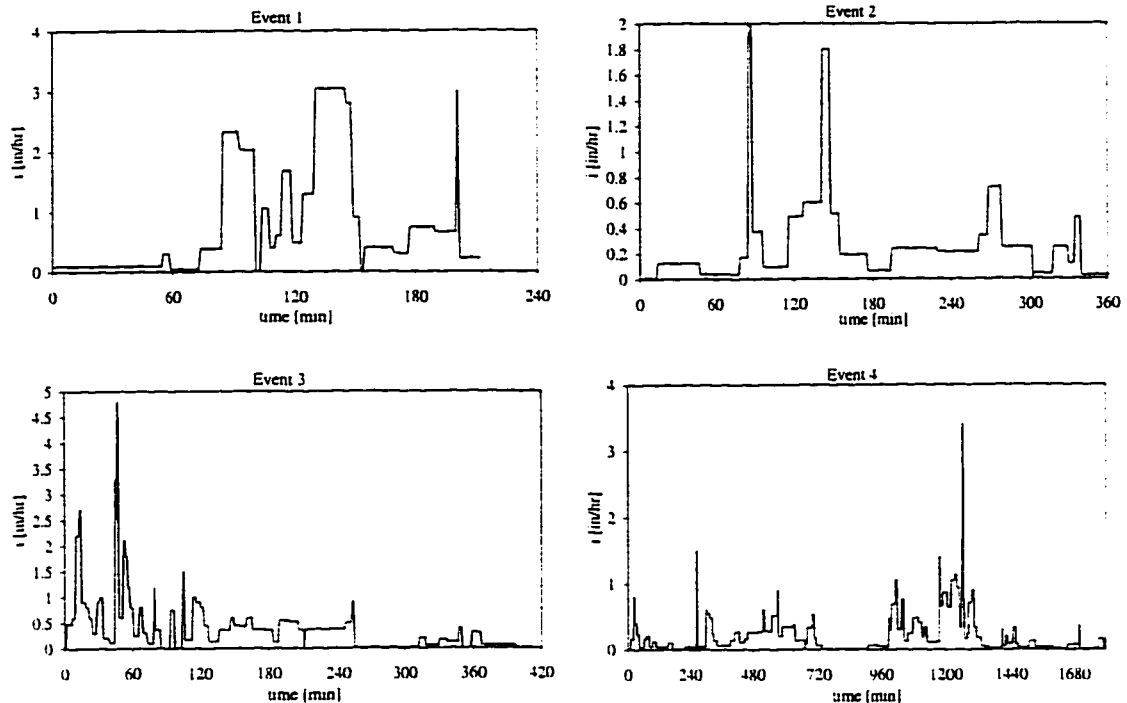


Fig. 4.5: Rainfall rates recorded at rain gage 1, located at the outlet

4.2 MODEL CALIBRATION AND VALIDATION

The CASC2D model was calibrated using events 1 and 2. The model is formulated using an explicit channel routing scheme, requiring that initial discharge in the channel be considered equal to zero. Once a simulation has been performed, baseflow can be added to the simulated runoff hydrograph, for comparison with the observed hydrograph. In simulating conditions on Goodwin Creek, the baseflow of less than 0.1 m^3/s at the outlet was considered negligible, as compared to measured peak runoff rates ranging between 30 m^3/s and 100 m^3/s (see Fig. B.1 in Appendix B).

Two approaches to calibrating were used. In both cases the criteria for calibration was to simulate observed values of peak discharge and time to peak. The volume of runoff was not considered in the calibration procedure.

The objective of the first calibration approach was to fit the simulated outlet hydrograph to the observed outlet hydrograph. Calibration was performed at each of the three cell resolutions: 416 ft, 832 ft, and 1248 ft. A comparison of the calibrated parameters at increasing grid sizes shows the effects of grid resolution on CASC2D simulations for basins on the order of 20 km². A comparison of discharge hydrographs for sub-basin areas, generated using parameters calibrated for the outlet, shows grid effects at the sub-basin level, where rainfall-runoff processes on upland areas play a significant role in defining the nature of the hydrograph.

The objective of the second calibration approach was to fit simulated to observed hydrographs at sub-basin gages. Calibration was performed by evaluating the sensitivity of runoff hydrographs at the sub-basin level to the model parameters. Using a 416 ft grid size, the parameters to which runoff was most sensitive were adjusted so as to simulate the peak discharge and time to peak at individual gages. These parameters were then applied at the larger grid sizes. A comparison of the runoff hydrographs corresponding to sub-basin gages shows the effects of grid resolution on the simulated runoff response of overland cells.

The model has been formulated using six parameters: S_d , K_s , H_f , M_d , n_{ol} , and n_{chan} . All parameters are directly related to physical processes governing rainfall-runoff generation. Detention storage (S_d) represents water which accumulates before overland runoff occurs, such as water retained by leaves or in depressions. Infiltration rates are determined by soil characteristics such as hydraulic conductivity (K_s), capillary pressure (H_f), and initial soil moisture deficit (M_d). Since two soil types exist in the basin (see Fig. 4.2b), soil parameters are defined for each of the soil types. Overland discharge rates are

evaluated as a function of the overland Manning roughness coefficient (n_{ol}). Three roughness coefficients were used to describe runoff conditions in upland areas, based on the landuse map (Fig. 4.2c). Runoff rates in the channel network are evaluated as a function of the channel roughness coefficient (n_{chan}).

4.2.1 CALIBRATING TO OUTLET CONDITIONS

The model was first calibrated using event 1, described in Table 4.2. The rainfall started at 9:19 PM on October 17th, 1981, lasting 3.5 hr. Precipitation measurements were available at all 17 rain gages. The event had an average rainfall intensity of 0.811 in/hr (20.6 mm/hr), with instantaneous measurements ranging up to 6.2 in/hr (157 mm/hr).

The criteria for model calibration was to simulate peak magnitude and time to peak. In order to calibrate the model, input parameters were varied at each grid resolution in order to obtain the best possible fit between simulated and observed outlet hydrographs. Numerous trial simulations were performed using the 416 ft, 832 ft, and 1248 ft grid sizes. Some of the hydrographs simulated as a result of calibration runs using a 416 ft grid size are shown in Fig. 4.6. More detailed results from all the trial calibration runs for 416 ft, 832 ft, and 1248 ft grid sizes are presented in Appendix C (Table C.1, C.2, C.3 and Fig. C.1, C.2, C.3).

As seen in Fig. 4.6, trial 1 resulted in the best fit, where best fit was defined as the simulated hydrograph which approximated as closely as possible first the magnitude of the peak discharge, then the time to peak. The variations in parameter inputs for trials 4, 6, 7, and 8 are summarized in Table 4.3, where the value (Δ) shown is evaluated as:

$$\Delta = \frac{(\text{value}_{\text{trial}} - \text{value}_{\text{trial 1}})}{\text{value}_{\text{trial 1}}} \quad (4.1)$$

where $\text{value}_{\text{trial}}$ = parameter value used in trial 4, trial 6, trial 7 or trial 8

$\text{value}_{\text{trial 1}}$ = parameter value used in trial 1

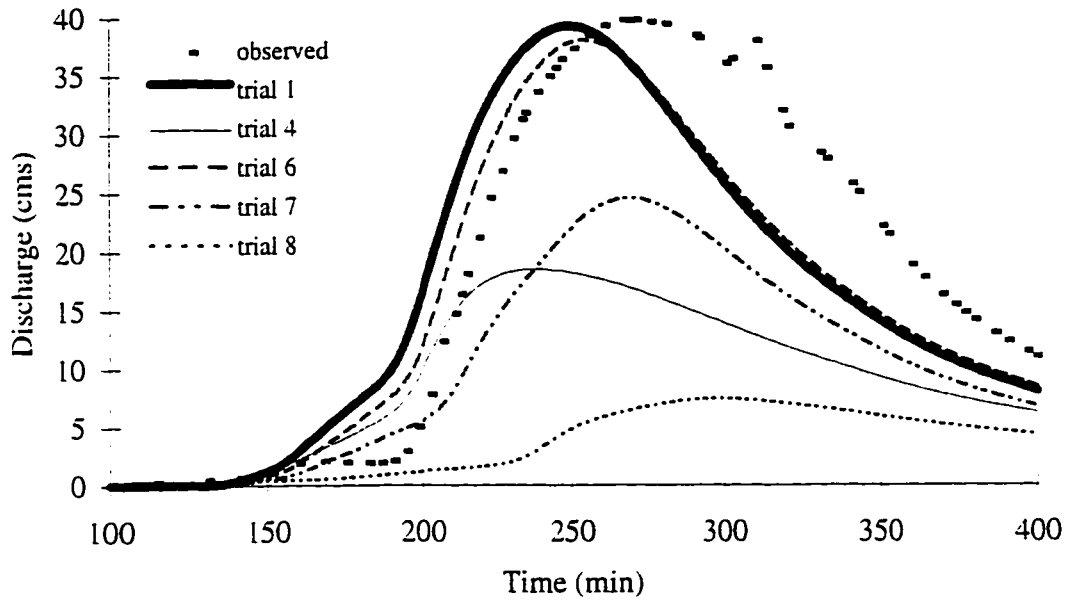


Fig. 4.6: Sample calibration results

Table 4.3: Variations in parameters calibrated for outlet conditions

	trial 4	trial 6	trial 7	trial 8
	Δ	Δ	Δ	Δ
S_d		0.333		
n_{ol} type1	61.5			11.5
n_{ol} type2	2.75			5.25
n_{ol} type3	0.875			5.25
K_s soil 1			0.392	0.392
K_s soil 2			0.377	0.377
H_f soil 1			0.043	0.043
H_f soil 2			0.376	0.376
M_d soil 1	-0.875	-0.5		
M_d soil 1	-0.875	-0.5		

With reference to Fig. 4.6 and Table 4.3, the magnitude of peak discharge was greatly reduced by increasing overland roughness coefficients (n_{ol}), as seen in trials 4 and

8. Peak discharge was also decreased by reducing moisture deficit (M_d) or by increasing capillary pressure head (H_f), as seen in trials 4, 7, and 8. The timing of peak discharge was influenced by an increase in (H_f), seen in trials 7 and 8. Trial 6 resulted in similar results to trial 1, indicating that detention storage parameter (S_d) and moisture deficit parameter (M_d) counter-act each other.

A comparison of Q_p/Q_{obs} and T_p/T_{obs} for the trial simulations, at increasing grid size, (see Appendix C, Fig. C.4) showed the effects of grid size on model output. For all trial simulations, using a 416 ft grid size, Q_p was very sensitive to parameter changes ($0.2 < Q_p/Q_{obs} < 1$), while T_p was not sensitive to changes ($T_p/T_{obs} \equiv 1$). Using a 832 ft grid size, similar parameter changes showed greater sensitivity for Q_p ($0.4 < Q_p/Q_{obs} < 1$), than for T_p ($0.8 < T_p/T_{obs} < 1$). Using a 1248 ft grid size, Q_p was sensitive to parameter changes ($0.6 < Q_p/Q_{obs} < 1.4$), while T_p fluctuated very little ($0.7 < T_p/T_{obs} < 0.9$). The net effect of increasing grid size was increase peak discharge ($Q_p > Q_{obs}$) and decrease the time to peak ($T_p > T_{obs}$).

The parameters selected as a result of calibration to event 1, resulting in the best fit of simulated to observed outlet discharge at all three resolutions, are summarized in Table 4.4. As seen in the table, the parameters affected by increasing grid size were overland roughness (n_{ol}), channel roughness (n_{chan}), moisture deficit (M_d), and capillary pressure (H_f). The most significant changes were made to the overland roughness coefficients, which were increased from 0.08 to 0.15 as grid size increased.

Table 4.4: Model parameters determined as a result of calibration run 1

	416 ft (127 m)	832 ft (254 m)	1248 ft (380 m)
Overland detention storage S_d (m)	0.015	0.015	0.015
Overland roughness n_{oi}	0.08	0.09	0.15
Soil type 1: K_s (m/s)	1.30E-06	1.30E-06	1.30E-06
Soil type 1: H_f (m)	0.16	0.16	0.1668
Soil type 1: M_d	0.08	0.1	0.1
Soil type 2: K_s (m/s)	2.20E-06	2.20E-06	2.50E-06
Soil type 2: H_f (m)	0.08	0.08	0.080
Soil type 2: M_d	0.08	0.1	0.1
Channel roughness n_{ch}	0.037	0.037	0.04

A comparison of simulated hydrographs at increasing grid sizes is presented in Fig. 4.7.

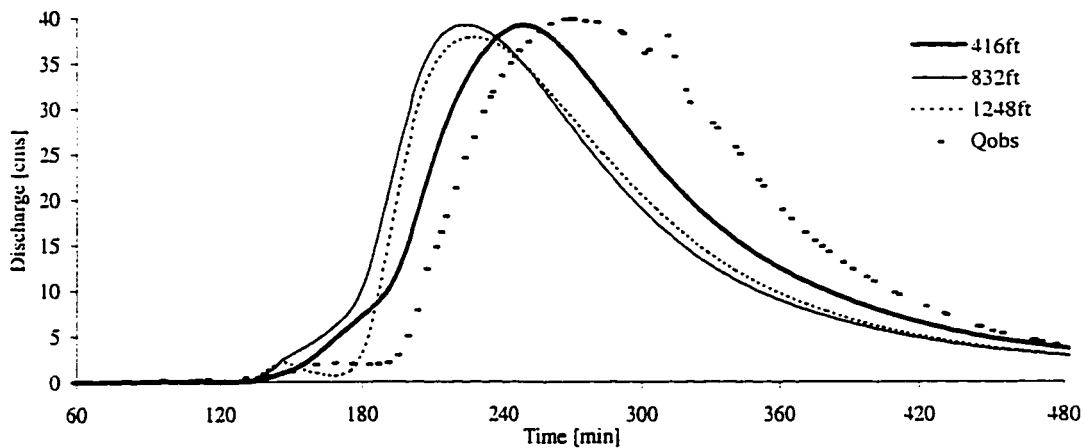
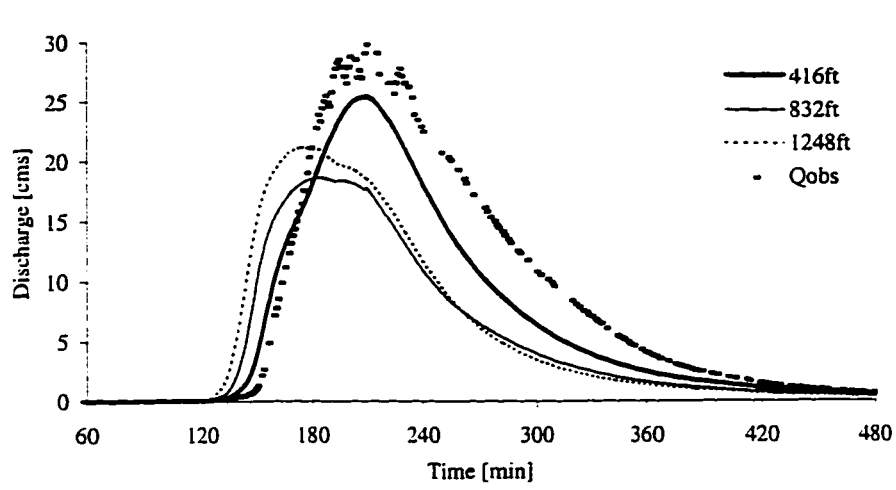
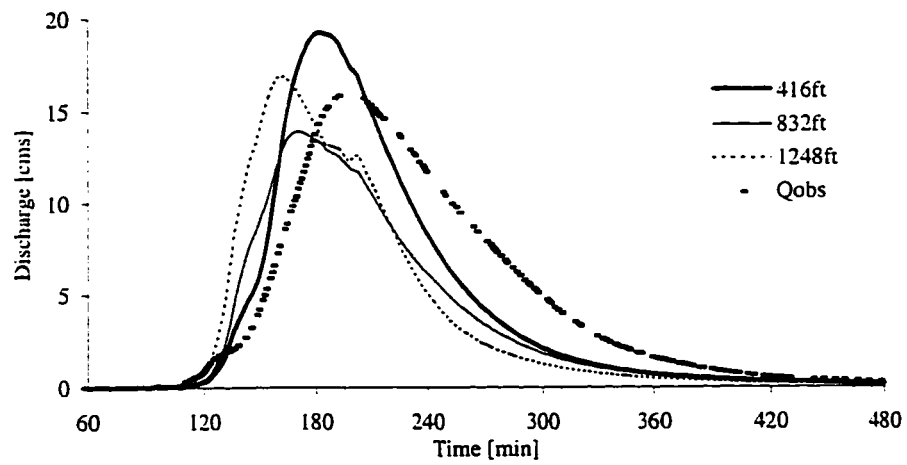


Fig. 4.7: Simulated outlet hydrograph for event 1

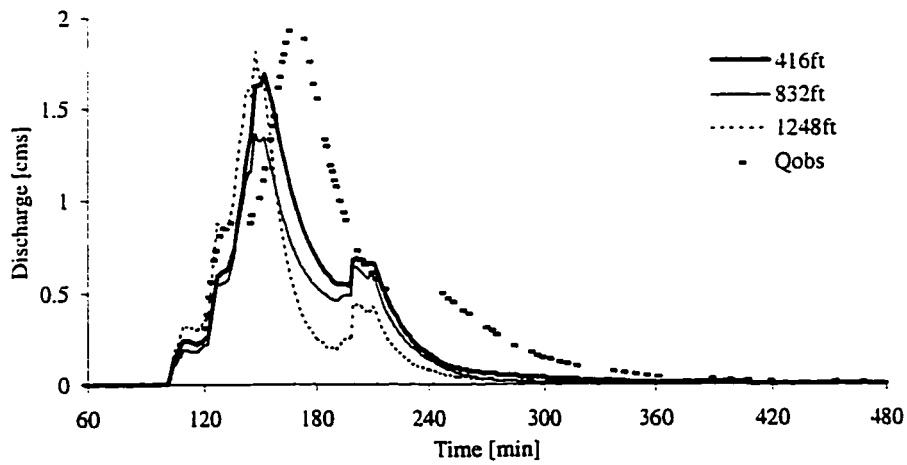
Having calibrated the model to outlet conditions, the simulated sub-basin hydrographs were evaluated for comparison with observed hydrographs. Gages 3, 5, and 12 were selected, with drainage areas of 8.78 km², 4.30 km², and 0.30 km² respectively. As one proceeds upstream from gage 3 to gage 12, channel routing is expected to play less of a role, while upland processes are expected to become more important. Simulated and observed hydrographs are shown in Fig. 4.8. At all resolutions, simulated sub-basin hydrographs repeatedly have low runoff rates and early times to peak. At gage 12, where peak discharge was only 2 m³/s, the results at the three resolutions are very similar.



Gage 3



Gage 5



Gage 12

Fig. 4.8: Simulated sub-basin hydrographs for event 1

CASC2D is a single event model. In the course of model calibration, it was found that the moisture deficit and overland detention storage parameters are closely related to rainfall conditions prior to the event. When soil is saturated, overland runoff occurs much more rapidly, particularly when events have high rainfall intensities. Of the four events chosen for the analysis, there were two different antecedent moisture conditions.

For events preceded by large amounts of rainfall, calibration was again performed this time using event 2. The calibrated parameters for event 1 were modified so as to take into consideration high antecedent moisture conditions. This required changing the infiltration parameters and overland detention storage. Table 4.5 summarizes the parameters determined as a result of calibration using event 2.

The soil parameters and the detention storage were not affected by increasing grid size. The overland roughness coefficients and channel roughness were the same as those calibrated for event 1. The simulated and observed outlet hydrographs are plotted in Fig. 4.9. All three resolutions reproduce the observed peak discharge to within 10% and the time to peak to within 30 min.

Table 4.5: Model parameters determined as a result of calibration run 2

	416 ft (127 m)	832 ft (254 m)	1248 ft (380 m)
Overland detention storage S_d (m)	0.00	0.00	0.00
Overland roughness n_{ol}	0.08	0.09	0.15
Soil type 1: K_s (m/s)	1.00E-07	1.00E-07	1.00E-07
Soil type 1: H_f (m)	0.01	0.01	0.01
Soil type 1: M_d	0.0	0.0	0.0
Soil type 2: K_s (m/s)	1.50E-07	1.50E-07	1.50E-07
Soil type 2: H_f (m)	0.01	0.01	0.01
Soil type 2: M_d	0.0	0.0	0.0
Channel roughness n_{ch}	0.037	0.037	0.04

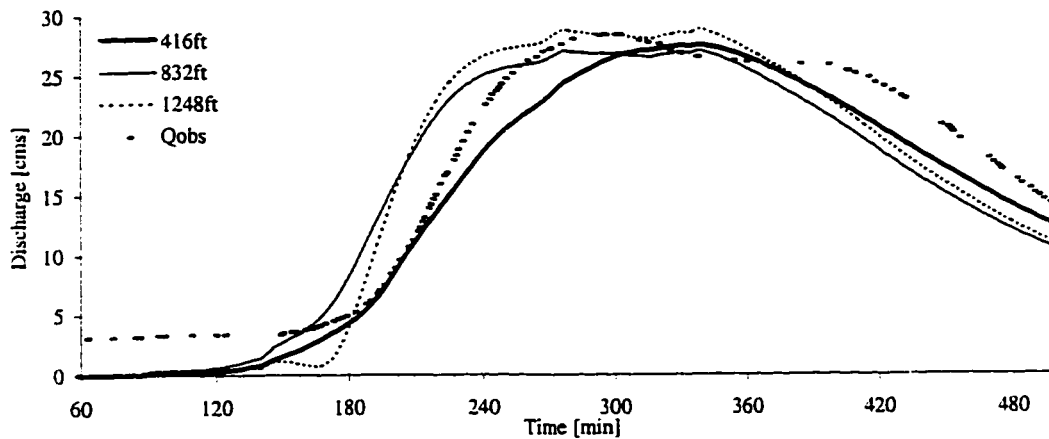
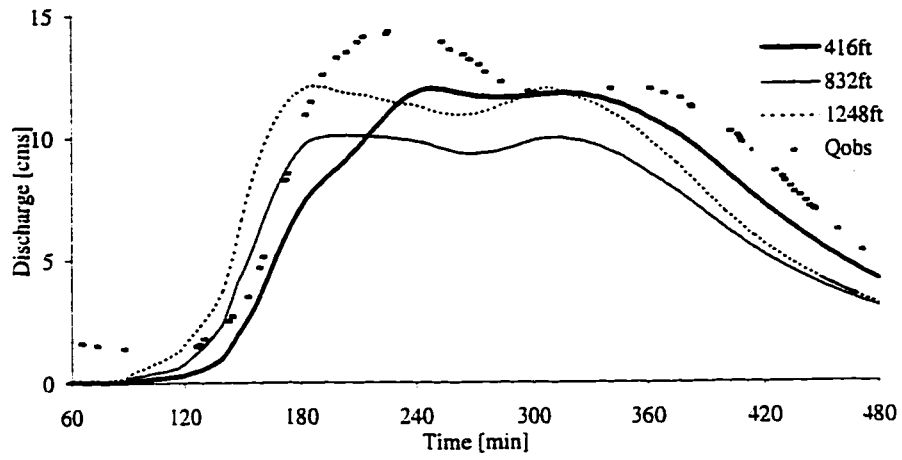


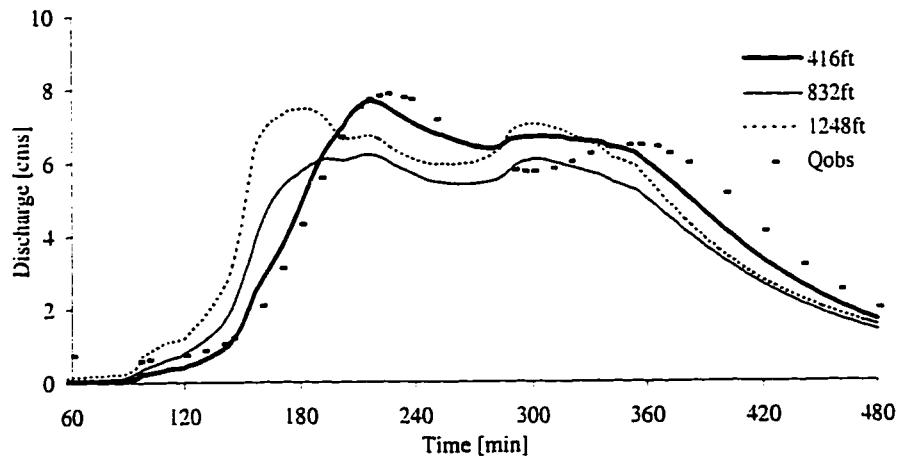
Fig. 4.9: Simulated outlet discharge for event 2

Sub-basin hydrographs were simulated for gages 3, 5, and 12, with drainage areas of 8.78 km², 4.30 km², and 0.30 km² respectively. The hydrographs are shown in Fig. 4.10. The three resolutions show similar results at the sub-basin level: simulated peak discharge is always lower than the observed value, and the time to peak is almost always early.

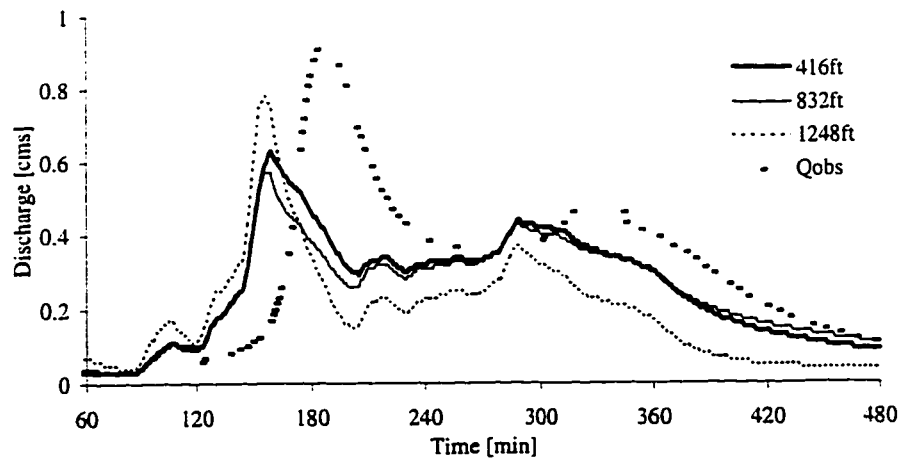
The results from the calibration runs for events 1 and 2 show that the CASC2D model is capable of accurately simulating observed peak discharge and time to peak at the outlet, using grid sizes ranging from 416 ft to 1248 ft, as long as the model is calibrated independently at each grid size. The primary effect of increasing grid size is to require an increase in the overland and channel roughness coefficients, as shown in Tables 4.4 and 4.5. This increase is related to the representation of characteristics influencing overland and channel flow. When initial soil moisture was high, the soil and detention storage parameters were the same regardless of grid size (see Table 4.5), indicating that the use of coarser grid resolutions will have less of an effect under such conditions.



Gage 3



Gage 5



Gage 12

Fig. 4.10: Simulated sub-basin hydrographs for event 2

4.2.2 CALIBRATING TO SUB-BASIN CONDITIONS

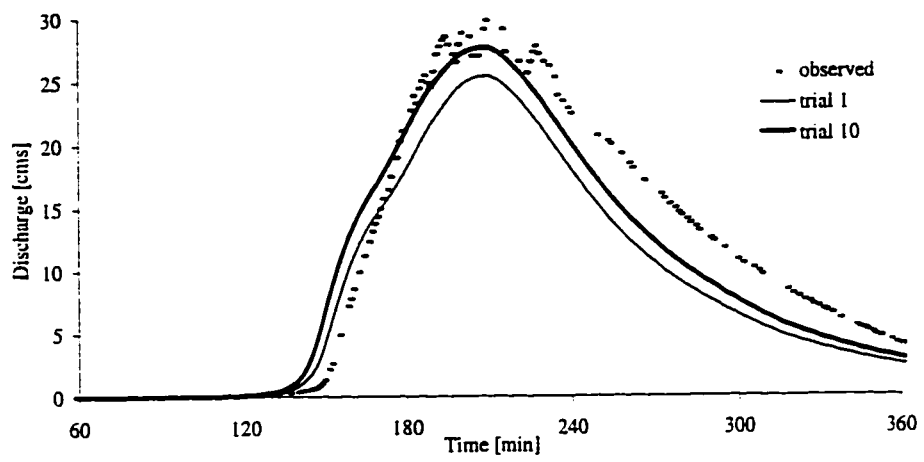
The simulation of sub-basin hydrographs using parameters calibrated to outlet conditions consistently led to low peak runoff rates and early times to peak, as seen in Fig. 4.8 and 4.10. A closer look at the role of changing parameters at the sub-basin level provides additional information on the effects of grid resolution on CASC2D simulations. Consequently, the model was calibrated for each of three sub-basin gages, in order to obtain the best possible fit between simulated and observed peak discharge and time to peak. Using a 416 ft grid size, parameters were calibrated for event 1, then for event 2.

Parameters from the calibration of event 1 to outlet conditions (see Table 4.4) were used as reference values, as trial 1. These parameters were then changed in trial simulations (see Appendix B, Table C.4). The simulated hydrographs are presented in Fig. 4.11.

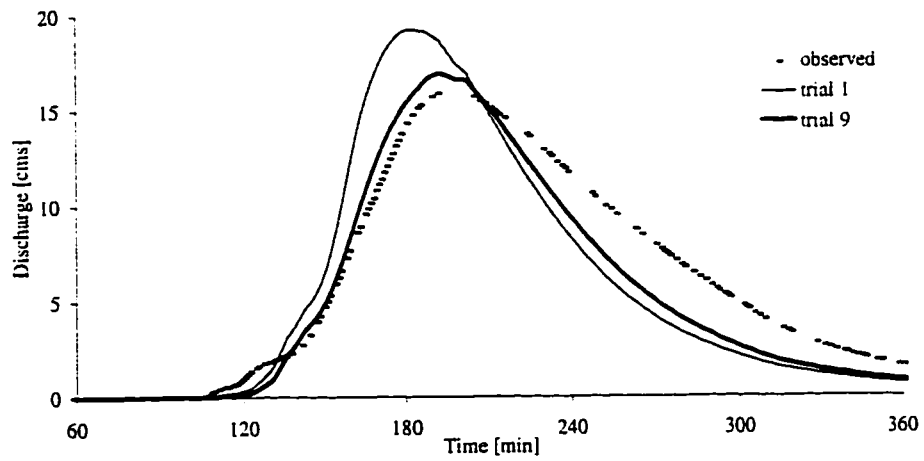
The required parameter changes are summarized in Table 4.6, where the value shown (Δ) represents a variation as compared to the parameter value evaluated as a result of calibration to outlet conditions (see Section 4.2.1 for details). According to the table, the simulation of runoff conditions at all three sub-basin gages required decreasing the moisture deficit parameter (M_d) by up to 75%, and increasing the overland roughness coefficient (n_{ol}) as much as 25%.

Table 4.6: Variations in parameters in sub-basin calibration of event 1

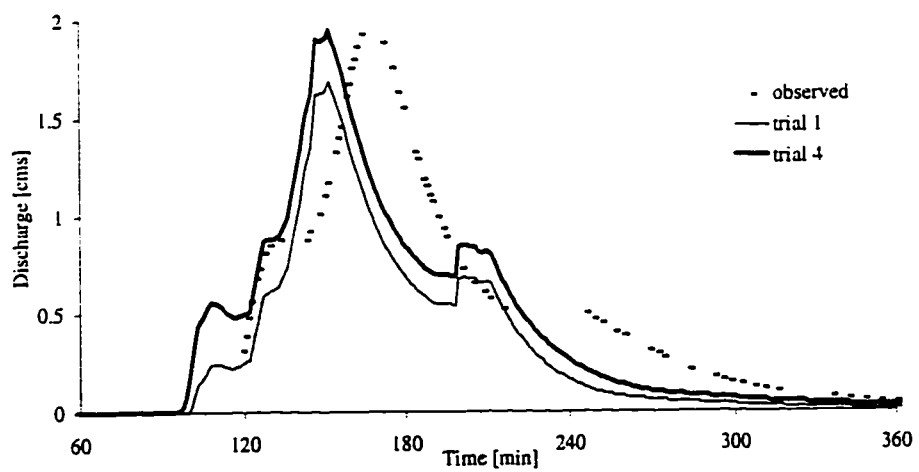
	gage 12	gage 5	gage 3
	Δ	Δ	Δ
S_d		0.333	
n_{ol} type1		0.25	0.25
n_{ol} type2		0.25	0.25
n_{ol} type3		0.25	0.25
M_d soil 1	-0.75	-0.5	-0.5
M_d soil 1	-0.75	-0.5	-0.5



Gage 3



Gage 5



Gage 12

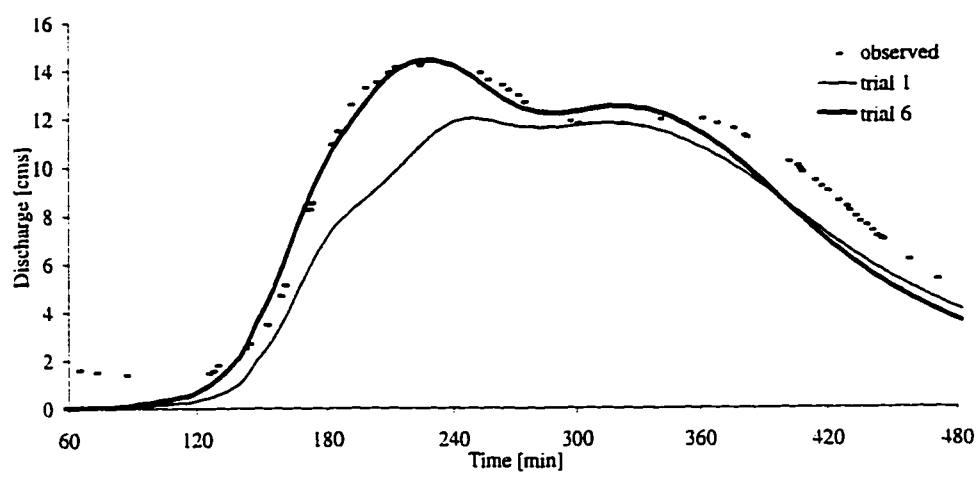
Fig. 4.11: Calibrating to sub-basin conditions, event 1

Trial simulations were also performed using the 832 ft and the 1248 ft grid size. The calibrated parameters resulting in the best fit at a 416 ft grid size were used in simulating runoff at gage 3, 5, and 12. A comparison of the simulated hydrographs at the three resolutions is presented in Appendix C, Fig. C.6. The parameters corresponding to a 416 ft grid size do not produce good results at gages 3 and 5, but at gage 12 the simulated hydrograph is hardly affected by grid resolution.

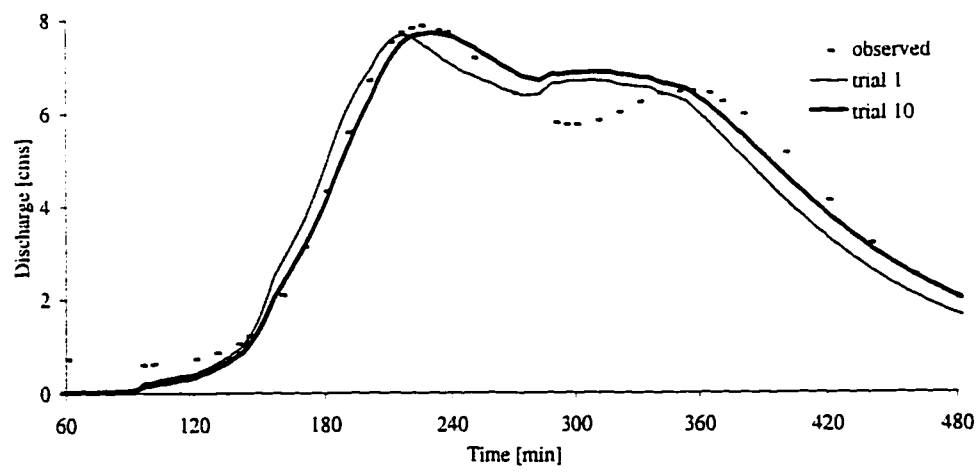
The same procedure used in calibrating to event 1 for sub-basin conditions was repeated for event 2. The simulated best-fit hydrographs are presented in Fig. 4.12, along with the simulated hydrographs using calibrated parameters for outlet conditions (trial 1). The calibrated parameters defined in simulating outlet conditions were used as reference values (see Table 4.5 for values). A number of trial simulations were performed (see Appendix C, Table C.5). The changes required in parameter values are summarized in Table 4.7, where Δ represents a variation from the value used in trial 1 (Section 4.2.1 for details). The simulation of runoff at gages 3 and 12 required decreasing the overland roughness coefficient (n_{oi}) and the hydraulic conductivity (K_s) by 50%, while at gage 5 the parameter values for n_{oi} , K_s , and H_f were all decreased.

Table 4.7: Variations in parameters in sub-basin calibration of event 2

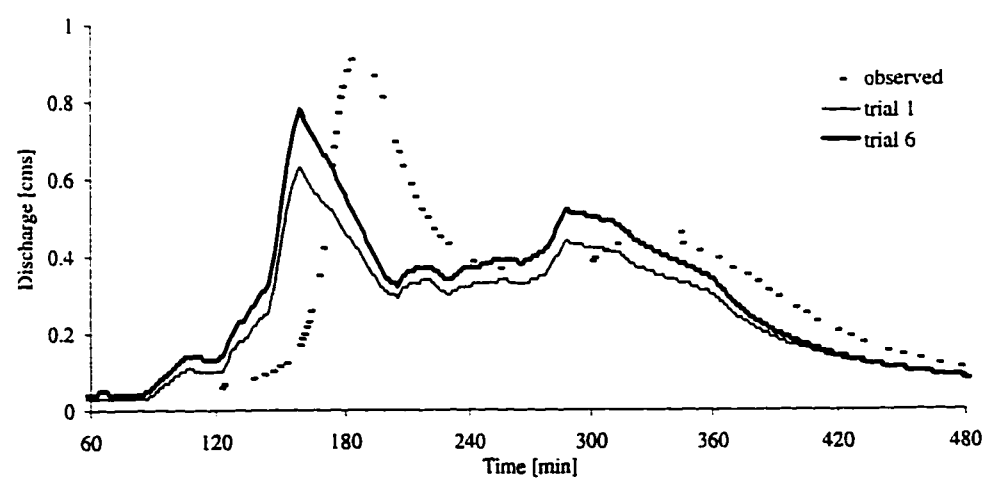
	gage 3 and 12	gage 5
	Δ	Δ
n_{ch}		0.6216
n_{oi} type1	-0.5	-0.25
n_{oi} type2	-0.5	-0.25
n_{oi} type3	-0.5	-0.25
K_s soil 1	-0.5	-0.5
K_s soil 2	-0.533	-0.533
H_f soil 1		-0.9
H_f soil 2		-0.9



Gage 3



Gage 5



Gage 12

Fig. 4.12: Calibrating to sub-basin conditions, event 2

The sub-basin calibrated parameters resulting in the best fit at the 416 ft grid size were applied at the 832 ft and 1248 ft grid sizes (see Appendix C, Fig. C.8). The effects of increasing grid size are similar to those observed on event 1. At gages 3 and 5 the simulated peak discharge and time to peak are affected by grid size. At gage 12 the simulated hydrographs are similar at the three grid resolutions.

4.2.3 VALIDATION RESULTS

Since the primary purpose of this study was to evaluate the applicability of CASC2D in simulating outlet hydrographs for large basins, the parameters calibrated to outlet conditions (Section 4.2.1) were used in the validation process. The model was validated using events 3 and 4 (see Table 4.2). These events were preceded by large amounts of rainfall, and therefore high antecedent soil moisture conditions existed. The model was validated using calibrated parameters from event 2 (Table 4.5).

The rainfall characteristics of the validation events were significantly different from the characteristics of the calibration event. During event 3, the total rainfall volume was almost twice that of event 2, yet both events lasted approximately the same amount of time. Event 4 lasted five times as long as event 2, and had a total rainfall volume four times the rainfall volume corresponding to event 2. The average rainfall rates for events 2, 3, and 4 were 0.224 in/hr, 0.340 in/hr, and 0.186 in/hr respectively (see Table 4.2).

Thus although calibrated parameters were used in the validation runs, slight adjustments were made to the parameters which were related to interception and soil moisture. Due to the large volume of water associated with event 3 and its high rainfall intensity (as compared to event 2), the storage detention parameter (S_d) was increased from 0.0 (the calibrated value for event 2) to 0.02, and the moisture deficit parameter

(M_d) was increased from 0.0 to 0.1. As a result of the large rainfall volume corresponding to event 4 and its lower rainfall intensity (as compared to event 2), the storage detention parameter (S_d) was increasing from 0.0 to 0.005. None of the other parameters required changing. The same changes were made at all three resolutions.

The validation runs produced fairly good fits between simulated and observed peak discharge rates and times to peak, at the outlet and at the sub-basin level (gage 3). The simulated runoff volume, for the duration of the event, did not reproduce actual conditions very well (particularly for event 3). The results are shown in Fig. 4.13a-4.13b for event 3 and in Fig. 4.14a-4.14b for event 2.

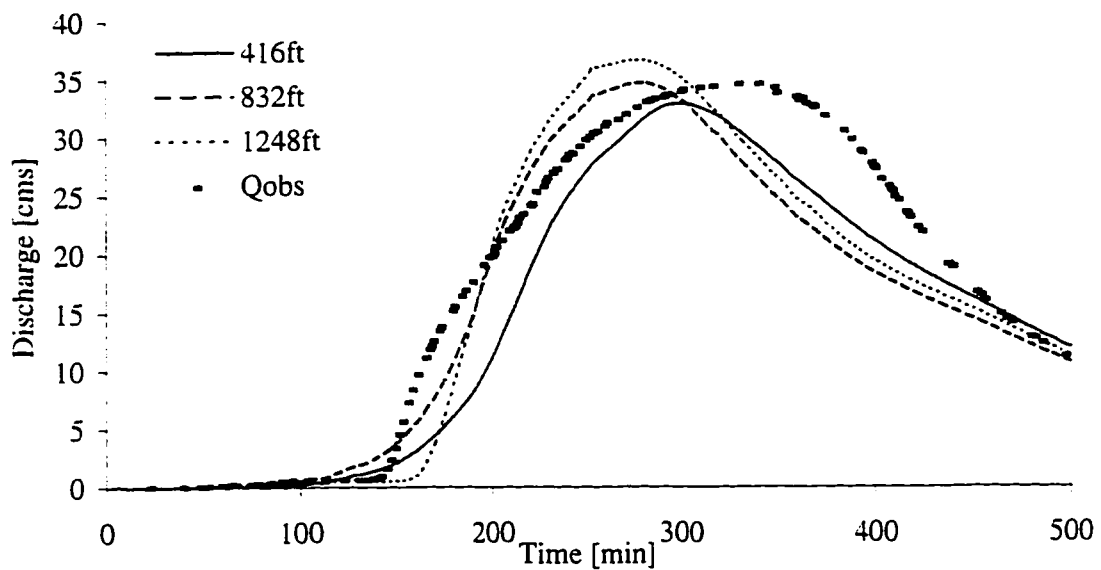


Fig. 4.13a: Goodwin Creek simulated outlet discharge, event 3

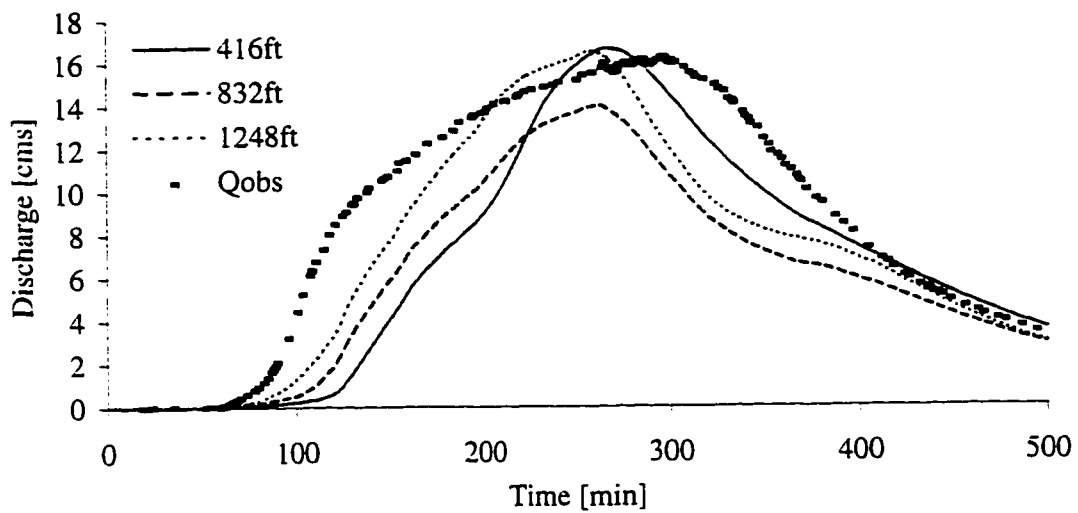


Fig. 4.13b: Goodwin Creek simulated discharge at gage 3, event 3

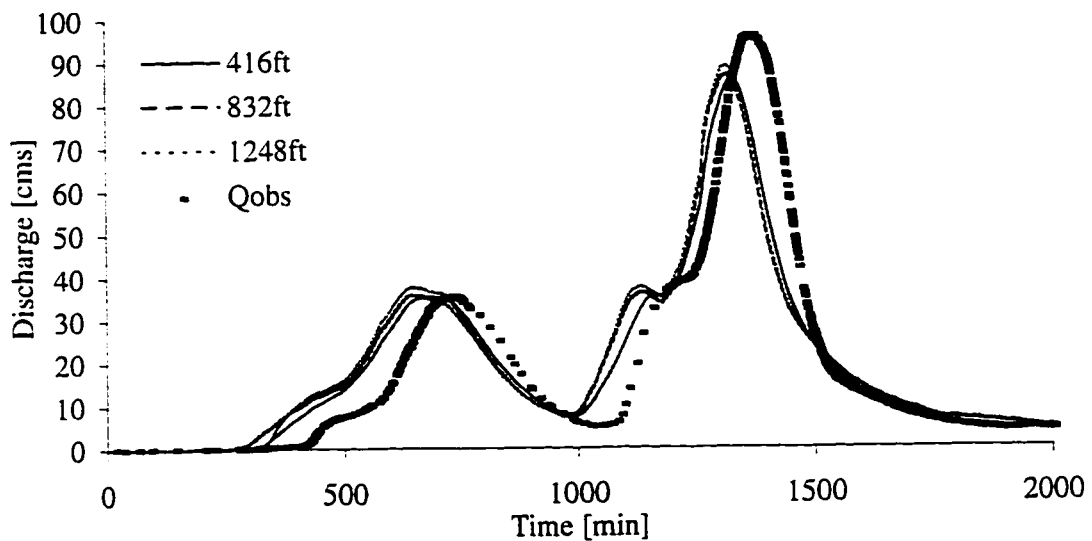


Fig. 4.14a: Goodwin Creek simulated discharge, event 4

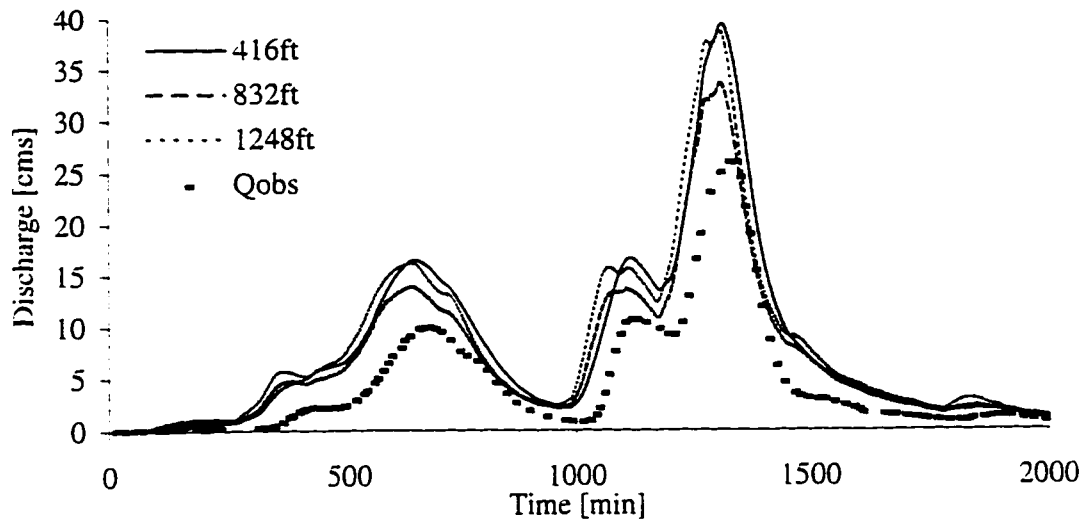


Fig. 4.14b: Goodwin Creek simulated discharge at gage 3, event 4

In simulating event 4, which lasted 31 hr and required small computational time steps because of the high discharge rates at the outlet (up to $100 \text{ m}^3/\text{s}$), the total computation time was greatly reduced at the coarser resolution. In terms of the magnitude of peak discharge and the time to peak, the simulated outlet hydrographs at increasing grid size lead to similar results. At all three resolutions the magnitude of the simulated hydrograph was within 10 percent of the observed discharge, and the simulated time to peak was within 60 min of the observed time to peak. Based on simulations results, it can thus be stated that the coarsest resolution (1248 ft) is a resolution which will lead to fairly accurate estimates of the peak magnitude and the time to peak corresponding to a given rainfall event, and will result in much shorter computation times.

4.3 SUMMARY

The GRASS capabilities for data analysis were used in evaluating watershed characteristics at increasing grid sizes. As demonstrated in Table 4.1, the effects of coarser grid resolutions on the representation of watershed characteristics include: 1) a decrease in the total number of cells representing the watershed from 1290 cells to 140 cells; 2) an increase in the percentage of channel cells as compared to the total number of cells from 16.4 percent to 43.6 percent ; 3) a decrease in the percentage of overland cells as compared to the total cells from 83.6 percent to 56.4 percent; and 4) a decrease in drainage density from 1.30 km^{-1} to 1.15 km^{-1} . The reduction in the total number of cells results in faster simulation times. The increase in the percentage of channel cells as compared to the percentage of overland cells causes overland flow to reach the channel more rapidly. The shortened channel length also affects channel routing conditions.

In the calibration runs, coarser resolutions consistently resulted in higher runoff rates and shorter times to peak. Due to the representation of watershed characteristics at large grid sizes, runoff from upland regions reaches the channels more rapidly, and is transmitted more quickly to the outlet. At coarser resolutions it was found that peak discharge could be reduced and time to peak increased by increasing the values of roughness coefficients for both overland flow (n_{ol}) and channel flow (n_{ch}).

In upland regions, rainfall-runoff generation is significantly affected by soil characteristics. At the sub-basin level the role of channel routing becomes less important, while upland processes of infiltration and runoff become very important. Calibrating the model to sub-basin conditions required different parameters than those calibrated for outlet conditions. Event 1 was preceded by very little rainfall, and infiltration was

significant during the event. At the sub-basin level, runoff was found to be sensitive to moisture deficit (M_d), detention storage (S_d), and the overland roughness coefficient (n_{ol}). Moisture deficit was reduced by up to 75 percent, while soil detention and overland roughness were increased by 25 percent (see Table 4.6). Sub-basin runoff was simulated for event 2, which had high antecedent moisture conditions, by reducing both hydraulic conductivity (K_s) and the overland roughness coefficient (n_{ol}) by up to 50 percent (see Table 4.7). Yet although sub-basin runoff was more accurately simulated by changing parameters such as M_d , S_d , n_{ol} , and K_s , approximate estimates of peak discharge and time to peak were obtained using parameters calibrated to outlet conditions (see Fig. 4.8, and Fig. 4.10).

On Goodwin Creek, the validation runs demonstrated the applicability of coarse resolutions in simulating the magnitude of peak discharge and the time to peak at the outlet. For event 4, which lasted more than a day, the larger grid sizes were as effective in simulated outlet discharges as the finest grid size, and required much shorter computation times. The validation results confirmed that large grid sizes can be used in CASC2D simulations, as long as the model is calibrated at the coarse resolution. Calibrating the model at each resolution provides more accurate simulation results by taking into consideration the effects of grid size on the representation of watershed characteristics governing hydrologic and hydraulic processes.

Chapter V

LARGE-SCALE SIMULATIONS

5.1 HICKAHALA-SENATOBIA INPUT DATA

The Hickahala-Senatobia basin, covering a 560 km² drainage area in north-western Mississippi, has been selected for the evaluation of grid size effects on large-scale simulations (Fig. 5.1).

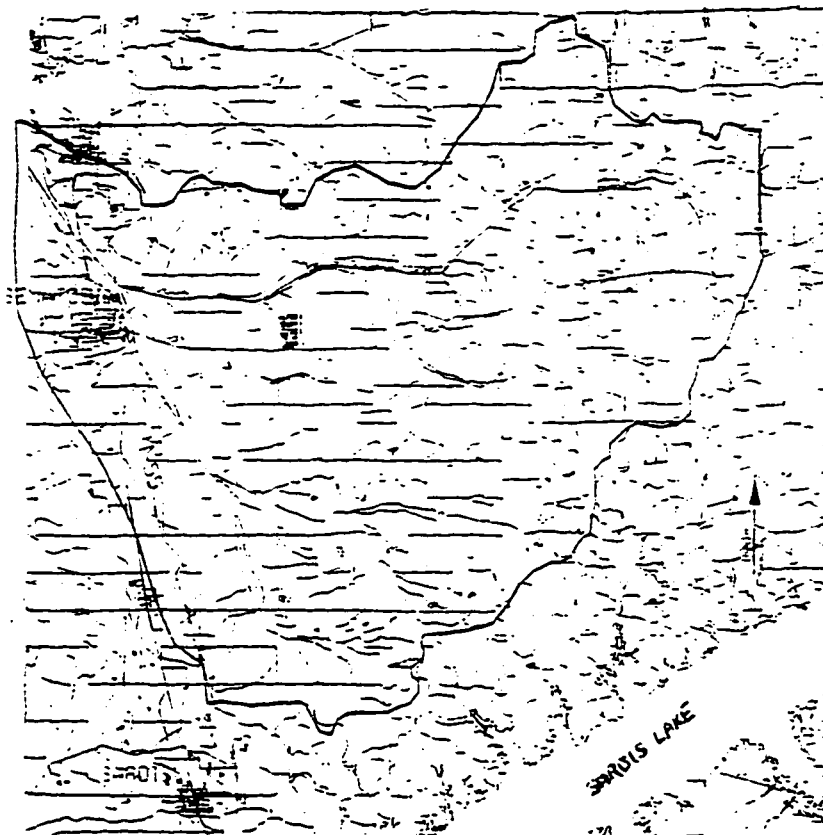


Fig. 5.1: Hickahala-Senatobia basin
(from Johnson, 1993)

The two main tributaries of the watershed are Hickahala Creek and Senatobia Creek. Elevations in the watershed range from 170 m to 64 m. Landuse types include agriculture (24%), pasture (49%), forest (26%), and residential (1%). The two general categories of soil types are fine sandy loam (20%) and silt loam (80%). Average slopes in the channel network range from 0.003 in upstream links to 0.0007 in the main channel. The outlet of the basin flows into Arkabutla Dam, on the north-west end of the watershed.

Input data for simulations on Hickahala-Senatobia were available through contacts at Waterways Experiment Station (WES) in Mississippi. Watershed characteristics including elevation, soil type, and landuse were obtained in the form of raster maps at a 100 ft grid size. Fig. 5.2 shows the topography of the watershed at a 100 ft grid size. This raster map was critical in defining runoff conditions at coarser resolutions.

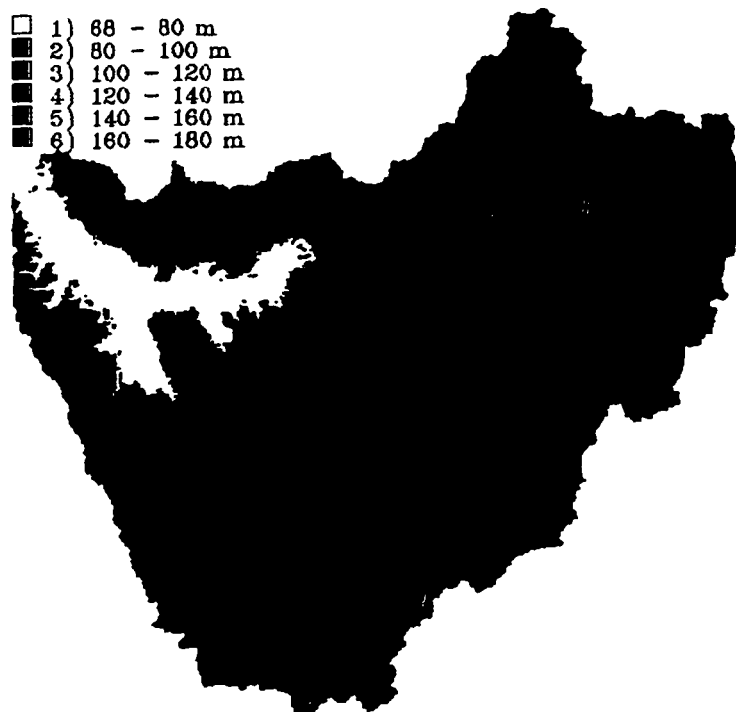


Fig. 5.2: Hickahala-Senatobia digital elevation map (100 ft grid size)

Channel network characteristics defining channel width, depth, and Manning roughness coefficients were compiled from various sources. The basin covers such a large area that reliable precipitation and discharge measurements were not available for the entire watershed. Model calibration and validation runs could not be performed using actual rainfall-runoff events. Goodwin Creek is located within the same geographical region, in north-western Mississippi, and has similar watershed characteristics including landuse types, soil types, and overland slope values. Calibrated parameters from Goodwin Creek simulations were therefore used in the Hickahala-Senatobia simulations.

From the analysis of rainfall-runoff conditions on Goodwin Creek, it was determined that a grid size as large as 1248 ft would be adequate for CASC2D simulations. In order to extend the analysis to coarser resolutions, the three resolutions selected for simulations on the Hickahala-Senatobia basin were 1000 ft (305 m), 2000 ft (610 m), and 3000 ft (914 m). These grid sizes were chosen, being multiples of the original 100 ft input data in raster format. GRASS commands were used to aggregate input data to larger grid sizes, as described in Section 4.1.1 (also see Appendix D for details). The *g.region* command was first used in creating raster maps at increasing grid sizes, by overlaying a grid mesh of given dimensions on the watershed. The original elevation, landuse, and soil maps were aggregated at 1000 ft, 2000 ft, and 3000 ft grid sizes. The *r.watershed* command was then used to define sub-basin areas and the location of the channel at larger grid sizes. Based on an elevation map, the command extracts information about drainage patterns in the watershed. A threshold value is identified as the minimum value required for the initiation of a stream node. For Hickahala-Senatobia a threshold of 10 km² was assumed, so as to limit the total number

of channel cells representing the network. The sub-basin map generated at a 1000 ft grid size is presented in Fig. 5.3, where each color represents a single sub-basin, and the channel network (in blue) is overlaid on the sub-basin map.

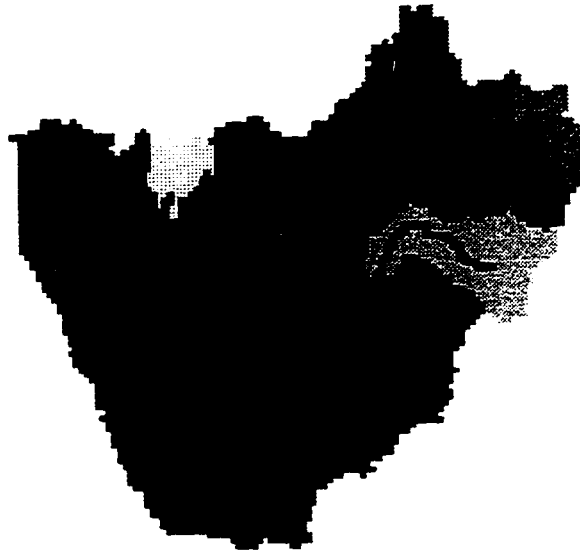


Fig. 5.3: Hickahala-Senatobia sub-basins and network at a 1000 ft grid size

GRASS commands were used to evaluate the effects of increasing grid size on the representation of watershed characteristics. Table 5.1 summarizes the results for grid sizes ranging from 100 ft to 3000 ft. As grid size increases, the total number of cells decreases from 614,896 cells to 661 cells. At the same time, the ratio of channel cells (defined as cells through which the channel network passes) to total cells increases from 0.87 percent (at 100 ft grid size) to 19.97 percent (at a 3000 ft grid size). In addition, the Hickahala drainage density, defined as the total channel length divided by the drainage area, decreases from 0.287 km^{-1} at a 100 ft grid size to 0.218 km^{-1} at a 3000 ft grid size. These changes in the representation of watershed characteristics are similar to the changes observed on Goodwin Creek (see Table 4.1), and will have a similar effect on modeling

hydrologic and hydraulic processes, as seen in the calibration and validation runs on Goodwin Creek.

Table 5.1: Hickahala-Senatobia watershed characteristics

	100 ft (30 m)	1000 ft (305 m)	2000 ft (610 m)	3000 ft (914 m)
Drainage area [km ²]	571.26	566.62	573.77	552.68
Total number of cells	614,896	6,099	1,544	661
Number of channel cells	5,375	484	223	132
Ratio of channel cells to total cells [%]	0.87	7.94	14.44	19.97
Ratio of overland cells to total cells [%]	99.13	92.06	85.56	80.03
Total length of channel [km]	163.83	147.52	135.94	120.70
Drainage density [km ⁻¹]	0.287	0.260	0.237	0.218

An increase in grid size also results in the loss of information with regard to the spatial variability of elevation. As demonstrated in Section 4.1.1 (Chapter 4), estimated upland slopes are affected by grid resolution. Hickahala-Senatobia slopes for grid sizes ranging from 100 ft to 3000 ft are shown in Fig. 5.4.

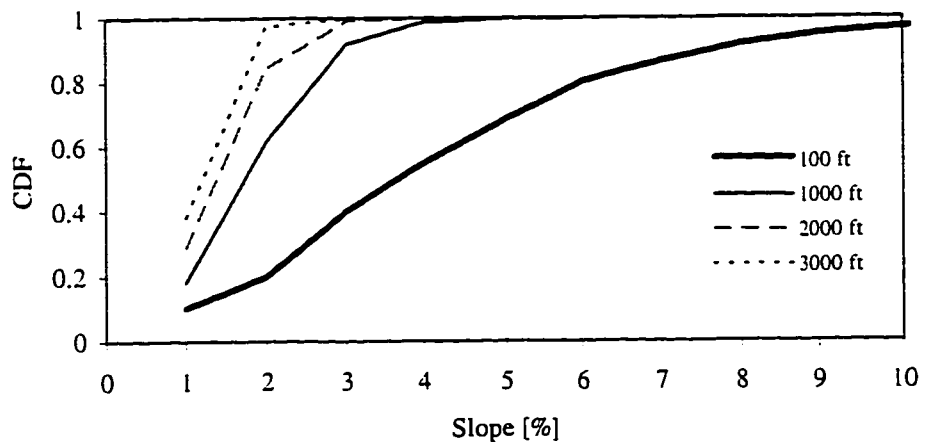


Fig. 5.4: Hickahala-Senatobia upland slopes at increasing grid size

Based on calibration runs on Goodwin Creek, it was found that the effects of grid size could be accounted for through the parameters representing overland and channel roughness. In the simulation of outlet conditions for events with high rainfall intensities

and/or long rainfall durations, an accurate description of hydraulic processes becomes very important. A detailed description of the spatial variability affecting hydrologic processes in upland areas is not as important.

Hydraulic processes are evaluated as a function of slope. In the CASC2D formulation, grid elevations are used to determine the rate and direction of runoff. As grid size increases, detail is lost in the digital elevation map (DEM). At the 1000 ft, 2000 ft, and 3000 ft grid sizes, various techniques were used in smoothing the DEM, so as to closer reflect conditions in upland areas. Any potholes which existed as a result of data aggregation were filled. Within the channel, link slopes were known from cross-section surveys. Talweg values were defined at each resolution so as to preserve the original values of channel slopes. Channel dimensions were also the same at all resolutions.

5.2 CASC2D SIMULATIONS

5.2.1 FINE GRID RESOLUTION

The applicability of CASC2D for large-scale simulations was first tested at the finest resolution available, which was the resolution of the original input data (100 ft). Due to the large number of grid cells representing the basin, the GRASS version of CASC2D was used (all other simulations were performed using the FORTRAN version of CASC2D). The matrix of 1023x1058 cells, representing the entire basin of 560 km², was easily managed by the GRASS version of CASC2D. This version of CASC2D requires raster maps as input for simulations and generates water depth raster maps at specific intervals throughout the simulation. An original elevation map for Hickahala-Senatobia was available at a 100 ft grid size. The channel network was extracted using the *r.watershed* command, as described in Section 5.1. If channel routing were to be

included at this resolution, channel characteristics would have to be defined for every channel cell. Due to the complexity of the stream network (5,375 cells), channel routing was not included.

In order to simulate runoff conditions in the channel, a constant depth, width, and channel roughness were assumed as average values representing the entire channel network. Based on cross-section measurements, an average depth of 3 m, an average width of 20 m, and a channel roughness coefficient of 0.04 were assumed as constant values representing conditions throughout the network. For all grid cells corresponding to channel cells, the channel depth (3 m) was subtracted from the elevation values in the DEM. This caused flow to automatically drain towards the channel cells. In addition, an equivalent channel roughness (n_{eq}) corresponding to the channel network was evaluated, assuming that the channel instead of being 20 m wide (the average observed width), was as wide as the grid size ($\cong 30$ m). The equivalent roughness coefficient was calculated as (see Appendix F for details):

$$n_{eq} = n_{ch} \left(\frac{W_{ch}}{W} \right)^{2/3} = 0.04 \left(\frac{20 \text{ m}}{30 \text{ m}} \right)^{2/3} = 0.031 \quad (5.1)$$

where n_{ch} and W_{ch} represent actual channel characteristics.

All channel cells were thus assigned a roughness coefficient of 0.031. Based on Goodwin Creek results, overland roughness (n_{ol}) was assumed to be 0.08 for the entire watershed.

Since rainfall and runoff data were not available for actual events, simulations were performed at a 100 ft grid size assuming uniform rainfall conditions. A uniform rainfall intensity of 0.50 in/hr was applied, for a duration of 6 hr. Soil parameters calibrated for Goodwin Creek, assuming low antecedent moisture conditions, were used

(see Table 4.4 for values). Output included a runoff hydrograph at the outlet and depth maps generated at 1 hr intervals. The raster depth maps are shown in Fig. 5.5, for simulation times of 2, 4, 6, 8, 10, and 12 hr. The total time simulated was 24 hr. During the rainfall event, infiltration occurs and excess rainfall begins to accumulate on hillslopes, then in the channels. This is seen in the depth maps at 2, 4, and 6 hr. Once rainfall has stopped, water begins to drain from upland areas and concentrates in the lowest elevations, where the channel is located.

In order to prevent numerical instabilities resulting from the finite difference representation of physically-based mathematical equations, the Courant number (C) must be less than or equal to 1 (Fletcher, 1987). Since the Courant number is calculated as a function of dt/dx , a decrease in the value of dx requires a decrease in the value of dt . In CASC2D simulations, dx represents the cell width and dt represents the computational time step. For simulations using a 100 ft grid size, it was found that a computational time step of 1 second had to be used in order to maintain stability. Longer time steps will result in stable solutions only if coarser grid resolutions are used. Extensive calculations were performed in simulating runoff at a 100 ft grid size, due to the 1 second time step required at this resolution, and due to the large number of cells representing the watershed.

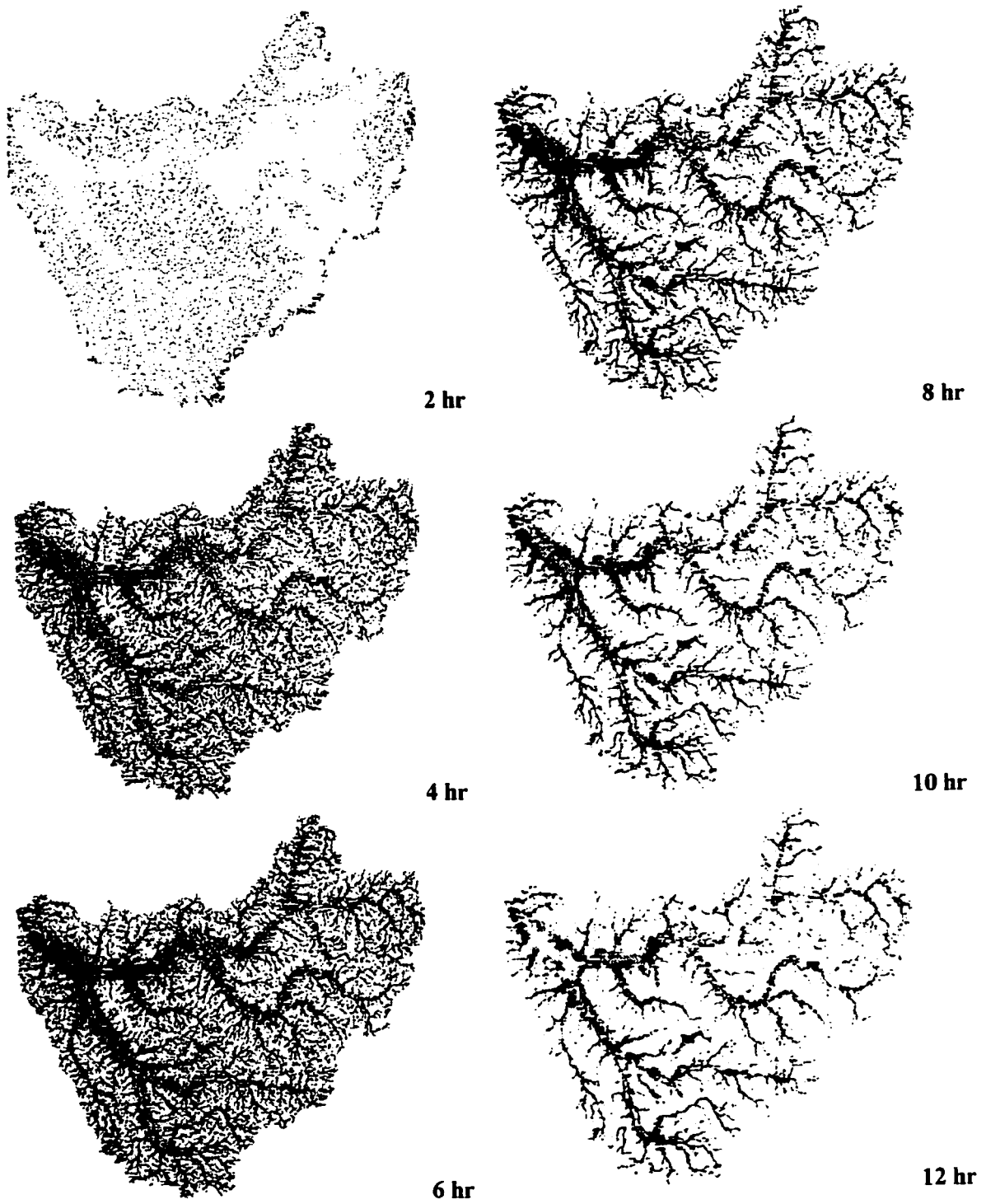


Fig. 5.5: Hickahala-Senatobia simulation results at a 100 ft grid size

At each 1 sec time step, calculations were performed for each grid cell, resulting in 614,896 calculations per time step. In order to simulate a total duration of 24 hr, including the duration of the rainfall event and the time required for runoff to drain to the outlet, 86,400 iterations were needed. At 614,896 calculations per iteration, the total number of calculations performed was 5.3×10^{10} . The actual computer time (using a HP735) required to do these calculations was approximately 10 days (240 hr), which corresponds to a ratio of 10:1 in terms of computer time versus real time.

Although input data is available at a 100 ft grid size and it has been shown that large-scale rainfall-runoff simulations can be performed at this fine resolution, coarser resolutions are more attractive for such simulations. Not only are calculations performed much more rapidly, due to fewer grid cells representing the watershed and the longer computational times steps, but less detailed input data is also required at the coarser resolutions.

5.2.2 COARSE GRID RESOLUTIONS

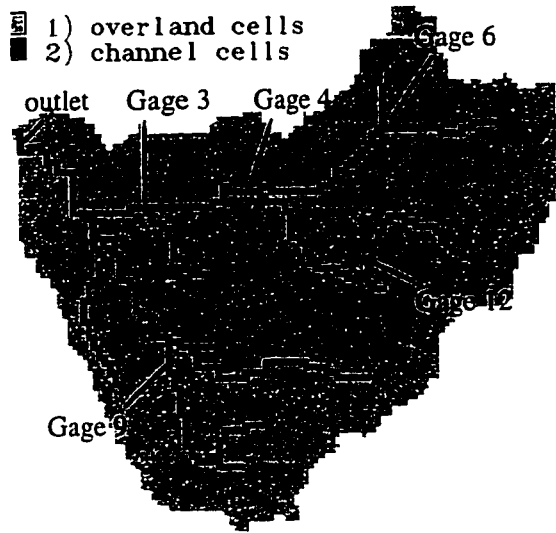
Clearly increasing the grid size from 100 ft to grid sizes ten, twenty, and thirty times as large results in the loss of information. At coarser resolutions, the representation of the spatial variability of upland characteristics such as slope, roughness coefficients, and infiltration parameters is altered. Small-scale heterogeneity is lost. Yet from calibration and validation runs on Goodwin Creek, it was found that the runoff response, could be simulated using a single value of the overland roughness coefficient (see Tables 4.4 and 4.5). In addition, the representation of upland and channel slopes has a major impact on the runoff response. Great care was therefore taken to fill all the depressions

which may have been created as a result of increasing grid size, and channel bed elevations were defined so as to maintain the original channel slope at all resolutions.

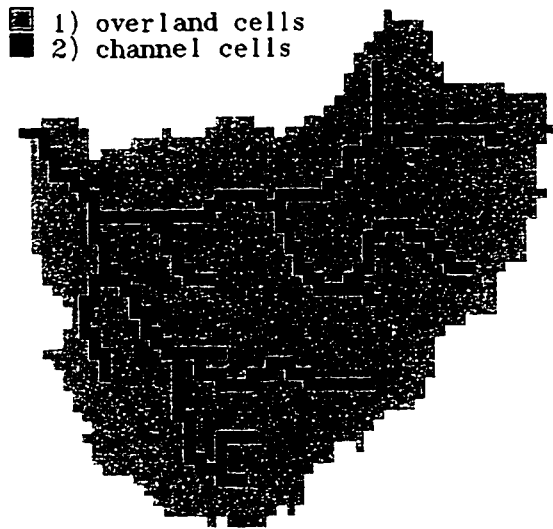
At coarser grid resolutions channel routing could be included. This was made possible by the reduction in the total number of cells representing the channel network. As described earlier, *r.watershed* was used to extract the network at each grid resolution. Having defined channel locations at the three resolutions, the network was divided into 30 separate segments, each segment having approximately the same number of cells. The drainage basin and network at increasing grid size are shown in Fig. 5.6. The gage locations shown at a 1000 ft grid size represent channel cells at which hydrographs corresponding to sub-basin areas were simulated.

Using available data on channel slopes in Hickahala-Senatobia, bed elevations were defined for each channel node. Many drop structures exist along the network. These were not taken into consideration in the modeling of rainfall-runoff conditions. Average channel slopes were used. Channel characteristics, including width, depth, and roughness coefficient, were defined for each cell, based on observed cross-section values (see Appendix B).

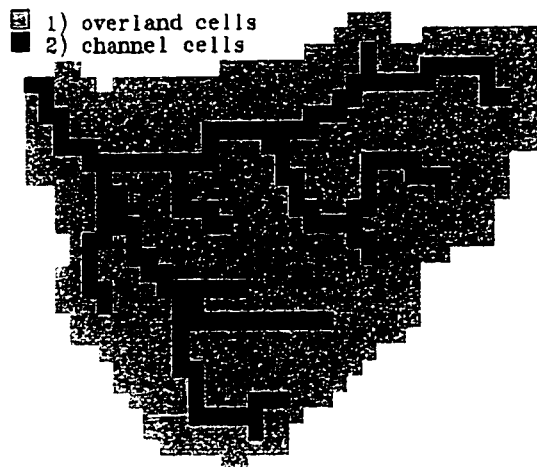
As was the case at 100 ft grid size, soil and overland roughness coefficients were defined based on Goodwin Creek calibration runs. In calibrating the model to Goodwin Creek conditions, the overland roughness coefficients corresponding to 416 ft, 832 ft, and 1248 ft, were 0.80, 0.9, and 0.15 respectively (see Tables 4.4 and 4.5). For Hickahala-Senatobia simulations, a constant overland roughness coefficient (n_{ol}) of 0.10 was assumed for the coarser resolutions (1000 ft, 2000 ft, and 3000 ft).



1000 ft grid size



2000 ft grid size



3000 ft grid size

5.6: Hickahala-Senatobia at increasing grid sizes

In order to evaluate grid size effects on rainfall-runoff simulations, both impervious and pervious conditions were simulated. An event with a constant rainfall intensity of 0.5 in/hr (12.7 mm/hr) and a duration of 3 hr was used for the impervious simulations. The hydrographs generated at each resolution are presented in Fig. 5.7a- Fig.5.7c. The response of smaller sub-basins (see gages 9 and 12) is directly related to the rainfall duration, while the response of larger sub-basins (gages 4, 3, and outlet) is delayed as a result of the time required for flow to travel through the network. The time lag between the end of the rainfall event and the time to peak increases as the drainage area increases. As seen in the simulated hydrograph at the outlet, the time to peak occurs 5 hr after the rainfall has stopped. This lag time is representative of the wave travel time through the entire channel network.

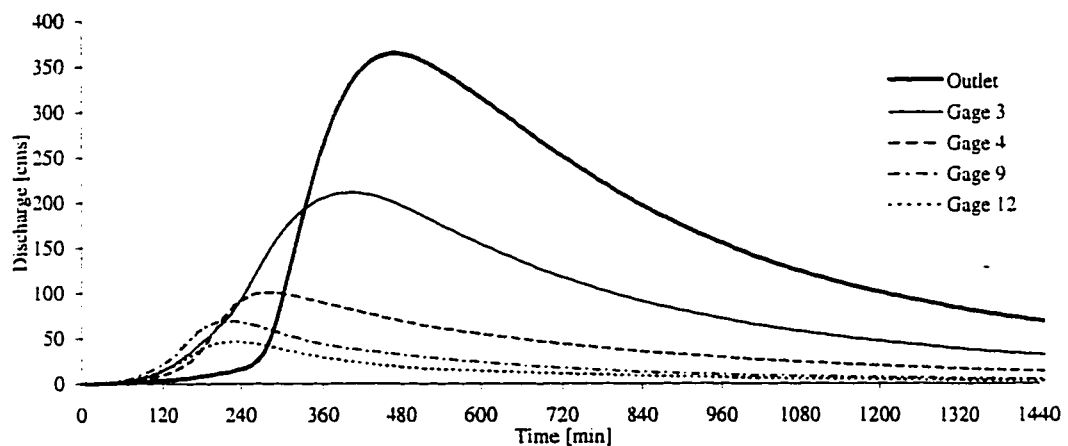


Fig. 5.7a: Simulated runoff hydrographs at 1000 ft grid size with impervious conditions

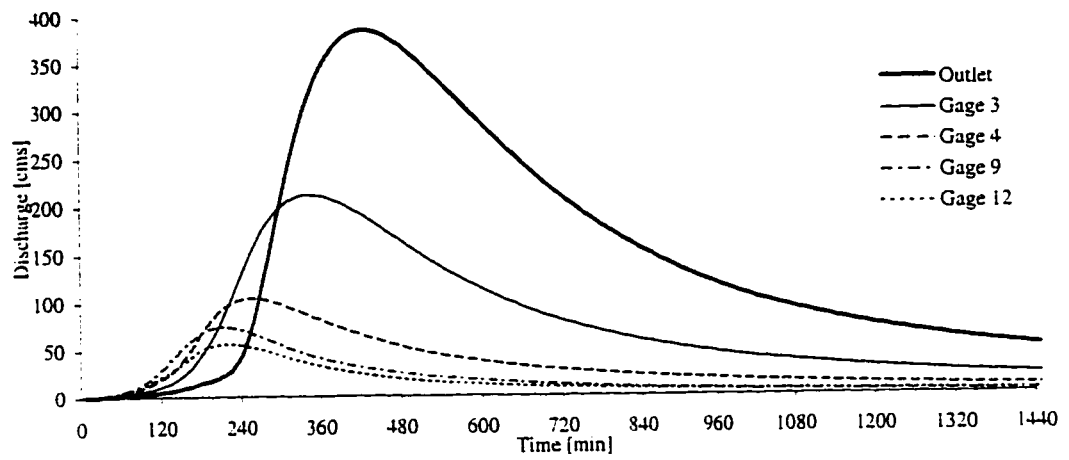


Fig. 5.7b: Simulated runoff hydrographs at 2000 ft grid size with impervious conditions

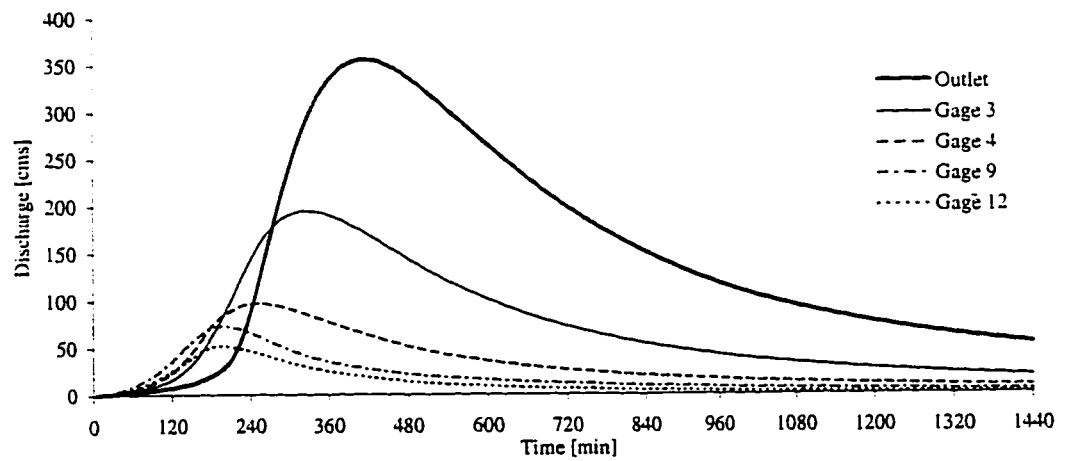


Fig. 5.7c: Simulated runoff hydrographs at 3000 ft grid size with impervious conditions

The drainage areas (A_d) corresponding to the location of sub-basin gages and the outlet vary as a function of grid size, as seen in Table 5.2. This is a result of the changes in the representation of topography at the different resolutions. Drainage patterns are slightly modified, as is the location of the channel network. Since drainage areas corresponding to individual gages are not the same, a direct comparison of simulated runoff hydrographs at these gages will therefore not give a true representation of the on rainfall processes, particularly on the smaller sub-basins.

Table 5.2: Drainage areas associated with sub-basins at increasing grid sizes

Gage number	1000 ft resolution	2000 ft resolution	3000 ft resolution
	A_d [km ²]	A_d [km ²]	A_d [km ²]
Outlet	566.62	573.77	552.68
3	302.77	301.75	247.49
4	134.24	127.09	207.36
6	64.38	64.29	55.18
9	68.75	70.61	107.02
12	36.98	48.31	55.18

Pervious simulations were performed assuming a rainfall intensity of 0.5 in/hr (12.7 mm/hr) and a duration of 6 hr. A longer rainfall duration was necessary in order to generate runoff in upland areas. The hydrographs at increasing grid sizes are displayed in Fig. 5.8a-Fig.5.8c. As was the case for the impervious simulations, peak discharge on sub-basins (gages 9 and 12) directly reflects overland flow conditions. The runoff hydrograph peaks when rainfall stops, after 6 hr. At gage 4 and at the outlet, the peak response is delayed by the time required for the wave to travel through the channel network. At the outlet, the time to peak is approximately 11 hr, which represents a 5 hr delay in the runoff response. This delay is indicative of the wave travel time through the entire channel network, and is equal to the delay seen in the impervious simulations.

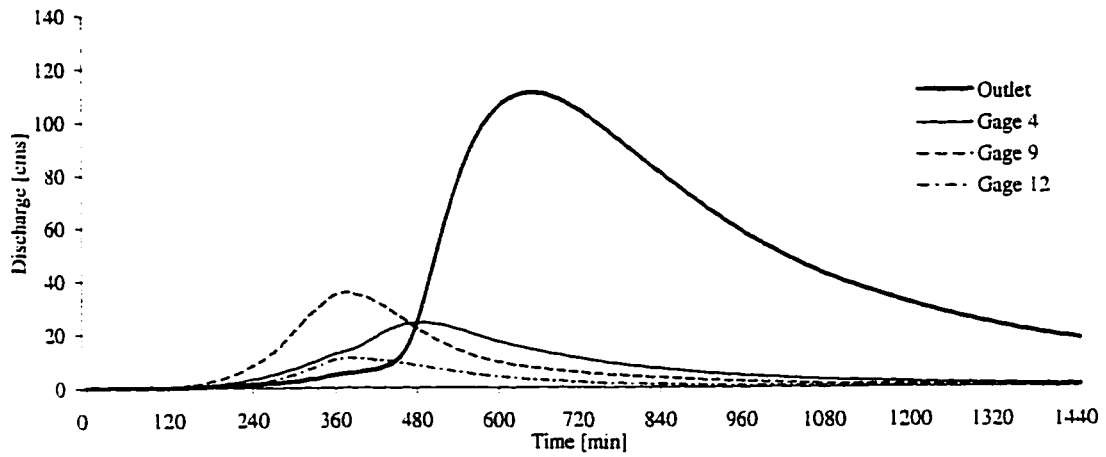


Fig. 5.8a: Simulated runoff hydrographs at 1000 ft grid size with pervious conditions

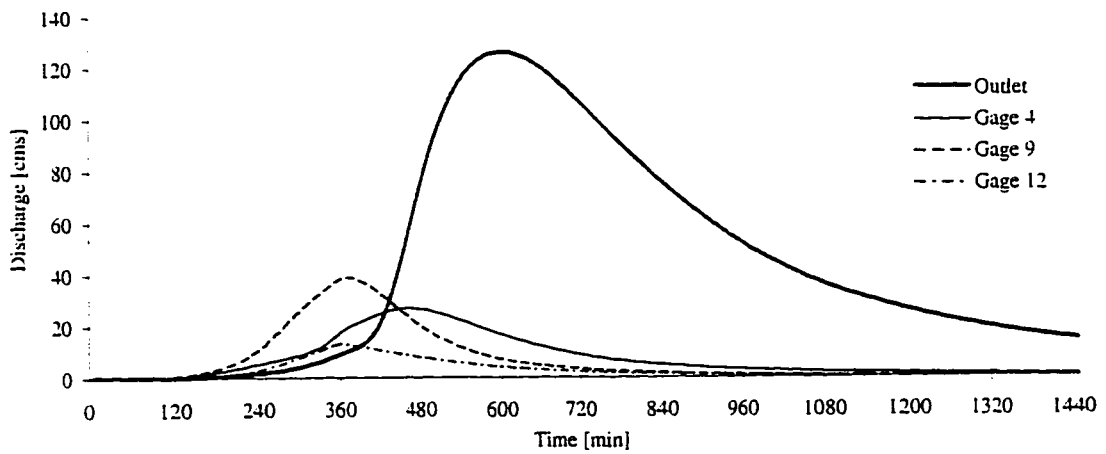


Fig. 5.8b: Simulated runoff hydrographs at 2000 ft grid size with pervious conditions

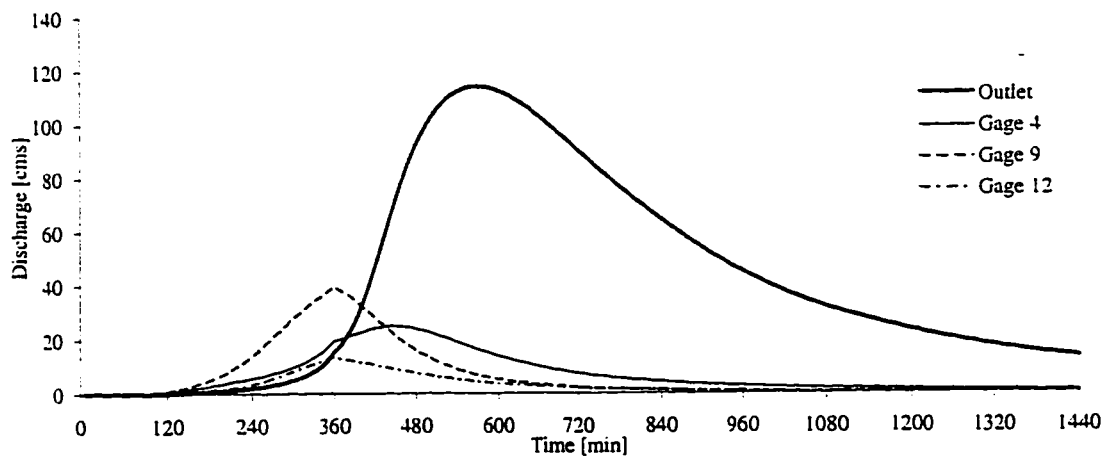


Fig. 5.8c: Simulated runoff hydrographs at 3000 ft grid size with pervious conditions

The simulated hydrographs at the outlet and at gages 4, 6, and 12 are shown for increasing grid sizes in Fig. 5.9. These hydrographs correspond to pervious conditions, with a rainfall intensity of 0.5 in/hr (12.7 mm/hr) and a rainfall duration of 6 hr. The drainage areas corresponding to the outlet and the sub-basin gages are approximately 560 km², 130 km², 60 km², and 40 km² respectively.

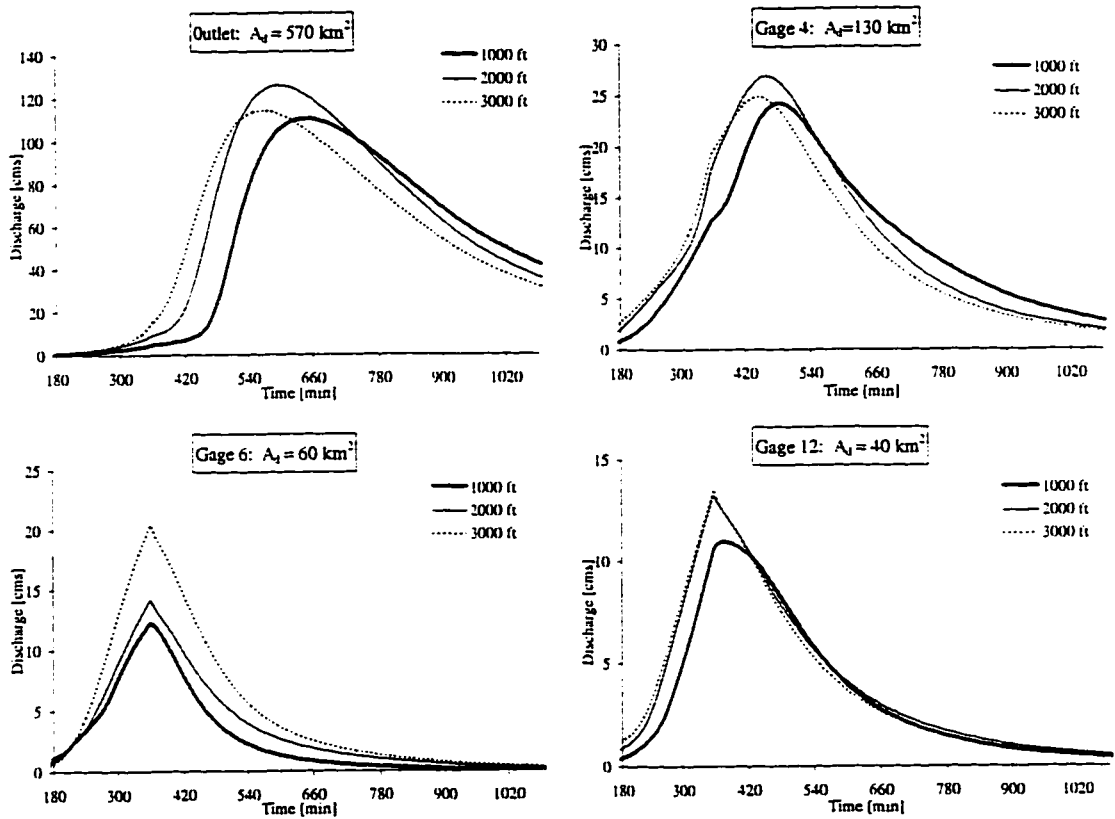


Fig. 5.9: Simulated discharge at increasing grid resolution

Since the drainage areas corresponding to the individual gages are not exactly the same (see Table 5.2), quantitative conclusions regarding the net effect of increasing grid size cannot be made based on the simulated hydrographs shown in Fig. 5.9. Using the 1000 ft grid size as a reference, it can only be said that the coarser resolutions tend to decrease the time to peak and increase the magnitude of the peak discharge. At the outlet

and at gage 4, the shape of the runoff hydrograph is similar at all three grid sizes. At these gage locations, channel routing plays an important role. At the sub-basin level, at gages 6 and 12, the coarser resolutions result in triangular-shaped hydrographs. These gages, as previously discussed, primarily represent runoff from upland areas. Channel routing plays a minor role. The triangular-shaped hydrographs at coarser resolutions do not represent the natural response of upland areas to rainfall. Based on these results, it appears that coarser resolutions would not be appropriate in simulating runoff at the sub-basin level (less than 60 km²) on Hickahala-Senatobia. Recall though that in defining the channel network, for modeling purposes, the minimum drainage area corresponding to channel cells was set at 10 km². This coarse representation of the channel network has a direct influence on the evaluation of runoff hydrographs at the sub-basin level. It can be concluded that the use of coarser resolutions is warranted if outlet conditions rather than sub-basin conditions are to be evaluated.

5.3 SUMMARY

GRASS commands were used to define the watershed at coarser resolutions, based on original input data at a 100 ft grid size, and to extract the channel network (see Fig. 5.3 and 5.6). The raster-based data was evaluated and watershed characteristics at increasing grid sizes determined. The effects of increasing grid size are summarized in Table 5.1. As was the case on Goodwin Creek, the coarser resolutions resulted in a reduced number of cells representing the watershed, an increased percentage of channel cells as compared to the total number of cells, a decreased percentage of overland cells, and a decrease in drainage density. Upland slopes were also found to decrease at coarser resolutions. Calibration runs on Goodwin Creek showed that in order to simulate

rainfall-runoff conditions at increasing grid size, the overland roughness coefficient and the channel roughness coefficient had to be increased. This change was necessary as a result of the effects of grid size on the representation of watershed characteristics. Since Goodwin Creek and Hickahala-Senatobia were in the same geographic region and had similar features (soil types, landuse types, slopes), the calibrated parameters from Goodwin Creek simulations were assumed to be valid for the Hickahala-Senatobia simulations. On Hickahala-Senatobia grid sizes ranged from 100 ft to 3000 ft.

It has been shown that the CASC2D model is capable of simulating runoff on a large watersheds using a fine grid resolution (100 ft). Yet the time required to simulate an event on a watershed the size of Hickahala-Senatobia (560 km²), or larger, is unrealistic if the modeler's intent is to evaluate real time scenarios. The simulation of a 24 hr event required ten days of computation time. The use of coarser resolutions for large-scale simulations is much more attractive, as a result of the reduction in computation time. Fig. 5.10 summarizes the expected calculation time as a function of the total number of cells in a basin, for the simulation of a 12 hr event (using an HP735). Due to the constraints imposed by the Courant number, so as to maintain numerical stability in the finite difference calculations, the computation time step Δt increases as grid size Δx increases. As shown in Fig. 5.10, for a drainage area of 600 km², simulations using a 30 m grid size must be performed at a 1 second time step, requiring a total calculation time of 100 hr (number of cells \cong 600,000). If a 1 km grid size were used, simulations could be performed at a 10 second time step, resulting in a total calculation time of 0.1 hr (number of cells \cong 600). Clearly a 1 km grid size is a much more feasible selection for large-scale simulations.

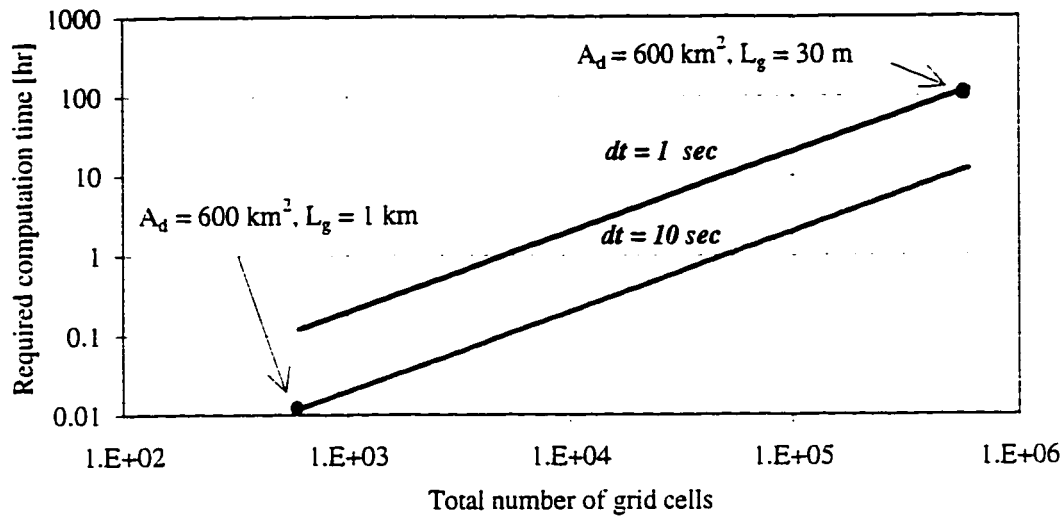


Fig. 5.10: Required calculation time for the simulation of a 12 hr event

Impervious simulations on Hickahala-Senatobia using coarse resolutions (300 m - 900 m) showed that grid resolution does not have much of an effect on the model output when infiltration is not considered. The simulated outlet hydrographs were comparable at increasing grid sizes. All resolutions showed a time lag between the end of rainfall and the time to peak at the outlet, with similar peak magnitudes. At the sub-basin level results were also comparable at increasing grid sizes.

The pervious simulations on Hickahala-Senatobia showed that the use of larger grid sizes could lead to decreased times to peak and increased peak discharges at the outlet. Simulated outlet hydrographs were similar at the three resolutions used in the analysis (1000 ft, 2000 ft, and 3000 ft). At the sub-basin level, where overland flow plays a major role, the primary effect of increasing grid size was to increase the magnitude of peak discharge. The simulated hydrographs at coarser resolutions were triangular in shape, indicating that at these resolutions overland flow was not accurately represented.

At the outlet, the use of coarse resolutions resulted in the simulation of similar runoff hydrographs. As shown by the delayed response of runoff, channel routing becomes an important feature in simulating the rainfall-runoff response at the outlet. Due to the long time required for the wave to travel through the channel network, the effects of spatial variability in upland areas become attenuated and have a less significant effect on the nature of the outlet hydrograph. It can therefore be concluded that coarser grid resolutions can be considered appropriate for simulations on large watersheds, particularly if the objective is to model outlet conditions.

Chapter VI

SIMULATING IMPERVIOUS RUNOFF CONDITIONS

6.1 INTRODUCTION

As discussed in Chapter 2 (Section 2.4), the hydraulic response of a basin to rainfall can be described using the concept of a watershed time to equilibrium (T_e), where T_e represents the wave travel time to the outlet of the basin. The time to equilibrium is evaluated as a function of watershed physical and geometrical properties, and as a function of storm characteristics. Steady state is achieved at times greater than the time to equilibrium, when the output of the system (runoff) is equal to the input to the system (rainfall). The nature of the surface runoff hydrograph, under uniform rainfall conditions, will depend on the rainfall duration. Assuming impervious conditions, if the rainfall duration (T_r) is longer than the time required to reach equilibrium ($T_r/T_e > 1$), then complete equilibrium occurs. Peak discharge is a constant value, defined as the equilibrium discharge, and is a linearly related to rainfall intensity. If the rainfall duration (T_r) is less than the time to reach equilibrium ($T_r/T_e < 1$), then partial equilibrium conditions exist and the peak discharge is described as a non-linear function of rainfall intensity (see Fig. 2.1).

Recent studies have evaluated the effects of spatial variability in watershed characteristics and rainfall properties on the time to equilibrium of small scale basins (see

Chapter 2). Sivapalan and Wood (1986) concluded that rainfall will have an important effect on rainfall-runoff modeling since the correlation length of rainfall is usually larger than that of infiltration parameters. In their analysis of 1-D systems, Julien and Moglen (1990) found that the time to equilibrium of spatially varied systems can be approximated by using spatially averaged values of hydrologic parameters. They defined a length scale at which spatial variability does not have a significant effect on runoff, and concluded that it should be possible to analyze extreme events (high intensity, long duration) with larger grid sizes, as long as the grids have a runoff length which is greater than the length scale. Saghafian and Julien (1995), in their studies of the effects of infiltration on time to equilibrium, concluded that the delay in reaching equilibrium is significant only when δ/K (where $\delta = (1-S)\theta_e H_f$) is large. They also determined that when the ratio of the stream response time to the catchment response time is small, the grid size used in calculations should be much less than the overland runoff length. Ogden (1992) looked at the effects of T_r/T_e on peak discharge and determined that under partial equilibrium conditions peak discharge will be highly variable, but under complete equilibrium peak discharge will not vary.

The intent of this research is to build on previous studies by extending the analysis of the concept of a watershed time to equilibrium to large scales. The effects of spatial variability of input parameters on time to equilibrium and peak discharge will be evaluated by simulating runoff conditions using a range of grid resolutions. The dimensionless parameters Q^* and T^* , where $Q^* = Q_p/Q_e$ and $T^* = T_r/T_e$, will provide a measure of the relative effects of grid size on runoff conditions, and will be used in determining appropriate grid sizes for simulations on large watersheds.

Under equilibrium conditions peak discharge is constant. It is anticipated that grid resolution will not affect runoff rates. When partial equilibrium conditions exist, grid resolution may have an impact on rainfall-runoff conditions. The concept of a watershed time to equilibrium was tested by simulating a rainstorm of constant rainfall intensity and of a duration long enough to produce equilibrium conditions at the outlet. Since equilibrium conditions were achieved at the outlet, it was assumed that all other grid cells in the basin had also reached equilibrium. Being in equilibrium, the peak discharge (Q_p) on each cell was a constant value equal to the equilibrium discharge (Q_e). It has been shown that under equilibrium, unit discharge (q) is equal to the product of rainfall intensity (i) and the runoff length (L) (see Fig. 2.1). Assuming that the drainage area (A_d) corresponding to runoff length (L) can be approximated as L^2 , equilibrium discharge is defined as:

$$Q_e = (iL)L = iA_d \quad (6.1)$$

Using GIS-GRASS capabilities for data analysis (see Appendix D, *r.mapcalc* program), the equilibrium discharge corresponding to a constant rainfall intensity is used to evaluate the drainage area (A_d) corresponding to every grid cell in the watershed. This drainage area (A_d), in contrast to drainage areas evaluated based on topography alone, is representative of the 2-D overland routing capabilities of the CASC2D model. Traditional methods of evaluated drainage patterns, based solely on elevation maps, allow for overland flow in a single direction. Using these methods, the minimum equilibrium discharge will correspond to runoff from a single cell. The CASC2D model allows for overland runoff to flow in two directions, resulting in drainage areas corresponding to overland cells which are less than the equilibrium discharge of a single cell.

The raster-based watershed data describes watershed characteristics. It can be used in calculating the time to equilibrium (T_e) for every pixel within the basin, corresponding to a uniform rainfall intensity (i), and assuming spatially averaged values of hydrologic parameters. As shown in Eq. (2.1), the time to equilibrium is evaluated as a function of parameters governing hydraulic runoff conditions. In this case two assumptions are made in order to simplify the evaluation of the time to equilibrium corresponding to individual cells. The first assumption is that the average overland roughness coefficient (\bar{n}_{ol}) and the average upland slope (\bar{S}) can be used in calculating time to equilibrium. The second assumption is that runoff length (L) is equal to $A_d^{0.5}$. It has been argued that $L \propto A_d^{0.6}$ (Hack, 1957), particularly as drainage areas increase (i.e. elongation of basins). Since runoff is to be evaluated for a large range of drainage areas, including drainage areas corresponding to upland and channel cells, the assumption of L equal to $A_d^{0.5}$ is made for all cells in the basin. The time to equilibrium (T_e) corresponding impervious runoff conditions and a given rainfall intensity (i), for any point in the basin with drainage area (A_d), is thus evaluated as:

$$T_e \equiv \left(\frac{\bar{n}_{ol} A_d^{1/2}}{i^{2/3} \bar{S}^{1/2}} \right)^{3/5} \quad (6.2)$$

As shown in Eq. (6.2), the time to equilibrium decreases as rainfall intensity increases. In relation to the drainage area, equilibrium is reached more quickly in upland areas, where A_d values are small, while the longest time to equilibrium corresponds to the outlet, which drains the largest area.

The approach used in this chapter is as follows. Raster maps displaying the drainage areas (A_d) corresponding to individual basins are developed for the two

watersheds described in Chapters 4 and 5. Maps representing the spatial distributions of Q_e and T_e for given rainfall intensities are also generated, based on Eq. (6.1) and (6.2). Impervious simulations are then performed with rainstorms of varying durations (T_r), in order to generate a range of T^* values (where $T^* = T_r/T_e$) representing partial and complete equilibrium conditions. Results from both watersheds were then compiled to evaluate a relationships between Q^* and T^* corresponding to complete and partial equilibrium conditions, assuming impervious runoff.

6.2 GOODWIN CREEK

6.2.1 EVALUATING COMPLETE EQUILIBRIUM CONDITIONS

For a given constant rainfall intensity, the equilibrium discharge (Q_e) and the time equilibrium (T_e) can be evaluated for any point in the watershed, assuming an average Manning overland roughness (\bar{n}_{o1}), and average upland slope (\bar{S}), and knowing the drainage area (A_d) corresponding to that point. The theory was tested by assuming impervious conditions on the basin and by applying Eq. (6.1) and (6.2). The equilibrium discharge at the outlet of the watershed, which drains a total area of 21 km², for a constant rainfall intensity of 0.5 in/hr ($3.528 \cdot 10^{-6}$ m/s) is calculated as:

$$Q_e = 0.000003528 \frac{\text{m}}{\text{s}} * 21,000,000 \text{ m}^2 \quad (6.3)$$

$$Q_e = 74 \text{ m}^3 / \text{s} \quad (6.4)$$

The time to equilibrium at the outlet is calculated assuming an average overland roughness coefficient of 0.08, an average slope of 0.015, and a runoff length of $A_d^{0.5}$ (where $A_d = 21 \text{ km}^2$):

$$T_e = \left(\frac{0.08 * 4,583}{0.000003528^{2/3} 0.015^{1/2}} \right)^{3/5} \quad (6.5)$$

$$T_e = 18,479 \text{ sec} = 308 \text{ min} = 5 \text{ hr } 8 \text{ min} \quad (6.6)$$

According to the above calculations, a rainstorm with a constant rainfall intensity of 0.5 in/hr and lasting longer than 308 min should result in equilibrium conditions at the outlet and throughout the basin. In order to ensure reaching equilibrium conditions throughout the basin, a rainfall duration of 900 min (15 hr) and an intensity of 0.5 in/hr was used in simulating impervious runoff. Equilibrium conditions were reached throughout the basin, as shown in Fig. 6.1. The drainage areas corresponding to the outlet, gage 3, gage 5, and gage 12 are approximately 21 km², 9 km², 4 km², and 0.3 km². The maximum runoff rates at the respective gages were 66 m³/s, 27 m³/s, 15 m³/s, and 1 m³/s.

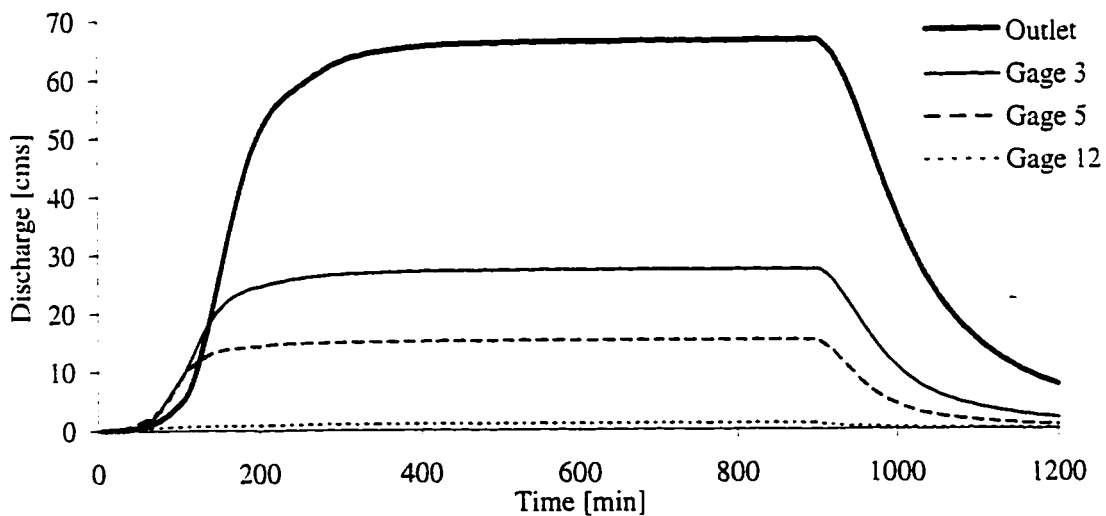


Fig. 6.1: Goodwin Creek equilibrium discharge hydrographs

Equilibrium discharge hydrographs at 832 ft and 1248 ft were identical. As expected, grid resolution did not affect the nature of the runoff hydrographs under complete equilibrium conditions.

Working within a raster-based environment, the peak discharge at every pixel was recorded for the impervious simulation. Since equilibrium has been reached, the peak discharge corresponds to the equilibrium discharge of the cell. The raster map depicting basin-wide spatial variability of Q_e , resulting from a uniform rainstorm of constant intensity, is presented in Fig. 6.2.

Equilibrium discharge is lower in the upland areas ($Q_e < 1 \text{ m}^3/\text{s}$) than in the channel ($100 \text{ m}^3/\text{s} > Q_e > 1 \text{ m}^3/\text{s}$). The highest equilibrium discharge occurs at the outlet, which drains the entire basin. The drainage area associated with each pixel is evaluated using Eq. (6.1), based on the raster map of equilibrium discharge (Fig. 6.2). The raster map depicting drainage areas associated with individual pixels is presented in Fig. 6.3.

The time to equilibrium corresponding to a uniform rainfall intensity of 0.5 in/hr (12.7 mm/hr) is then evaluated for every pixel by applying Eq. (6.2), based on the raster map of drainage areas (Fig. 6.3). An average value of Manning roughness and overland slope is used for all cells. The runoff length is calculated as $A_d^{0.5}$, as described in Section 6.1. Results are shown in Fig. 6.4. The times to equilibrium corresponding to individual cells throughout the basin range from 15 min in upland areas to 300 min at the outlet.

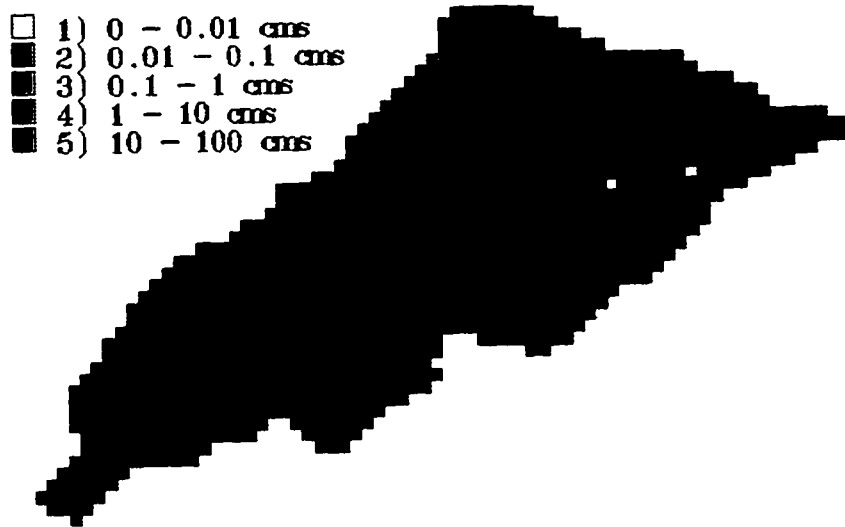


Fig. 6.2: Spatial variability of equilibrium discharge on the Goodwin Creek basin

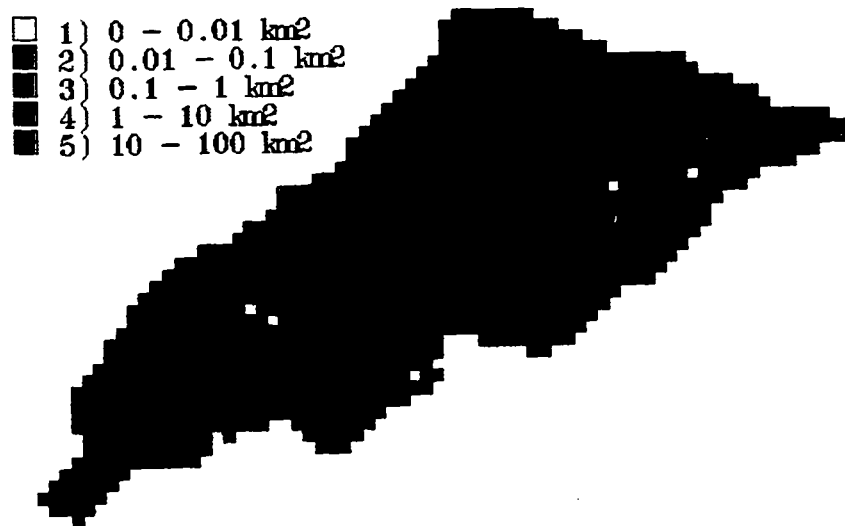


Fig. 6.3: Spatial variability of drainage area on the Goodwin Creek basin

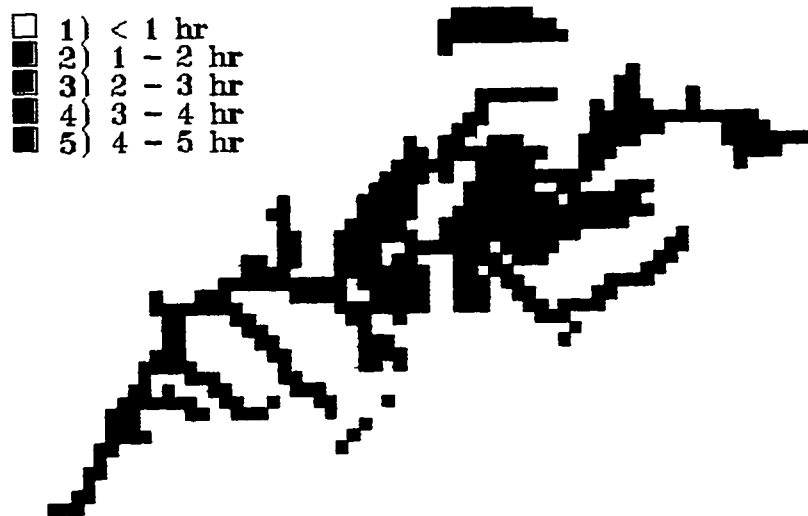


Fig. 6.4: Spatial variability of time to equilibrium on the Goodwin Creek basin

The drainage area (A_d) corresponding to individual grid cells will always be the same value, regardless of rainfall intensity. Equilibrium discharge (Q_e) and time to equilibrium (T_e) will vary as a function of rainfall intensity. Raster maps describing Q_e , A_d , T_e , and were generated at a 832 ft grid size and a 1248 ft grid size, using the techniques described above. Basin-wide Q_e values were evaluated as the peak runoff rates on individual cells, corresponding to a rainfall event of 0.5 in/hr and lasting 15 hr, assuming impervious conditions. The equilibrium discharge values were then used to generate raster maps depicting the drainage areas and times to equilibrium of individual cells. A comparison of the spatial basin-wide distributions of Q_e , A_d , and T_e at different grid resolutions is presented in Fig. 6.6a, 6.6b, and 6.6c.

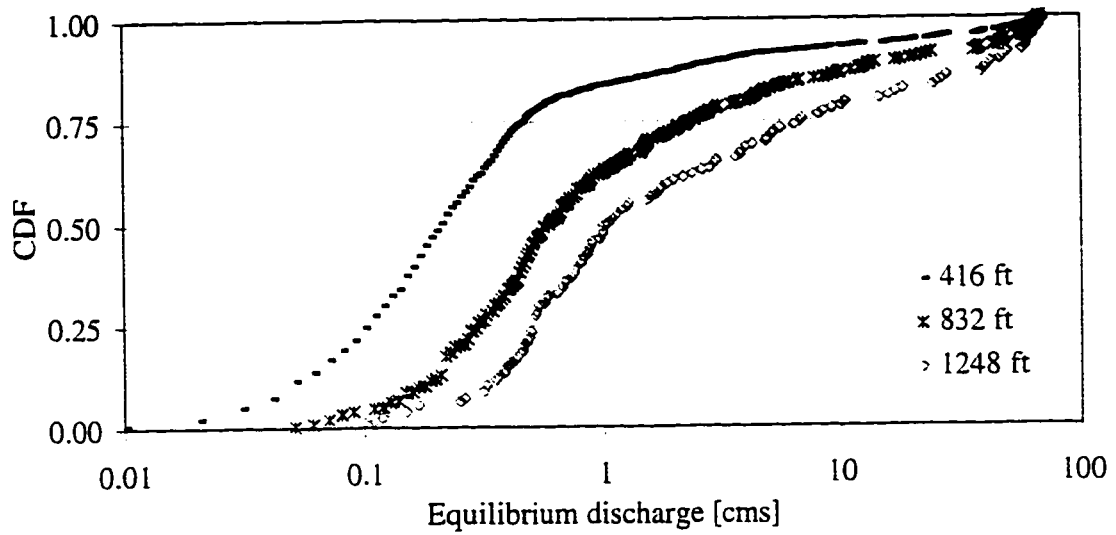


Fig. 6.6a: Distribution of basin-wide Q_e at increasing grid size, Goodwin Creek

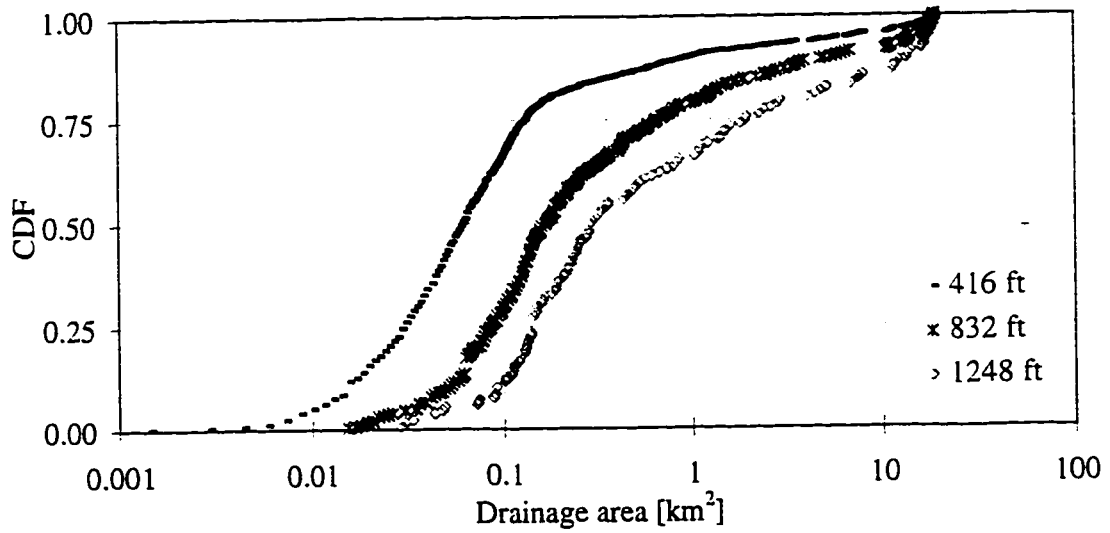


Fig. 6.6b: Distribution of basin-wide A_d at increasing grid size, Goodwin Creek

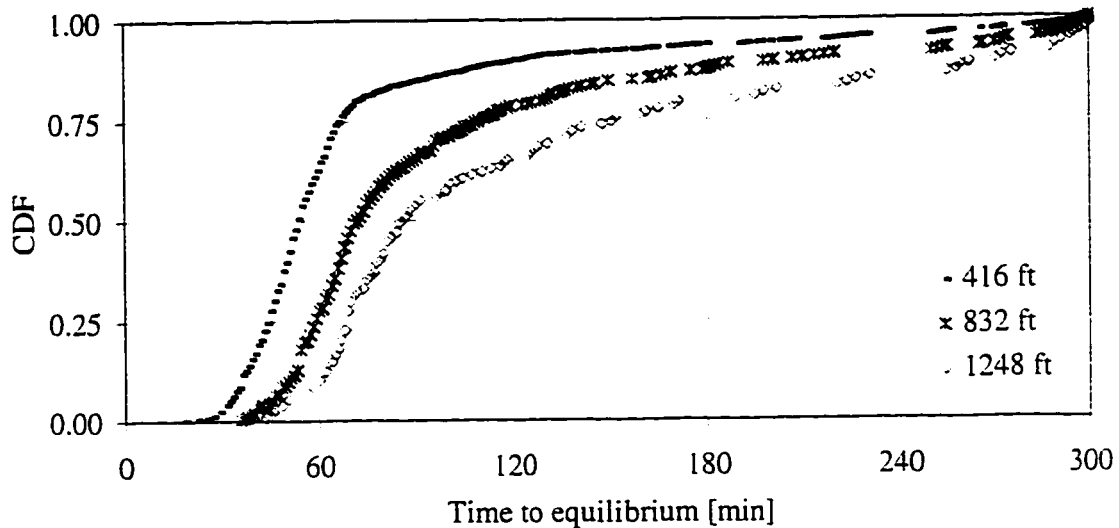


Fig. 6.6c: Distribution of basin-wide T_e at increasing grid size, Goodwin Creek

The effect of grid size on drainage area is to increase the areas associated with individual cells. At a 416 ft grid size, 50 percent of the cells (CDF = 0.5) have drainage areas less than 0.06 km^2 , while at the coarser resolutions 50 percent of the cells have drainage areas less than 0.2 km^2 and 0.3 km^2 . These cells represent upland runoff conditions. Since time to equilibrium and equilibrium discharge are directly related to drainage area, with $T_e \propto A_d^{0.3}$ and $Q_e \propto A_d$, similar patterns are seen in the distributions of time to equilibrium and equilibrium discharge at increasing grid size. Larger grid sizes result in higher values of drainage areas corresponding to individual cells, and therefore longer times are required before equilibrium is reached, particularly in upland areas. The implication of these results is that in order for equilibrium conditions

to exist in upland areas, using large grid sizes, long rainfall durations and/or high intensity rainfall events will be required.

6.2.2 PEAK DISCHARGE AS A FUNCTION OF T^*

Once equilibrium conditions (Q_e and T_e) had been determined for each pixel in the basin, simulations for a range of rainfall durations (T_r) were performed in order to evaluate Q^* as a function of T^* (where $Q^* = Q_p/Q_e$ and $T^* = T_r/T_e$). A constant rainfall intensity of 0.5 in/hr was used and the rainfall events lasted anywhere from 10 min to 2 hr. Peak discharges (Q_p) at every pixel were recorded for each simulation. The ratios of Q_p/Q_e were then plotted as a function of T_r/T_e , where Q_e and T_e were determined from raster maps such as the ones presented in Fig. 6.2 and 6.4. The results from the impervious simulations with $T_r = 40, 60, 80$ min are summarized in Fig. 6.7a-6.7c, for the three grid resolutions used in the analysis.

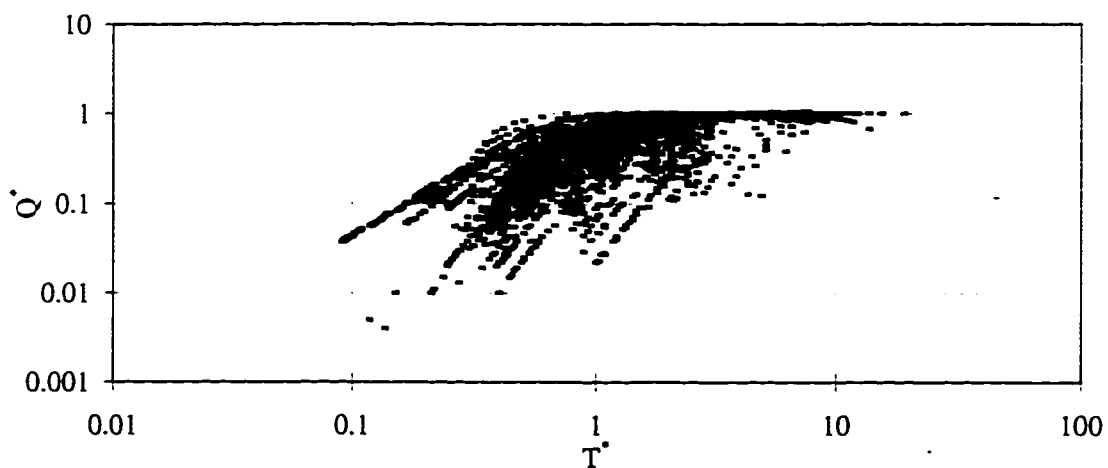


Fig. 6.7a: Peak discharge assuming impervious conditions (416 ft grid size)

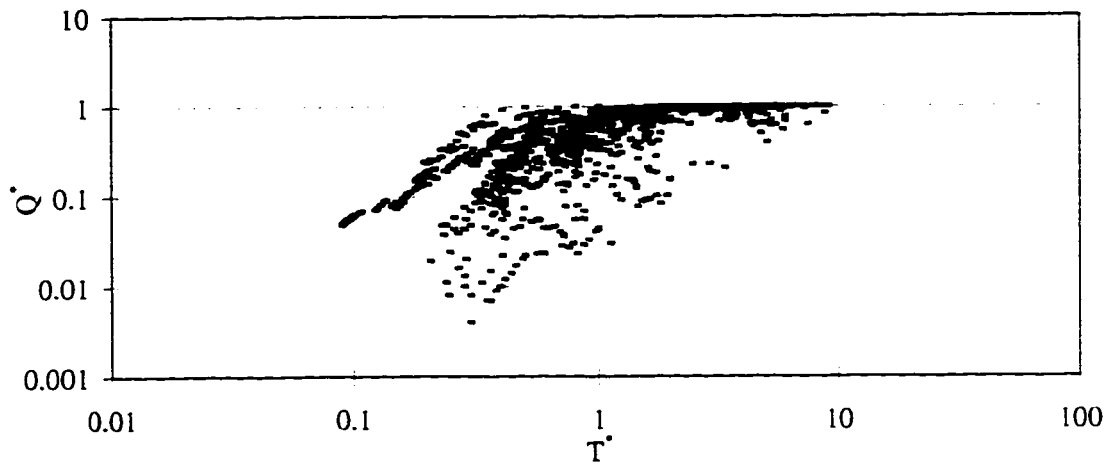


Fig. 6.7b: Peak discharge assuming impervious conditions (832 ft grid size)

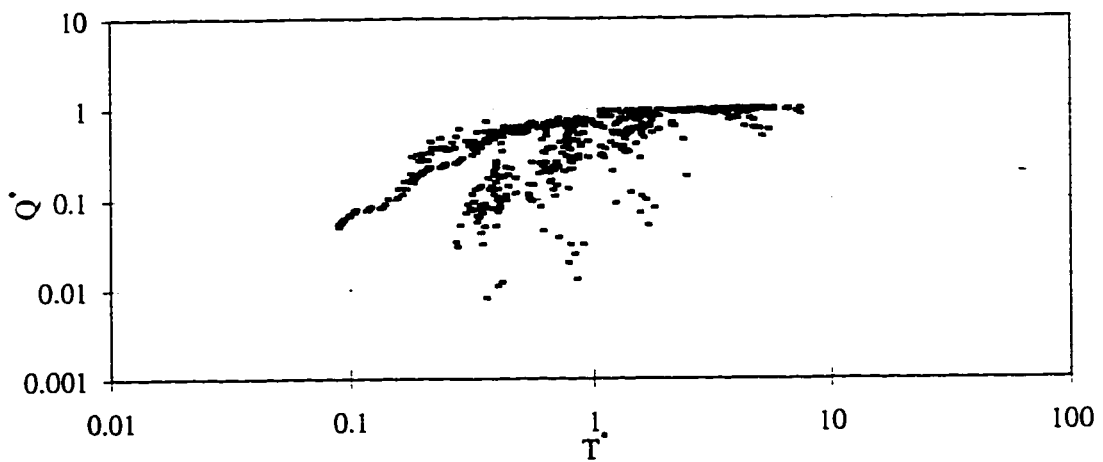


Fig. 6.7c: Peak discharge assuming impervious conditions (1248 ft grid size)

During the shorter rainstorm events, $T^* < 1$ on most of the grid cells, resulting in partial equilibrium conditions. During the longer rainstorm events, a larger percentage of the grid cells reached equilibrium. As seen in Fig. 6.7a - 6.7c, grid size does not have much of an affect on the relationships between Q^* and T^* , for both partial ($T^* < 1$) and complete ($T^* > 1$) equilibrium conditions. The results at coarser resolutions mimic those at the finest resolution, with fewer data points due to the reduced number of cells representing the watershed. As expected, Q^* tends towards 1 when $T^* > 1$, and Q^* never exceeds 1. Although a range of Q^* values exist even when complete equilibrium is reached, the empirical points tend towards a single value of Q^* when $T^* = 10$ (see Fig. 6.7a). The minimum value of T^* occurs at the outlet, where T^* and Q^* are both less than 0.1, and partial equilibrium conditions dominate the nature of runoff.

The results from impervious simulations on Goodwin Creek reflect theoretical solutions to the evaluation of complete and partial equilibrium conditions, indicating that the initial assumptions made in applying the concept are acceptable. These assumptions include the use of average values of overland slope (\bar{S}) and overland roughness coefficient (\bar{n}_{ol}), and the assumption that runoff length (L) is equal to $A_d^{0.5}$.

6.3 HICKAHALA - SENATOBIA

6.3.1 EVALUATING COMPLETE EQUILIBRIUM CONDITIONS

Assuming impervious conditions, equilibrium discharge (Q_e) and time to equilibrium (T_e) at the outlet of the Hickahala-Senatobia basin can also be evaluated. The watershed drains a total area of 560 km². The equilibrium discharge at the outlet of the basin, assuming a constant rainfall intensity of 0.5 in/hr, is calculated as:

$$Q_e = 0.000003528 \frac{\text{m}}{\text{s}} * 560,000,000 \text{ m}^2 \quad (6.7)$$

$$Q_e = 1976 \text{ m}^3 / \text{s} \quad (6.8)$$

The time to equilibrium at the outlet is calculated assuming an average Manning roughness of 0.08, an average slope of 0.01, and a runoff length equal to $A_d^{0.5}$ such that:

$$T_e = \left(\frac{0.08 * 23,664}{0.000003528^{2/3} * 0.01^{1/2}} \right)^{3/5} \quad (6.9)$$

$$T_e = 55,885 \text{ sec} = 931 \text{ min} = 15 \text{ hr } 30 \text{ min} \quad (6.10)$$

According to the above calculations, a rainstorm with a constant rainfall intensity of 0.5 in/hr and lasting longer than 16 hr should result in equilibrium conditions at the outlet and throughout the basin. The total volume of water corresponding to a constant rainstorm intensity of 0.5 in/hr, lasting 16 hr, would be approximately 10^8 m^3 . It was not possible to simulate an event of such a magnitude on Hickahala-Senatobia, nor was the equilibrium outlet discharge of $1976 \text{ m}^3/\text{s}$ feasible, given the hydraulic geometry of the channel network. Rather than simulating equilibrium conditions throughout the basin, as was the procedure used on Goodwin Creek, an alternative method was applied in order to determine A_d , Q_e , and T_e for all cells within the basin.

Within GRASS the program *r.watershed* (see Appendix D), uses a digital elevation map (DEM) to evaluate the accumulated number of cells draining to any given cell. Knowing the accumulated number of cells draining to each grid cell, a raster map depicting the drainage area (A_d) associated with every pixel can be created. This method was used to develop raster maps representing drainage areas (A_d) corresponding to individual grid cells in the Hickahala-Senatobia basin.

The location of the channel network was defined in the DEM by using channel bed elevations in the grid cells through which the channel network passed. This ensured that water drained into the channels and through the network towards the outlet. The raster map showing the spatial distribution of A_d at a 1000 ft grid size is presented in Fig. 6.8. At this resolution, most upland cells have drainage areas less than 1 km². Drainage areas corresponding to channel cells range from 10 km² to 560 km².

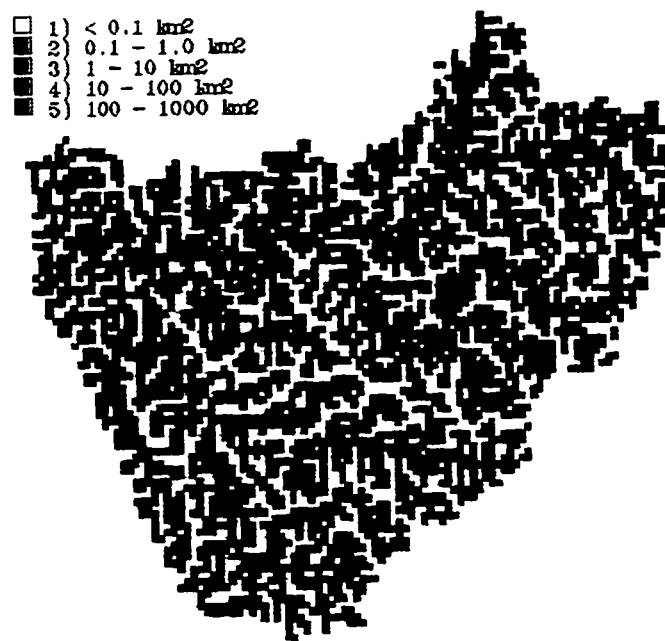


Fig. 6.8: Spatial variability of drainage area on the Hickahala-Senatobia basin

Once drainage areas per pixel were determined, the equilibrium discharge and the time to equilibrium corresponding to a constant rainstorm intensity of 0.5 in/hr were calculated. Eq. (6.1) and (6.2) were applied to every cell in the basin, using the GRASS program *r.mapcalc* (see Appendix D for details), assuming a runoff length of $A_d^{0.5}$ and average values of overland roughness and slope. The raster maps representing the spatial

variability of Q_e and T_e using a 1000 ft grid size are shown in Fig. 6.9 and 6.10. In upland areas, most grid cells have equilibrium runoff rates less than $10 \text{ m}^3/\text{s}$ and times to equilibrium less than 4 hr. In the channel network, equilibrium runoff rates exceed $100 \text{ m}^3/\text{s}$ and times to equilibrium are greater than 6 hr.

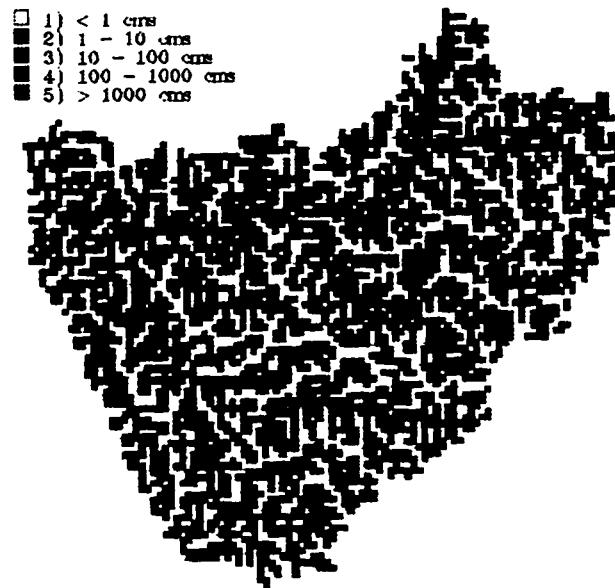


Fig. 6.9: Spatial variability of equilibrium discharge on the Hickahala-Senatobia basin

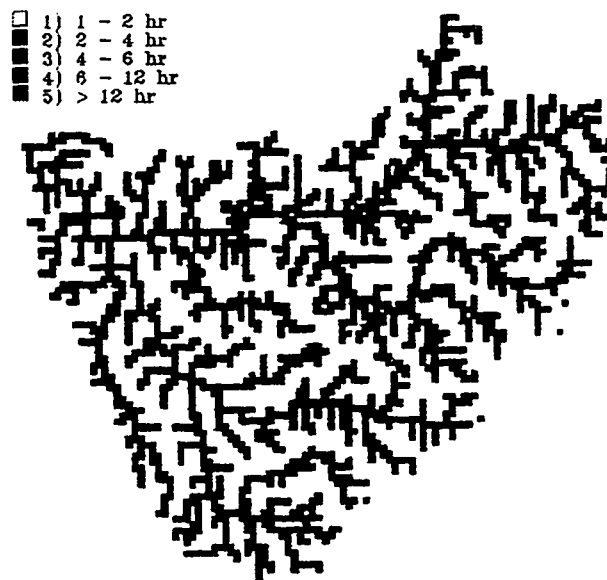


Fig. 6.10: Spatial variability of the time to equilibrium on the Hickahala-Senatobia basin

A similar analysis was performed using a 2000 ft and a 3000 ft grid size. The drainage areas corresponding to each grid cell were evaluated using the GRASS program *r.watershed*. Time to equilibrium and equilibrium discharge for individual cells were then calculated, assuming a constant rainfall intensity of 0.5 in/hr. Comparisons of the spatial basin-wide distributions of A_d , Q_e , and T_e are presented in Fig. 6.11a-6.11c.

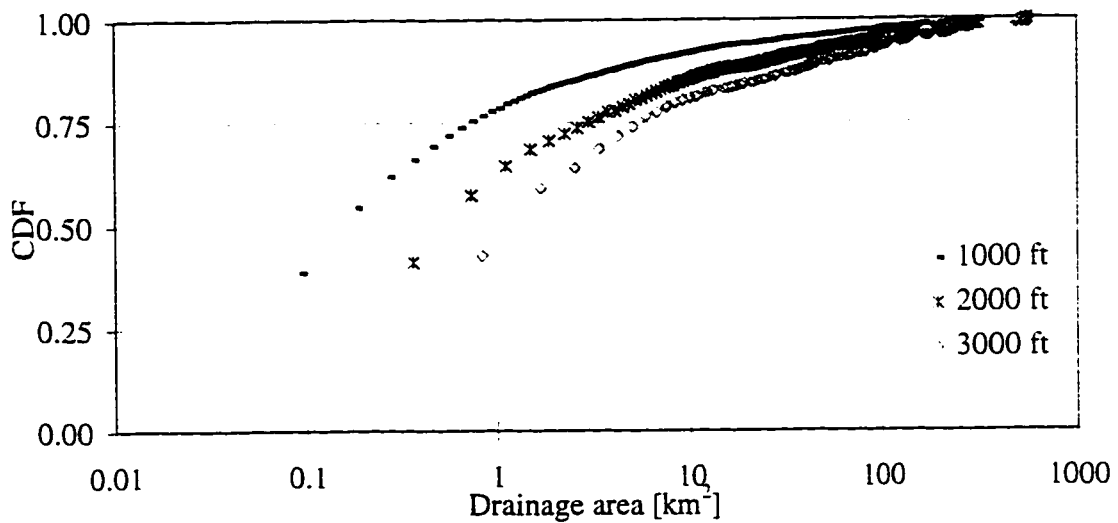


Fig. 6.11a: Distribution of basin-wide A_d at increasing grid size, Hickahala-Senatobia

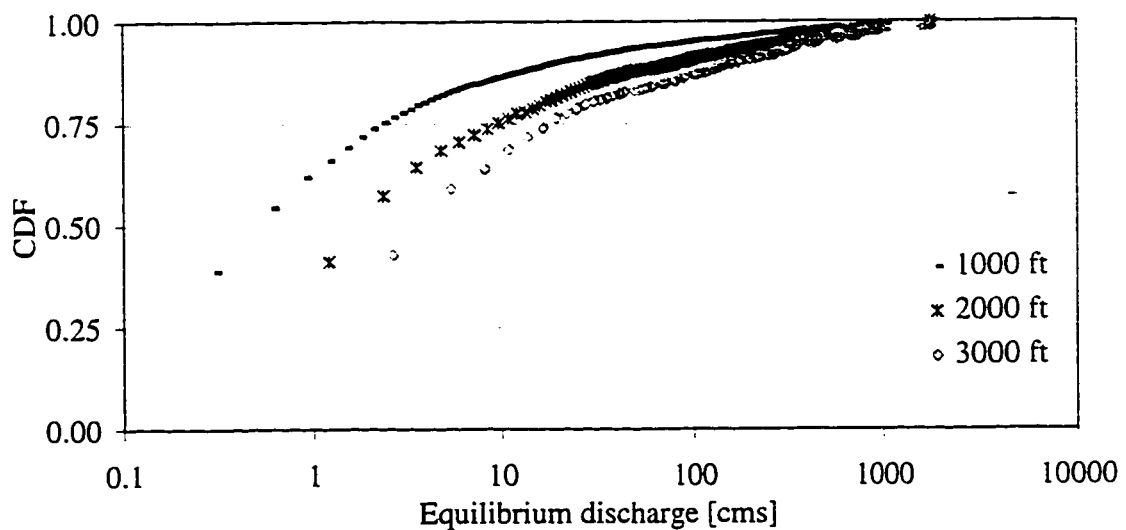


Fig. 6.11b: Distribution of basin-wide Q_e at increasing grid size, Hickahala-Senatobia

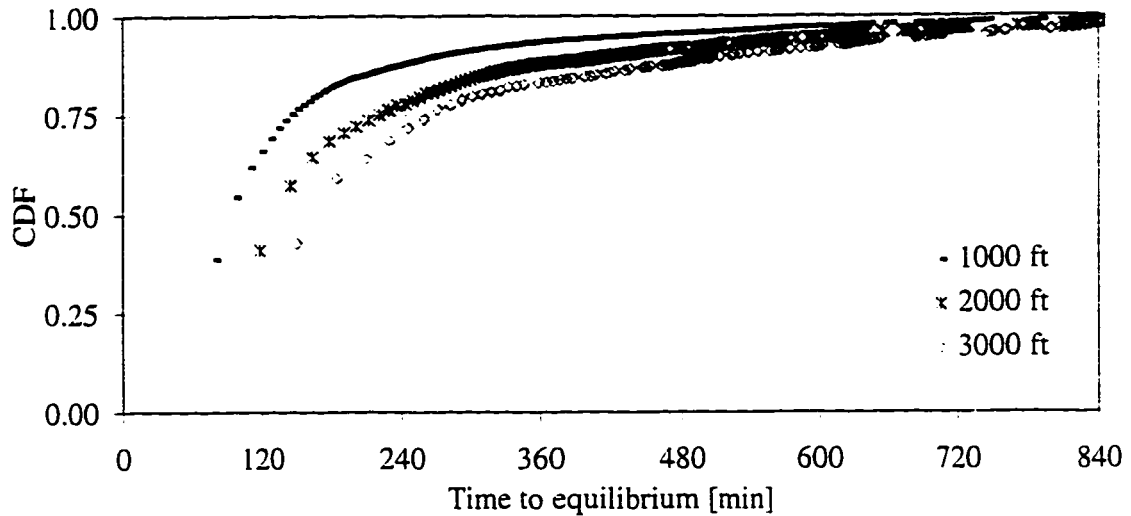


Fig. 6.11c: Distribution of basin-wide T_e at increasing grid size, Hickahala-Senatobia

The smallest drainage area at each grid size corresponds to the drainage area of a single cell. The cells with drainage areas less than 10 km^2 are overland cells. Grid resolution has more of an effect on drainage patterns in upland areas than it does on drainage patterns of channel cells, where $A_d > 10 \text{ km}^2$. The distribution of A_d at increasing grid size is reflected in the distributions of Q_e , and T_e , since $Q_e \propto A_d$ and $T_e \propto A_d^{0.3}$.

6.3.2 PEAK DISCHARGE AS A FUNCTION OF T^*

Partial and complete equilibrium conditions on Hickahala-Senatobia were simulated by applying rainfall events of constant intensity and durations ranging from 15 min to 2hr. Peak discharge (Q_p) for each simulation was recorded at every pixel. The values of Q^* were then plotted as a function of T^* , where Q_e and T_e were determined from raster maps such as the ones shown in Fig. 6.9 and Fig. 6.10. Results from impervious simulations, with $T_r = 1 \text{ hr}$, at the three resolutions used in the analysis are shown in Fig.

6.12a-6.12c. Since the minimum value of T_e , basin-wide, is greater than 1 hr (see Fig. 6.10), T^* is always less than 1 and all cells are in partial equilibrium.

At the three resolutions channel cells and overland cells show similar trends. Peak runoff rates are within the same range ($0.001 < Q^* < 1$), although at the finer resolution there is greater variability in the distribution of Q^* . The maximum value of T^* changes as a function of grid resolution because it corresponds to cells with the smallest drainage area (where $A_d = 1$ cell).

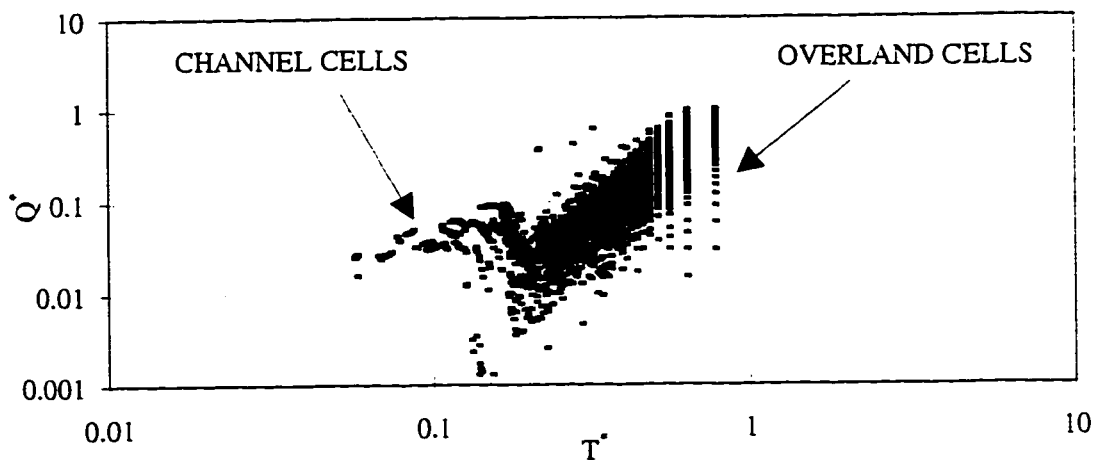


Fig. 6.12a: Peak discharge assuming impervious conditions (1000 ft grid size)

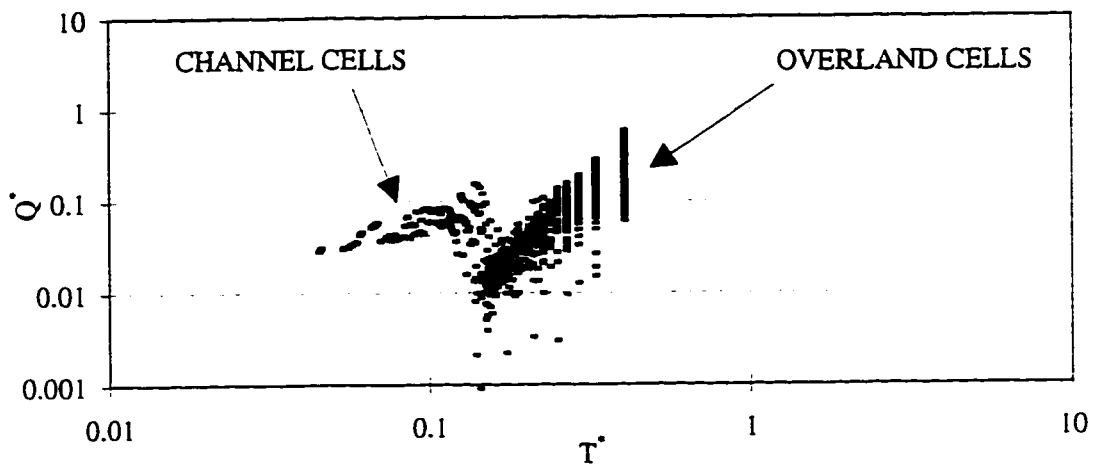


Fig. 6.12b: Peak discharge assuming impervious conditions (2000 ft grid size)

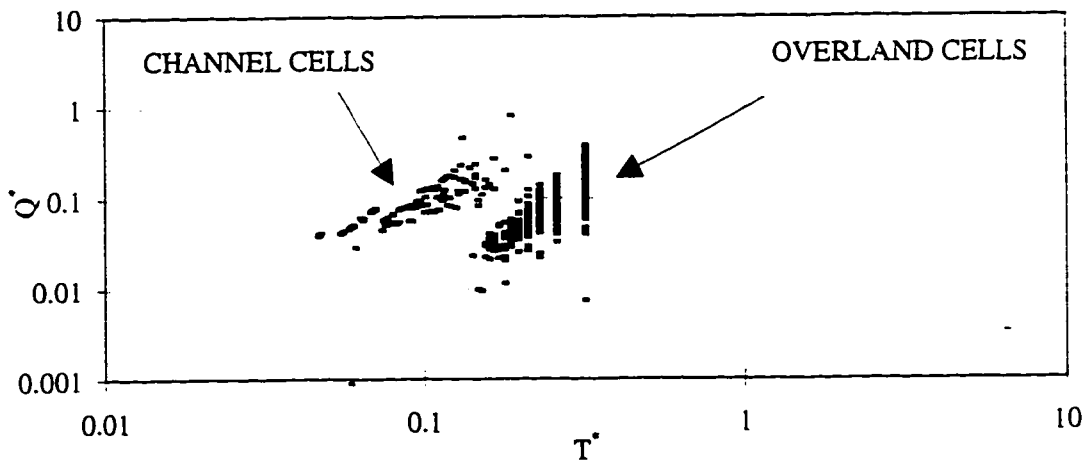


Fig. 6.12c: Peak discharge assuming impervious conditions (3000 ft grid size)

The results at a 1000 ft grid size, with $T_r = 15$ min and $T_r = 120$ min, are shown in Fig. 6.13 in order to further emphasize the difference between the runoff response of channel cells and the response of overland cells. Channel cells have smaller T^* values

and higher Q^* values than the overland cells. The time required to reach equilibrium in the channel network is longer, since these cells drain larger areas, resulting in smaller T_r/T_e values. The peak runoff rates in the network are high, resulting in higher Q_p/Q_e values, because runoff becomes concentrated in the channel cells and flow is confined by the dimensions of the channel cross-section. As seen in Fig. 6.12a, 6.12b, 6.12c, and 6.13, unique relationships define the behavior of Q^* as a function of T^* for channel cells and for overland cells.

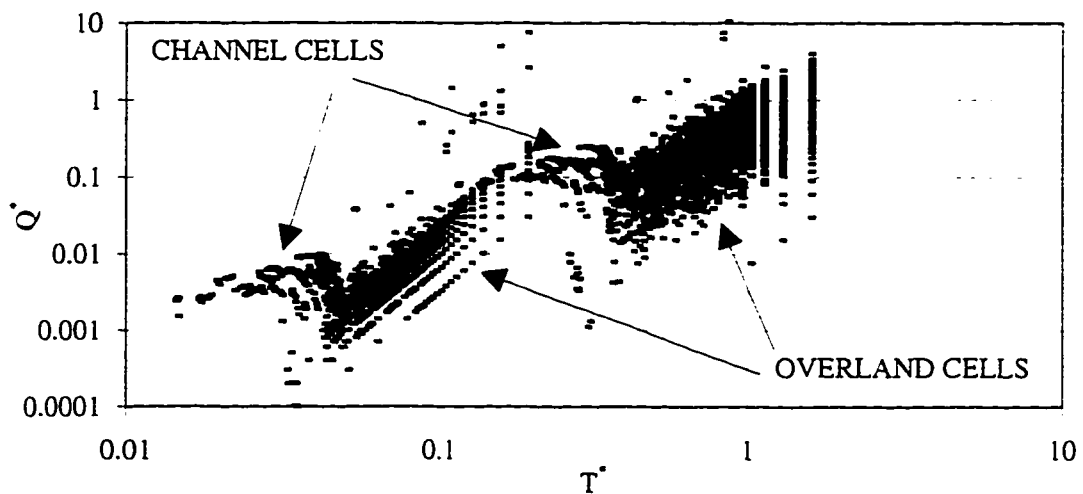


Fig. 6.13: Range of peak overland discharge and peak channel discharge

6.4 EFFECTS OF GRID SIZE ON CELL DRAINAGE AREA

Two methods were used in determining the drainage areas corresponding to individual cells. On Goodwin Creek, equilibrium runoff conditions could be simulated for the entire basin. The equilibrium discharge was then used to evaluate drainage area. On Hickahala-Senatobia, equilibrium conditions could not be simulated for the entire

basin, due to long time required to reach equilibrium at the outlet (15 hr). Drainage areas on the basin were instead evaluated using the GRASS program *r.watershed* (see Appendix D for details). A comparison was made of the drainage areas determined using the *r.watershed* program (*r.watershed*) and the drainage areas calculated using the CASC2D model ($A_d = Q_e/i$), for Goodwin Creek conditions. As seen in Fig. 6.14, the results from the two methods are similar for drainage areas larger than 1 km² (channel cells) but when drainage areas are less than 1 km² (overland cells) the methods do not have similar results.

As noted previously (see Section 6.1), methods such as the GRASS program *r.watershed*, which evaluate drainage area as a function of topography are limiting in that flow can only be routed in a single direction and the minimum drainage area achievable is the area corresponding to a single cell. As seen in Fig. 6.14, the CASC2D method of evaluating drainage areas leads to minimum drainage areas less than the area of a single cell, since this method allows for two-dimensional flow routing. In determining the distribution of drainage areas corresponding to grid cells in the Hickahala-Senatobia basin, the *r.watershed* program was used, with the acknowledgment that drainage areas defined for upland regions may not correspond directly to the drainage patterns of overland flow routed using the CASC2D model.

Results on Goodwin Creek are also used to show the difference between drainage areas corresponding to overland cells and drainage areas corresponding to channel cells. Fig. 6.15a and 6.16b show the effects of increasing grid size on overland and channel cells.

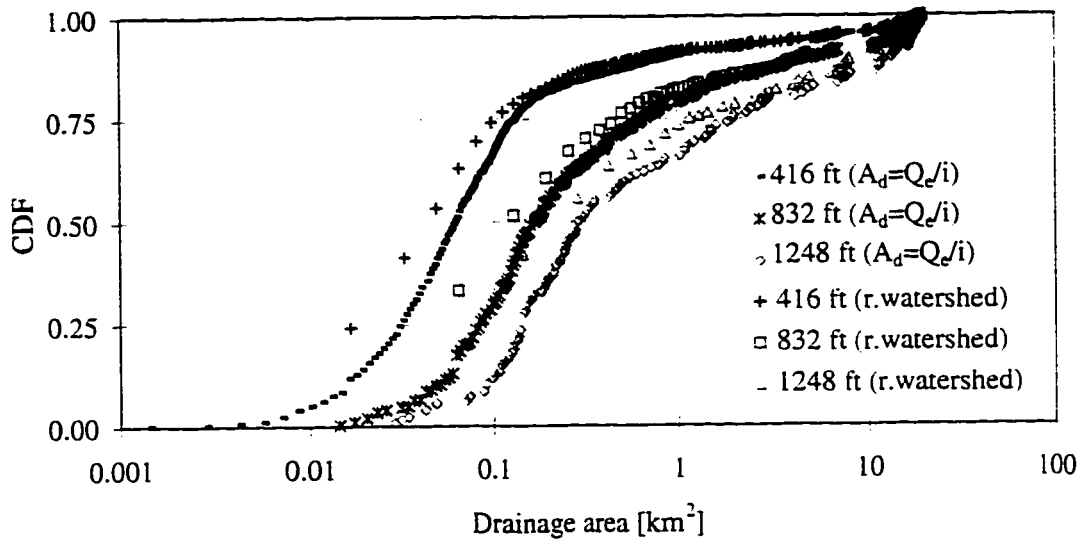


Fig. 6.14: Distribution of A_d on Goodwin Creek as determined by GRASS

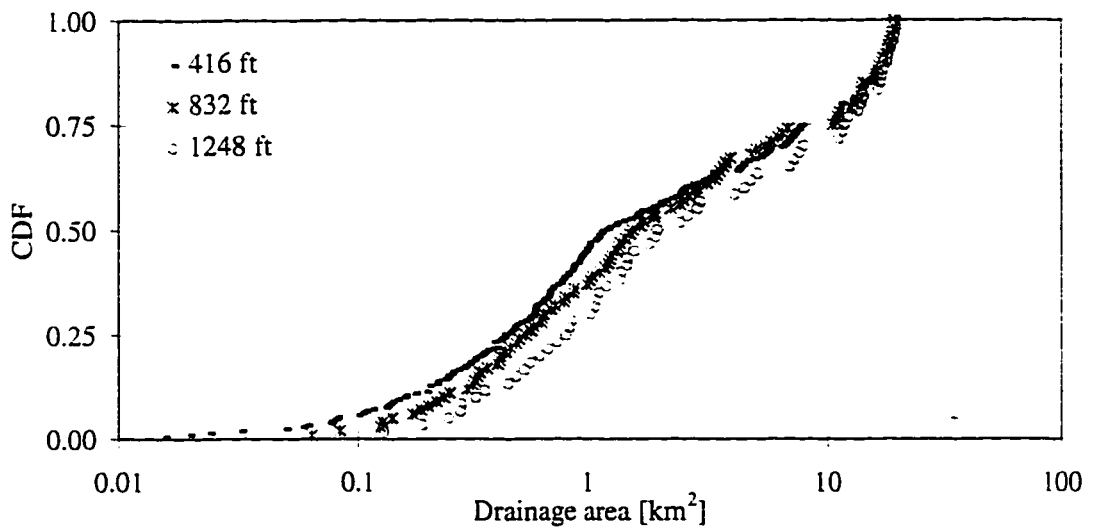


Fig. 6.15a: Distribution of A_d corresponding to Goodwin Creek channel cells

Channel drainage patterns are similar at all resolutions, particularly for CDF values greater than 0.50 (towards the outlet of the basin). At a 416 ft grid size there is clearly a change in the nature of the distribution of drainage areas at 1 km^2 . Overland drainage patterns are affected by grid resolution. The coarser resolutions lead to larger

drainage areas associated with individual cells. The fine resolution provides a smoother description of drainage patterns. Note that drainage areas corresponding to overland cells are less than 1 km^2 .

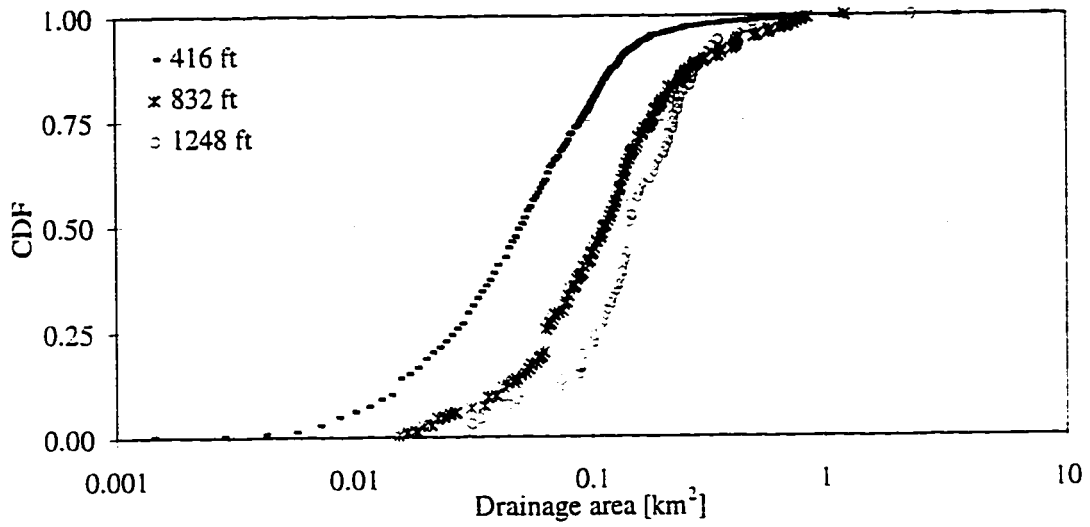


Fig. 6.15b: Distribution of A_d corresponding to Goodwin Creek overland cells

The distribution of drainage areas was also evaluated at a 100 ft grid size for Goodwin Creek. A comparison of the distribution of drainage areas for Goodwin Creek and Hickahala-Senatobia, using grid sizes ranging from 100 ft to 3000 ft, shows that the tendency at increasing grid sizes is for drainage areas to increase (Fig. 6.16a). Drainage patterns on large watersheds such as Hickahala-Senatobia are similar to those on smaller watersheds, particularly when drainage areas exceed 0.1 km^2 . On both watersheds, overland cells accounted for at least 50 percent (CDF = 0.5) of the total number of cells. The effect of grid size is most noticeable on these cells. Channel cells represented the upper 20 percent of the drainage area distribution (CDF > 0.8), and were not as influenced by grid resolution. Since the time to equilibrium and equilibrium discharge

are both related to A_d , the effect of grid resolution is not expected to be significant when runoff is evaluated at the outlet, due to similarities in the drainage patterns of channel cells.

Assuming that the area of a single grid cell is equal to A_g , the distribution of A_d/A_g is evaluated at each resolution. The results, as shown in Fig. 6.16b, indicate that similarity in drainage patterns exists at increasing grid size, regardless of the watershed.

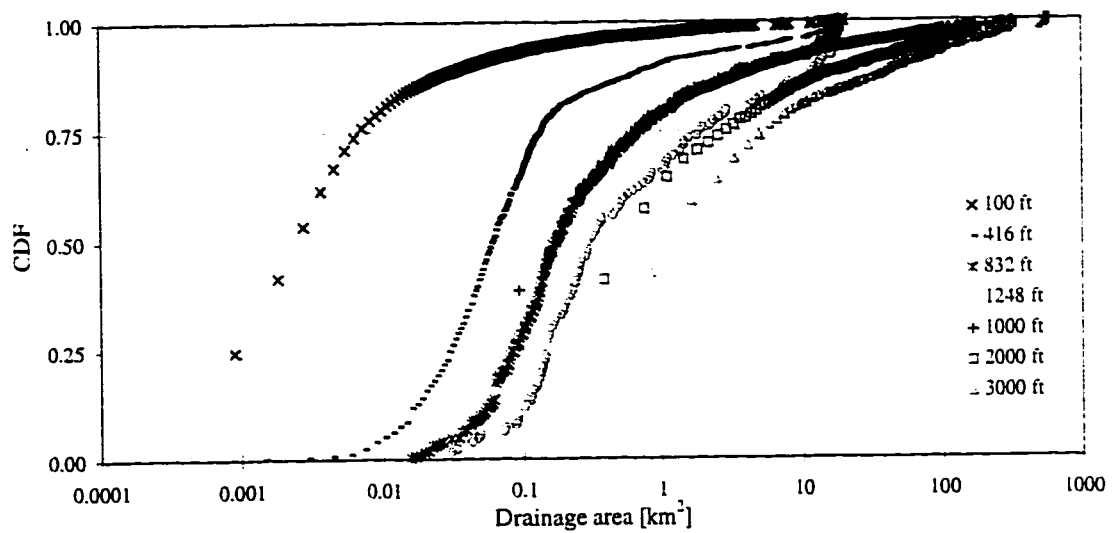


Fig. 6.16a: Distribution of A_d as a function of grid resolution

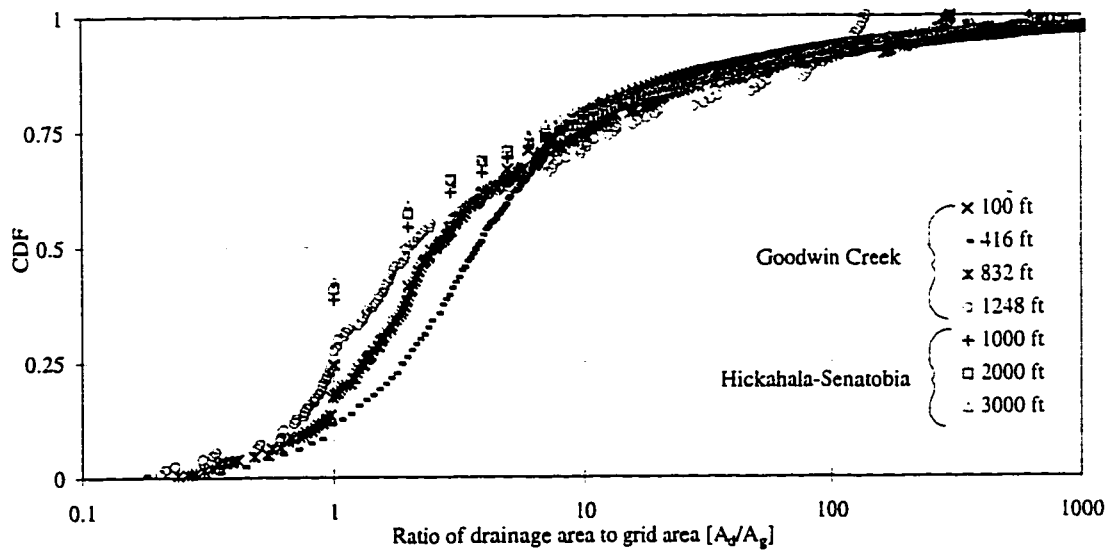


Fig. 6.16b: Distribution of A_d/A_g as a function of grid resolution

On Goodwin Creek, channel cells had minimum drainage areas (A_{d_min}) of approximately 0.1 km^2 (see Fig. 6.15a). On Hickahala-Senatobia, due to the size of the watershed, the minimum drainage area corresponding to channel cells was set at 10 km^2 . These minimum drainage areas allowed for detailed modeling of channel routing conditions. At a 416 ft grid size, the total number of channel cells on Goodwin Creek was 212 cells (see Table 4.1). At a 1000 ft grid size, the total number of channel cells on Hickahala-Senatobia was 484 cells (see Table 5.1). In modeling channel routing conditions, channel characteristics (width, depth, slope, roughness coefficient) had to be defined for every channel cell. This was feasible on Hickahala-Senatobia, having assumed a minimum drainage area of 10 km^2 for channel cells. If a threshold of 0.1 km^2 had been used, the number of channel cells would have increased dramatically.

Based on the definition of Goodwin Creek and Hickahala-Senatobia channel networks, for modeling purposes, an empirical equation was developed to be used in determining the minimum drainage area (A_{d_min}) corresponding to the initiation of the channel network. The minimum drainage area is evaluated as a function of the total drainage area of the basin (A_{d_bas}). Using the Goodwin Creek and Hickahala-Senatobia total drainage areas of 21 km^2 and 560 km^2 , with minimum drainage areas of 0.1 km^2 and 10 km^2 , the following equation was defined:

$$A_{d_min} = 0.0015 A_{d_bas}^{1.4} \quad (6.11)$$

where A_{d_min} and A_{d_bas} are both in km^2 .

Fig. 6.17 shows A_{d_min} as a function of A_{d_bas} , for drainage areas up to $10,000 \text{ km}^2$. The points corresponding to the Goodwin Creek and Hickahala-Senatobia are specified on the figure.

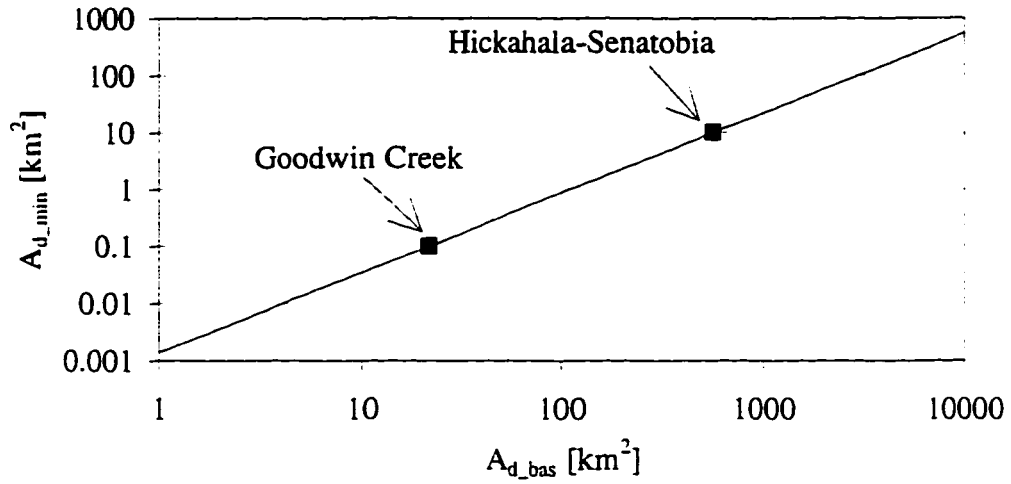


Fig. 6.17: Defining the minimum channel drainage area as a function of total area

The minimum runoff length (L_{d_min}) associated with A_{d_min} is assumed to be $A_{d_min}^{0.5}$, as has been the convention throughout this study (see Section 6.1). Based on Eq. (6.11) the equation used to evaluate L_{d_min} is:

$$L_{d_min} = (0.0015 A_{d_bas}^{1.4})^{0.5} \quad (6.12a)$$

$$L_{d_min} = 0.04 A_{d_bas}^{0.7} \quad (6.12b)$$

where L_{d_min} in km and A_{d_bas} in km^2 .

Minimum runoff length is plotted as a function of total drainage area in Fig. 6.18, with the lengths corresponding to Goodwin Creek and Hickahala-Senatobia shown on the graph. Although Eq. (6.11), (6.12a), and (6.12b) have been empirically derived, they can be used as a guideline in evaluating appropriate thresholds for the definition of the channel network on large watersheds. This is important in order to be able to simulate channel routing conditions using models such as CASC2D.

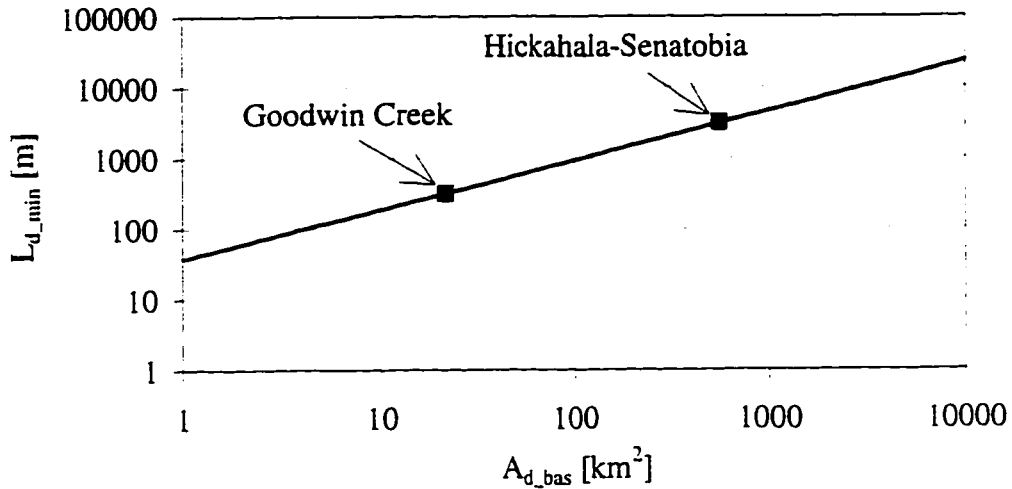


Fig. 6.18: Runoff length as a function of total drainage area

6.5 ANALYSIS OF IMPERVIOUS RUNOFF ON TWO WATERSHEDS

The results for all impervious simulations of Q^* as a function of T^* , for partial and complete equilibrium conditions on both watersheds, were evaluated. Equations were empirically derived to describe the nature of runoff hydrographs. Under complete equilibrium, when $T^* > 1$, all cells tend toward a Q^* value of 1.0. Peak discharge (Q_p) is equal to equilibrium discharge (Q_e). The dimensionless parameter representing complete equilibrium discharges (Q_{ce}^*) is evaluated as:

$$Q_{ce}^* = \frac{Q_p}{Q_e} = 1 \quad (6.13)$$

Under partial equilibrium conditions ($T^* < 1$), peak discharge conditions are defined separately for upland cells and for channel cells. In upland areas, a range of Q^* values can occur, where the maximum value is Q_{max}^* and the minimum value is Q_{min}^* . In the channel network, peak discharge conditions are described using the parameter Q_{ch}^* .

The equations corresponding to partial equilibrium, derived from empirical results, are as follows:

$$Q^*_{\max} = 7.5 T^{*3} \quad (6.14)$$

$$Q^*_{\min} = 0.2 T^{*3} \quad (6.15)$$

$$Q^*_{\text{ch}} = 2.5 T^{*5/3} \quad (6.16)$$

Combining results from Goodwin Creek and Hickahala-Senatobia impervious simulations, simulated values of Q^* are plotted as a function of T^* (see Fig. 6.19). The lines corresponding to Eq. (6.14), (6.15), and (6.16) are overlaid on the empirical data values. The point corresponding to complete equilibrium conditions ($Q^*_{\text{ce}}, T^*_{\text{ce}}$) is also shown on the graph.

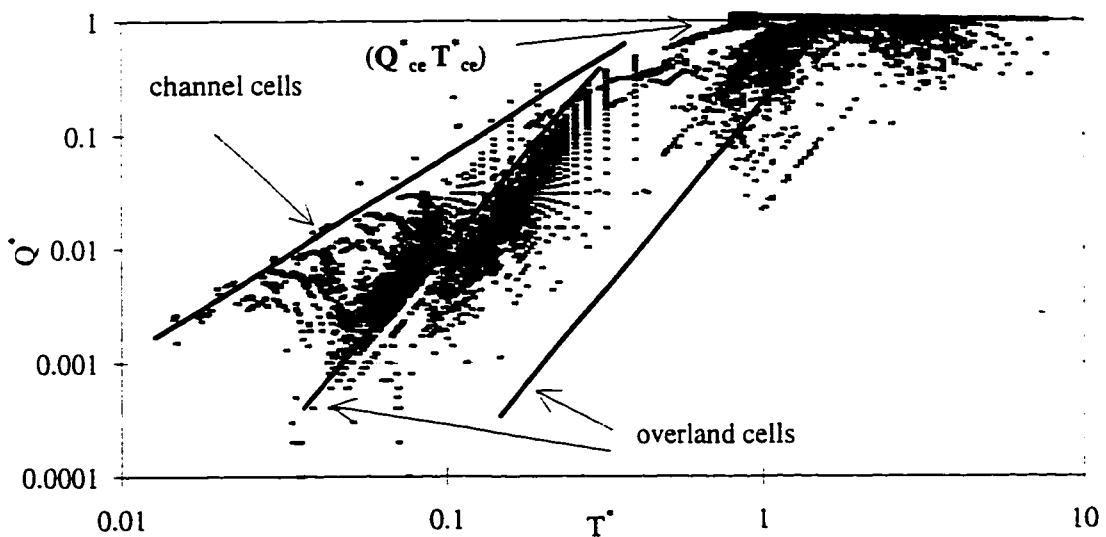


Fig. 6.19: Partial and complete equilibrium conditions on an impervious watershed

Under partial equilibrium conditions, it has been shown that discharge is evaluated as (see Section 2.4):

$$q = \alpha (i T_r^m) \quad (6.17)$$

Using the Manning resistance equation, the constants α and m are:

$$\alpha = \frac{S_f^{0.5}}{n} \quad (6.18)$$

$$m = \frac{5}{3} \quad (6.19)$$

Substituting Eq. (6.19) into Eq. (6.17), discharge is related to T_r as:

$$q \propto T_r^{5/3} \quad (6.20)$$

Therefore, relating Eq. (6.20) to the evaluation of Q^* as a function of T^* , the following relationship should exist:

$$\frac{Q_p}{Q_e} \propto \frac{T_r^{5/3}}{T_e} \quad (6.21a)$$

$$Q^* \propto T^{*5/3} \quad (6.21b)$$

As seen in Eq. (6.16), the empirical evaluation of runoff rates corresponding to channel cells results in Q^* values proportional to $T^{*5/3}$. The evaluation of runoff rates corresponding to overland cells leads to Q^* values proportional to T^{*3} , which is representative of laminar type flow (with $m = 3$). A possible explanation for this condition could be that the use of coarse resolutions in the simulations resulted in small depths associated with flow on overland cells (flow depth is uniform over the entire cell), leading to laminar-type flow.

6.6 SUMMARY

Using GRASS programs, it was possible to evaluate basin-wide values of A_d , Q_e , and T_e for individual pixels. Raster maps were generated for Goodwin Creek (see Fig.

6.2, 6.3, 6.4) and Hickahala-Senatobia (see Fig. 6.8, 6.9, 6.10). The cumulative distribution function of drainage areas at increasing grid sizes provided an indication of the effects of grid size on runoff conditions in upland areas and in the channel network. It was determined that conditions in the channel are not significantly affected by increasing grid resolutions.

All impervious simulations were performed assuming a uniform rainfall intensity. As seen in Fig. 6.19, the results indicate that when there is no temporal variability, at large values of T^* ($T^* > 10$) peak discharge conditions show very little variation. For small values of T^* ($T^* < 0.1$) there is great variability in peak discharge. Since empirical results reproduced the results expected from the theoretical development of the concept of a watershed time to equilibrium, the assumptions made in evaluating T_e (\bar{S} , \bar{n}_{01} , and $L=A_d^{0.5}$) were acceptable. Runoff conditions were evaluated using Q^* and T^* , where $Q^*=Q_p/Q_e$ and $T^*=T_r/T_e$.

The simulation of impervious watershed conditions led to the determination of unique equations governing the relationships between Q^* and T^* in upland areas and in the channel. Complete equilibrium conditions are reached when $T^*=T_{ce}^*=1$. The corresponding peak discharge condition is $Q^*=Q_{ce}^*=1$. Under partial equilibrium conditions, when $T^* < 1$, peak discharge conditions in upland areas are defined as $Q^* \propto T^{*3}$, Eq. (6.14) and Eq. (6.15), and in the channel network peak runoff conditions are defined as $Q^* \propto T^{*5/3}$, Eq. (6.16). These results are indicative of laminar-type flow in overland regions ($m=3$) and turbulent flow ($m = 5/3$) in the channel.

Chapter VII

PERVIOUS CONDITIONS

7.1 INTRODUCTION

The evaluation of runoff on pervious surfaces is complicated by the loss of water through interception, infiltration, and evapo-transpiration mechanisms. Under pervious conditions the reduced amount of water available for runoff will cause the value of Q^* to always be less than 1. Peak discharge (Q_p) will never be equal to equilibrium discharge (Q_e). In CASC2D the parameters which lead to a decrease in runoff rates, as compared to impervious conditions, are detention storage (S_d), soil hydraulic conductivity (K_s), capillary pressure (H_f), and moisture deficit (M_d).

The approach used in determining Q^* and T^* values for impervious simulations was applied on Goodwin Creek and Hickahala-Senatobia, assuming pervious conditions. Uniform rainfall events of three different intensities were simulated. The ratio of the average hydraulic conductivity (\bar{K}_s) to a uniform rainfall intensity (i) was used in selecting appropriate rainfall intensities, where \bar{K}_s was taken as the average hydraulic conductivity value corresponding to the entire watershed. The soil parameter values calibration runs on Goodwin Creek (see Table 4.4) were used to define pervious runoff conditions for both watersheds.

The rainfall rates corresponding to \bar{K}_s / i values of 0.2, 0.5, and 1.0 were 1.25 in/hr (8.8E-06 m/s), 0.50 in/hr (3.5E-06 m/s), and 0.28 in/hr (2.0E-06 m/s) respectively. The raster maps of A_d , generated in Chapter 6 (see Fig. 6.3 and 6.8), were used in calculating the basin-wide values of Q_e and T_e corresponding to impervious conditions for each of the three rainfall intensities. Simulations were performed, peak discharge (Q_p) was determined for each pixel, and the basin-wide results were presented in the form of Q^* as a function of T^* , where $Q^* = Q_p / Q_e$ and $T^* = T_r / T_e$.

Simulations were then performed in order to quantify the effects of infiltration. Conditions were first evaluated assuming a uniform rainfall intensity (no temporal variability). An equivalent rainfall intensity (i_{eq}), representative of the amount of water available for runoff, was defined as a function of rainfall intensity (i) and hydraulic conductivity (\bar{K}_s). Storms of very long durations were applied. Once equilibrium was reached, the discharge corresponding to equilibrium assuming pervious conditions (Q_{e_eq}) was used to evaluate the equivalent rainfall intensity (i_{eq}) as:

$$Q_{e_eq} = i_{eq} A_d \quad (7.1)$$

The assumptions were made that the runoff length (L) can be evaluated as $A_d^{0.5}$, and that spatially averaged values of hydrologic parameters in upland areas can be used to calculate the time to equilibrium (see Chapter 6, Section 6.1). Having determined i_{eq} , the time to equilibrium corresponding to pervious conditions (T_{e_eq}) could be evaluated as:

$$T_{e_eq} = \left(\frac{\bar{n}_{01} A_d^{1/2}}{i_{eq}^{2/3} \bar{S}^{1/2}} \right)^{3/5} \quad (7.2)$$

As seen in Eq. (7.1) and (7.2), since i_{eq} will always be less than i , the effect of infiltration is to reduce the equilibrium discharge ($Q_{e_eq} < Q_e$) and increase the time to equilibrium ($T_{e_eq} > T_e$).

Infiltration conditions were also evaluated for events 1, 2, and 3 on Goodwin Creek (see Table 4.2). The average rainfall intensity for each event was used to calculate T_e and Q_e values for individual grid cells, based on drainage area (A_d). Peak runoff rates recorded at each pixel were used in determining Q^* values (where $Q^* = Q_p/Q_e$), which were then plotted as a function of T^* (where $T^* = T_p/T_e$). The results from the events show the effects of temporal rainfall variability on Q^* and T^* .

7.2 GOODWIN CREEK

Constant rainfall intensities of 0.28 in/hr ($\bar{K}_s / i = 1.0$), 0.50 in/hr ($\bar{K}_s / i = 0.5$), and 1.25 in/hr ($\bar{K}_s / i = 0.2$) were applied to Goodwin Creek, assuming a wide range of rainfall durations. The peak discharge at every grid cell in the basin was recorded for each simulation. For each rainfall intensity, values of Q_e and T_e were evaluated, assuming impervious conditions, based on the drainage areas (see Chapter 6, Eq. (6.1) and (6.2)). For a given rainfall duration, basin-wide values of Q^* were then plotted as a function of T^* .

Results from pervious simulations at a 416 ft grid size are shown in Fig. 7.1a-7.1c. As the value of \bar{K}_s / i decreases, the maximum value of Q^* increases, tending towards 1. More of the rainfall becomes available for runoff. The values of T^* are high for all three \bar{K}_s / i ratios, due to the delayed response of the basin as a result of infiltration. The highest rainfall intensity (1.25 in/hr) required a shorter rainfall duration to achieve

runoff ($T_r = 2$ hr), while the lowest rainfall intensity required a rainfall duration of 6 hr in order to generate runoff. There are some outlying points, particularly when $T^f > 10$, which could be a result of the incorrect determination of drainage area corresponding to these cells (i.e. points near the boundary of the watersheds).

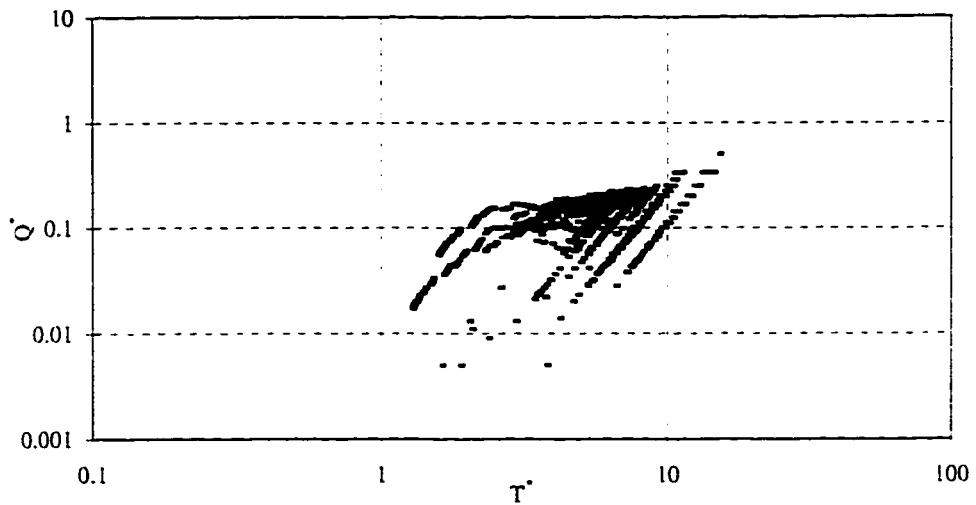


Fig.7.1a: Peak runoff rates on Goodwin Creek for $\bar{K}_s / i = 1.0$

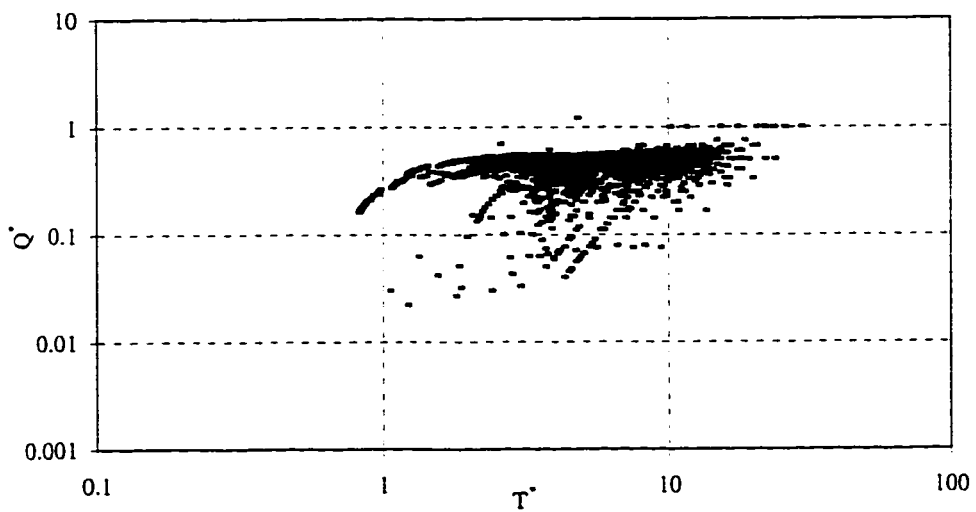


Fig. 7.1b: Peak runoff rates for on Goodwin Creek $\bar{K}_s / i = 0.5$

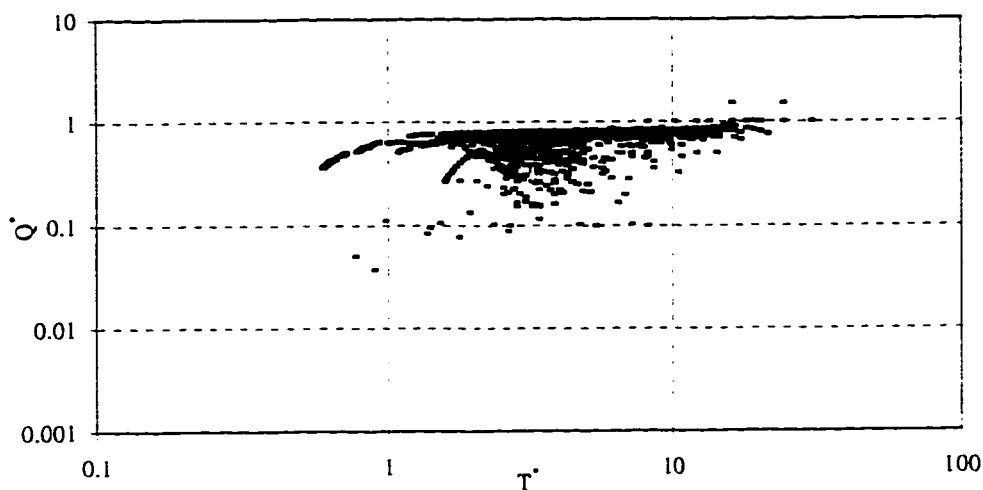


Fig. 7.1c: Peak runoff rates on Goodwin Creek for $\bar{K}_s / i = 0.2$

Pervious simulations at a 832 ft grid size and a 1248 ft grid size led to identical results (see Appendix E, Fig. E.1 and Fig. E.2). Regardless of the grid resolution, the nature of runoff hydrographs showed similar trends for all three conditions of infiltration ($\bar{K}_s / i = 1, 0.5, 0.2$). As complete equilibrium conditions were approached, peak discharge stabilized at a constant value. When \bar{K}_s / i is equal to 0.2, peak runoff rates are similar to those of impervious conditions. When \bar{K}_s / i is equal to 1.0, peak discharge remains very low, due to high infiltration losses.

7.3 HICKAHALA-SENATOBIA

The approach used on Goodwin Creek was repeated on Hickahala-Senatobia. Constant rainfall intensities of 0.28 in/hr ($\bar{K}_s / i = 1.0$), 0.50 in/hr ($\bar{K}_s / i = 0.5$), and 1.25 in/hr ($\bar{K}_s / i = 0.2$) were applied. A range of rainfall durations were used in order to simulate partial and complete equilibrium conditions. Peak discharge (Q_p) at every grid cell was recorded for the pervious simulations. The raster map of drainage areas (see

Chapter 6) was used to evaluate time to equilibrium and equilibrium discharge for each of the three rainfall intensities. Basin-wide values of Q^* and T^* were then determined, based on individual cell values of Q_p , Q_e , and T_e . The results from the simulations at a 1000 ft grid size are shown in Fig. 7.2a-7.2c.

As seen in Fig. 7.2a-7.2c, values of Q^* decrease as the ratio of \bar{K}_s / i increases, due to infiltration. The more pervious the watershed, the longer the rainfall durations required in order to generate runoff. When a rainfall intensity of 1.25 in/hr was applied to the basin, a 1 hr rainfall duration was sufficient to generate runoff. When 0.5 in/hr intensity was applied, a rainfall duration of 6 hr was necessary before runoff occurred. At higher values of T^* , particularly when $T^* > 1$, results in Fig. 7.2a-7.2c show points where the value of Q^* exceeds 1. These points correspond to overland cells, where T_e is short. As discussed previously, Q^* should never exceed 1. The most likely explanation for this occurrence on the Hickahala-Senatobia basin is that the drainage areas were defined using the GRASS program *r.watershed*. As shown in Fig. 6.14, the determination of drainage areas using GRASS (based on topography) or CASC2D (2-D flow routing) result in different distributions, particularly in upland areas. Equilibrium discharge is evaluated as a function of the drainage area. Since peak discharge (Q_p) was defined as a result of CASC2D simulations of two-dimensional flow, it is not surprising that some of the Q^* estimates are too high for those cells draining the smallest areas.

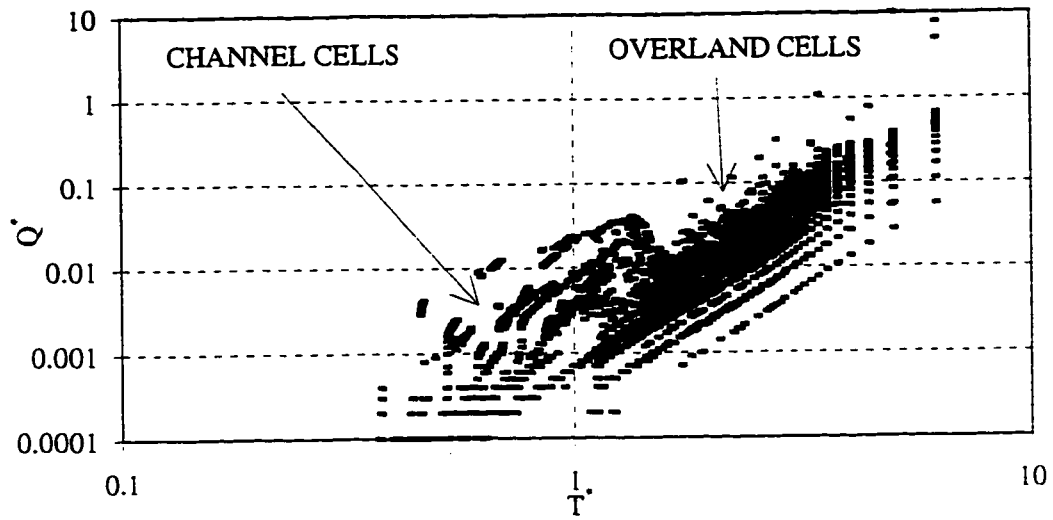


Fig. 7.2a: Peak runoff rates on Hickahala-Senatobia for $\bar{K}_s / i = 1.0$

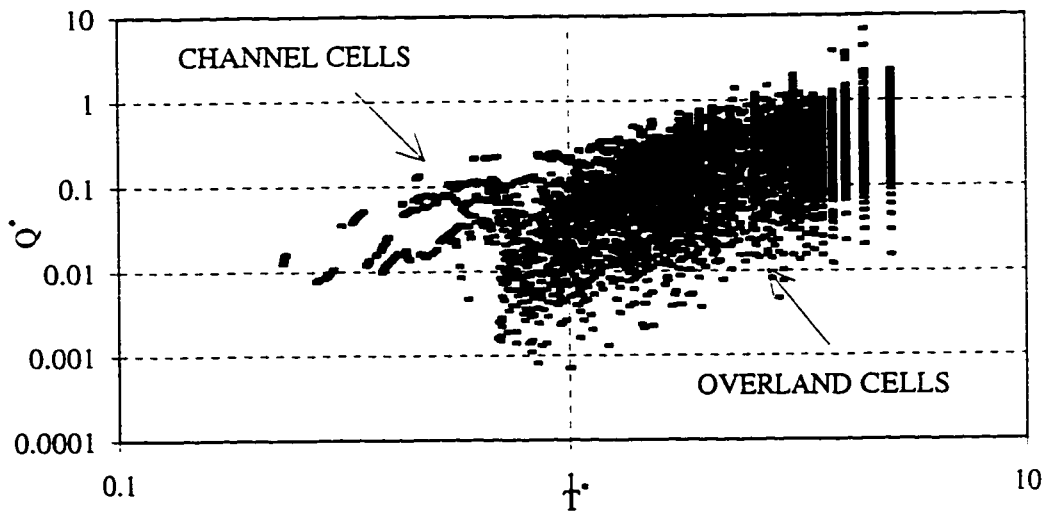


Fig. 7.2b: Peak runoff rates on Hickahala-Senatobia for $\bar{K}_s / i = 0.5$

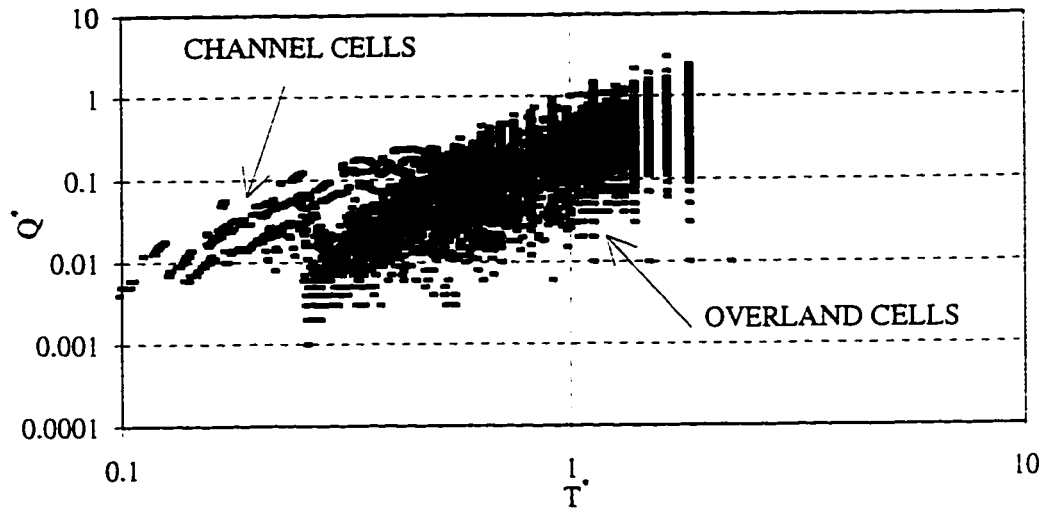


Fig. 7.2c: Peak runoff rates on Hickahala-Senatobia for $\bar{K}_s / i = 0.2$

Results from pervious simulations at the 2000 ft and 3000 ft grid sizes were identical to the 1000 ft simulations. The results are shown in Appendix E, Fig. E.3 and Fig. E.4. The role of infiltration, when evaluated in terms of Q^* and T^* , is not significantly affected by grid size. Peak runoff rates tend towards a constant value, which is a function of \bar{K}_s / i . Due to infiltration, the time to reach equilibrium is delayed, and peak discharge (Q_p) for pervious simulations is always be less than the impervious equilibrium discharge (Q_e), resulting in Q^* values less than 1. Again, some outlying points exist where Q^* does exceed 1, due to the inaccurate representation of drainage areas corresponding to some of the cells in upland areas.

7.4 QUANTIFYING INFILTRATION EFFECTS

7.4.1 SIMULATING COMPLETE EQUILIBRIUM CONDITIONS

Under pervious conditions, equilibrium conditions can be reached, but will be a function of an equivalent rainfall intensity (i_{eq}) rather than the rainfall intensity (i). Since

$i_{eq} < i$, a much longer rainstorm of duration (T_r) will be necessary in order to reach complete equilibrium. The equivalent rainfall intensity corresponding to given infiltration conditions can be determined by simulating complete equilibrium throughout the basin, assuming pervious conditions.

The procedure used in Chapter 6 to determine equilibrium discharge on a cell by cell basis was re-applied to Goodwin Creek. Hypothetical rainstorms were simulated, this time assuming pervious conditions, such that equilibrium was reached at the outlet. For rainfall intensities of 0.28 in/hr, 0.50 in/hr, and 1.25 in/hr, the rainfall durations required to reach equilibrium at the outlet were 72 hr, 50 hr, and 30 hr respectively.

As shown in Fig. 7.3a-7.3c, complete equilibrium conditions existed throughout the basin. Gages draining smaller areas reached equilibrium earlier than those draining large areas. Runoff was significantly delayed when \bar{K}_s / i was 1.0, and the peak discharge remained low ($9 \text{ m}^3/\text{s}$) due to the loss of water to infiltration. For near impervious conditions ($\bar{K}_s / i = 0.2$) runoff occurred rapidly and peak discharge at the outlet reached $140 \text{ m}^3/\text{s}$.

For each of the \bar{K}_s / i simulations, peak discharge (Q_p) corresponding to every pixel was recorded. Since equilibrium conditions were reached throughout the basin, this discharge was assumed to be the equivalent equilibrium discharge (Q_{e_eq}). Using the drainage area (A_d) evaluated for individual cells under impervious conditions, the equivalent rainfall intensity (i_{eq}) was then calculated according to Eq. (7.1). Next, for each cell, the calculated value of i_{eq} was compared to the actual rainfall intensity (i), which was kept constant throughout the simulations. The distributions of basin-wide

values of i_{eq}/i for each \bar{K}_s / i simulation at the three grid resolutions used on Goodwin Creek are shown in Fig. 7.4a-Fig. 7.4c.

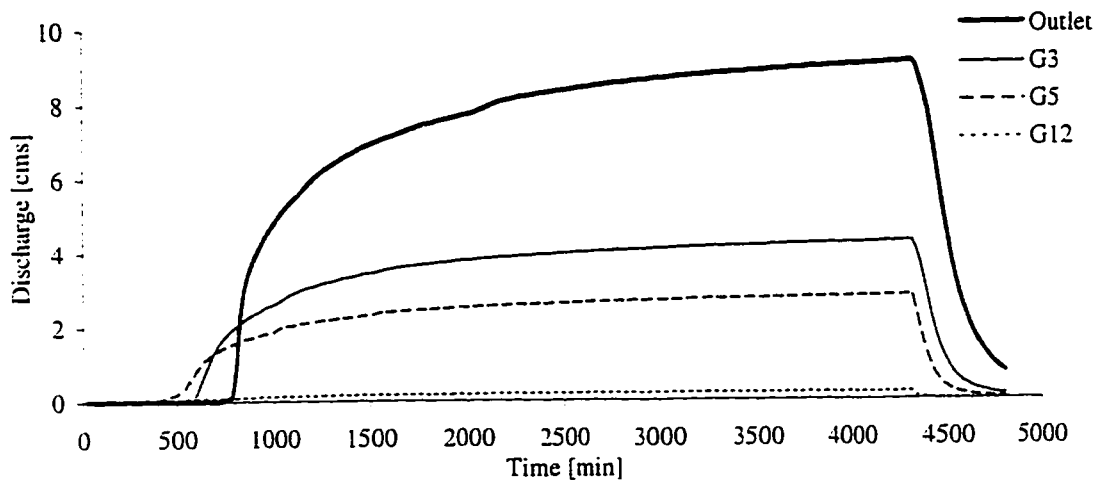


Fig. 7.3a: Equilibrium hydrographs $\bar{K}_s / i = 1.0$

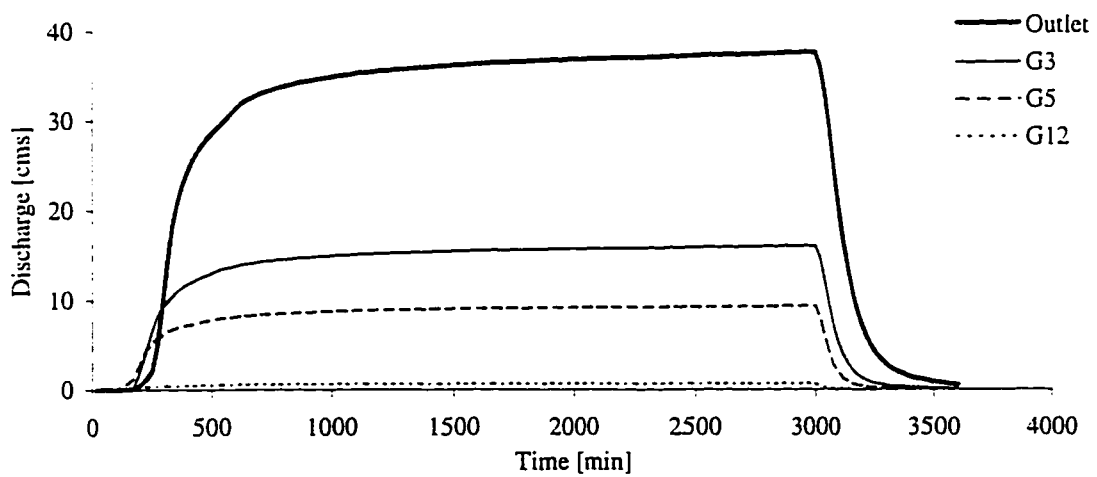


Fig. 7.3b: Equilibrium hydrographs $\bar{K}_s / i = 0.5$

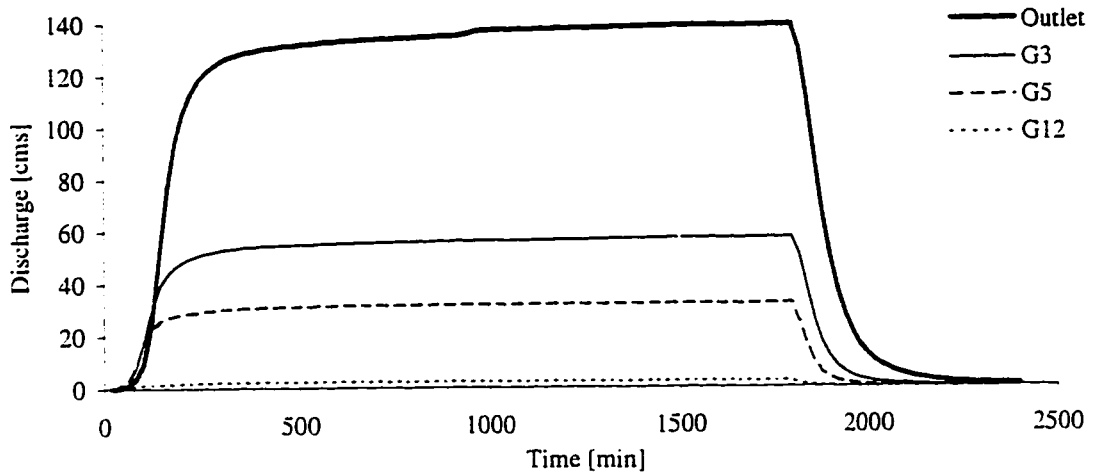


Fig. 7.3c: Equilibrium hydrographs $\bar{K}_s / i = 0.2$

The majority of the grid cells have a unique value of i_{eq}/i for each \bar{K}_s / i simulation. Results are similar at the three resolutions, although at 1248 ft the value of i_{eq}/i tends towards a single value, with less scatter. Based on simulation results, the relationship between i_{eq}/i and \bar{K}_s / i can be approximated by the following equation:

$$\frac{i_{eq}}{i} = 1 - \frac{2}{3} \left(\frac{\bar{K}_s}{i} \right) \quad (7.3)$$

The i_{eq}/i values for $\bar{K}_s / i = 1, 0.5,$ and 0.2 were calculated using Eq. (7.3). They are plotted on Fig. 7.4a-Fig. 7.4c, for comparison with the actual simulated values.

Based on Eq. (7.3), the equilibrium conditions for pervious simulations, as related to impervious conditions, can be evaluated as:

$$Q_{e_eq} = \frac{i_{eq}}{i} Q_e = \left[1 - \frac{2}{3} \left(\frac{\bar{K}_s}{i} \right) \right] Q_e \quad (7.4)$$

$$T_{e_eq} = \frac{i}{i_{eq}} T_e = \frac{T_e}{\left[1 - \frac{2}{3} \left(\frac{\bar{K}_s}{i} \right) \right]} \quad (7.5)$$

As expected, the effect of infiltration is to decrease equilibrium discharge and increase time to equilibrium. In the application of Eq. (7.4) and (7.5), the ratio of \bar{K}_s / i may range anywhere from $\bar{K}_s / i = 0$ (impervious conditions) to $\bar{K}_s / i = 1$ (highly pervious conditions).

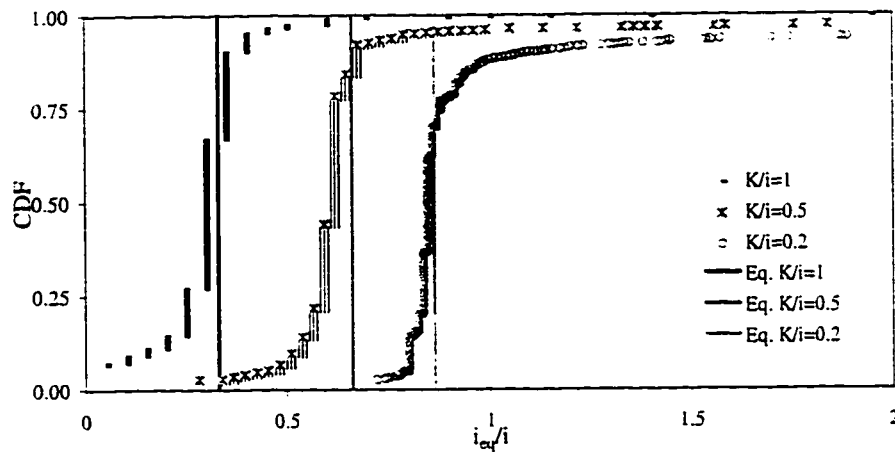


Fig. 7.4a: Distribution of basin-wide i_{eq}/i (416 ft grid size)

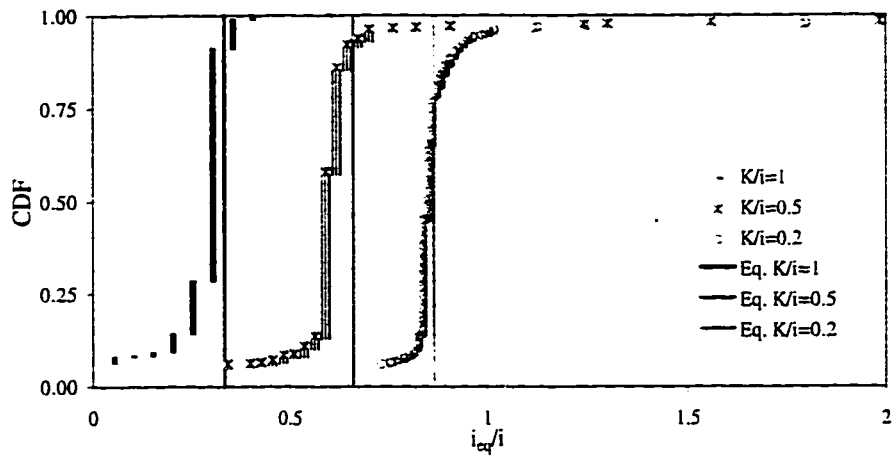


Fig. 7.4b: Distribution of basin-wide i_{eq}/i (832 ft grid size)

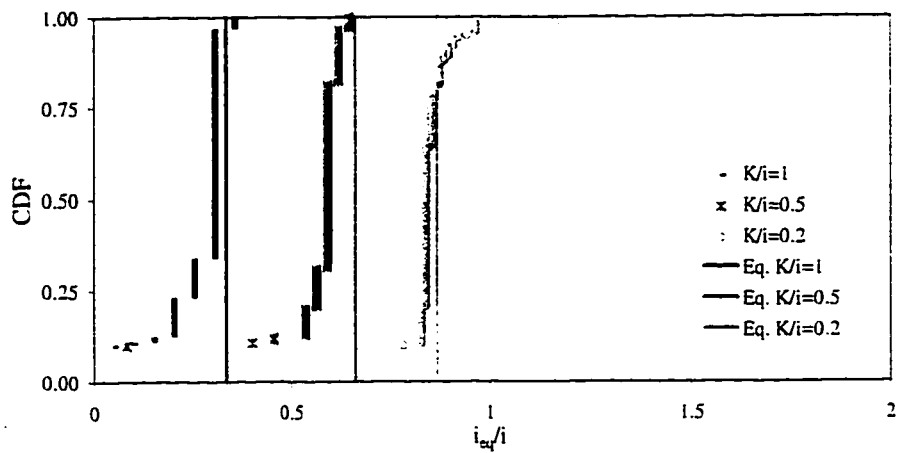


Fig. 7.4c: Distribution of basin-wide i_{eq}/i (1248 ft grid size)

The simulated values of i_{eq}/i were also evaluated as a function of drainage area (A_d), for both overland and channel cells. At the 416 ft grid size the results corresponding to the three \bar{K}_s / i values are presented in Fig. 7.5a and Fig. 7.5b. There is a great deal of variability in the values of i_{eq}/i corresponding to overland cells (Fig. 7.5a).

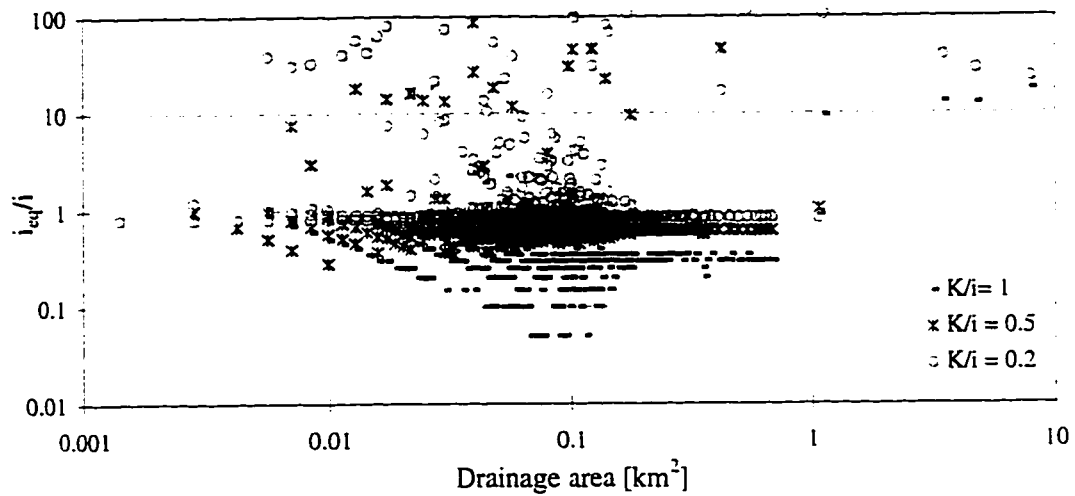


Fig. 7.5a: Effects of drainage area on i_{eq}/i for overland cells

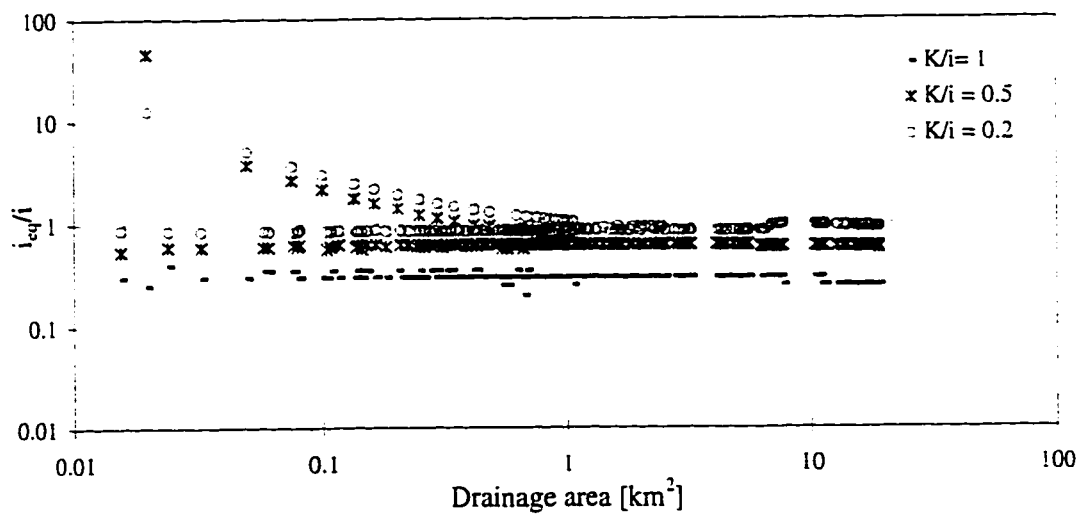


Fig. 7.5b: Effects of drainage area on i_{eq}/i for channel cells

The outlying points (large i_{eq}/i) are indicative of the effects of spatial variability in upland areas, particularly relating to the pervious soil conditions, and may also be attributed to the method used in evaluating drainage patterns. The value of i_{eq} was calculated as a function of the drainage areas corresponding to individual cells, where

$i_{eq} = Q_{e_eq} / A_d$. Drainage areas on Goodwin Creek were defined based on a two-dimensional overland flow scheme, assuming impervious runoff conditions. As shown in Fig. 6.14, based on topography alone (i.e. using *r.watershed*) drainage areas corresponding to overland cells are found to be higher. If drainage areas in upland areas were higher, as indicated by *r.watershed*, the calculated values of i_{eq} would decrease, and high values of i_{eq}/i seen in Fig. 7.5a would not occur.

For the cells defined as overland cells (Fig. 7.5a), the value of i_{eq}/i becomes approximately constant at drainage areas greater than 0.3 km^2 . This could be an indication of the threshold at which the real channel network begins. For channel cells (Fig. 7.5b), the value of i_{eq}/i shows very little variability, particularly when drainage areas are greater than 1 km^2 . These results indicate that the effects of spatial variability on the generation of excess rainfall become less significant as drainage areas increase ($A_d > 1 \text{ km}^2$). Consequently, Eq. (7.3), which describes the relationship between i_{eq} and i , can be considered applicable for all drainage areas greater than 1 km^2 , assuming uniform rainfall intensities.

7.4.2 GOODWIN CREEK RAINFALL EVENTS

Results from the simulation of events 1, 2, and 3 on Goodwin Creek were used to evaluate infiltration effects associated with temporally varying rainfall. For each event, the peak discharge at individual cells throughout the basin was recorded. The average rainfall rate (\bar{i}) for the events was used to calculate basin-wide values of equilibrium discharge (Q_e) and time to equilibrium (T_e), assuming impervious conditions (see Chapter 6, Section 6.1). The values of Q^* and T^* were then evaluated for individual cells, using the simulated peak discharge (Q_p) and the rainfall duration (T_r) of the event. The results

are shown in Fig. 7.6, where Q^* is plotted as a function of T^* and also as a function of drainage density (A_d).

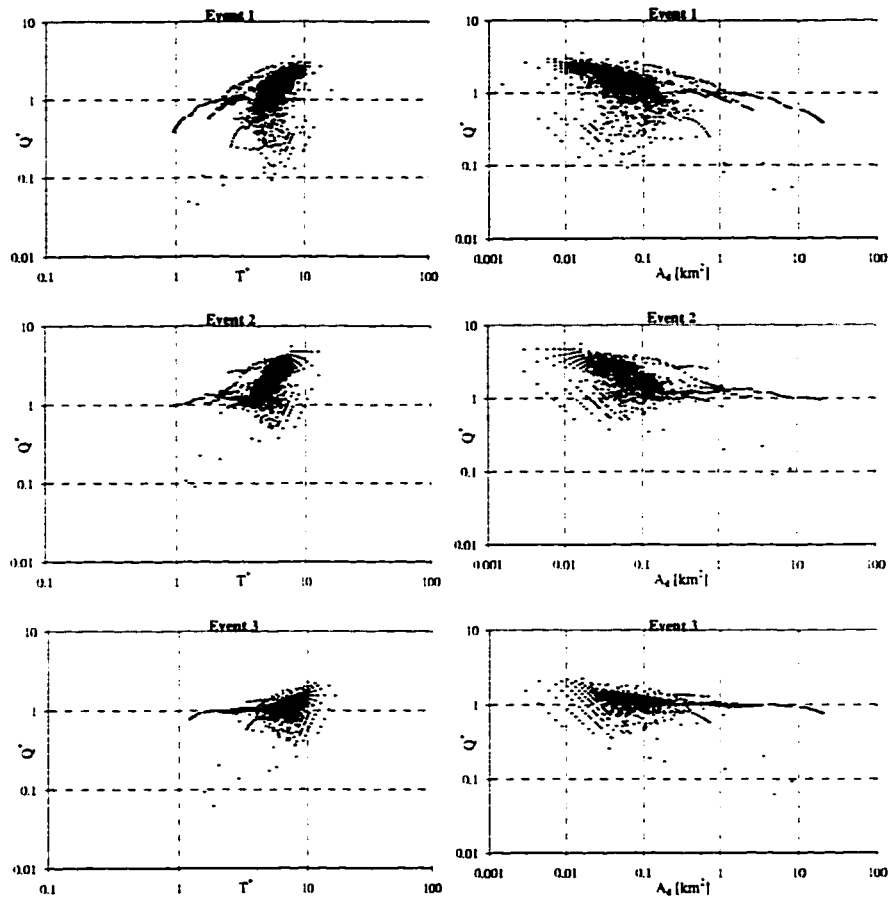


Fig. 7.6: Effect of rainfall variability on peak discharge for rainfall events on Goodwin Creek

As seen in Fig. 7.6, when non-uniform rainfall is simulated, there is a great deal of variability in the values of Q^* when T^* is large. These points represent cells in upland areas, which have small drainage areas and short times to equilibrium. The values of Q^* show little fluctuation when T^* is small. These points represent cells which drain larger areas values (channel cells) and have long times to equilibrium. An average rainfall intensity (\bar{i}) was assumed in calculating the equilibrium conditions ($Q_e \propto \bar{i}$ and $T_e \propto \bar{i}^{-0.4}$). Most of the values of Q^* in Fig. 7.6 are greater than 1, particularly in the case of

overland cells, indicating that the spatial variability of rainfall rates had a significant effect on peak runoff rates. The channel cells (small T^* values) have Q^* values less than 1, indicating that an average rainfall intensity can be used in evaluating peak discharge conditions. By the time runoff reaches channel cells, the effects of spatial variability in rainfall rates on peak discharge have been attenuated.

The graphs showing Q^* as a function of A_d demonstrate that the temporal variability of rainfall has a significant effect in the upland areas, where $A_d < 1 \text{ km}^2$. This is true for all three events. Clearly at 1 km^2 , conditions stabilize. Based on these results, the temporal variability of rainfall is shown to become unimportant for drainage areas greater 1 km^2 . An average rainfall intensity is considered appropriate for the evaluation of Q^* and T^* corresponding to $A_d > 1 \text{ km}^2$.

Table 7.1 summarizes the parameters used in the simulation of events 1, 2, and 3. For each event, average hydraulic conductivity (\bar{K}_s), average rainfall intensity (\bar{i}), and \bar{K}_s / \bar{i} have also been calculated and are shown in the table. \bar{K}_s / \bar{i} ratios for the events range from 0.254 for event 1, to 0.045 for event 3.

Table 7.1: Parameters from simulations using 416 ft grid size

	EVENT 1	EVENT 2	EVENT 3
Detention storage S_d	0.015	0.00	0.02
Soil type 1: K_s [m/s]	1.30E-06	1.00E-07	1.00E-07
Soil type 2: K_s [m/s]	2.20E-06	1.50E-07	1.50E-07
Soil type 1: H_f [m]	0.16	0.01	0.01
Soil type 2: H_f [m]	0.08	0.01	0.01
Soil type 1: M_d	0.08	0.0	0.1
Soil type 2: M_d	0.08	0.0	0.1
Average i [m/s]	5.72E-06	1.58E-06	2.40E-06
Average K_s [m/s]	1.45E-06	1.09E-07	1.09E-07
Average H_f [m]	0.144	0.01	0.01
Average M_d	0.08	0.0	0.1
\bar{K}_s / \bar{i}	0.25	0.07	0.045

The effects of infiltration on peak discharge are summarized in Table 7.2. For reference, outlet time to equilibrium (T_e) and equilibrium discharge (Q_e) have been calculated using average watershed and rainfall characteristics. The \bar{K}_s / \bar{i} ratios from Table 7.1 were used in estimating the equivalent time to equilibrium (T_{e_eq}) and the equivalent equilibrium discharge (Q_{e_eq}) for each of the three events. Eq. (7.5) was applied in calculating T_{e_eq} , and Eq. (7.4) was applied in calculating Q_{e_eq} .

Table 7.2: Infiltration effects at Goodwin Creek outlet

	EVENT 1	EVENT 2	EVENT 3
At outlet Q_e [m^3/s]	106	28	43
At outlet T_e [min]	222	406	348
T_r [min]	211	361	407
Q_p [m^3/s]	39	27	33
$T^* = T_r/T_e$	0.95	0.89	1.17
$Q^* = Q_p/Q_e$	0.37	0.96	0.77
T_{e_eq}	$1.20T_e$	$1.05T_e$	$1.03T_e$
Q_{e_eq}	$0.80Q_e$	$0.95Q_e$	$0.97Q_e$

According to Table 7.2, T_{e_eq} values at the outlet are $1.20T_e$, $1.05T_e$, and $1.03T_e$. These are an indication of the time at which equilibrium will be reached at the outlet, assuming pervious conditions. Infiltration does not have much of an effect on runoff conditions for events 2 and 3, where $T_{e_eq} \approx T_e$. At the outlet, T^* for events 2 and 3 has been calculated as 0.89 and 1.17. Conditions at the outlet are therefore expected to be very close to complete equilibrium. The actual values of Q^* for events 2 and 3 are almost equal to unity, as shown in Fig. 7.6. For event 1, infiltration is significant, resulting in a T_{e_eq} value of $1.20T_e$. Although T^* was calculated to be 0.95, partial equilibrium conditions exist at the outlet as a result of infiltration effects. As demonstrated in Fig. 7.6, Q^* for event 1 is much less than unity at the outlet.

In Eq. (7.3), (7.4), and (7.5), runoff conditions were found to be directly related to the ratio of \bar{K}_s / i . But when the moisture deficit (M_d) is relatively high, infiltration parameters other than the hydraulic conductivity (K_s) may cause a reduction in the amount of water available for runoff and may have a significant effect on runoff conditions. The effect of moisture deficit (M_d) was evaluated for events 1 and 3, which had M_d values of 0.08 and 0.1 respectively (see Table 7.1). According to the Green and Ampt equation, the infiltration rate (f) is calculated as:

$$f = K_s \left(1 - \frac{H_f M_d}{F} \right) \quad (7.6)$$

where K_s , H_f , and M_d are soil parameters defined for CASC2D simulations, and F is the total infiltrated depth.

As time increases, the infiltration rate approaches a constant value. Eq. (7.6) was applied for the events 1 and 3, for the duration of the events. The results indicate that the infiltration rate is greater than the hydraulic conductivity (Fig. 7.7).

The difference between rainfall intensity (i) and the infiltration rate (f) is excess water, and becomes available for runoff. In order to consider the effects of moisture deficit, runoff should be evaluated as a function of f / \bar{i} . Based on soil parameters, f / \bar{i} can be calculated as:

$$\frac{f}{\bar{i}} = \left(\frac{f}{\bar{K}_s} \right) \left(\frac{\bar{K}_s}{\bar{i}} \right) \quad (7.7)$$

$$\frac{f}{\bar{i}} = \left(1 - \frac{H_f M_d}{F} \right) * \left(\frac{\bar{K}_s}{\bar{i}} \right) \quad (7.8)$$

For values of M_d close to zero, the infiltration rate and hydraulic conductivity are equal. In this case excess water can be evaluated as the difference between rainfall intensity (i) and the hydraulic conductivity (K_s). As expected, Eq. (7.8) reduces to \bar{K}_s / \bar{i} for $M_d = 0$.

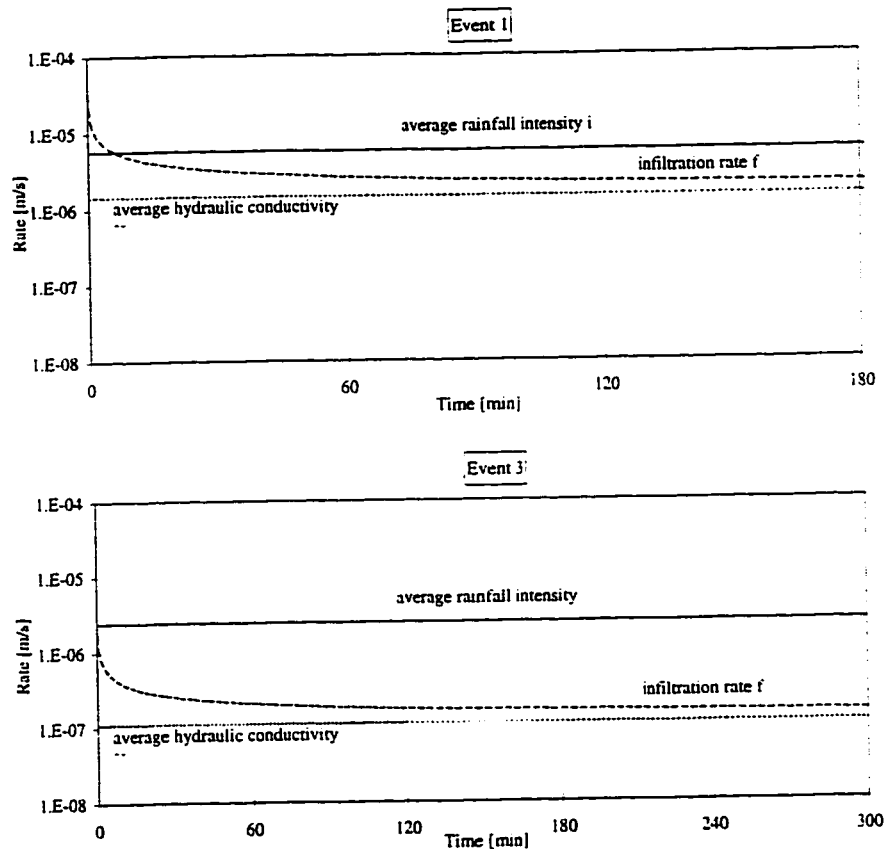


Fig. 7.7: Infiltration conditions for events 1 and 3

As seen in Fig. 7.7, the difference between hydraulic conductivity and the infiltration rate is very small. Evaluating discharge conditions using \bar{K}_s / \bar{i} instead of f / \bar{i} can still be considered adequate for these events. When M_d is greater than 0.5, a more accurate representation of infiltration effects will be achieved by replacing \bar{K}_s / \bar{i} with f / \bar{i} in Eq. (7.3), (7.4), and (7.5).

7.5 ANALYSIS OF PERVIOUS RUNOFF ON TWO WATERSHEDS

The values of Q^* as a function of T^* were evaluated for all pervious simulations, with $\bar{K}_s / i = 1.0, 0.5, \text{ and } 0.2$. Equations describing peak runoff rates were empirically derived for partial and complete equilibrium conditions. The effects of infiltration are quantified as a function of \bar{K}_s / i .

As a result of infiltration, equilibrium conditions on a pervious watershed will be delayed. Complete equilibrium conditions are reached at when $T^* = T_{ce}^*$, which is evaluated according to Eq. (7.5) as:

$$T_{ce}^* \equiv \frac{3}{3 - 2 \frac{\bar{K}_s}{i}} \quad (7.9)$$

The complete equilibrium discharge (Q_{ce}^*) corresponding to T_{ce}^* is calculated according to Eq. (7.4) as:

$$Q_{ce}^* \equiv 1 - \frac{2 \bar{K}_s}{3 i} \quad (7.10)$$

Fig. 7.8 summarizes the variation in T_{ce}^* and Q_{ce}^* as a function of \bar{K}_s / i . For a \bar{K}_s / i ratios of 0.2, 0.5, and 1.0, T_{ce}^* is equal to 1.15, 1.5, and 3.0 respectively. These ratios indicate that under pervious conditions, equilibrium will be reached at times greater than the time to equilibrium corresponding to impervious conditions. For the same \bar{K}_s / i ratios of 0.2, 0.5, and 1.0, Q_{ce}^* is calculated as 0.85, 0.65, and 0.30 respectively. The maximum possible discharge for the three conditions will be 85 percent, 65 percent, and 30 percent of the equilibrium discharge under impervious conditions.

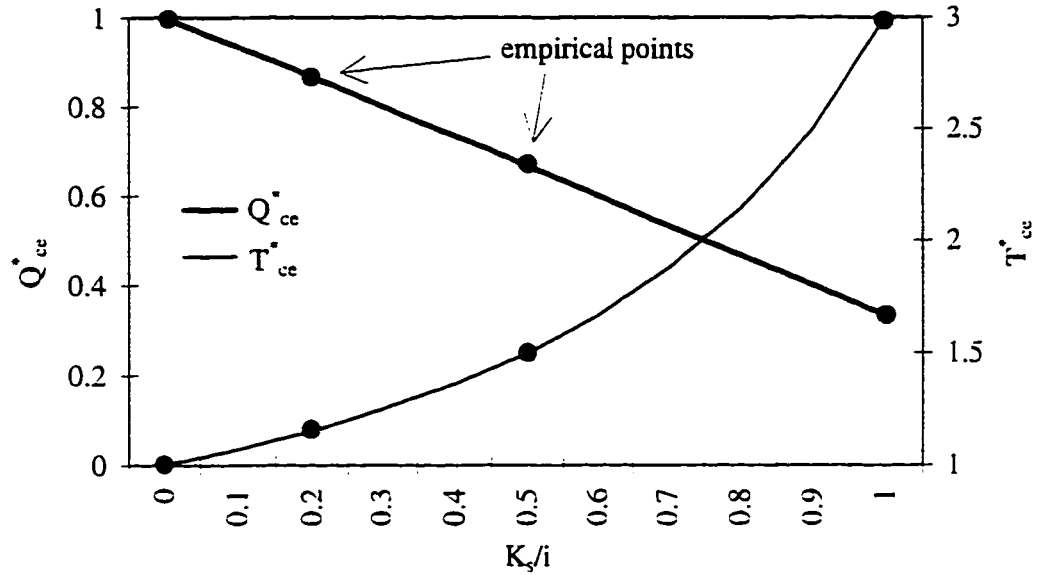


Fig. 7.8: Effects of infiltration on complete equilibrium conditions

Under partial equilibrium conditions, a range of Q^* values can occur. Different conditions exist for overland cells and for channel cells, but all Q^* values are a function of \bar{K}_s / i . In upland areas, the maximum possible value of Q^* is Q_{max}^* , and the minimum value is Q_{min}^* , both of which are related to T^* . In the channel, Q^* is defined as Q_{ch}^* . Based on empirical results, overland and channel partial equilibrium conditions are evaluated as:

$$Q_{max}^* = 0.0056 T^{*3} \left(\frac{\bar{K}_s}{i} \right)^{-3.5} \quad (7.11)$$

$$Q_{min}^* = 0.2 T^{*3} (0.0004) \bar{K}/i \quad (7.12)$$

$$Q_{ch}^* = 2.5 T^{*2} (0.008) \bar{K}/i \quad (7.13)$$

Eq. (7.11), (7.12), and (7.13) are valid for $0.2 < \bar{K}_s / i < 1.0$.

With reference to Section 6.5, the mathematical evaluation of discharge as a function of depth, using the Manning resistance coefficient and assuming turbulent flow, would indicate that Q^* should be proportional to $T^{*5/3}$. Eq. (7.11) and (7.12), based on empirical solutions, define $Q^* \propto T^{*3}$ on overland cells and Eq. (7.13) defines channel flow as $Q^* \propto T^{*2}$. Again, due to the use of coarse grid resolutions, the depth of flow in upland areas may result in laminar-type flow, which would lead to $Q^* \propto T^{*3}$.

Combining results from previous simulations on Goodwin Creek and Hickahala-Senatobia, simulated values of Q^* were plotted as a function of T^* for a conditions ranging from partial equilibrium to complete equilibrium. Fig. 7.8, 7.9, and 7.10 summarize the results for $\bar{K}_s / \bar{i} = 1.0, 0.5, \text{ and } 0.2$ simulations.

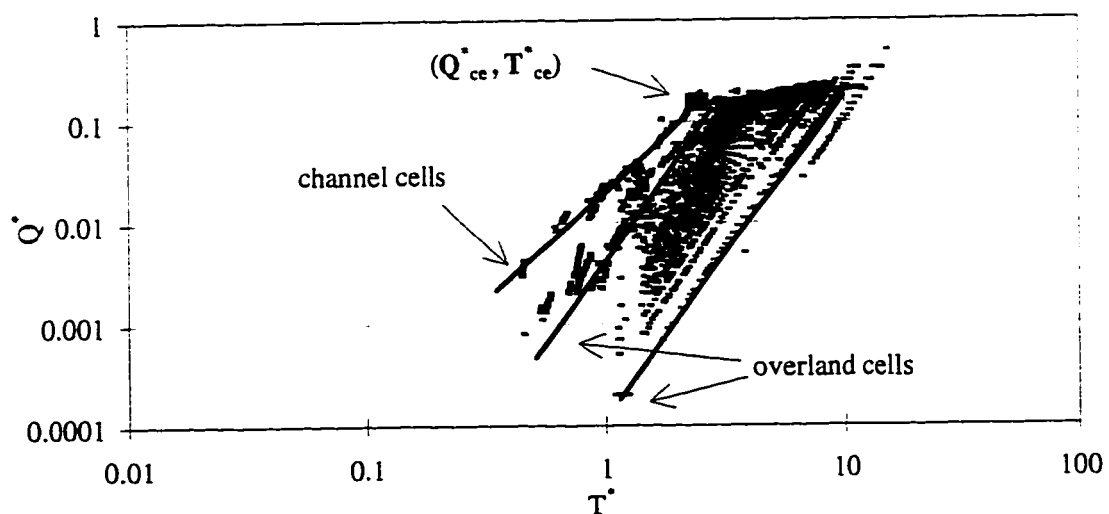


Fig. 7.9: Partial and complete equilibrium conditions at $\bar{K}_s / \bar{i} = 1.0$

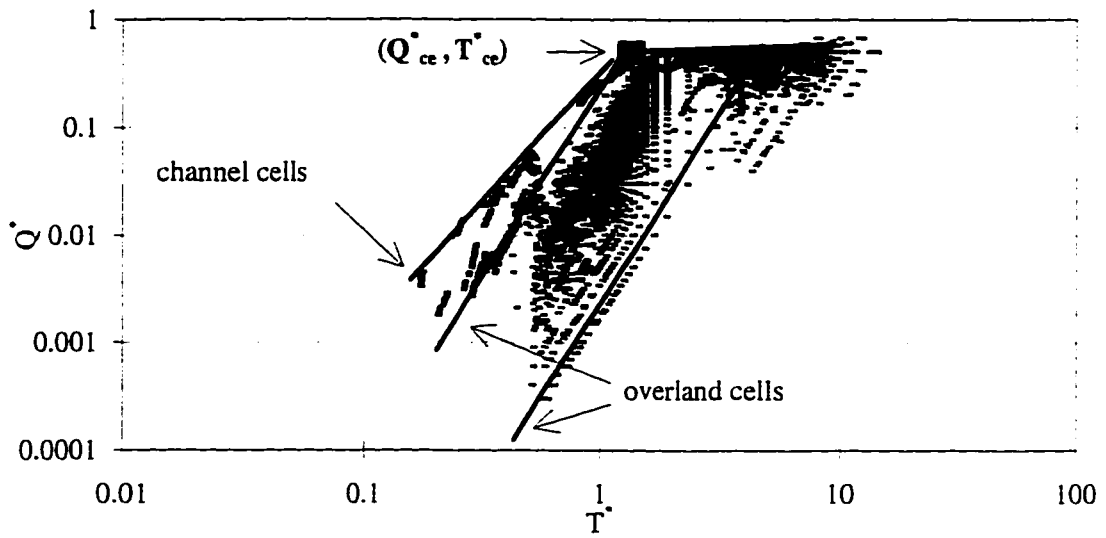


Fig. 7.10: Partial and complete equilibrium conditions at $\bar{K}_s / \bar{i} = 0.5$

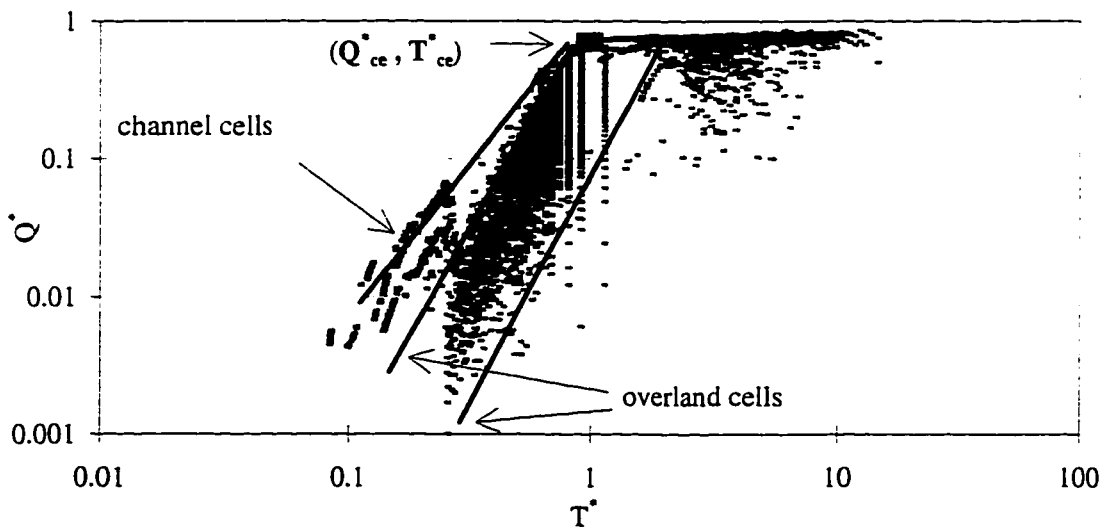


Fig. 7.11: Partial and complete equilibrium conditions at $\bar{K}_s / \bar{i} = 0.2$

Under pervious conditions the maximum possible value of Q^* is reduced. due to infiltration. In addition, it can be seen in Fig. 7.9, 7.10, and 7.11 that threshold values of T^* were required in order to generate runoff in upland areas. Minimum T^* values recorded for $\bar{K}_s / \bar{i} = 1.0, 0.5, \text{ and } 0.2$ were approximately 1, 0.5, and 0.2, indicating that rainfall durations equal to $1T_e, 0.5T_e, \text{ and } 0.2T_e$ were necessary before runoff could occur in upland areas.

Grid resolutions for large-scale simulations can be defined using the concept of a watershed time to equilibrium. As seen in Fig. 7.9, Fig. 7.10, and Fig. 7.11, complete equilibrium conditions are reached when $T^* = T_{ce}^*$. The runoff length corresponding to T_{ce}^* will thus ensure that equilibrium conditions are met on most grid cells in the basin. This is the largest grid size (L_{g_max}) which would be appropriate for rainfall-runoff simulations, and would result in complete equilibrium conditions on the majority of the cells in the basin. All points are shown to converge towards a single Q^* value at $T^* \approx 10T_{ce}^*$ (Fig. 7.9, 7.10, 7.11). The runoff length associated with $T^* = 10T_{ce}^*$ represents a minimum grid length (L_{g_min}) which will ensure complete equilibrium conditions on almost all cells in the basin. Any grid size within the range of L_{g_max} and L_{g_min} would therefore be appropriate. In addition, it has been shown that the effects of upland spatial variability on rainfall-runoff conditions become attenuated when $A_d > 1 \text{ km}^2$, which corresponds to a runoff length of 1 km. If $L_{g_min} < 1 \text{ km} < L_{g_max}$, a 1 km grid size would be appropriate choice for large scale simulations. A final factor to consider is the minimum drainage area (A_{d_min}) required for modeling purposes (see Fig. 6.17 and Fig. 6.18). If the grid size selected for simulations is larger than the runoff length (L_{d_min}) corresponding to the minimum drainage area, then a grid size the length of L_{d_min} should

be used instead, particularly if both overland and channel routing are to be included in the modeling of the rainfall-runoff response.

7.6 SUMMARY

Pervious simulations were performed assuming uniform rainfall intensities. The effects of infiltration were evaluated based on raster maps of Q_e and T_e corresponding to impervious equilibrium conditions. Assuming a uniform rainfall intensity, peak runoff rates were found to be related to an equivalent rainfall intensity (i_{eq}). The ratios of i_{eq}/i for overland cells and channel cells showed that beyond 1 km^2 , a constant value of i_{eq}/i exists (see Fig. 7.5a and 7.5b) and the spatial variability in upland characteristics does not have an effect on runoff conditions. Based on empirical results, Eq. (7.3) was developed in order to evaluate i_{eq}/i as a function of the average soil hydraulic conductivity (\bar{K}_s) and rainfall intensity (i).

Pervious simulations were also performed assuming non-uniform rainfall intensities. Q^* and T^* values corresponding to events 1, 2, and 3 on Goodwin Creek were evaluated in order to determine the effects of infiltration for temporally and spatially varying rainfall events. Peak discharge was found to be highly variable in upland areas, for drainage areas less than 1 km^2 (see Fig. 7.6). Outlet runoff conditions were found to be related to average rainfall rates and an average hydraulic conductivity. These results indicated that temporal and spatial variability in rainfall can be neglected on drainage areas larger than 1 km^2 .

When simulating pervious conditions, it has been shown that the time to equilibrium is increased and the equilibrium discharge is reduced. Peak runoff rates are related to the equivalent rainfall intensity (i_{eq}) and can be evaluated as a function of

\bar{K}_s / \bar{i} . When moisture deficit is high ($M_d > 0.5$), peak runoff rates should be evaluated as a function of f / \bar{i} rather than of \bar{K}_s / \bar{i} , where f / \bar{i} is calculated based on soil parameters K_s , H_f , and M_d and the total infiltrated depth F (see Eq. 7.8).

Based on pervious simulations, equations representing the relationships between Q^* and T^* were empirically derived. For complete equilibrium conditions, the time to reach equilibrium is evaluated using Eq. 7.9. Peak discharge tends towards a constant value which can be evaluated using Eq. 7.10. Under partial equilibrium, the relationships governing Q^* as a function of T^* differ for overland cells and for channel cells (see Eq. 7.11, 7.12, 7.13).

Since the objective of the study is to evaluate outlet conditions for large basins, the equation developed for channel runoff conditions is important. Q^* in the channel (Q_{ch}^*) is related to \bar{K}_s / \bar{i} . For complete equilibrium conditions, Q_{ch}^* is calculated by applying Eq. 7.10. For partial equilibrium conditions Q_{ch}^* is calculated using Eq. 7.13. The values of Q_{ch}^* corresponding to different \bar{K}_s / \bar{i} ratios are summarized in Fig. 7.12. Also shown on the figure are the points corresponding the T_{ce}^* , which will be used in evaluating the maximum grid size appropriate for rainfall-runoff simulations.

The developments in this chapter can be used in defining appropriate grid resolutions for large scale simulations, based on the need to reach complete equilibrium conditions on individual grid cells. A range of grid sizes can be defined, where L_{g_min} is the minimum grid size (corresponding to complete equilibrium conditions basin-wide) and L_{g_max} is the maximum grid size (corresponding to complete equilibrium on most cells). The final choice of a grid resolution will depend on the modeler's objective. For

modeling of purposes, a 1 km grid resolution has been shown to be a good choice, as long as the runoff length associated with the minimum drainage area is not less than 1 km.

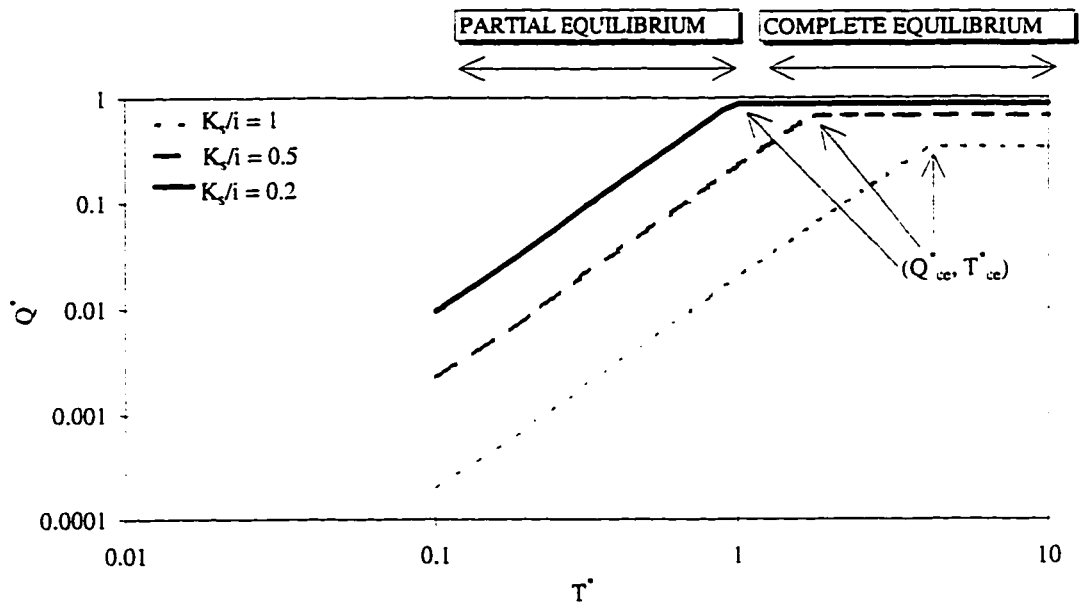


Fig. 7.12: Channel runoff conditions for pervious simulations

Chapter VIII

APPLICATION

8.1 METHODOLOGY

Based on results from this study, a method for selecting appropriate grid sizes for raster-based simulations of rainfall-runoff on large basins has been developed. These grid resolutions will ensure equilibrium conditions at the grid level, such that peak discharge on each cell will be a linear function of rainfall intensity. As described in Chapter 7, a range of grid resolutions will be appropriate: the maximum grid size is L_{g_max} and the minimum grid size is L_{g_min} . The grid size selected for modeling purposes will also be a function of data availability and model output requirements, and will be subject to limitations imposed by the need for a minimum drainage area (A_{d_min}) corresponding to channel cells (see Fig. 6.17).

Given the following watershed characteristics: drainage area (A_d), average slope (\bar{S}), average overland Manning roughness (\bar{n}_{ol}), average hydraulic conductivity (\bar{K}_s), grid size is selected as a function of a average rainfall intensity (\bar{i}) and rainfall duration (T_r). The steps to determine grid size are:

1. Calculate \bar{K}_s / \bar{i}
2. Evaluate complete equilibrium conditions using Eq. (7.9) and (7.10) as:

$$T_{ce}^* \equiv \frac{3}{3 - 2 \frac{\bar{K}_s}{i}} \quad (7.9)$$

$$Q_{ce}^* \equiv 1 - \frac{2 \bar{K}_s}{3 i} \quad (7.10)$$

3. Determine the time to equilibrium corresponding to the largest grid size, where:

$$T^* = T_{ce}^*$$

$$T_e = \frac{T_r}{T_{ce}^*}$$

4. Calculate the largest grid size (L_{g_max}) resulting in equilibrium conditions as:

$$L_{g_max} = T_e^{5/3} \left(\frac{\bar{i}^{2/3} \bar{S}^{1/2}}{\bar{n}_{ol}} \right)$$

5. Calculate the smallest grid size (L_{g_min}), defined for the point where $T^* = 10 T_{ce}^*$, as:

$$L_{g_min} = \frac{L_{g_max}}{10^{5/3}}$$

6. Calculate the runoff length (L_{d_min}) required in order to model channel runoff on a basin of drainage area A_d , based on empirically-derived equations, as:

$$L_{d_min} = 0.04 A_d^{0.7}$$

where A_d is in km^2 , and L_{d_min} is in km (see Eq. 6.11, 6.12a, and 6.12b).

7. Select grid size based on the following criteria:

- for complete equilibrium conditions basin-wide, and a very detailed description of rainfall-runoff processes throughout the basin, select L_{g_min} ;
- for complete equilibrium conditions on most pixels, and a less detailed description of rainfall-runoff process in upland areas, select L_{g_max} ;

- depending on modeling requirements and data availability, appropriate grid sizes will range between L_{g_min} and L_{g_max} ;
- if L_{d_min} is smaller than the grid size chosen for simulations, select a grid size equal to L_{d_min} in order to be able to reproduce channel routing conditions.

Once an appropriate grid size has been defined, an estimate of the peak discharge corresponding to a particular rainfall-runoff event, given specific watershed characteristics, can be evaluated as follows:

A. Calculate the time to equilibrium at the outlet of the watershed as:

$$T_{e_bas} = \left(\frac{\bar{n}_{ol} A_d^{1/2}}{\bar{i}^{2/3} \bar{S}^{1/2}} \right)^{3/5}$$

B. Evaluate T_{out}^* as T_r/T_{e_bas}

C. Evaluate Q_{out}^* according to the following criteria

- if $T_{out}^* > T_{ce}^*$, equilibrium conditions exist: $Q_{out}^* = Q_{ce}^*$
- if $T_{out}^* < T_{ce}^*$, partial equilibrium conditions exist and Eq. (7.13) is used to

$$\text{evaluate } Q_{out}^* \text{ as: } Q_{out}^* = 2.5 (T_{out}^*)^2 (0.008)^{\frac{\bar{K}_s}{\bar{i}}}$$

D. Peak discharge is estimated as: $Q_p = Q_{out}^* Q_e = Q_{out}^* (\bar{i} A_d)$

8.2 EXAMPLE

The concept of a watershed time to equilibrium and peak equilibrium were tested on Hickahala-Senatobia using a real event. Radar precipitation measurements were available for an event which occurred on January 19th, 1995. Discharge measurements were also available for Hickahala Creek and Senatobia Creek, the two main branches of the channel network. The event lasted approximately 3 hr, starting at 10 PM. The

average rainfall intensity was 9.62 mm/hr (2.7E-6 m/s). Assuming an average soil conductivity rate of 1.0E-7 m/s (the event was preceded by a significant amount of rainfall), a grid size for CASC2D simulations can be selected in the following manner:

Given:

$$A_d = 560 \text{ km}^2 \qquad \bar{n}_{ol} = 0.08 \qquad \bar{i} = 2.7\text{E-}6 \text{ m/s}$$

$$\bar{S} = 0.015 \qquad \bar{K}_s = 1.0\text{E}10\text{-}7 \text{ m/s} \qquad T_r = 3 \text{ hr}$$

Step 1. Calculate $\bar{K}_s / \bar{i} = 0.04$

Step 2. Evaluate complete equilibrium conditions corresponding to pervious runoff:

$$T_{ce}^* = \frac{3}{3 - 2\left(\frac{\bar{K}_s}{\bar{i}}\right)} = \frac{3}{3 - 2(0.04)} = 1.03$$

$$Q_{ce}^* = 1 - \frac{2}{3}\left(\frac{\bar{K}_s}{\bar{i}}\right) = 1 - \frac{2}{3}(0.04) = 0.97$$

Step 3. Determine the time to equilibrium corresponding to complete equilibrium conditions on the largest grid size, as:

$$T_e = \frac{T_r}{T_{ce}^*} = \frac{180 \text{ min}}{1.03} = 175 \text{ min} = 10500 \text{ sec}$$

Step 4. Calculate the largest grid size (L_{g_max}) as:

$$L_{g_max} = T_e^{5/3} \left(\frac{\bar{i}^{2/3} \bar{S}^{1/2}}{\bar{n}_{ol}} \right) = 10500^{5/3} \left(\frac{0.0000027^{2/3} 0.015^{1/2}}{0.08} \right)$$

$$L_{g_max} = 1495 \text{ m}$$

Step 5. Calculate the smallest grid size (L_{g_min}), as:

$$L_{g_min} = \frac{L_{g_max}}{10^{5/3}}$$

$$L_{g_min} = 32 \text{ m}$$

Step 6. Calculate the minimum length (L_{d_min}), required for channel routing, as:

$$L_{d_min} = 0.04 A_d^{0.7} = 0.04 (560^{0.7})$$

$$L_{d_min} = 3.36 \text{ km} = 3360 \text{ m}$$

Step 7. Select grid size based on the following criteria:

- for complete equilibrium conditions basin-wide, and a detailed description of rainfall-runoff processes basin-wide, select a grid size of 30 m;
- for complete equilibrium conditions on most grid cells, and a less detailed description of rainfall-runoff in upland areas, select a grid size of 1500 m;
- appropriate grid resolutions range between 1500 m and 30 m;
- based on modeling requirements and data availability, a 1 km grid size could be used in simulating this event on Hickahala-Senatobia;
- since L_{d_min} is larger than L_{g_max} ($3360 \text{ m} > 1500 \text{ m}$), a grid size as large as 1500 m could be used for simulations on Hickahala-Senatobia.

Having determined appropriate grid resolutions for the simulation of this particular event, an estimate of the peak discharge corresponding to the rainfall-runoff event can be evaluated as follows:

Step A. Calculate the time to equilibrium at the outlet of the watershed as:

$$T_{e_bas} = \left(\frac{\bar{n}_{ol} A_d^{1/2}}{\bar{i}^{2/3} \bar{S}^{1/2}} \right)^{3/5} = \left(\frac{0.08 (560,000,000)^{1/2}}{0.0000027^{2/3} 0.015^{1/2}} \right)^{3/5}$$

$$T_{e_bas} = 55073 \text{ sec} = 918 \text{ min}$$

Step B. Evaluate T_{out}^* as:

$$T_{out}^* = \frac{T_r}{T_{e_bas}} = \frac{180 \text{ min}}{918 \text{ min}}$$

$$T_{out}^* = 0.2$$

Step C. Since $T_{out}^* < T_{ce}^*$ ($0.2 < 1.03$), partial equilibrium conditions exist at the outlet and Q_{out}^* is evaluated using Eq. (7.13):

$$Q_{out}^* = 2.5(T_{out}^*)^2 (0.008)^{\frac{\bar{K}_s}{i}} = 2.5(0.2)^2 (0.008)^{0.04}$$

$$Q_{out}^* = 0.08$$

Step D. Peak discharge (Q_p) is estimated as:

$$Q_p = Q_{out}^* Q_e = Q_{out}^* (\bar{i} A_d)$$

$$Q_p = 0.08 (0.0000027 * 560,000,000)$$

$$Q_p = 121 \text{ m}^3 / \text{s}$$

Observed peak discharge measurements were only available for Hickahala Creek and Senatobia Creek. The drainage area corresponding to Hickahala Creek is approximately 310 km^2 (121 mi^2) and the drainage area corresponding to Senatobia Creek is approximately 210 km^2 (82 mi^2). The peak discharge at the sub-basin level can be evaluated by repeating Step A - Step D. The time to equilibrium (T_{e_bas}) of the two sub-basins (Step A) is calculated to be 769 min and 684 min. For a 3 hr rainfall duration (Step B), T_{out}^* corresponding to Hickahala Creek is 0.23 and T_{out}^* for Senatobia Creek is 0.26. Both values represent partial equilibrium conditions. Eq. (7.13) is used in

calculating Q_{out}^* (Step C). Q_{out}^* for the Hickahala sub-basin is 0.11 and for the Senatobia sub-basin Q_{out}^* is 0.14. The peak discharges are evaluated (Step D) as 92 m³/s for Hickahala Creek and 79 m³/s for Senatobia Creek.

Runoff hydrographs for the event were recorded on Hickahala Creek and Senatobia Creek. The peak discharge observed on Hickahala Creek was 82 m³/s. The peak discharge on Senatobia Creek was 130 m³/s. These values are within the range of the peak runoff rates calculated using the method developed in this study.

Chapter IX

SUMMARY AND CONCLUSIONS

In Chapters 4 and 5, the CASC2D model was applied using grid sizes ranging from 30x30 m to 1x1 km. The effects of grid size on runoff simulations were first evaluated using a 21 km² watershed. The model was calibrated and validated at three resolutions (416 ft, 832 ft, and 1248 ft). It was found that outlet and sub-basin runoff can be simulated using coarser resolutions, as long as the model is specifically calibrated at these resolutions (see Fig. 4.6, 4.7, 4.8, 4.9). At larger grid sizes, the percentage of channel cells, as compared to the total number of cells, is higher, and the estimated drainage density decreases (see Table 4.1). Under such conditions, in modeling runoff using the CASC2D model, overland flow reaches the channel more quickly, and runoff is conveyed to the outlet more rapidly. It was found that in order to account for the effects of increasing grid size, overland roughness coefficients had to be increased from 0.08 at a 416 ft grid size to 0.15 at a 1248 ft grid size.

The results from calibration and validation runs on the small-scale watershed were used in evaluating runoff on a large-scale watershed of 560 km². The effects of increasing grid sizes (100 ft, 1000 ft, 2000 ft, 3000 ft) on basin and network characteristics resulted in a higher percentage of channel cells and decreased drainage density (see Table 5.1). Upland slopes also decreased (see Fig. 5.4). In simulating outlet

conditions, it was found that the runoff response was delayed as a result of the time required for the wave to travel through the entire network. At the outlet, conditions in the channel have more of an impact on the nature of the hydrograph than the spatial variability of overland characteristics.

It was shown that the CASC2D model is capable of simulating rainfall events on large watersheds using fine grid resolutions. Using a 100 ft grid size, the Hickahala-Senatobia watershed was represented by 600,000 cells, with approximately 5,000 cells representing the channel network (see Table 5.1). Despite the large number of grid cells and the short computational time step required to maintain stability, it was possible to simulate runoff on a 560 km² watershed. As shown in Fig. 5.10, the calculation time required for simulations on large watersheds is greatly reduced when coarser resolutions are used. Coarser resolutions are typically more practical for large-scale simulations, due to the reduced computation time and the fewer input data requirements.

In Chapters 5 and 6, the concept of a watershed time to equilibrium (T_e) was used in evaluating basin-wide rainfall-runoff conditions. Complete and partial equilibrium hydrographs were simulated on the 21 km² watershed and the 560 km² watershed, assuming impervious and pervious conditions. The grid sizes used in the analyses ranged from 416 ft (127 m) to 3000 ft (914 m). GIS raster maps representing the spatial variability of drainage areas (A_d) were generated using GRASS programs (see Fig. 6.2 and 6.8). At increasing grid sizes, the cumulative distribution function of drainage areas shifted towards larger values of A_d (see Fig. 6.16a). In addition, it was found that grid size has an impact on the distribution of drainage areas corresponding to overland cells (Fig. 6.15b), but has very little effect on the distribution of drainage areas corresponding

to channel cells (6.15a). This was an important finding, since it had already been determined that channel routing controls the nature of runoff hydrographs on large-watersheds. If the distribution of drainage areas corresponding to channel cells is accurately reproduced at coarser grid resolutions, then these resolutions will provide reliable estimates of runoff in large-scale simulations.

Drainage areas associated with individual grid cells were used to evaluate the time to equilibrium (T_e) and the equilibrium discharge (Q_e) corresponding to constant rainfall intensities (see Fig. 6.3, 6.4, 6.9, 6.10). The results from pervious and impervious simulations were presented in the form of Q^* as a function of T^* , where $Q^* = Q_p/Q_e$ and $T^* = T_r/T_e$. The effect of infiltration can be quantified using the ratio of i_{eq}/i , where i_{eq} is an equivalent rainfall intensity corresponding to pervious conditions. Assuming a constant rainfall intensity, it was found that i_{eq}/i is constant for drainage areas greater than 1 km^2 (see Fig. 7.5a and 7.5b). According to these results, when $A_d > 1 \text{ km}^2$, the spatial variability of infiltration effects can be neglected, and i_{eq}/i can be evaluated as a function of \bar{K}_s / i (see Eq. 7.3). For non-uniform rainfall events, the value of i_{eq}/i also became constant for drainage areas greater than 1 km^2 (see Fig. 7.6). This indicates that at 1 km^2 , spatial and temporal rainfall variability become negligible, and i_{eq}/i can be evaluated as a function of \bar{K}_s / \bar{i} . Based on results from pervious simulations using uniform and non-uniform rainfall intensities, it can be concluded \bar{K}_s / \bar{i} can be used in estimating runoff conditions on drainage areas larger than 1 km^2 .

As demonstrated in Fig. 6.18, 7.9, 7.10, and 7.11, specific relationships were found to exist between the values of Q^* and T^* , for complete and partial equilibrium

conditions. Complete equilibrium is reached when $T^* = T_{ce}^*$. At complete equilibrium $Q^* = Q_{ce}^*$. The values of T_{ce}^* and Q_{ce}^* corresponding to specific infiltration conditions are related to \bar{K}_s / i , as seen in Eq. (7.9) and Eq. (7.10). The variation in T_{ce}^* and Q_{ce}^* as a function of \bar{K}_s / i was shown in Fig. 7.8, where T_{ce}^* ranged from 0.0 to 3, and Q_{ce}^* ranged from 0.3 to 1. When $T^* < T_{ce}^*$, partial equilibrium conditions exist, and runoff conditions are defined by a range of Q^* values. As seen in Eq. (7.11), (7.12), and (7.13), runoff on overland cells and channel cells can be evaluated as a function of \bar{K}_s / i and T^* . Since channel conditions have been found to be particularly important for large-scale simulations, the effect of \bar{K}_s / i on Q^* and T^* , for both complete and partial equilibrium conditions, is summarized in Fig. 7.13. At increasing values of \bar{K}_s / i (from pervious to impervious), the equilibrium discharge increases, and the time to reach equilibrium decreases.

As shown in Chapter 7 (Section 7.6), results from the dimensional analyses relating Q^* and T^* can be used in defining appropriate grid sizes for large-scale simulations. A method was developed to select grid sizes for 2-D hydrologic modeling of large watersheds, based on the results found in Chapters 6 and 7. Grid sizes are determined as a function of watershed characteristics (A_d , S , n_{ol} , K_s) and rainfall characteristics (i , T_r). A range of appropriate grid resolutions exists which will result in equilibrium conditions on individual grid cells. The grid size selected for runoff simulations will depend on the modeler's objective. For detailed and accurate representation of upland and channel runoff processes, the finer resolutions should be used. If input data is scarce and the objective is to simulate outlet conditions, coarser

resolutions can be used. The method for grid size selection was tested on the 560 km² basin, for a specific rainfall event. Appropriate grid sizes, based on watershed and rainfall characteristics, were calculated as ranging between 1500 m and 30 m.

Considering data availability and modeling requirements, a grid size of 1000 m was recommended as an ideal grid size for the large-scale simulation of this particular event.

In summary, referring back to the original objectives of this study, CASC2D simulations were performed on two watersheds using grid sizes ranging from 30x30 m to 1x1 km, in order to evaluate the effects of grid size on the representation of watershed characteristics and on the rainfall-runoff response. The feasibility of large scale simulations using fine resolutions was also evaluated. The concept of a watershed time to equilibrium was then applied in evaluating peak discharge rates throughout the basin, assuming impervious and pervious conditions. The dimensionless parameters Q^* and T^* were used to describe complete and partial equilibrium conditions. A method for grid size selection was developed as a result of the relationships governing Q^* and T^* , such that appropriate grid sizes were defined as a function of watershed and rainfall properties.

REFERENCES

- Agiralioglu, N., (1984), 'Effect of catchment geometry on time of concentration', *Proc. 3rd Int. Conf. On Urban Storm Drainage*, Göteborg, Sweden, **1**, 177-184.
- Agiralioglu, N., (1988), 'Estimation of the time of concentration for diverging surfaces', *J. Hydrol. Sci.*, **33(2)**, 173-179.
- Beven, K., (1985), 'Distributed models', in Anderson, M.G. and T.P. Burt (Eds), *Hydrological Forecasting*, John Wiley and Sons, Chichester, UK, Chp. 13.
- Beven, K., Wood, E.F., and Sivapalan, M. (1988), 'On hydrological heterogeneity — catchment morphology and catchment response', *J. Hydrol.*, **100**, 353-375.
- Beven, K., (1989), 'Changing ideas in hydrology — the case of physically based models', *J. Hydrol.*, **105**, 157-172.
- Beven, K., (1983), 'Surface water hydrology: Runoff generation and basin structure', *Rev. of Geophys.*, **21(3)**, 721-729.
- Beven, K., (1995), 'Linking parameters across scales: subgrid parameterizations and scale dependent hydrological models, in Kalma, J.D. and M. Sivapalan (Eds), *Scale Issues in Hydrological Modeling*, Advances in Hydrological Processes, John Wiley and Sons, New York, NY, 263-281.
- Black, P.E., (1970), 'Runoff from watershed models', *Wat. Resour. Res.*, Vol. 6, No. 2.
- Black, P.E., (1972), 'Hydrograph responses to geomorphic model watershed characteristics and precipitation variables', *J. Hydrol.*, **17**, 309-329.
- Black, P.E., and Cronn, J.W., (1975), 'Hydrograph responses to watershed model size and similitude relations', *J. Hydrol.*, **26**, 255-266.
- Blackmarr, W.A. (Ed.), 1995, 'Documentation of hydrologic, geomorphic, and sediment transport measurements on Goodwin Creek experimental watershed, Northern Mississippi, for the period 1982-1993 -- Preliminary release', ARS USDA, Oxford, MS, pp.141.

- Blösch, G., and M. Sivapalan, (1995), 'Scale issues in hydrological modeling: a review', *Hydrol. Process.*, **9**(3/4), 251.
- Blösch, G., R.B. Grayson, and M. Sivapalan, (1995), 'On the representative elementary area (REA) concept and its utility for distributed rainfall-runoff modeling, in J.D. Kalma, and M. Sivapalan (Eds), *Scale Issues in Hydrological Modeling*, Advances in Hydrological Processes, John Wiley and Sons, 71-88.
- Bruneau, P., Gascuel-Oudou, C., Robin, P., Merot, Ph., Beven, K. (1995), "Sensitivity of space and time resolution of a hydrological model using digital elevation data", *Hydrological Processes*, **9**, 69-81.
- Chairat, S. and J.W. Delleur, (1993), 'Effects of the topographic index distribution on predicted runoff using GRASS', *Water Resour. Bul.*, **29** (6), 1029-1034.
- DeCoursey, D.G., (1996), 'Hydrological, climatological and ecological systems scaling: A review of selected literature and comments', Interim Progress Report, USDA-ARS-NPA Great Plains Systems Research Unit, Ft. Collins, CO, pp.120.
- Doe, W.W. and B. Saghafian, (1992), 'Spatial and temporal effects of army maneuvers on watershed response: The integration of GRASS and a 2-D hydrologic model', *Proc. 7th Annual GRASS Users Conference*, National Park Service Technical Report NPS/NRG15D/NRTR-93/13, Lakewood, Colorado, 91-165.
- Dunne, T., (1982), 'Models of runoff processes and their significance', in *Scientific Basis of Water Resource Management*, National Academy Press, Washington, D.C., 17-30.
- Farajalla, N.S., and B.E. Vieux, (1995), 'Capturing the essential spatial variability in distributed hydrological modelling: infiltration parameters, *Hydrol. Process.*, **9**, 55-68.
- Fletcher, C.A.L., (1987), 'Computational Techniques for Fluid Dynamics 1. Fundamental and General Techniques', from the *Springer Series in Computational Physics*, Glowinski, R., Holt, M., Hut, P., Keller, H.B., Killeen, J., Orszag, S.A., and V.V. Rusanov (Eds), Second Edition, Springer-Verlag.
- Gao, X., Sorooshian, S., and D.C. Goodrich, (1993), 'Linkage of a GIS to a distributed rainfall-runoff model', in Goodchild, M.F., Parks, B.O., and L.T. Steyaert, (Eds), *Geographic Information Systems and Environmental Modeling*, Oxford University Press, Oxford, 182-186.
- Garbrecht, J. and L. Martz (1994), 'Grid size dependency of parameters extracted from digital elevation models', *Computers & Geosciences*, **20**(1), 85-87.

- Goodrich, D.C. and Woolhiser, D.A., (1991), 'Catchment hydrology', *Rev. of Geophys., Supplement: U.S. National Report to International Union of Geodesy and Geophysics 1987-1990*, 202-209.
- Goodrich, D.C., D.A. Woolhiser, and S. Sorooshian, (1993), 'A stabilization measure for stream network complexity and application of REA concepts to semi-arid watersheds', A preprint paper presented at the Robertson, NSW, Australia workshop on Scale Issues in Hydrological/Environmental Modeling, Abstract in Kalma, J., M. Sivapalan, and E. Wood, (Eds and Convenors), *Scale Issues in Hydrological/Environmental Modeling*, CSIRO-UAW-ANU, a Special publication, pp.36.
- Grayson, R.B., I.D. Moore, and T.A. McMahon, (1992a), 'Physically based hydrologic modeling, 1, A terrain-based model for investigative purposes', *Wat. Resour. Res.*, **28**, 2639-2658.
- Grayson, R.B., Moore, I.D., and McMahon, T.A. (1992b), 'Physically-based hydrologic modelling: 2. Is the concept realistic?', *Wat. Resour. Res.*, **26**, 2659-2666.
- Gupta, V.K., Waymire, E.D., and Wang, C.T., (1980), 'A representation of an instantaneous unit hydrograph from geomorphology', *Wat. Resour. Res.*, **16**(5), 855-862.
- Hack, J.T., (1957), 'Studies of longitudinal stream profiles in Virginia and Maryland', *U.S. Geol. Surv. Prof. Pap.*, **294-B**, 45-97.
- Henderson, F.M., and R.A. Wooding, (1964), 'Overland and groundwater flow from a steady rainfall of finite duration', *J. Geophys. Res.*, **69**(8), 1531-1540.
- Hillel, D., (1986), 'Modeling in soil physics: A critical review', In: *Future Developments in Soil Science Research*, A collection of Soil Sci. Soc. Am. Golden Anniversary contributions presented at Annual Meeting, New Orleans, 35-42.
- James, L.D., and S.J. Burges, (1982), 'Selection, calibration, and testing of hydrologic models', in Haan, C.T., Johnson, H.P., and D.L. Brakensiek (Eds), *Hydrological Modeling of Small Watersheds*, Am. Soc. Agr. Eng., St. Joseph, Mich., Monogr. Ser., **5**, 435-472.
- Julien, P.Y., and Moglen, G.E. (1990), 'Similarity and length scale for spatially varied overland flow', *Wat. Resour. Res.*, **26**, 1819-1832.
- Julien, P.Y., and Saghafian, B., (1991), 'A two-dimensional watershed rainfall-runoff model -- User's manual', Center for Geosciences, C.S.U., Ft. Collins, Colorado, pp.66.

- Julien, P.Y., Saghafian, B., and F.L. Ogden, (1995), 'Raster-based hydrological modeling of spatially-varied surface runoff', *Wat. Resour. Res.*, **31** (3), 523-535.
- Johnson, B.E., (1993), "Comparison of distributed vs. lumped rainfall-runoff modeling techniques", M.S. Thesis, Memphis State.
- Johnson, B.E., N.K. Raphael, and J.C. Willis, (1993), 'Verification of hydrologic modeling systems', *Proc. Federal Water Agency Workshop on Hydrologic Modeling Demands for the 90's*, USGS Water Resources Investigations Report 93-4018, June 6-9, Sec. 8., 9-10.
- Kirkby, M.J. (1976), 'Tests of the random network model and its applications to basin hydrology', *Earth Surf. Process.*, **1**, 197-212.
- Klein, M., (1976), 'Hydrograph peakedness and basin area', *Earth Surf. Process.*, **1**, 27-30.
- Klemes, V., (1986), 'Dilettantism in hydrology: transition or destiny?', *Water Resour. Res.*, **22**, 177S-188S.
- Lighthill, M.H., and G.B. Whitham, (1955), 'On kinetic waves, I, Flood movement in long rivers', *Proc. R. Soc. London, Ser. A*, **229**, 281-316.
- Loague, K.M., (1988), Streamflow generation: Equally likely realizations of a single stochastic process, In: *Modeling Agricultural, Forest, and Rangeland Hydrology*, Am. Soc. Agr. Eng., St. Joseph, Michigan, 420-426.
- Maidment, D.R., (1993), 'GIS and hydrologic modeling', in Goodchild, M.F., Parks, B.O., and L.T. Steyaert (Eds), *Geographic Information Systems and Environmental Modeling*, Oxford University Press, Oxford, 147-167.
- Milly, P.C.D., and P.S. Eagleson, (1987), 'Effect of spatial variability on average annual water balance', *Water Resour. Res.*, **23**, 2135-2143.
- Moore, I.D., A.K. Turner, J.P. Wilson, S.K. Jenson, and L.E. Band (1991), 'GIS and land surface-subsurface process modelling', paper presented at *First International Conference on Integrating Geographic Information systems and Environmental Modeling*, Natl. Center for Geogr. Inf. and Anal., Boulder, Colo., Sept. 15-18.
- Moore, I.D., Turner, A.K., Wilson, J.P., Jenson, S.K., and Band, L.E., (1993), 'GIS and land surface-subsurface process modeling' in Goodchild, M.F., Parks, B.O., and Steyaert, L.T. (Eds), *Geographic Information Systems and Environmental Modeling*, Oxford University Press, Oxford, 196-230.

- Ogden, F. (1992), 'Two-dimensional runoff modeling with weather radar data', Ph.D. dissertation, Colorado State University, Ft. Collins, Colorado.
- Rawls, W.J., Brakensiek, D.L., and N. Miller, (1983), 'Green-Ampt infiltration parameters from soils data, *J. Hydraul. Eng.*, **109(1)**, 62-70.
- Rodriguez-Iturbe, I.R. and Valdes, J.B., (1979), 'The geomorphic structure of hydrologic response', *Wat. Resour. Res.*, **15(6)**, 1409-1420.
- Saghafian, B. (1992), 'Hydrologic analysis of watershed response to spatially varied infiltration', Ph.D. dissertation, Colorado State University, Ft. Collins, Colorado.
- Saghafian, B., Julien, P.Y., (1995), 'Time to equilibrium for spatially variable watersheds', *J. Hydrol.*, **172**, 231-245.
- Sivapalan, M. and Wood, E.F. (1986), 'Spatial heterogeneity and scale in the infiltration response of catchments' in Gupta, V.K., Rodríguez-Iturbe, I., and Wood, E.F. (Eds), *Scale Problems in Hydrology*, D. Reidel, Dordrecht, 81-106.
- Sivapalan, M., Beven, K., and H.F. Wood, (1987), 'On hydrologic similarity, 2, A scaled model of storm runoff production', *Water Resour. Res.*, **23(12)**, 2266-2278.
- United States Army Corps of Engineers, (1993), 'GRASS 4.1 User's Reference Manual', Compiled at the Construction Engineering Research Laboratories, Champaign, Illinois, pp.458.
- Vieux, B.E. and N.S. Farajalla, (1994), 'Capturing the essential spatial variability in distributed hydrological modelling: hydraulic roughness', *Hydrol. Process.*, **8**, 221-236.
- Warwick, J.J., and S.J. Hanes, 1994, 'Efficacy of ARC/INFO GIS application to hydrologic modeling', *J. Water Resour. Plan. Mgt.*, **120(3)**, 366-379.
- Wood, E.F., (1983), 'Hydrology 1979-1982', *Rev. of Geophys.*, **21(3)**, 697-698.
- Wood, E.F., Sivapalan, M., Beven, K., and Band, L., (1988), 'Effects of spatial variability and scale with implications to hydrologic modeling', *J. Hydrol.*, **102**, 29-47.
- Wood, E.F., M. Sivapalan, and K.J. Beven, (1990), 'Similarity and scale in catchment storm response', *Rev. of Geophys.*, **28(1)**, 1-18.
- Wood, E.F., and V. Lakshmi, (1993), 'Scaling water and energy fluxes in climate systems: Three land-atmosphere modeling experiments', *Am. Met. Soc., J. of Climate*, **6**, 839-857.

- Wooding, R.A., (1965a), 'A hydraulic model for the catchment-stream problem, I. Kinematic-wave theory', *J. Hydrol.*, **3**, 254-267.
- Wooding, R.A., (1965b), 'A hydraulic model for the catchment-stream problem, II. Numerical solutions', *J. Hydrol.*, **3**, 268-282.
- Wooding, R.A., (1966), 'A hydraulic model for the catchment-stream problem, III. Comparison with runoff observations', *J. Hydrol.*, **4**, 21-37.
- Woolhiser, D.A., (1975), 'Simulation of unsteady overland flow', in *Unsteady Flow in Open Channels*, edited by K. Mahmood and V. Yevjevich, Vol. II, Water Resources Pub., Ft. Collins, Co.
- Woolhiser, D.A., (1977), 'Unsteady free-surface flow problems', in *Mathematical Models for Surface Water Hydrology*, Wiley, N.Y., 195-213.
- Woolhiser, D.A. and Goodrich, D., (1988), 'Effect of storm rainfall intensity patterns on surface runoff', *J. Hydrol.*, **102**, 335-354.

APPENDIX A
CASC2D SOURCE CODE

```
INTEGER ISHP(200,200), IMAN(200,200), ISOIL(200,200), KKK, ILL,  
+   NITER, ICHN(30,30,2), IQ(20,2), DIRROW(200,200),  
+   DIRCOL(200,200), DIRCOLMAX(200,200),DIRROWMAX(200,200)  
REAL E(200,200), H(200,200), RINT(200,200), DT, VINP(200,200),  
+   DQOV(200,200), DQCH(200,200), HCH(200,200), XRG(17),  
+   YRG(17), RRG(17), PMAN(10), PINF(10,3), TMAX(200,200),  
+   QCHNMAX(200,200),TCHNMAX(200,200),QFLOW(200,200),  
+   QROW(200,200),QCOL(200,200),TPEAK,QPEAK,  
+   RAVG(200,200),RTOT(200,200),RMAX(200,200)  
  
C   CALL GETTIM(IHR,IMIN,ISEC,I100)  
C   -----  
C   OPENING FILES  
C   -----  
OPEN(UNIT=21,FILE='SHAPE')  
OPEN(UNIT=22,FILE='ELEVATION')  
OPEN(UNIT=23,FILE='RAIN.DAT')  
OPEN(UNIT=24,FILE='SOIL')  
OPEN(UNIT=25,FILE='IN_DATA')  
OPEN(UNIT=26,FILE='CHANNEL_DATA')  
OPEN(UNIT=27,FILE='HYD.OUT')  
OPEN(UNIT=28,FILE='IMAN')
```

```

OPEN(UNIT=29,FILE='DISCH.OUT')
OPEN(UNIT=36,FILE='DEPTH.OUT')
OPEN(UNIT=60,FILE='QMAX.OUT')
OPEN(UNIT=61,FILE='TMAX.OUT')
OPEN(UNIT=62,FILE='DIRROW.OUT')
OPEN(UNIT=63,FILE='DIRCOL.OUT')
OPEN(UNIT=64,FILE='RAINAvg.OUT')
OPEN(UNIT=65,FILE='RAINMAX.OUT')
C -----
C  READING INPUT DATA - IN_DATA and CHANNEL
C -----
WRITE(27,222)
READ(25,*) M,N,W,NMAN,SDEP
READ(25,*) DT,NITER,NITRN,NPRN
READ(25,*) JOUT,KOUT,SOUT,WCHOUT,DCHOUT,RMANOUT
READ(25,*) INDEXINF,NSOIL
READ(25,*) NCHN,MAXCHN
READ(25,*) IRAIN
IF(IRAIN.EQ.0) READ(25,*) CRAIN
IF(IRAIN.EQ.1) READ(25,*) NRG,NREAD
IF(IRAIN.EQ.1) READ(25,*) (XRG(L),YRG(L),L=1,NRG)
READ(25,*) (PMAN(J),J=1,NMAN)
IF(INDEXINF.EQ.1)READ(25,*) ((PINF(J,K),K=1,3),J=1,NSOIL)
READ(25,*) INDEXDIS,NDIS
IF(INDEXDIS.EQ.1)READ(25,*) ((IQ(J,K),K=1,2),J=1,NDIS)
IF(NCHN.NE.0) READ(26,*) ((CHP(L,K),K=1,3),L=1,NCHN)
IF(NCHN.NE.0) READ(26,128) (((ICHN(L,J,K),J=1,MAXCHN),
+           K=1,2),L=1,NCHN)
128 FORMAT(/16I3/16I3)
WRITE(29,229) ((IQ(J,K),K=1,2),J=1,NDIS)

```

```

C -----
C  READING SHAPE, ELEVATIONS, AND MANNING N --
C -----
      DO I = 1,6
      READ(21,902)NO
      READ(22,902)NO
      READ(24,902)NO
      READ(28,902)NO
902  FORMAT(A100)
      ENDDO
      DO 150 J=1,M
          READ(21,*)(ISHP(J,K),K=1,N)
          READ(22,*)(E(J,K),K=1,N)
          DO 140 K=1,N
              E(J,K)=E(J,K)/100.
140  CONTINUE
          READ(24,*)(ISOIL(J,K),K=1,N)
          READ(28,*)(IMAN(J,K),K=1,N)
          H(J,K)=0.
          HCH(J,K)=0.
          DQOV(J,K)=0.
          DQCH(J,K)=0.
          VINP(J,K)=0.
          RTOT(J,K)=0.
          RAVG(J,K)=0.
          RMAX(J,K)=0.
150  CONTINUE
C -----
C  INITIALIZE MATRIX FOR LOCATION OF CHANNEL NODES
C -----

```

```

DO 160 IC=1,NCHN,1
  DO 175 L=1,MAXCHN,1
    J=ICHN(IC,L,1)
    K=ICHN(IC,L,2)
    IF(J.LE.0) GO TO 160
    ISHP(J,K)=2
175  CONTINUE
160  CONTINUE
    VIN=0.
    VOUT=0.
    VSUR=0.
    VINFTOT=0.
    RINDEX=1.
    KKK=0
C  -----
C  TIME LOOP
C  -----
DO 10 I=1,NITER
  ICALL=0
  IF(I.GT.NITRN) RINDEX=0.
  IF(I.LE.NITRN.AND.IRAIN.EQ.1) THEN
    IF(((I-1)/NREAD)*NREAD.EQ.(I-1)) THEN
      ICALL=1
      READ(23,124) (RRG(L),L=1,NRG)
124  FORMAT(17F9.3)
    ENDIF
  ENDIF
C  -----
C  UPDATE OVERLAND DEPTH AND FLOW
C  -----

```

```

DO 1 J=1,M
  DO 1 K=1,N
    IF(ISHP(J,K).EQ.0) GO TO 1
    IF(IRAIN.EQ.0) THEN
      RINT(J,K)=CRAIN
    ELSE
      IF(ICALL.EQ.1)CALL RAIN(J,K,NRG,XRG,YRG,RRG,RINT)
    ENDIF
    IF(RINT(J,K).GT.RMAX(J,K)) RMAX(J,K)=RINT(J,K)
    IF(I.GT.NITRN) RINT(J,K)=0.
    RTOT(J,K)=RTOT(J,K)+(RINT(J,K)*DT)
    HOV=DQOV(J,K)*DT/(W*W)
    HOV=HOV+H(J,K)+RINDEX*RINT(J,K)*DT
    IF(HOV.LT.0) GO TO 170
    IF(INDEXINF.EQ.1)CALL INFILT(J,K,DT,ISOIL,VINF,
+      PINF,HOV)
    H(J,K)=HOV
    DQOV(J,K)=0.
    VIN=VIN+RINDEX*RINT(J,K)*DT*W*W
    IF(I.EQ.NITER) VINFTOT=VINFTOT+VINF(J,K)*W*W
    IF(I.EQ.NITER.AND.ISHP(J,K).EQ.1)VSUR=VSUR+H(J,K)*W*W
1  CONTINUE
C  -----
C  UPDATE CHANNEL DEPTH
C  -----
  DO 2 IC=1,NCHN,1
    DO 3 L=1,MAXCHN,1
      J=ICHN(IC,L,1)
      K=ICHN(IC,L,2)
      JJ=ICHN(IC,L+1,1)

```

```

IF(J.LE.0) GO TO 2
IF(JJ.LT.0) GO TO 2
WCH=CHP(IC,1)
DCH=CHP(IC,2)
DHCH=DQCH(J,K)*DT/(W*WCH)
HCH(J,K)=HCH(J,K)+DHCH
IF(H(J,K).GT.SDEP) THEN
    HCH(J,K)=HCH(J,K)+(H(J,K)-SDEP)*W/WCH
    H(J,K)=SDEP
ENDIF
HTOP=DCH+H(J,K)
IF(HCH(J,K).GT.HTOP) THEN
    DH=(HCH(J,K)-HTOP)*WCH/W
    H(J,K)=H(J,K)+DH
    HCH(J,K)=HTOP+DH
ENDIF
IF(HCH(J,K).LT.0) GO TO 170
DQCH(J,K)=0.
IF(I.EQ.NITER) VSUR=VSUR+HCH(J,K)*W*WCH+H(J,K)*W*W
3   CONTINUE
2   CONTINUE
C   -----
C   OVERLAND FLOW ROUTING
C   -----
11  DO 20 J=1,M
    DO 30 K=1,N
        IF(ISHP(J,K).EQ.0) GO TO 30
        DO 40 L=-1,0,1
            JJ=J+L+1
            KK=K-L

```

```

        IF(JJ.GT.M.OR.KK.GT.N.OR.ISHP(JJ,KK).EQ.0) GO TO 40
        CALL OVRL(W,IMAN,PMAN,SDEP,J,K,JJ,KK,E,H,
+         DIRROW,DIRCOL,DQOV,QROW,QCOL,L)
40     CONTINUE
30     CONTINUE
20     CONTINUE
C     -----
C     CHANNEL FLOW ROUTING
C     -----
        DO 50 IC=1,NCHN,1
            WCH=CHP(IC,1)
            DCH=CHP(IC,2)
            RMANCH=CHP(IC,3)
            DO 60 L=1,MAXCHN-1,1
                J=ICHN(IC,L,1)
                K=ICHN(IC,L,2)
                JJ=ICHN(IC,L+1,1)
                KK=ICHN(IC,L+1,2)
                JJJ=ICHN(IC,L+2,1)
                IF(JJ.LE.0) GO TO 50
                CALL CHNCHN(NCHN,W,WCH,DCH,RMANCH,J,K,JJ,KK,JJJ,I,
+                E,HCH,ICHN,CHP,DQCH,NDIS,IQ,Q,QCHNMAX,TCHNMAX,DT)
60     CONTINUE
50     CONTINUE
C     -----
C     OUTFLOW DISCHARGE
C     -----
            HOUT=H(JOUT,KOUT)
            ALFA=SQRT(SOUT)/PMAN(IMAN(JOUT,KOUT))
            QOUTOV=0.

```

```

IF(HOUT.GT.SDEP) QOUTOV=W*ALFA*((HOUT-SDEP)**1.667)
H(JOUT,KOUT)=HOUT-QOUTOV*DT/(W*W)
HOUT=HCH(JOUT,KOUT)
WPOUT=WCHOUT+2.*HOUT
IF(HOUT.GT.DCHOUT) WPOUT=WCHOUT+2.*DCHOUT
AREAOUT=WCHOUT*HOUT
ALFA=SQRT(SOUT)/RMANOUT
QOUTCH=ALFA*(AREAOUT**1.6667)/(WPOUT**0.6667)
HCH(JOUT,KOUT)=HOUT-QOUTCH*DT/(W*WCHOUT)
QOUT=QOUTOV+QOUTCH
VOUT=VOUT+QOUT*DT

IF(I.EQ.1) THEN
  QPEAK=0.
  TPEAK=0.
ENDIF
IF(QOUT.GT.QPEAK) THEN
  QPEAK=QOUT
  TPEAK=REAL(I)*DT/60.
ENDIF
IF((1/NPRN)*NPRN.EQ.I) WRITE(27,111) I*DT/60.,QOUT
IF((1/NPRN)*NPRN.EQ.I) THEN
  WRITE(29,112) I*DT/60.,(Q(ILL),ILL=1,NDIS)
  KKK=KKK+1
  DO 1004 ILL=1,NDIS
    DISCH(KKK,ILL)=Q(ILL)
1004  CONTINUE
ENDIF
C -----
C  EVALUATING QMAX
C -----

```



```

DO 1099 J=1,M
DO 1099 K=1,N
IF(I.EQ.1) THEN
    QMAX(J,K)=0.0
    DIRROW(J,K)=0
    DIRCOL(J,K)=0
ELSE
    QFLOW(J,K)=QROW(J,K)+QCOL(J,K)
ENDIF
IF(QFLOW(J,K).GT.QMAX(J,K)) THEN
    QMAX(J,K)=QFLOW(J,K)
    TMAX(J,K)=REAL(I)*DT/60.
    DIRROWMAX(J,K)=DIRROW(J,K)
    DIRCOLMAX(J,K)=DIRCOL(J,K)
ENDIF
1099 CONTINUE
10 CONTINUE
C -----
C END OF TIME LOOP
C -----
C -----WRITING OUTPUT-----
WRITE(36,898)
DO 899 J=1,M
DO 899 K=1,N
    RAVG(J,K) = RTOT(J,K)*10000000./(DT*NITRN)
    RMAX(J,K) = RMAX(J,K)*10000000.
    IF(QCHNMAX(J,K).EQ.0) GO TO 899
    IF(QCHNMAX(J,K).GT.QMAX(J,K))THEN
        QMAX(J,K)=QCHNMAX(J,K)
        TMAX(J,K)=TCHNMAX(J,K)

```

```

        ENDIF
    IF(ISHP(J,K).EQ.0) GO TO 899
    WRITE(36,891) J,K,1000.*H(J,K),1000.*VIN(J,K)
899 CONTINUE
    DO 999 J=1,M
    WRITE(60,998)(QMAX(J,K),K=1,N)
    WRITE(61,998)(TMAX(J,K),K=1,N)
    WRITE(62,998)(DIRROWMAX(J,K),K=1,N)
    WRITE(63,998)(DIRCOLMAX(J,K),K=1,N)
    WRITE(64,998)(RAVG(J,K),K=1,N)
    WRITE(65,998)(RMAX(J,K),K=1,N)
999 CONTINUE
998 FORMAT(110F8.4)
    WRITE(27,113) QPEAK,TPEAK,VIN,VOUT,VSUR,VINFTOT
    GO TO 172
170 WRITE(27,171) J,K,I*DT,HOV
172 CONTINUE
C   CALL GETTIM(IHR,IMIN,ISEC,I100)
C   WRITE(27,(''Stopped at'',I2,':',I2,':',I2))IHR,IMIN,ISEC

222 FORMAT(/' TIME(MIN) DISCHARGE(CMS)'/)
229 FORMAT(/'DISCHARGE AT:',20(2I5,' ')/
+ 'TIME [MIN]',' DISCHARGE [CMS]'/)
111 FORMAT(2X,F7.2,F10.2)
112 FORMAT(2X,F5.1,20F7.2)
113 FORMAT(/' PEAK DISCHARGE IN CMS = ',F15.2/
+ ' TIME TO PEAK IN MIN = ',F15.2/
+ ' VOLUME IN M3 = ',F15.2/
+ ' VOLUME OUT IN M3 = ',F15.2/
+ ' SURFACE VOLUME IN M3= ',F15.2/

```

```

+      ' VOLUME INFILTRATED IN M3 =' ,F15.2/)
171 FORMAT(/'PROGRAM STOPPED FOR NEGATIVE DEPTH' ,2I4,2F15.6)
1054 FORMAT(I10)
550 FORMAT(I4)
898 FORMAT( ' ROW COLUMN DEPTH (MM) INFILTRATION (MM)')
891 FORMAT(2I6,2F10.0)

      END

C =====
      SUBROUTINE RAIN(J,K,NRG,XRG,YRG,RRG,RINT)
C =====
      DIMENSION XRG(NRG),YRG(NRG),RINT(200,200),RRG(NRG)
      RINT(J,K)=0.
      TOTDIST=0.
      TOTRAIN=0.
      DO 1 L=1,NRG
          REALJ=J
          REALK=K
          DIST=SQRT((REALJ-YRG(L))**2+(REALK-XRG(L))**2)
          IF(DIST.LT.1E-5) THEN
              RINT(J,K)=RRG(L)
              GO TO 2
          ENDIF
          TOTDIST=TOTDIST+1./(DIST**2)
          TOTRAIN=TOTRAIN+RRG(L)/(DIST**2)
1      CONTINUE
          RINT(J,K)=TOTRAIN/TOTDIST
C----->>>  UNIT CHANGE FROM in/hr TO m/s
2      RINT(J,K)=RINT(J,K)*0.0254/3600.
      RETURN
      END

```

```

C =====
SUBROUTINE INFILT(J,K,DT,ISOIL,VINF,PINF,HOV)
C =====
INTEGER ISOIL(200,200)
DIMENSION VINF(200,200),PINF(10,3)
IINF=ISOIL(J,K)
HYDCON=PINF(IINF,1)
CS=PINF(IINF,2)
SMD=PINF(IINF,3)
P1=HYDCON*DT-2.*VINF(J,K)
P2=HYDCON*(VINF(J,K)+CS*SMD)
RINF=(P1+SQRT(P1**2+8.*P2*DT))/(2.*DT)
IF((HOV/DT).LE.RINF) THEN
    RINF=HOV/DT
    HOV=0
ELSE
    HOV=HOV-RINF*DT
ENDIF
VINF(J,K)=VINF(J,K)+RINF*DT
RETURN
END
C =====
SUBROUTINE OVRL(W,IMAN,PMAN,SDEP,J,K,JJ,KK,E,H,
+ DIRROW,DIRCOL,DQOV,QROW,QCOL,L)
C =====
DIMENSION E(200,200),H(200,200),DQOV(200,200),PMAN(10),
+ QROW(200,200),QCOL(200,200)
INTEGER IMAN(200,200),L,DIRROW(200,200),DIRCOL(200,200)
DATA A/1./
S0=(E(J,K)-E(JJ,KK))/W

```

```

DHDX=(H(JJ,KK)-H(J,K))/W
SF=S0-DHDX+1E-30
IF(ABS(SF).LT.1E-20) SF=1E-20
HH=H(J,K)
RMAN=PMAN(IMAN(J,K))
IF(SF.LT.0) HH=H(JJ,KK)
IF(SF.LT.0) RMAN=PMAN(IMAN(JJ,KK))
IF(HH.LT.SDEP) RETURN
ALFA=(ABS(SF)**0.5)/RMAN
DQQ=SIGN(A,SF)*W*ALFA*((HH-SDEP)**1.667)
DQOV(J,K)=DQOV(J,K)-DQQ
DQOV(JJ,KK)=DQOV(JJ,KK)+DQQ
  IF(L.EQ.-1) THEN
    IF (DQQ.GT.0) THEN
      QROW(J,K)=DQQ
      DIRROW(J,K)=1
    ELSE
      QROW(J,K)=-DQQ
      DIRROW(J,K)=2
    ENDIF
  ENDIF
  IF(L.EQ.0) THEN
    IF (DQQ.GT.0) THEN
      QCOL(J,K)=DQQ
      DIRCOL(J,K)=3
    ELSE
      QCOL(J,K)=-DQQ
      DIRCOL(J,K)=4
    ENDIF
  ENDIF

```

RETURN

END

C =====
SUBROUTINE CHNCHN(NCHN,W,WCH,DCH,RMANCH,J,K,JJ,KK,JJJ,I,
+ E,HCH,ICHN,CHP,DQCH,NDIS,IQ,Q,QCHNMAX,TCHNMAX,DT)

C =====
DIMENSION HCH(200,200),ICHN(30,30,2),CHP(30,3),
+ DQCH(200,200),IQ(20,2),Q(20),E(200,200),
+ QCHNMAX(200,200),TCHNMAX(200,200)

REAL DT

DATA A/1./

S0=(E(J,K)-DCH-E(JJ,KK)+DCH)/W

IF(JJJ.LT.0) THEN

DO 5 IIC=1,NCHN,1

IF(JJ.EQ.ICHN(IIC,1,1).AND.KK.EQ.ICHN(IIC,1,2)) THEN

S0=(E(J,K)-DCH-E(JJ,KK)+CHP(IIC,2))/W

IJUN=IIC

GO TO 7

ENDIF

5 CONTINUE

ENDIF

7 DHDX=(HCH(JJ,KK)-HCH(J,K))/W

SF=S0-DHDX+1E-30

IF(ABS(SF).LT.1E-20) SF=1E-20

HH=HCH(J,K)

IF(SF.LT.0) THEN

WCH=CHP(IJUN,1)

DCH=CHP(IJUN,2)

RMANCH=CHP(IJUN,3)

HH=HCH(JJ,KK)

```

ENDIF
WP=WCH+2.*HH
IF(HH.GT.DCH) WP=WCH+2.*DCH
AREA=WCH*HH
DQ=SIGN(A,SF)*(SQRT(ABS(SF))/RMANCH)*(AREA**1.6667)/(WP**0.6667)
DQCH(J,K)=DQCH(J,K)-DQ
DQCH(JJ,KK)=DQCH(JJ,KK)+DQ
    IF(I.EQ.1) THEN
        QCHNMAX(J,K)=0.
        TCHNMAX(J,K)=0.
    ENDIF
    IF(DQ.GT.QCHNMAX(J,K)) THEN
        QCHNMAX(J,K)=DQ
        TCHNMAX(J,K)=REAL(I)*DT/60.
    ENDIF
DO 367 ILL=1,NDIS
C   IF(SF.GE.0) THEN
    IF(J.EQ.IQ(ILL,1).AND.K.EQ.IQ(ILL,2)) Q(ILL)=DQ
C   ELSE
C   IF(JJ.EQ.IQ(ILL,1).AND.KK.EQ.IQ(ILL,2)) Q(ILL)=-1.*DQ
C   ENDIF
367 CONTINUE
RETURN
END

```

APPENDIX B

INPUT DATA

The following raster maps were required as input to CASC2D simulations (see CASC2D source code, Appendix A):

1. SHAPE – describes the shape of the watershed
2. ELEVATION - digital elevation values for all cells
3. SOIL – soil types for all cells
4. IMAN – basin-wide variability in overland roughness coefficient (n)

The map of soil types (SOIL) was used to determine Green and Ampt infiltration parameters based on Table B.1, which has been reproduced from Rawls et al. (1983).

The parameters required to calculate the infiltration rate in the CASC2D formulation are the wetted front capillary head (H_f), hydraulic conductivity (K_s), and soil moisture deficit (M_d). Soil moisture deficit is equal to the difference between effective porosity (θ_e) and initial soil moisture (θ_i).

The map of basin-wide variability in overland roughness coefficients (IMAN) was derived from the landuse-types in the watershed. Specific values of overland Manning (n) are determined by calibrating the model.

Additional input data is specified in the 'IN_DATA' file and in the 'CHANNEL_DATA' file. Examples of these files for Goodwin Creek and Hickahala-

Senatobia are presented. The parameters in the IN_DATA file are described in Table

B.2.

Table B.1: Green-Ampt parameters based on soil texture

Soil Texture	Total Porosity	Effective Porosity	Wetted Front Capillary Head (m)	Hydraulic Conductivity (m/s)
sand	0.437	0.417	0.0495	3.27E-5
loamy sand	0.437	0.401	0.0613	8.31E-6
sandy loam	0.453	0.412	0.1101	3.03E-6
loam	0.463	0.434	0.0889	9.44E-7
silt loam	0.501	0.486	0.1668	1.81E-6
sandy clay loam	0.398	0.330	0.2185	4.17E-7
clay loam	0.464	0.309	0.2088	2.78E-7
silty clay loam	0.471	0.432	0.2730	2.78E-7
sandy clay	0.430	0.321	0.2390	1.67E-7
silty clay	0.479	0.423	0.2922	1.39E-7
clay	0.475	0.385	0.3163	8.33E-8

Table B.2: Description of CASC2D input parameters

INPUT PARAMETER	DESCRIPTION
M, N	Number of rows, number of columns
W	Width of grid cells
NMAN	Number of overland roughness coefficients
SDEP	Detention storage
DT	Time step
NITER	Number of total iterations
NITRN	Number of rainfall iterations
NPRN	Frequency of writing output
JOUT, KOUT, SOUT	Outlet row number, column number, and slope
WCHOUT, DCHOUT, RMANOUT	Outlet width, depth, and roughness coefficient
INDEXINF	Infiltration index, where 0=no infiltration, 1=with infiltration
NSOIL	Number of soil types
NCHN	Number of channel links
MAXCHN	Maximum number of nodes per link
IRAIN	Rain index, where 0=uniform rainfall, 1=non-uniform rainfall
NRG, NREAD	Number of raingages, frequency of gage data
XRG, YRG	Raingage location, column number and row number
PMAN	Manning coefficient
PINF	Infiltration parameters (K_s , H_f , M_d)
INDEXDIS	Index for sub-basin hydrograph determination
NDIS	Number of sub-basin hydrographs desired
IQ (J,K)	Location of sub-basin hydrographs, row and column

GOODWIN CREEK IN_DATA FILE (simulation of event 1 at a 416 ft grid size)

47	75	126.83	3	0.000	→ M,N,W,NMAN,SDEP
10.	3000	1266	30		→ DT,NITER,NITRN,NPRN
44	3	0.002	23.63	6.05	0.037 → JOUT,KOUT,SOUT,WCHOUT,DCHOUT,RMANOUT
1	3				→ INDEXINF,NSOIL
19	16				→ NCHN,MAXCHN
1					→ IRAIN
17	6				→ NRG,NREAD
4.5	43.5				→ XRG(L),YRG(L) for L=1,NRG
15.5	26.5				
33.5	20.5				
45.5	16.5				
41.5	9.5				
44.5	25.5				
58.5	11.5				
57.5	16.5				
62.5	14.5				
19.5	26.5				
28.5	26.5				
33.5	23.5				
22.5	34.5				
30.5	33.5				
37.5	29.5				
39.5	18.5				
52.5	19.5				
0.08					→ PMAN(J) for J=1,NMAN
0.08					
0.08					
1.30E-6	0.16	0.1			→ PINF(J,K),K=1,3 for J=1,NSOIL
1.30E-6	0.16	0.1			
2.20E-6	0.08	0.1			
1	5				→ INDEXDIS,NDIS
37	9				→ IQ(J,K),K=1,2 for J=1,NDIS
20	33				
13	38				
23	39				
17	54				

HICKAHALA-SENATOBIA IN_DATA FILE (simulation of constant rainfall intensity at
1000 ft grid size)

104	108	304.80	1	0.0	→ M,N,W,NMAN,SDEP
1.	108000	300			→ DT,NITER,NITRN,NPRN
26	3	0.001	60.00	7.0	0.038 → JOUT,KOUT,SOUT,WCHOUT,DCHOUT,RMANOUT
1	2				→ INDEXINF,NSOIL
30	27				→ NCHN,MAXCHN
0					→ IRAIN
0.0000035280					→ CRAIN
0.1					→ PMAN(J) for J=1,NMAN

2.5E-06	0.08	0.1	→ PINF(J,K),K=1,3 for J=1,NSOIL
1.3E-06	0.1668	0.1	
1	4		→ INDEXDIS,NDIS
42	17		→ IQ(J,K),K=1,2 for J=1,NDIS
39	49		
26	74		
70	32		

The CHANNEL_DATA file provides information on channel characteristics corresponding to individual channel links. The location of all channel cells is defined using (J) and (K) coordinates, where (J) represents the row number and (K) represents the column number, and -1 signifies the end of a link.

GOODWIN CREEK CHANNEL_DATA FILE (416 ft simulation, total of 19 links)

28.99	4.00	0.037	→ Width [m], Depth [m], Channel roughness
32.71	4.20	0.037	Link 1 through Link 19
23.45	4.34	0.037	
18.35	4.34	0.037	
15.24	4.50	0.037	
17.70	4.70	0.037	
37.97	4.97	0.037	
28.24	5.32	0.037	
23.63	6.05	0.037	
12.88	3.87	0.037	
22.42	3.98	0.037	
14.48	4.11	0.037	
15.70	3.40	0.037	
16.32	3.55	0.037	
13.65	3.83	0.037	
8.58	4.30	0.037	
7.42	4.50	0.037	
6.00	3.00	0.037	
7.00	3.50	0.037	

13 13 13 13 13 13 12 12 12 11 11 11 11 11 11 -1	Link1
69 68 67 66 65 64 64 63 62 62 61 60 59 58 57 -1	

11 11 12 12 12 12 12 13 14 14 15 15 16 16 16 -1	Link2
57 56 56 55 54 53 52 52 52 51 51 50 50 49 48 -1	

16 16 16 16 16 15 15 15 14 14 14 14 14 -1 0 0	Link3
48 47 46 45 44 44 43 42 42 41 40 39 38 -1 0 0	

.....Etc.

As rainfall input, either a constant rainfall rate or recorded raingage data can be used. Five events selected for simulations on Goodwin Creek are summarized in Table B.3. Fig. B.1 shows observed runoff hydrographs and stage measurements corresponding to the four events.

Table B.3: Goodwin Creek rainfall events

	Date	Time begin	Time end	Duration
Event 1	Oct 17, 1981	9:19 PM	12:50 AM (next day)	3hr 31min
Event 2	Feb 8, 1982	7:00 PM	1:01 AM (next day)	6hr 01min
Event 3	Dec 27, 1988	8:31 PM	5:07 AM (next day)	6hr 47min
Event 4	Dec 2, 1983	12:00 AM	7:06 AM (next day)	3 1hr 09min

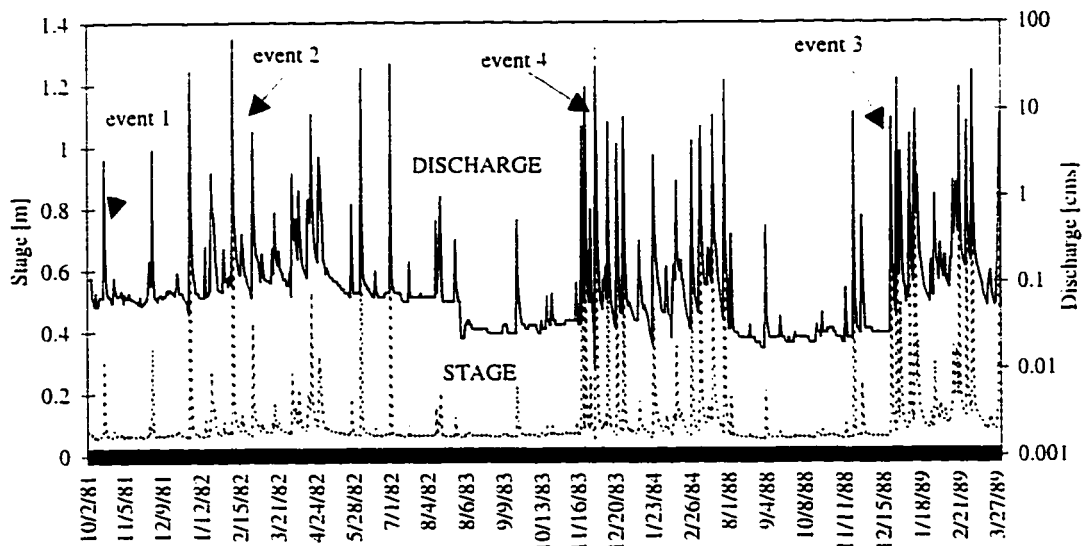


Fig. B.1: Goodwin Creek observed stage and discharge

The spatial variability of rainfall rates for each event is evaluated by calculating the coefficient of variation of the average and maximum rainfall rates corresponding to individual grid cells, where the coefficient of variation is calculated as:

$$C_v = \frac{\text{value} - \text{mean value}}{\text{mean value}} \quad (\text{B.1})$$

Raster maps showing the spatial variability of average and maximum coefficients of variation are shown in Fig. B.2 and B.3, where Eq. (B.1) was applied using values corresponding first to the average rainfall rate on each cell and then using values corresponding to the maximum rainfall rate on each cell.

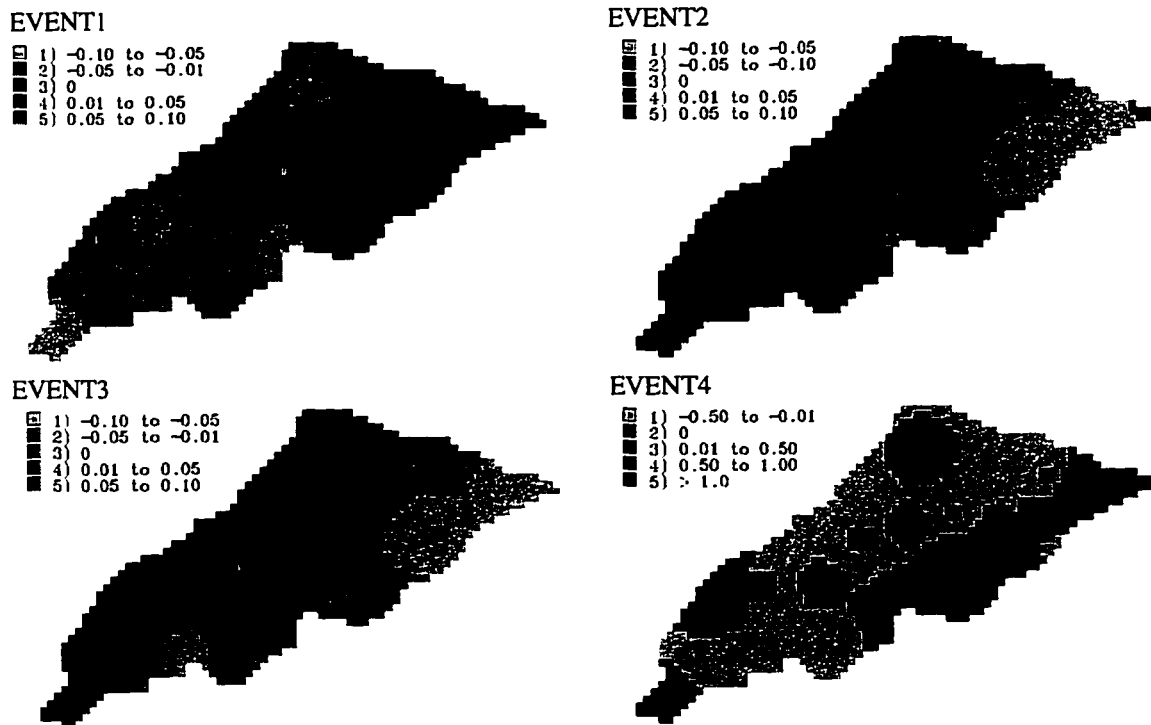


Fig. B.2: Coefficient of variation of average rainfall rates for Goodwin Creek events

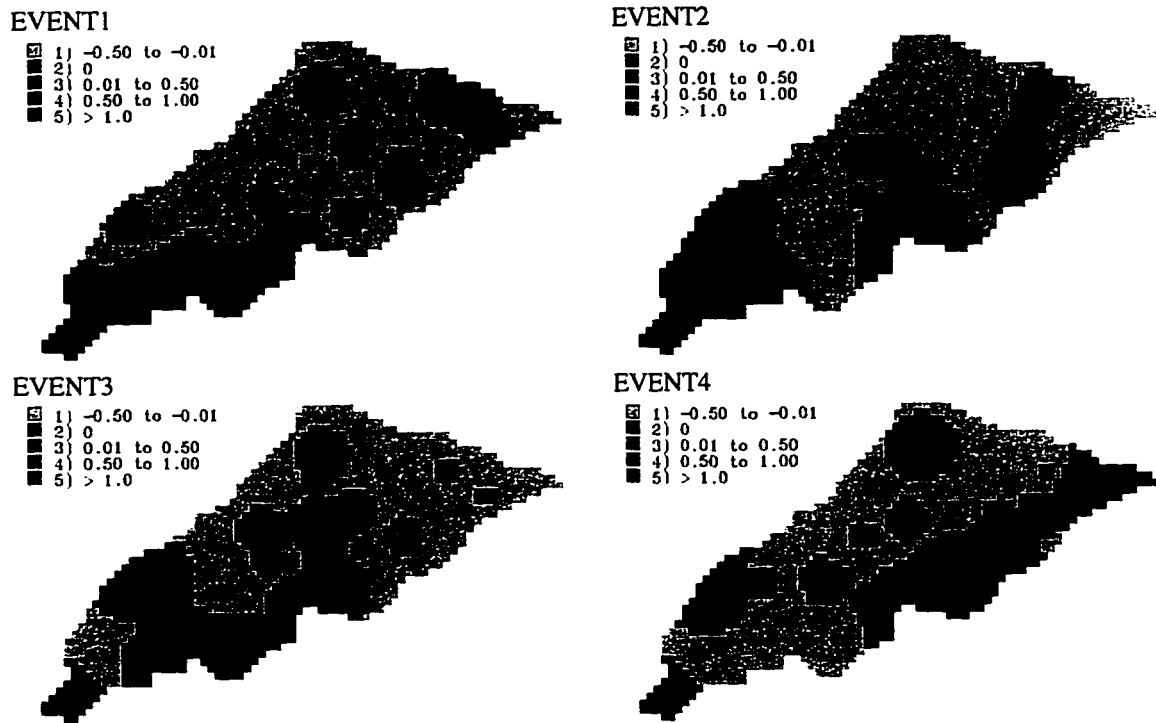


Fig. B.3: Coefficient of variation of maximum rainfall rates for Goodwin Creek events

APPENDIX C
CALIBRATION DATA

Modeling calibration was performed for Goodwin Creek using event 1, first with the objective of minimizing the differences between simulated and observed peak discharge and time to peak at the outlet. Three resolutions were used. The parameters corresponding to eight of the trial simulations are presented in Tables C.1-C.3. The hydrographs corresponding to the trial simulations are shown in Fig. C.1- C.3.

Calibration runs at increasing grid sizes showed the effects of parameters on peak discharge and time to peak at the respective resolutions. The results for eight of the trial simulations at a 416 ft grid size are summarized in Fig. C.4, where Q_p/Q_{obs} and T_p/T_{obs} are shown.

Table C.1: Parameter values used for trial simulations at a 416 ft grid size

	Trial 1	Trial 2	Trial 3	Trial 4	Trial 5	Trial 6	Trial 7	Trial 8
S_d	0.015	0.015	0.015	0.015	0.02	0.02	0.015	0.015
$n_{channel}$	0.037	0.037	0.037	0.037	0.037	0.037	0.037	0.037
$n_{ol\ type1}$	0.08	1	1	5	0.09	0.08	0.08	1
$n_{ol\ type2}$	0.08	0.2	0.3	0.3	0.09	0.08	0.08	0.5
$n_{ol\ type3}$	0.08	0.15	0.15	0.15	0.09	0.08	0.08	0.5
$K_s\ soil\ 1$	1.3E-6	1.3E-6	1.3E-6	1.3E-6	1.3E-6	1.3E-6	1.81E-6	1.81E-6
$K_s\ soil\ 2$	2.2E-6	2.2E-6	2.2E-6	2.2E-6	2.2E-6	2.2E-6	3.03E-6	3.03E-6
$H_f\ soil\ 1$	0.16	0.16	0.16	0.16	0.16	0.16	0.1668	0.1668
$H_f\ soil\ 2$	0.08	0.08	0.08	0.08	0.08	0.08	0.1101	0.1101
$M_d\ soil\ 1$	0.08	0.1	0.01	0.01	0.05	0.04	0.08	0.08
$M_d\ soil\ 1$	0.08	0.1	0.01	0.01	0.05	0.04	0.08	0.08

Table C.2: Parameter values used for trial simulations at a 832 ft grid size

	Trial 1	Trial 2	Trial 3	Trial 4	Trial 5	Trial 6	Trial 7	Trial 8
S_d	0.015	0.015	0.015	0.015	0.02	0.02	0.015	0.015
$n_{channel}$	0.037	0.037	0.037	0.037	0.037	0.037	0.037	0.037
n_{oi} type 1	0.09	1	5	5	0.09	0.09	0.09	1
n_{oi} type 2	0.09	0.2	0.3	0.3	0.09	0.09	0.09	0.5
n_{oi} type 3	0.09	0.15	0.15	0.15	0.09	0.09	0.09	0.5
K_s soil 1	1.3E-6	1.3E-6	1.3E-6	1.3E-6	1.3E-6	1.3E-6	1.81E-6	1.81E-6
K_s soil 2	2.2E-6	2.2E-6	2.2E-6	2.2E-6	2.2E-6	2.2E-6	3.03E-6	3.03E-6
H_f soil 1	0.16	0.16	0.16	0.16	0.16	0.16	0.1668	0.1668
H_f soil 2	0.08	0.08	0.08	0.08	0.08	0.08	0.1101	0.1101
M_d soil 1	0.1	0.1	0.1	0.1	0.05	0.15	0.1	0.1
M_d soil 1	0.1	0.1	0.1	0.1	0.05	0.15	0.1	0.1

Table C.3: Parameter values used for trial simulations at a 1248 ft grid size

	Trial 1	Trial 2	Trial 3	Trial 4	Trial 5	Trial 6	Trial 7	Trial 8
S_d	0.015	0.015	0.015	0.015	0.02	0.02	0.015	0.015
$n_{channel}$	0.04	0.04	0.04	0.04	0.04	0.04	0.04	0.04
n_{oi} type 1	0.15	1	5	5	0.15	0.15	0.15	1
n_{oi} type 2	0.15	0.2	0.3	0.3	0.15	0.15	0.15	0.5
n_{oi} type 3	0.15	0.15	0.15	0.15	0.15	0.15	0.15	0.5
K_s soil 1	1.3E-6	1.3E-6	1.3E-6	1.3E-6	1.3E-6	1.3E-6	1.81E-6	1.81E-6
K_s soil 2	2.5E-6	2.2E-6	2.5E-6	2.5E-6	2.5E-6	2.5E-6	3.03E-6	3.03E-6
H_f soil 1	0.1668	0.1668	0.1668	0.1668	0.1668	0.1668	0.1668	0.1668
H_f soil 2	0.08	0.08	0.08	0.08	0.08	0.08	0.1101	0.1101
M_d soil 1	0.1	0.1	0.1	0.1	0.1	0.15	0.1	0.1
M_d soil 1	0.1	0.1	0.1	0.1	0.1	0.15	0.1	0.1

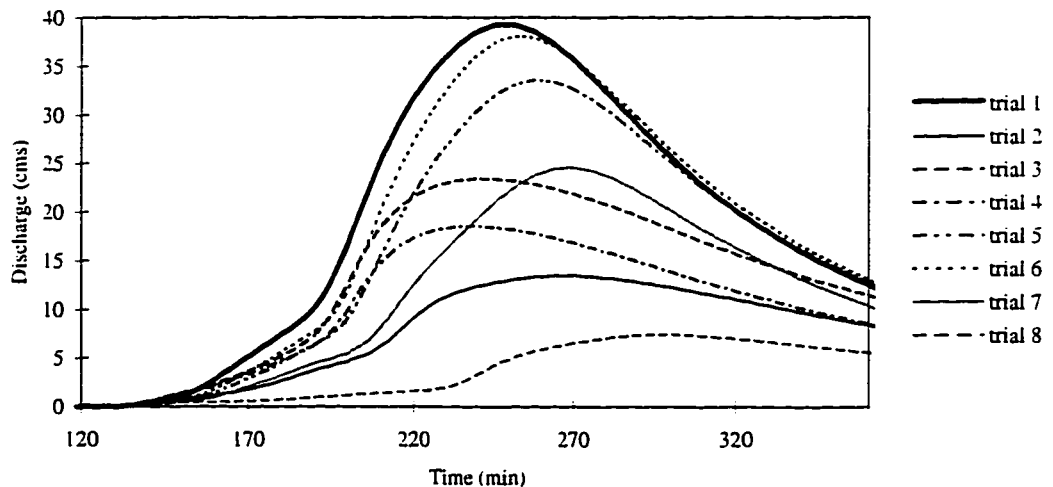


Fig. C.1: Simulated hydrographs from calibration runs at a 416 ft grid size

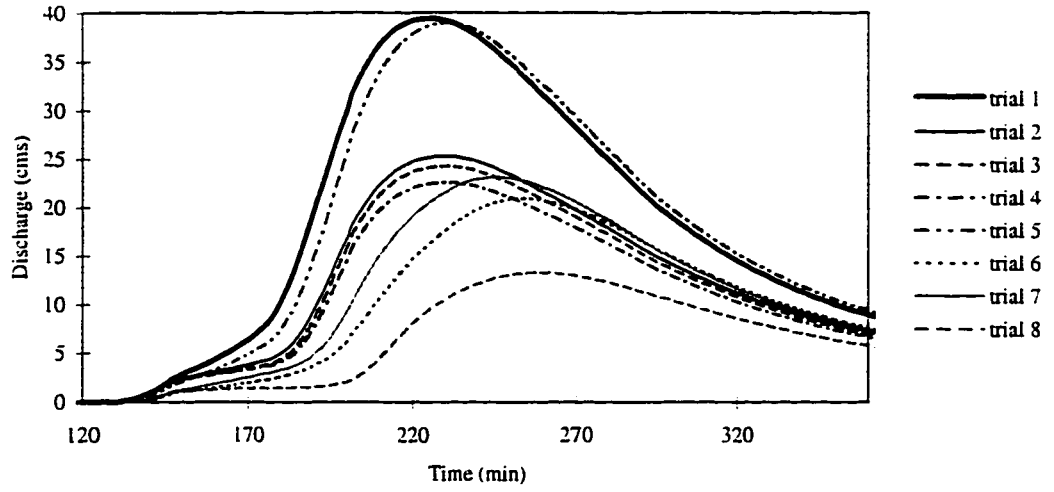


Fig. C.2: Simulated hydrographs from calibration runs at a 832 ft grid size

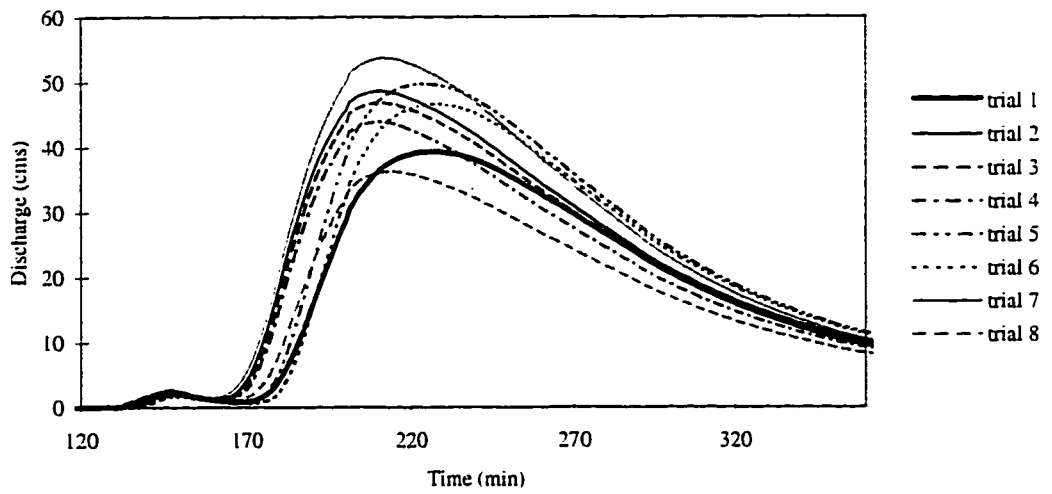


Fig. C.3: Simulated hydrographs from calibration runs at a 1248 ft grid size

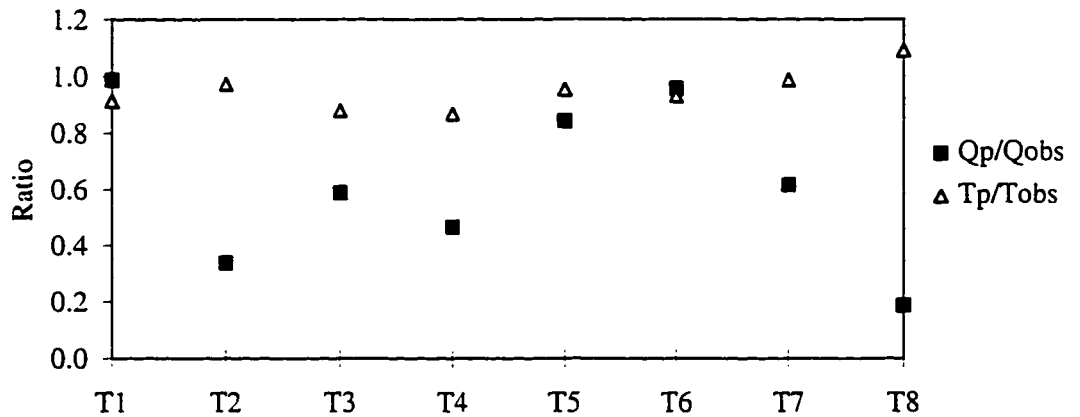


Fig. C.4: Peak discharge and time to peak for trial calibration runs

Calibration was also performed at the sub-basin level, where parameter values were modified so as to obtain the best possible fit between observed and simulated hydrographs at gages 3, 5, and 12. Trial simulations were performed at a 416 ft grid size. The changes in parameters for ten trial simulations of event 1 are presented in Table C.4. The ratio (Δ) shown in the table was defined in Eq. 4.1 (Section 4.2.1, Chapter 4). Trial 1, the parameters calibrated for outlet conditions, was used as a reference (see Table 4.4 for actual parameter values).

Table C.4: Parameter calibration for sub-basins (event 1)

	trial 2	trial 3	trial 4	trial 5	trial 6	trial 7	trial 8	trial 9	trial 10
	Δ	Δ	Δ	Δ	Δ	Δ	Δ	Δ	Δ
S_d	0.33			-0.93	0.33	0.33	0.33	0.33	
n_{oi} type1		-0.5				0.25	0.25	0.25	0.25
n_{oi} type2		-0.5				0.25	0.25	0.25	0.25
n_{oi} type3		-0.5				0.25	0.25	0.25	0.25
K_s soil 1		0.39							
K_s soil 2		0.38							
H_f soil 1		0.04							
H_f soil 2		0.38							
M_d soil 1	-0.5	-0.38	-0.75		-0.75	-0.75	-0.63	-0.5	-0.5
M_d soil 1	-0.5	-0.38	-0.75		-0.75	-0.75	-0.63	-0.5	-0.5

The effects of changing parameters on peak discharge are shown in Fig. C.5.

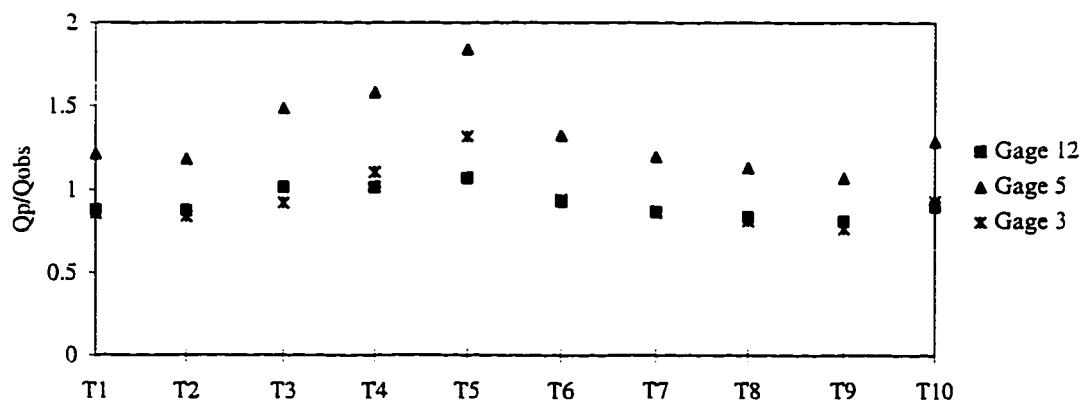


Fig. C.5: Peak discharge for sub-basin calibration runs (event 1)

The parameters resulting in the best fit at a 416 ft grid size were used at the coarser resolutions. The results at each sub-basin gage are shown in Fig. C.6

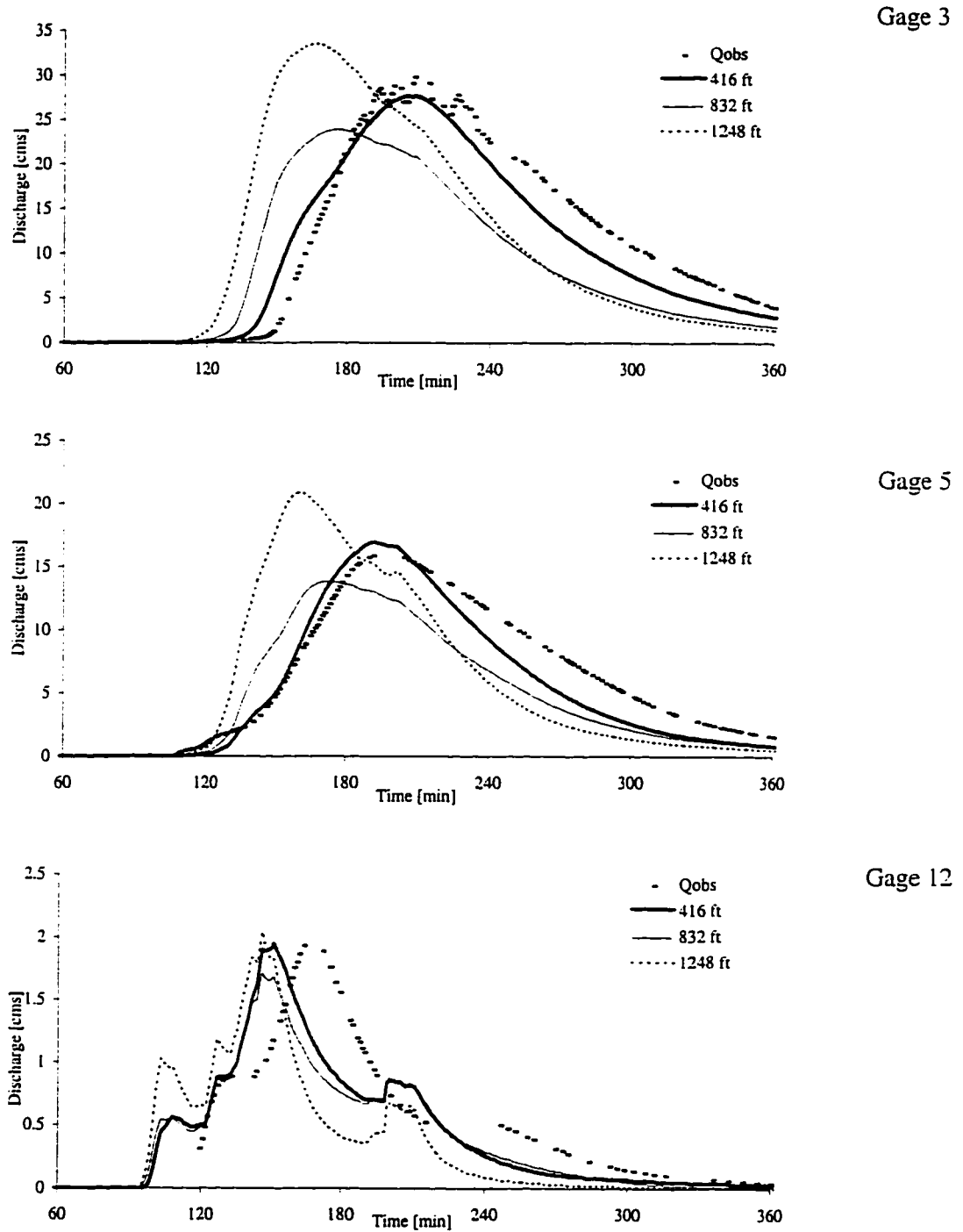


Fig. C.6: Effects of increasing grid size on sub-basin hydrographs (event 1)

The changes in parameters for ten trial simulations of event 2, at a 416 ft grid size, are presented in Table C.5. Trial 1, the parameters calibrated for outlet conditions, is used as a reference (see Table 4.5 for actual values). Trial 3 was simulated using the hydraulic conductivity values corresponding to event 1.

Table C.5: Parameter calibration for sub-basins (event 2)

	trial 2	trial 3	trial 4	trial 5	trial 6	trial 7	trial 8	trial 9	trial 10
	Δ	Δ	Δ	Δ	Δ	Δ	Δ	Δ	Δ
n_{channel}							0.08	0.62	0.62
$n_{\text{ol type1}}$					-0.5	-0.25	-0.25	-0.25	-0.25
$n_{\text{ol type2}}$					-0.5	-0.25	-0.25	-0.25	-0.25
$n_{\text{ol type3}}$					-0.5	-0.25	-0.25	-0.25	-0.25
$K_s \text{ soil 1}$		12		-0.5	-0.5	-0.5	-0.5	-0.5	-0.5
$K_s \text{ soil 2}$		13.67		-0.533	-0.53	-0.53	-0.53	-0.53	-0.53
$H_f \text{ soil 1}$			15						-0.9
$H_f \text{ soil 2}$			7						-0.9
$M_d \text{ soil 1}$	$\Delta=0.1$								
$M_d \text{ soil 1}$	$\Delta=0.1$								

The effect of parameter changes is summarized in Fig. C.7, where Q_p/Q_{obs} is shown of each trial simulation.

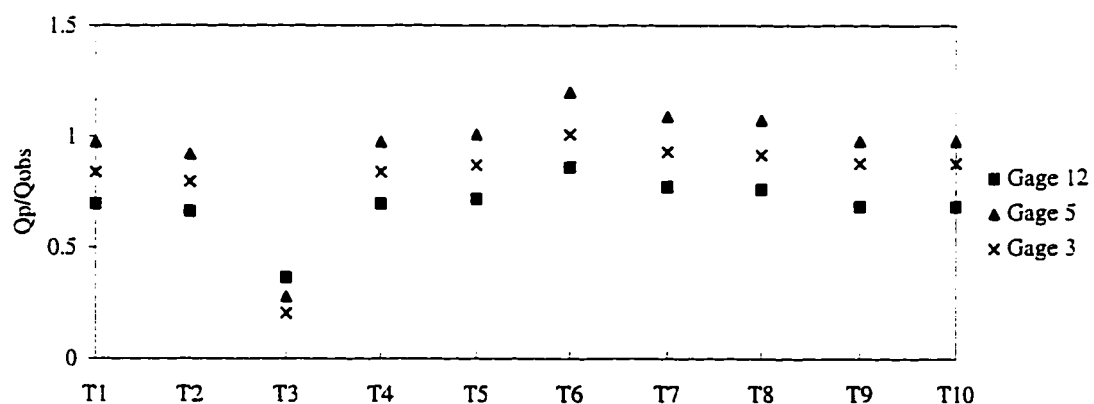
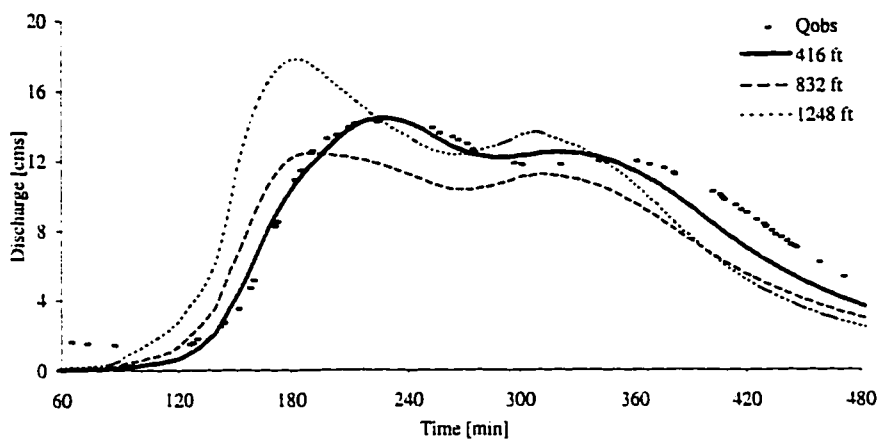
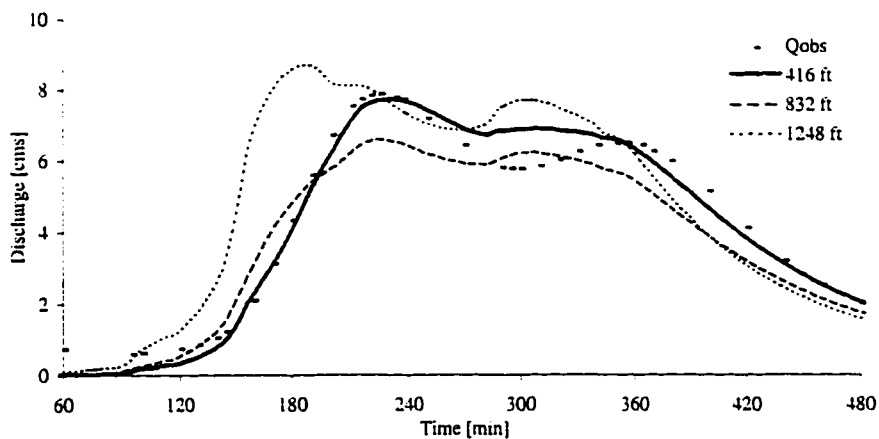


Fig. C.7: Peak discharge for sub-basin calibration runs (event 2)

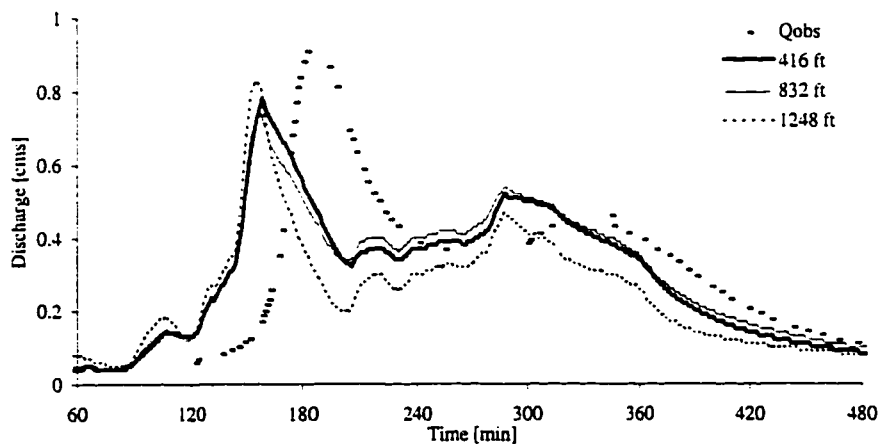
The 416 ft grid size parameter values resulting in the best fit at the sub-basin level were used at the coarser resolution. The effects of increasing grid size are shown in Fig. C.8 for gages 3, 5, and 12.



Gage 3



Gage 5



Gage 12

Fig. C.8: Effects of increasing grid size on sub-basin hydrographs (event 2)

APPENDIX D

GRASS PROGRAMS USED IN ANALYSIS

The Geographical Resources Analysis Support System (GRASS) is a public domain system which was originally developed by researchers in the Environmental Division of the US Army Construction Engineering Research Laboratories (USACERL) in Champaign, Illinois. The GRASS system is used to manipulate and analyze geographic data. The following GRASS programs were used in synthesizing input data for CASC2D simulations (United States Army Corps of Engineers, 1993):

g.region: defines the watershed region as a function of north, south, east, and west coordinates and a grid resolution. When the grid size is increased, the value corresponding to the grid cell closest to the center of the larger cell is chosen to represent the larger scale.

r.mapcalc: performs mathematical operations on raster maps and can be used to create new maps.

r.slope.aspect: determines the slope and aspect corresponding to individual cells, based on a DEM.

r.stats: summarizes the statistics corresponding to any raster map. It can be used in evaluating the spatial distribution of parameter values.

r.watershed: based on a DEM, it evaluates drainage patterns on a watershed and generates raster maps depicting sub-basin areas, the location of the stream network, the accumulated drainage area corresponding to each cell, and the drainage direction at each cell. Drainage can be specified to occur horizontally or vertically, but not cross-diagonally between cells.

APPENDIX E

RESULTS FROM PERVIOUS SIMULATIONS AT COARSE RESOLUTIONS

Pervious simulations were performed on Goodwin Creek and Hickahala-Senatobia for \bar{K}_s / i ratios of 1.0, 0.5, and 0.2, using a wide range of rainfall durations (T_r). Peak discharge was determined at individual grid cells, and basin-wide values of Q^* were evaluated as a function of T_r^* . The values of Q^* as a function of T_r^* were not significantly affected by grid size. The only difference was that at coarse resolutions fewer data points existed, since the watershed was represented by fewer cells.

The results for the 416 ft grid size on Goodwin Creek were presented in Chapter 7, Section 7.2. Results at a 832 ft grid size are shown in Fig. E.1a-E.1c for \bar{K}_s / i equal to 1.0, 0.5, and 0.2. Results at a 1248 ft grid size are shown in Fig. E.2a-E.2c for \bar{K}_s / i of 1.0, 0.5, and 0.2.

The results from the 1000 ft grid size on Hickahala-Senatobia, were presented in Chapter 7, Section 7.3. Results at a 2000 ft grid size are shown in Fig. E.3a-E.3c for \bar{K}_s / i equal to 1.0, 0.5, and 0.2. Results at a 3000 ft grid size are shown in Fig. E.4a-E.4c for \bar{K}_s / i of 1.0, 0.5, and 0.2. The outlying points, where $Q^* > 1$, correspond to overland cells where drainage areas may not have been correctly assessed (see discussion, Section 6.3).

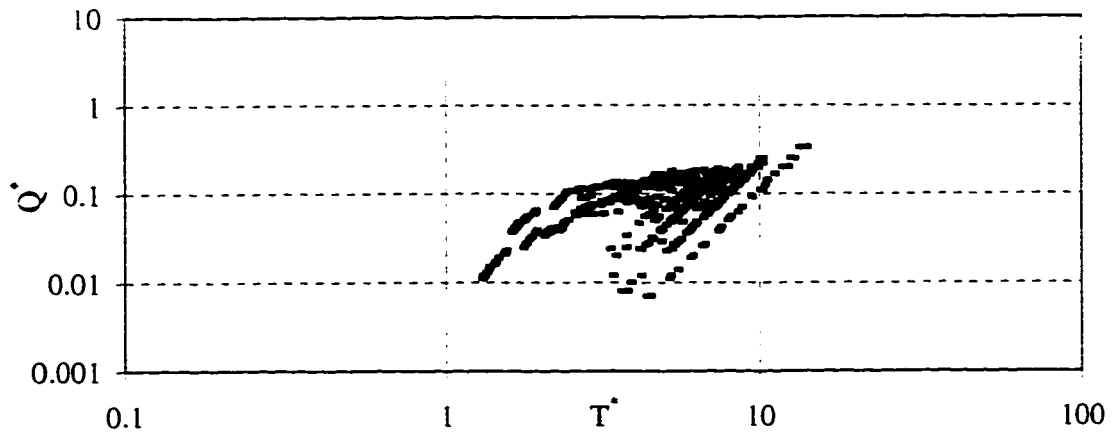


Fig.E.1a: Peak runoff rates on Goodwin Creek for $\bar{K}_s / i = 1.0$ (832 ft grid size)

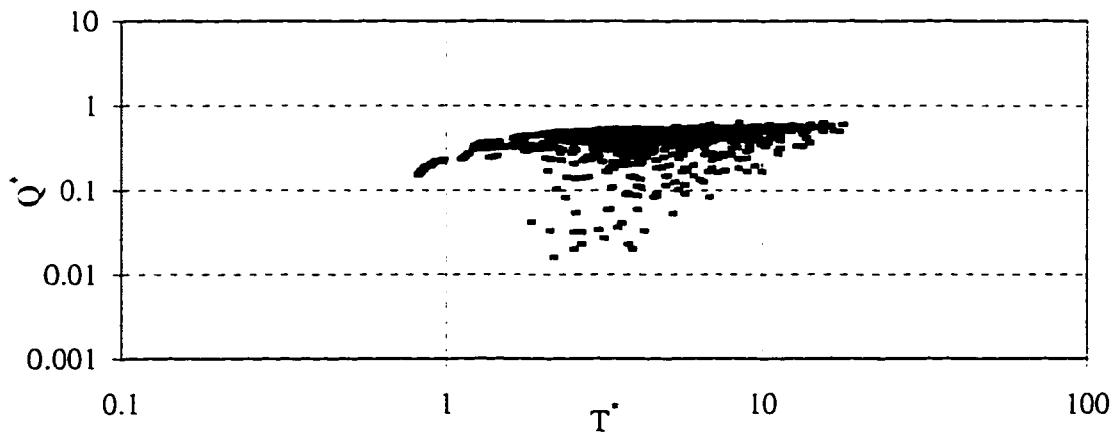


Fig. E.1b: Peak runoff rates for on Goodwin Creek $\bar{K}_s / i = 0.5$ (832 ft grid size)

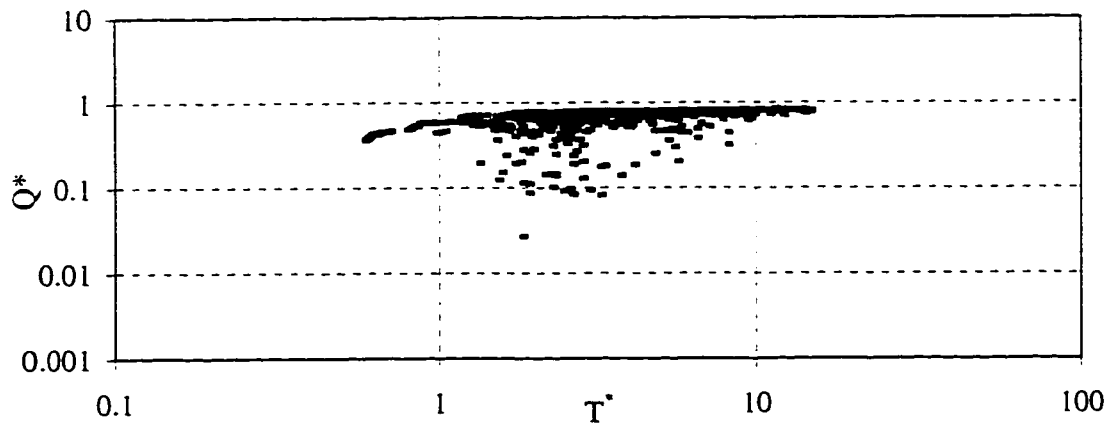


Fig. E.1c: Peak runoff rates on Goodwin Creek for $\bar{K}_s / i = 0.2$ (832 ft grid size)

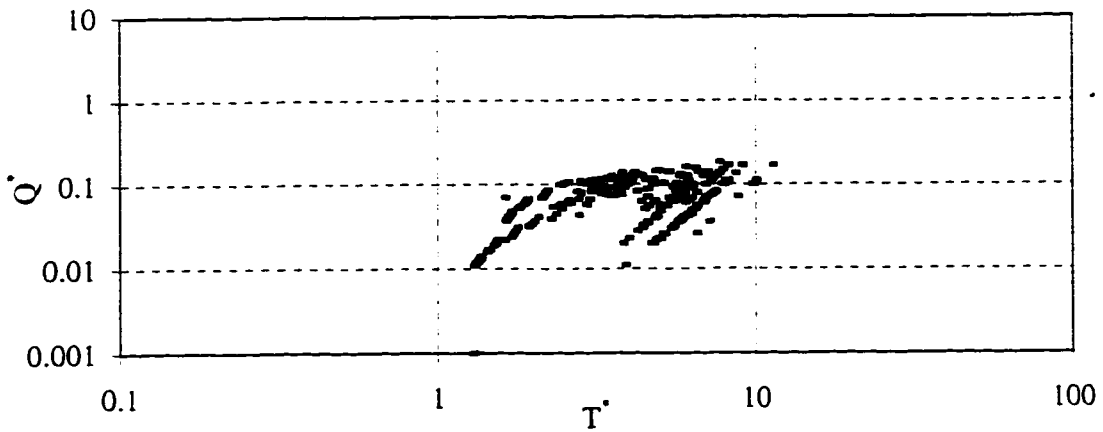


Fig.E.2a: Peak runoff rates on Goodwin Creek for $\bar{K}_s / i = 1.0$ (1248 ft grid size)

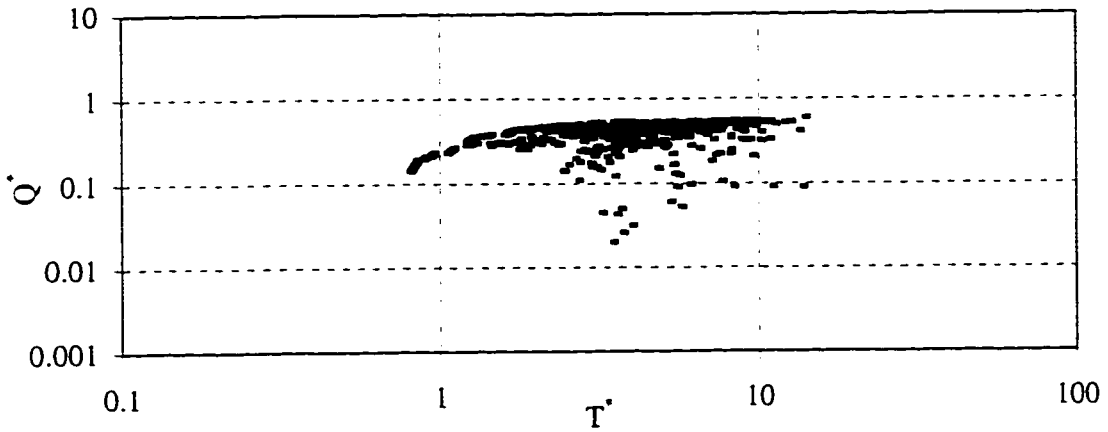


Fig. E.2b: Peak runoff rates for on Goodwin Creek $\bar{K}_s / i = 0.5$ (1248 ft grid size)

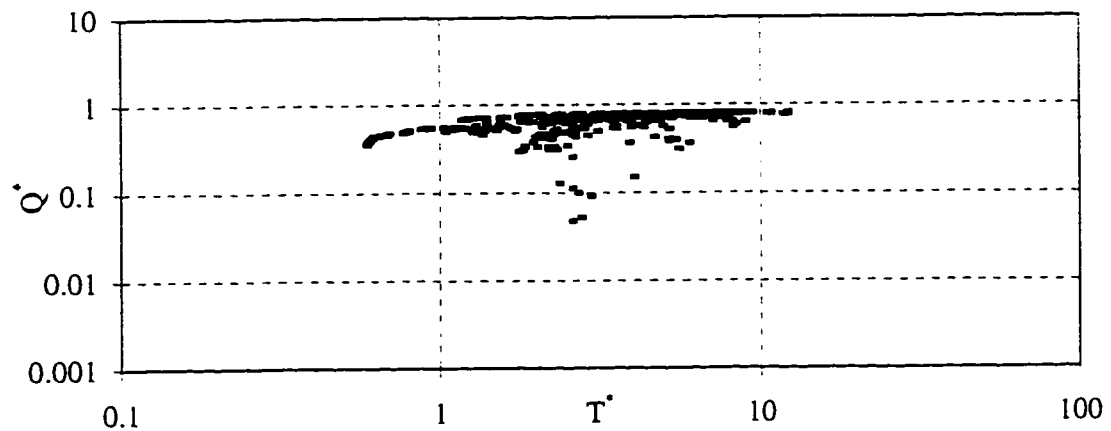


Fig.E.2c: Peak runoff rates on Goodwin Creek for $\bar{K}_s / i = 0.2$ (1248 ft grid size)

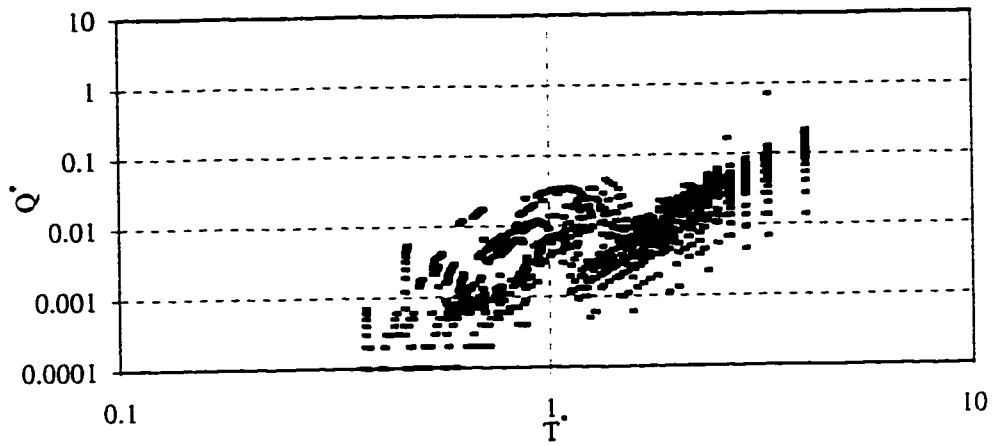


Fig. E.3a: Peak runoff rates on Hickahala-Senatobia for $\bar{K}_s / i = 1.0$ (2000 ft grid size)

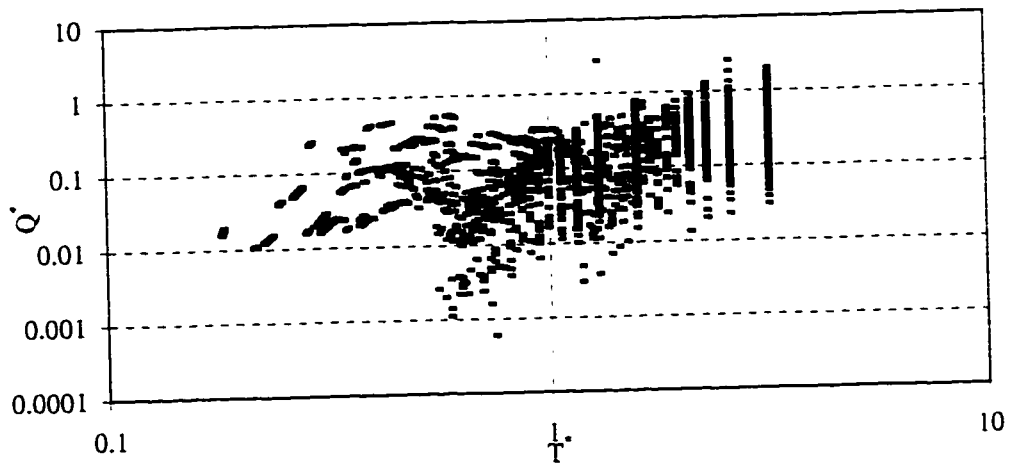


Fig. E.3b: Peak runoff rates on Hickahala-Senatobia for $\bar{K}_s / i = 0.5$ (2000 ft grid size)

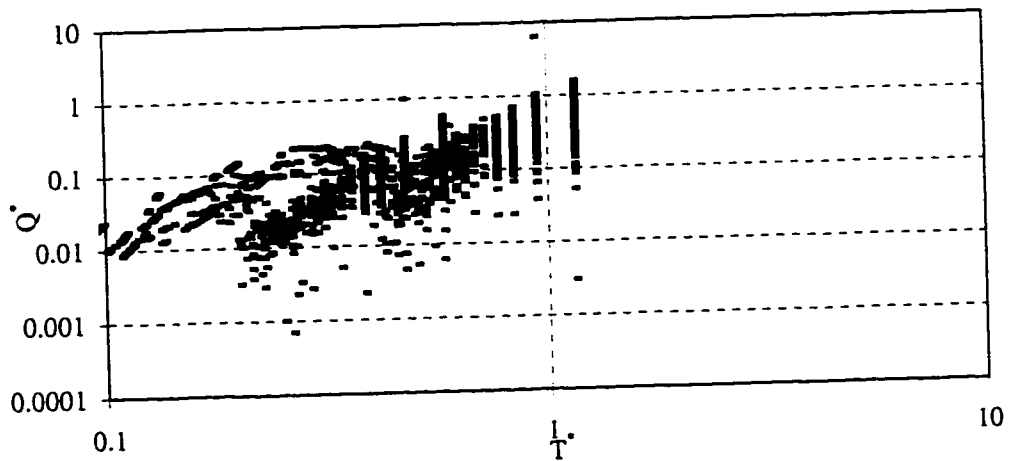


Fig. E.3c: Peak runoff rates on Hickahala-Senatobia for $\bar{K}_s / i = 0.2$ (2000 ft grid size)

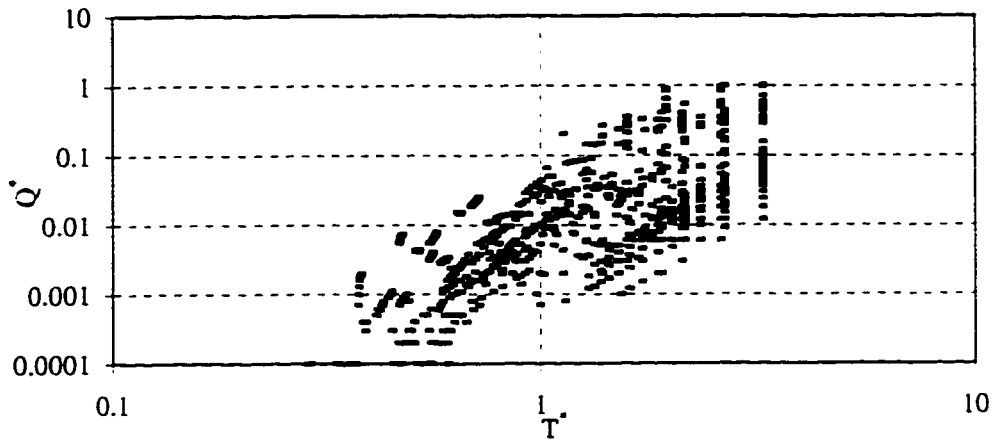


Fig. E.4a: Peak runoff rates on Hickahala-Senatobia for $\bar{K}_s / i = 1.0$ (3000 ft grid size)

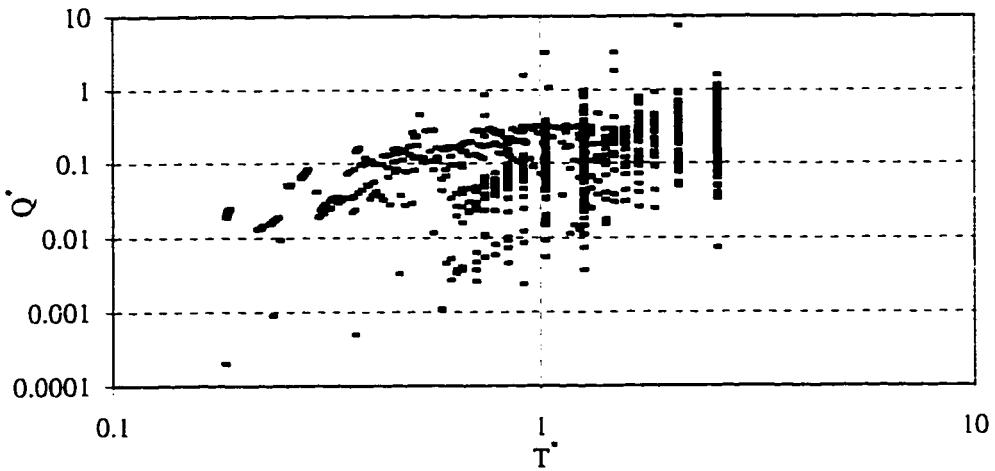


Fig. E.4b: Peak runoff rates on Hickahala-Senatobia for $\bar{K}_s / i = 0.5$ (3000 ft grid size)

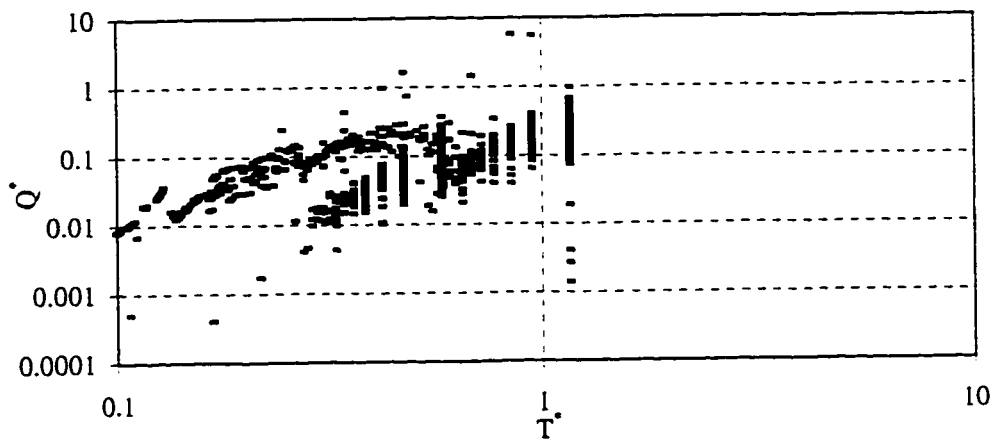
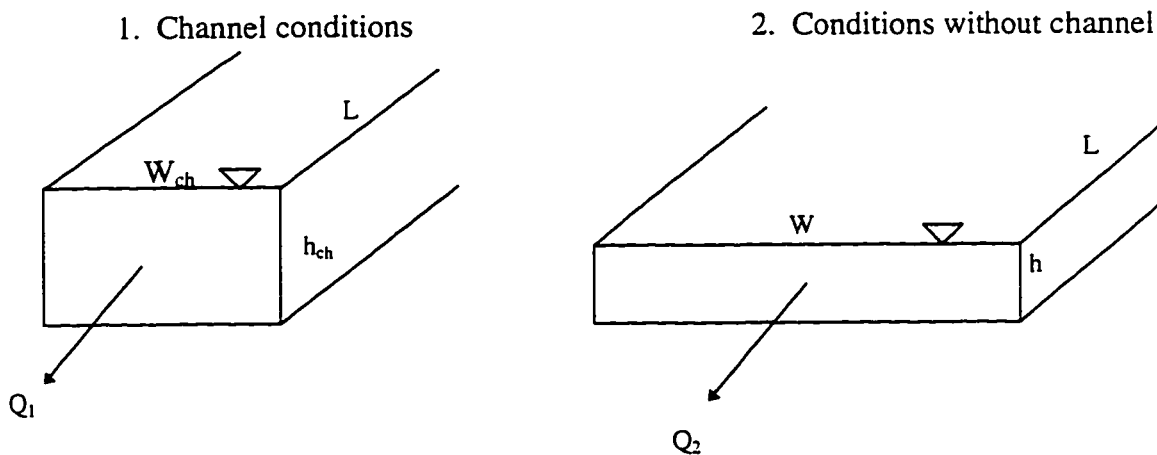


Fig. E.4c: Peak runoff rates on Hickahala-Senatobia for $\bar{K}_s / i = 0.2$ (3000 ft grid size)

APPENDIX E

CALCULATING AN EQUIVALENT CHANNEL ROUGHNESS

In order to perform channel routing, CASC2D requires channel information (width, depth, Manning n) for every channel cell, and the connectivity of the channel links must also be specified. On large watersheds, when very fine resolutions are used, the channel network becomes too complex to define. A method was developed in order to evaluate the equivalent channel roughness (n_{eq}) if the channel of width (W_{ch}) were to be replaced by a grid cell of width (W). By specifying an equivalent channel roughness, channel routing can be neglected.



Step 1: Assume the same volume of water is in 1 (with channel) and 2 (without channel):

$$V_1 = h_{ch} W_{ch} L \quad (E.1)$$

$$V_2 = hWL \quad (\text{E.2})$$

Step 2: Evaluate depth as a function of width, where $V_1 = V_2$:

$$h_{ch}W_{ch}L = hWL \quad (\text{E.3})$$

$$\frac{h}{h_{ch}} = \frac{W_{ch}}{W} \quad (\text{E.4})$$

Step 3: Assume the same discharge in 1 (with channel) and 2 (without channel):

$$Q_1 = W_{ch}h_{ch} \left(\frac{1}{n_{ch}} h_{ch}^{2/3} S_f^{1/2} \right) \quad (\text{E.5})$$

$$Q_2 = Wh \left(\frac{1}{n_{eq}} h^{2/3} S_f^{1/2} \right) \quad (\text{E.6})$$

Step 4: Evaluate Manning roughness as a function of width, where $Q_1 = Q_2$:

$$W_{ch}h_{ch} \left(\frac{1}{n_{ch}} h_{ch}^{2/3} S_f^{1/2} \right) = Wh \left(\frac{1}{n_{eq}} h^{2/3} S_f^{1/2} \right) \quad (\text{E.7})$$

$$\frac{n_{eq}}{n_{ch}} = \frac{W}{W_{ch}} \left(\frac{h}{h_{ch}} \right)^{5/3} = \frac{W}{W_{ch}} \left(\frac{W_{ch}}{W} \right)^{5/3} \quad (\text{E.8})$$

$$n_{eq} = n_{ch} \left(\frac{W_{ch}}{W} \right)^{2/3} \quad (\text{E.9})$$